

# Hydrogeochemical, Mineralogical and Microbial Processes Occurring in Old Sulfide-Rich Tailings

by

Michael Campbell Moncur

A thesis

presented to the University of Waterloo

in fulfillment of the

thesis requirement for the degree of

Doctor of Philosophy

in

Earth Sciences

Waterloo, Ontario, Canada, 2015

©Michael Campbell Moncur 2015

## **Author's Declaration**

This thesis consists of material all of which I authored or co-authored: see Statement of Contributions included in the thesis. This is a true copy of the thesis, including any required final revisions, as accepted by my examiners.

I understand that my thesis may be made electronically available to the public.

## Statement of Contributions

- Chapter 1: Michael Moncur wrote the chapter.
- Chapter 2: Michael Moncur conducted the field work, compiled the data set, and participated in designing the study and writing the manuscript.
- Chapter 3: Michael Moncur conducted the field work, built the laboratory equipment, compiled the data set, participated in designing the study, and wrote the manuscript.
- Chapter 4: Michael Moncur designed the study, conducted the field work, performed the modeling, compiled the data, assisted with XANES analyses, microbial enumerations, mineralogy, and wrote the manuscript.
- Chapter 5: Michael Moncur designed the study, conducted the field work, compiled the data, performed the modeling, and wrote the manuscript.
- Chapter 6: Michael Moncur designed the study, conducted the field work, compiled the data, performed the modeling, assisted with the mineralogy, and wrote the manuscript.
- Chapter 7: Michael Moncur designed the study, conducted the field work, compiled the data, did the mass loading calculations, performed the modeling, did the mineralogy, and wrote the manuscript.
- Chapter 8: Michael Moncur designed the study, conducted the field work, compiled the data, performed the modeling, and contributed to the mineralogy, and wrote the manuscript.
- Chapter 9: Michael Moncur wrote the chapter.

## Abstract

The former Sherritt-Gordon Mine, located in Sherridon Manitoba, processed approximately 7.7 Mt of sulfide ore between 1931 and 1951. The Zn-Cu volcanic massive-sulfide ore body yielded Zn and Cu concentrates with minor amounts of Au and Ag. The tailings derived from the ore extraction activities contain up to 60 wt. % as sulfide, mainly as pyrrhotite  $[\text{Fe}_{1-x}\text{S}]$  and pyrite  $[\text{FeS}_2]$ , with pyrrhotite equaling or exceeding pyrite in all samples. Other primary sulfide minerals in the tailings include minor amounts of sphalerite  $[(\text{Zn},\text{Fe})\text{S}]$ , chalcopyrite  $[\text{CuFeS}_2]$ , and trace amounts of arsenopyrite  $[\text{FeAsS}]$  and galena  $[\text{PbS}]$ . Tailings were discharged into three separate impoundments; the Camp tailings deposited between 1931 and 1932; the Woods tailings deposited between 1937 and 1951; and the subaqueous Fox tailings deposited near the end of mining operations in 1951. During the past ~80 years, extensive oxidation of sulfide minerals in the Camp tailings has resulted in extremely high concentrations of dissolved  $\text{SO}_4$  and metals in the tailings porewater, among some of the highest reported in the literature.

Mineralogical analyses of the Camp tailings found that the pyrrhotite was the first mineral consumed during oxidation followed by sphalerite, then pyrite. Dissolved Ni and Co released from pyrrhotite, and dissolved Zn and Cd from sphalerite, were attenuated when they were sequestered in early-formed Fe oxyhydroxides. The sorptive capacity of Fe oxyhydroxides decreases over time, and with continued exposure to low-pH porewater, the Ni, Co, Zn and Cd initially sequestered in the Fe-oxyhydroxides may eventually be released back to the porewater. Elements such as Cu, Pb and Cr were observed to form distinct secondary mineral phases or remained incorporated into mature Fe oxyhydroxides, however, Ni and Zn were mobile.

Magnetite was relatively stable except under extremely low-pH conditions, where it became a source of Fe(II), Fe(III) and potentially Cr.

Mineralogical and geochemical characterization of the submerged Fox tailings focused on two contrasting areas of this deposit: sub-aerial tailings with the water table positioned at a depth of 50 cm; and sub-aqueous tailings stored under a 100 cm water cover. The sub-aerial tailings showed a zone of extensive sulfide-mineral alteration extending 40 cm below the tailings surface with moderate alteration restricted to depths >60 cm. In contrast, sulfide-mineral alteration within the submerged tailings was limited to a <6 cm zone located below the water-tailings interface. Porewater within the upper 40 cm of the sub-aerial tailings was characterized by low pH (1.9–4.2), depleted alkalinity, elevated dissolved SO<sub>4</sub> and metals, and abundant populations of acidophilic sulfur-oxidizing bacteria. Conversely, pore-water in the sub-aqueous tailings was characterized by a circumneutral pH, moderate alkalinity, and low concentrations of dissolved SO<sub>4</sub> and metals. The primary control of water chemistry in the sub-aqueous tailings appeared to be dissimilatory sulfate reduction (DSR), evident from elevated concentrations of pore-water H<sub>2</sub>S, large shifts in δ<sup>13</sup>C-DIC and δ<sup>34</sup>S-SO<sub>4</sub> consistent with fractionation during DSR, and elevated populations of sulfate reducing bacteria. In addition, mineralogical investigation revealed the presence of secondary sulfide coatings on primary sulfide minerals that may control metal mobility within the sub-aqueous tailings.

Surface water discharging from the Fox tailings flowed into the Woods tailings. Similar to the Camp tailings, extensive sulfide oxidation had occurred in the Woods tailings during the past 60 years resulting in elevated concentrations of sulfide oxidation products and low pH values in the unsaturated tailings porewater. During precipitation events and the spring freshet, surface seeps developed along the flanks of the tailings impoundment discharging groundwater with very low pH values (*e.g.*, as low as 0.39) and elevated concentrations of dissolved metals

(*e.g.*, SO<sub>4</sub> up to 203 g L<sup>-1</sup>; Fe up to 68 g L<sup>-1</sup>). Efflorescent minerals, including melanterite, rozenite, halotrichite, chalcantite, alpersite, copiapite, hexahydrite, jurbanite, pickeringite, jarosite and gypsum were observed within these groundwater seepage areas. The formation of these secondary efflorescent minerals removes SO<sub>4</sub> and metals from solution. Laboratory dissolution experiments found that these minerals rapidly dissolved in water, indicating that this removal would only be temporary, and that there is still the potential for increased loadings of dissolved metals and SO<sub>4</sub> during precipitation events. Below the vadose zone in the saturated tailings, concentrations of dissolved metals and SO<sub>4</sub> decreased, but remained elevated in deeper groundwater. Along the groundwater flowpath, near the border between the Woods tailings and the discharge area into Woods Lake, concentrations of metals and SO<sub>4</sub> abruptly decreased, coinciding with strong shift towards more positive δ<sup>34</sup>S-SO<sub>4</sub> values, consistent with the influence of DSR on water chemistry rather than simple dilution. DSR currently occurring at the tailings edge appears to lead to a substantial decrease in loading of dissolved metals, SO<sub>4</sub> and low pH groundwater to Woods Lake.

Groundwater and surface water discharging from the Sherridon tailings impoundments discharge directly into Camp Lake. A 5-year hydrological and geochemical sampling program was initiated at Camp Lake to identify the mass-loadings and seasonal distributions of dissolved metals and SO<sub>4</sub> discharging from the lake to the receiving Kississing Lake. Outflow from Camp Lake was sampled weekly and biweekly and dissolved ion concentrations and pH showed a strong seasonal cycle in mass-loadings. During winter months when the lake was ice-covered, discharge water from Camp Lake had a neutral pH with low concentrations of dissolved metals and SO<sub>4</sub> similar to background concentrations. The Camp Lake discharge had an abrupt increase in dissolved metal and SO<sub>4</sub> concentrations and decreases in pH during the spring freshet that remained relatively constant until fall freeze-up, when dissolved metal concentrations and pH

returned to winter values. The annual and interannual variations in loadings measured in Camp Lake were different from those measured at the two streams feeding Camp Lake, revealing the contribution of high-salinity groundwater discharge from the tailings to the lake during dry years and the potential for significant loadings due to the dissolution of efflorescent minerals or enhanced transport of solutes through the thick unsaturated zone in the tailings during relatively wet years. The abrupt changes in pH, metal and  $\text{SO}_4$  concentrations, and the timing of these changes with the appearance and disappearance of ice-cover on the lakes, suggests a combination of physical and geochemical controls related to shifts in sources of water, mixing and changes in solubility. Despite fairly low average annual metal concentrations measured in Camp Lake discharge, concentrations of Zn and Cu were elevated above background in bottom sediments of Kississing Lake in a zone extending  $9.5 \text{ km}^2$  from the location of Camp Lake inflow.

The insight gained from studying metal release from sulfide-rich tailings was used to identify processes and controls on the release of metal(loid)s from Quaternary sediments and influence on background water quality in Alberta's Southern Oil Sands Regions. A survey of over 800 groundwater wells completed in sand and gravel aquifers found that 50% of the wells contained As concentrations exceeding drinking water guidelines of  $10 \mu\text{g L}$ . The same geochemical, mineralogical and isotopic methods used to investigate sulfide oxidation processes in the Sherridon tailings were applied to these glaciofluvial sediments to identify As sources. Unoxidized sediments collected from below the water table contained abundant arsenian framboidal pyrite and As-bearing Fe oxyhydroxides. Speciation model calculations showed that the majority of groundwater samples were undersaturated with respect to ferrihydrite, suggesting that reductive dissolution of As-bearing Fe oxyhydroxides may be the source of some As in deeper reduced groundwater. In contrast, the oxidized sediments above the water table did not contain framboidal pyrite, but exhibited spheroidal Fe oxyhydroxide grains with elevated As

concentrations. The habit and composition suggest that these Fe oxyhydroxide grains in the oxidized sediment were an alteration product of former framboidal pyrite grains. The results of the mineralogical analyses indicate that the oxidation of framboidal pyrite during weathering may be the source of As released to shallow aquifers and reductive dissolution of Fe oxyhydroxides may be the source of As in deeper aquifers.



## Acknowledgements

First I would like to thank my advisor and mentor Dr. Carol Ptacek for her support, encouragement, patience, and convincing me to pursue this thesis. I thank my co-advisor Dr. David Blowes for his mentoring and introducing me to the world of mine tailings geochemistry. I benefited greatly from their insight, knowledge and enthusiasm. During my studies they encouraged me to apply a multi-disciplinary approach to my research incorporating geochemistry, mineralogy, hydrogeology, microbiology, hydrology, isotope geochemistry and modeling which helped define this research and introduced me to new concepts.

I would like to thank my committee members Dr. Douglas Gould and Dr. Richard Amos for committing their time and providing insightful comments during meetings and review of this thesis. I also thank my external examiners Dr. Katie Walton-Day and Dr. Jonathan Price for taking time out of their busy schedules to carefully and critically review this thesis.

I was extremely fortunate to have had the opportunity to work with Dr. Matthew Lindsay, the late Dr. John Jambor, Dr. Bernhard Mayer, Dr. Masaki Hayashi, Dr. Dogan Paktunc, and Dr. Ron Peterson. Many research ideas were developed through discussions and assistance from these talented individuals.

This research would not have been possible without the technical assistance of numerous individuals in the field and laboratory, including many insightful discussions. These outstanding people include:

**University of Waterloo;** Laura Groza, Joy Hu, Michael Gunsinger (Golder), Jeff Bain, Lianna Smith, Andrea Brookfield (Kansas Geological Survey), Dr. William Robertson, Corina McDonald, Randy Stotler (University of Kansas), Dr. Shaun Frape, Sue Fisher.

**Alberta Innovates – Technology Futures;** Dr. Jean Birks, Larry Roy, Dr. John Gibson, Cathie Thompson, Don Jones.

**Community of Sherridon;** Denis Hatch, Fred Schurko, Nick Benyk, Ernie Lapensee. Johan Krebs, Debbie Hatch.

**University of Calgary;** Maurice Shevalier, Michael Nightingale, George Kominek, Steve Taylor, Jesusa Pontoy, Dr. Michael Wieser, Farzin Malekani.

**Alberta Government:** Brent Welsh (AER), Joe Prusak (AESRD), Debra Mooney  
(Alberta Health).

**Manitoba Conservation and Water Stewardship;** Special thanks to Dave Green for  
initiating this project.

Thanks to Tom Wingrove and Doug Bright for providing access to lake sediment data.

I would like to express my gratitude to my family: Mark and Marilyn Moncur, my mother Ellen Moncur, and my beautiful daughters Rowan and Isla, for their encouragement and patience. I am grateful that my father got me interested in hydrogeology at a young age and introduced to the University of Waterloo. I am grateful for the friendship of many people during this thesis, particularly Mike Baker who traveled to UW to celebrate the post-defence beveraging.

Finally, I thank my lovely wife Dr. Jean Birks, who is an inspiration, providing me with unwavering support, encouragement, and exceptional guidance during this research. Without Jean's support, completion of this thesis would not have been achievable.

This research was made possible through funding provided by the Natural Sciences and Engineering Research Council of Canada (NSERC), the Toxic Substances Research Initiative managed jointly by Health Canada and Environment Canada, Alberta Innovates — Technology Futures, Manitoba Conservation and Water Stewardship, Alberta Health and Wellness, Alberta Environment, and the Beaver River Watershed Alliance. Synchrotron-based research described in Chapter 4 was performed at the Canadian Light Source in Saskatoon, SK, which is funded by the Canada Foundation for Innovation, NSERC, the National Research Council of Canada, the Canadian Institutes of Health Research, the Government of Saskatchewan, Western Economic Diversification Canada, and the University of Saskatchewan. The XAFS experiments in Chapter 8 were performed at the PNC/XOR beamline, Advanced Photon Source, Argonne National Laboratory in Lemont, IL, which is supported by the US Department of Energy under Contracts W-31-109-Eng-38 (APS) and DE-FG03-97ER45628 (PNC-CAT). The XAFS experiments were also supported by NSERC through a MRS Grant and funding from Alberta Environment.

# Dedication

This thesis is dedicated to  
the memory of  
Virginia “Ginny” Moncur

# Table of Contents

Author's Declaration.....	ii
Statement of Contributions .....	iii
Abstract.....	iv
Acknowledgements.....	ix
Dedication.....	xi
Table of Contents.....	xii
List of Tables .....	xvi
List of Figures.....	xix
Chapter 1: Introduction .....	1
1.1 Geochemical Processes in Mine Tailings .....	2
1.1.1 Sulfide Oxidation .....	2
1.1.2 Acid Neutralization .....	4
1.1.3 Sulfate Reduction .....	6
1.2 Research Objectives.....	7
1.3 Thesis Organization .....	7
Chapter 2: Mine Drainage From the Weathering of Sulfide Minerals and Magnetite.....	9
2.1 Executive Summary .....	11
2.2 Introduction.....	11
2.3 Oxidation of the Sulfide Minerals.....	13
2.4 Trace Element Mineral Associations .....	15
2.5 Mineralogical and Geochemical Behavior.....	16
2.6 Progression of Sulfide Alteration.....	23
2.7 Geochemical Variations with Depth.....	26
2.8 Generalized Paragenesis .....	29
2.9 Conclusions.....	34
Chapter 3: Pore-water Extraction From the Unsaturated and Saturated Zones .....	35
3.1 Executive Summary .....	36
3.2 Introduction.....	36
3.3 Methods and Materials.....	39
3.3.1 Core Collection.....	39
3.3.2 Squeezer Construction.....	41
3.3.3 Squeezing Procedure .....	44
3.3.4 Case Study Field Methods.....	47
3.4 Progression of Sulfide Alteration.....	49
3.4.1 Unsaturated Profile.....	50
3.4.2 Surface Water – Groundwater Interface.....	52
3.5 Conclusions.....	54
Chapter 4: Long-term Mineralogical and Geochemical Evolution of Sulfide Mine Tailings Under A Shallow Water Cover.....	56

4.1	Executive Summary .....	57
4.2	Introduction.....	58
4.3	Study Site.....	59
4.4	Methods.....	62
	4.4.1 Core Collection and Piezometer Installation.....	62
	4.4.2 Solid Phase Analyses and Mineralogy .....	63
	4.4.3 Aqueous Geochemistry .....	65
	4.4.4 Microbial Enumerations .....	67
	4.4.5 Geochemical Modeling .....	68
4.5	Results and Discussion .....	68
	4.5.1 Fox Lake Water Level.....	68
	4.5.2 Physical Tailings Characteristics.....	69
	4.5.3 Mineralogy .....	70
	4.5.4 Sub-Aerial Tailings .....	71
	4.5.5 Sub-Aqueous Tailings .....	74
	4.5.6 Solid-Phase Geochemistry .....	77
	4.5.7 X-ray Absorption Spectroscopy .....	80
	4.5.8 Porewater Chemistry .....	83
	4.5.8.1 Sub-Aerial Tailings.....	83
	4.5.9 Sulfate Reduction .....	88
	4.5.10 Microbial Enumerations .....	92
	4.5.11 Fox Lake Water Quality .....	94
4.6	Conclusions.....	95
Chapter 5:	Tracing The Sulfur Cycle At An Abandoned High-Sulfide Tailings Impoundment Using Chemical and Isotopic Techniques.....	97
5.1	Executive Summary .....	98
5.2	Introduction.....	98
5.3	Site Background.....	99
5.4	Methods.....	100
5.5	Results and Discussion .....	101
5.6	Conclusions.....	107
Chapter 6:	Occurrence and Implications of Efflorescent Sulfate Minerals From The Former Sherritt-Gordon Zn-Cu Mine .....	109
6.1	Executive Summary .....	110
6.2	Introduction.....	111
6.3	Site Background.....	112
6.4	Methods.....	116
	6.4.1 Mineral Sampling and Analyses.....	116
	6.4.2 Seep Water Chemistry.....	117
	6.4.3 Speciation Modeling.....	118
	6.4.4 Laboratory Dissolution Experiments.....	118
6.5	Results and Discussion .....	119
	6.5.1 Woods Seep.....	119
	6.5.2 Seepage Valley .....	119
	6.5.3 Speciation Modeling.....	126

	6.5.4	Dissolution Experiments .....	128
	6.5.5	Environmental Implication.....	131
	6.6	Conclusions.....	135
Chapter 7:		Seasonal Cycling and Mass-Loading of Dissolved Metals and Sulfate Discharging From an Abandoned Mine Site in Northern Canada .....	136
	7.1	Executive Summary .....	137
	7.2	Introduction.....	138
	7.3	Study Area .....	139
	7.4	Methods.....	142
		7.4.1 Hydrology.....	142
		7.4.2 Surface Water Quality .....	143
		7.4.3 Geochemical Modeling .....	145
		7.4.4 Lakebed Sediments and Secondary Precipitates .....	145
	7.5	Results and Discussion .....	146
		7.5.1 Camp Lake Hydrology .....	146
		7.5.2 Woods Weir Watershed.....	147
		7.5.3 Acid Pond.....	153
		7.5.4 Sherlett Creek Watershed.....	153
		7.5.5 Camp Weir .....	158
		7.5.6 Metal and SO <sub>4</sub> Loading .....	161
		7.5.7 Down-Stream Impact to Cold Lake.....	164
	7.6	Conclusions.....	167
Chapter 8:		Source and Distribution of Naturally Occurring Arsenic in Groundwater From Alberta's Southern Oil Sands Region .....	169
	8.1	Executive Summary .....	170
	8.2	Introduction.....	171
	8.3	Study Area .....	176
	8.4	Geological and Hydrogeological Setting.....	176
	8.5	Methods.....	178
		8.5.1 Groundwater Chemistry .....	178
		8.5.2 Arsenic Speciation.....	180
		8.5.3 Geochemical Modeling .....	180
		8.5.4 Solid Phase Analyses and Mineralogy .....	181
	8.6	Results and Discussion .....	182
		8.6.1 Sources and Controls of Arsenic .....	182
		8.6.2 Arsenic Distribution in Groundwater .....	190
		8.6.3 Long-Term Arsenic Variations .....	199
	8.7	Conclusions.....	201
Chapter 9:		Conclusions .....	203
	9.1	Summary of Results .....	204
	9.2	Scientific Contributions .....	213
	9.3	Recommendations.....	214

References .....218

## List of Tables

Table 2-1:	Schematic of relative resistance of sulfides and magnetite in oxidized tailings.....	17
Table 2-2:	Sulfide alteration index (SAI) of the Sherridon tailings (revised after Blowes and Jambor, 1990; Moncur et al., 2005).....	19
Table 2-3:	Schematic representation of the progressive oxidation of a unit of mine waste containing a mixed assemblage of pyrrhotite (po) and pyrite (py). In the earliest stage of oxidation, the secondary products are formed predominantly from pyrrhotite, with native sulfur and marcasite derived exclusively from pyrrhotite; the Fe oxyhydroxides may include ‘amorphous’ material and ferrihydrite, but typically consist predominantly of very fine-grained goethite with a high sorptive capacity. In the late stage, following consumption of the sulfides, pH will eventually rise and jarosite will therefore also be unstable. Photomicrographs of the Sherridon tailings; (a) earliest to (d) late. (a) Unaltered grains of pyrite, sphalerite (sp) and chalcopyrite (ch) with grains of pyrrhotite rimmed by secondary marcasite (mr). (b) Near the center of the photo is a particle consisting of a core of pyrrhotite, a dark intermediate zone, and a rind of marcasite. The dark zone is vacant, but local areas of Fe SO <sub>4</sub> are detectable. Pyrite and sphalerite grains are unaltered. (c) Whitish grains are pyrite and chalcopyrite accompanied by two grains of magnetite (m). On the right is a large particle of goethite. Pyrrhotite is no longer present. (d) On the left is a whitish grain of pitted magnetite and on the right are two particles of compact goethite. Note the absence of sulfide minerals. ....	30
Table 3-1.	Materials and dimensions for 5.1 cm (2-in.) and 7.6 cm (3-in.) squeezer components. ....	43
Table 4-1:	Results of LCF analysis of S K-edge XANES spectra for sub-aerial (FX) and sub-aqueous (FXS) tailings. Fitted reference spectra included pyrite (py) and marcasite (mr), pyrrhotite (po), chalcopyrite (cp), sphalerite (sp), gypsum (gp), jarosite (ja), and covellite (cv). The R factor is the mean-square misfit between the measured and modeled spectra. ....	82
Table 4-2:	Porewater chemistry measured from the land-based (FX) and submerged (FXS) tailings in 2001 and 2009.....	87
Table 4-3:	Water chemistry measured from Fox Lake (FL) surface water between 1983 and 2009. Median calculations for FL and Sherlett Lake (SL) were determined from 2002 to 2009 data. GPAL refers to the Canadian guidelines for the protection of aquatic life (CCME, 2007). Historical values from Beck <sup>a</sup> (1983) and Beck <sup>b</sup> (1988). Detection limit represented by dl. Hyphens indicate that parameter was not determined. ....	94
Table 6-1:	Primary sulfide minerals observed in the ore (O) by Farley (1949) and the tailings (T) by Moncur et al. (2005). ....	113



Table 6-2:	Secondary sulfate and Fe(III)-oxyhydroxide minerals observed in the hardpan layers (Moncur et al., 2005).....	115
Table 6-3:	Secondary sulfate minerals observed at seepage zones. ....	124
Table 6-4:	Speciation modeling results of the seep waters from Woods Seep (WS), Valley Seep (VS) and Seep Pool (SP). The density and ionic strength of the waters were calculated using the Pitzer database. Mineral compositions are listed in Table 6.3 except schwertmannite $[\text{Fe}_8\text{O}_8(\text{OH})_6(\text{SO}_4)\cdot n\text{H}_2\text{O}]$ . ....	127
Table 6-5:	Results from the dissolution experiments showing concentrations of dissolved sulfate and metal(oid)s. Abbreviations refer to melanterite (Mel), alpersite (Alp), chalcantite (Chl), halotrichite (Hal), pickeringite (Pkt), hexahydrate (Hex), birnessite (Bir) and gypsum (Gyp). ....	131
Table 6-6:	Speciation modeling results of the seep waters from Woods Seep (WS), Valley Seep (VS) and Seep Pool (SP). The density and ionic strength of the waters were calculated using the Pitzer database. Mineral compositions are listed in Table 6.3 except schwertmannite $[\text{Fe}_8\text{O}_8(\text{OH})_6(\text{SO}_4)\cdot n\text{H}_2\text{O}]$ . Selected water chemistry from the Woods Seep (WS) and Valley Seep (VS). All concentrations are in $\text{mg L}^{-1}$ . A negative % change refers to a decrease in concentration. Concentrations in $\text{mg L}^{-1}$ . ....	132
Table 7-1:	Annual precipitation during the study period for the Sherridon area. Total snowfall was measured in Flin Flon, 60 km SW of Sherridon. ....	147
Table 7-2:	Average and median concentration of pH, $\text{SO}_4$ and metals from Sherlett Creek, Woods Weir and Camp Lake from July 2001 to September 2006. n refers to the number of samples analyzed; CDWS is the Canadian drinking water standards and GPAL is the Canadian guidelines for the protection of aquatic life. All concentrations in $\text{mg L}^{-1}$ , except pH which is unitless. Exceeding refers to percentage of average concentrations that exceed regulatory guidelines.....	151
Table 7-3:	Whole-rock analyses ( $\text{mg kg}^{-1}$ ) of secondary precipitates collected from Woods Weir (WWOR) and Camp Weir (CWOR). Each location is an average of three analyses except for WWWWHT, which is for one sample. Subscript OR refers to orange precipitates and WHT refers to a white precipitate.....	153
Table 8-1:	Examples of natural and anthropogenic occurrences of As in groundwater across Canada. ....	173
Table 8-2:	Physical properties of the eight formations in the CLBR glacial drift deposits (revised after Parks et al. (2005)).....	177
Table 8-3:	Total As concentrations measured in sediments from the CLBR basin, including data from Andriashek (2000), Fennell (2008) and this study. All values are in ppm. BR refers to bedrock and n refers to number of samples. ....	183
Table 8-4:	Arsenic concentration (ppm) of Fe(III)-oxyhydroxide $[\text{FeOOH}]$ and pyrite grains in sediments from Sites 1 and 2, determined by WDS-EPMA.....	187

Table 8-5: Primary sulfide minerals observed in the ore (O) by Farley (1949) and the tailings.....193

Table 8-6: Stable isotope and radiocarbon data from groundwater in the CLBR basin. NETPATH was used to correct groundwater ages. Number of wells sampled is represented by n. VCDT refers to Vienna Canyon Diablo Troilite. ....199

## List of Figures

- Figure 2-1: Map of Canada showing the locations of Sherridon, Manitoba, and other mine sites investigated by the authors that contributed to this manuscript.....13
- Figure 2-2: Cross-section through the center of the older Sherridon tailings impoundment, showing the mineralogical changes rated according to a sulfide alteration index (SAI) (after Moncur et al., 2005), which is a relative scale of alteration intensity. At SAI = 10, the sulfides have been almost completely obliterated (Fig. 2.6); at SAI = 3, remnant cores of pyrrhotite are abundant; at SAI = 1, the alteration occurs only as narrow rims on pyrrhotite (Fig. 2.7e,f). A continuous hardpan extends from 0.9 m to 2 m. The photo to the right of the SAI plot shows fresh exposed tailings on the left adjacent to extensive development of surface blooms of tertiary rozenite (white mineral) that formed shortly after the Fe<sup>2+</sup>-rich continuous hardpan was exposed to O<sub>2</sub> (right half of the photo). Analysis of the rozenite showed that Zn is present in trace amounts. The static water table is at approximately 4 m below ground surface.....20
- Figure 2-3: Variation in O<sub>2</sub> and CO<sub>2</sub> gas, percent sulfur and calcium carbonate [CaCO<sub>3</sub>], volumetric moisture content [ $\Theta$ : where ((mass<sub>water</sub>/density<sub>water</sub>)/volume<sub>total</sub>)], porosity (n), and saturation, and pore water density, in the Sherridon tailings. The solid horizontal line shows the top of the main hardpan. The static water table is at approximately 4 m below ground surface. Data from Moncur et al. (2005). .....22
- Figure 2-4: Sulfide alteration index (SAI) and bulk-sample X-ray diffractometry data for the Sherridon tailings. Plotted points for the diffractometry data represent the X-ray peak height (generally the highest peak in the diffraction pattern of the mineral) as follows: nd not detected; vw very low (very weak) peak height; w weak; m medium; st strong. In the plot for goethite, L is for lepidocrocite [ $\gamma$ -FeOOH], and in the plot for the Fe sulfates, M is melanterite and R is rozenite. The solid horizontal line shows the top of the main hardpan. The static water table is approximately 4 m below ground surface.....22
- Figure 2-5: Tailings from the Sherridon sulfide-depleted zone at 20 cm depth. Photo to the left, in plain reflected light, width of field 2.6 mm, shows two adjacent residual grains of chalcopyrite (cp), which are the only remaining sulfides (the whitish grain 'il' on the left is ilmenite FeTiO<sub>3</sub>). The narrow grey rims, as at the arrow, are Fe oxyhydroxides, mainly goethite. Photo to the right is of the same field, but in plain transmitted light. The black areas are Fe oxyhydroxides that have formed as rims and pseudomorphs after Fe sulfides. ....24
- Figure 2-6: Photomicrographs of the Sherridon tailings; (a) to (e) are for plain reflected light. (a) Oxidized zone at 60 cm depth, showing complete replacement of

pyrrhotite, now represented by blackish pseudomorphs, but with no alteration evident for the whitish grains of pyrite. Width of field is 2.1 mm. **(b)** Top of the hardpan contact at 90 cm depth, showing unaltered pyrite (py), sphalerite (s, at center), and a grain of chalcopyrite (cp). The zoned grains, as at the arrow, are pseudomorphs after pyrrhotite, wherein the whitish rims are secondary marcasite. Width of field is 2.1 mm. **(c)** Hardpan contact at 90 cm depth; width of field is 0.625 mm. The white, homogeneous grains are pyrite (py). Pyrrhotite (po, and at the core of the triangular particle at the top) is variably rimmed by marcasite (mr); in the particle at the bottom right no pyrrhotite remains. The large grey grain is sphalerite (sp) containing, at the arrow, an inclusion of former pyrrhotite, now altered to marcasite. **(d)** Hardpan zone at 116–126 cm depth, showing white unaltered pyrite (py) and weak alteration of pyrrhotite (po) along the rim and basal parting, with a narrow outermost rind of marcasite. Width of field is 0.625 mm. **(e)** Hardpan zone at 112–118 cm depth, showing cores of pyrrhotite with a thin exterior of marcasite; the intermediate zone is a Fe sulfate, as is indicated by its low reflectance and spectrally high S content. Width of field is 0.625 mm. **(f)** Basal part of the hardpan zone at 185 cm depth; reflected light, internal reflection, polarizers almost crossed, width of field 0.625 mm. The grains showing the basal parting are marcasite after pyrrhotite, a few remnants of which are present, as at the arrow. The cementing material is yellowish in plain light (whitish in the reproduction), and is apparently a mixture of Fe oxyhydroxide and Fe sulfate. The unaltered grains at the top right and lower left are pyrite (py). .....25

Figure 2-7: Profiles of the water chemistry of the Sherridon tailings from August, 2001. The rectangular enclosure shows the position of the main hardpan, and the horizontal dashed line is the position of the static water table. Data from Moncur et al. (2005). .....27

Figure 2-8: Examples of well-developed alteration rims of Fe oxyhydroxide on pyrite in tailings from the Yellowknife gold-producing area, Northwest Territories, Canada. Photos (a) and (b) are backscattered-electron (BSE) images of oxyhydroxide-rimmed pyrite (py) and the corresponding x-ray maps that show the distribution of Fe, As, and S. The residual pyrite is outlined well by the maps for S. Note that As is concentrated in the Fe oxyhydroxides and has been sorbed from the pore waters rather than from the low-As host pyrite. The bar scales are 45 µm for (a) and 35 µm for (b). .....32

Figure 2-9: (a) BSE image of remnant arsenopyrite (asp) and (b) a pseudomorph of Fe oxyhydroxide after arsenopyrite in tailings from the Yellowknife area, Northwest Territories, Canada. The bar scales are 50 $\mu\text{m}$ and 25 $\mu\text{m}$ , respectively. The black areas within the pseudomorph are voids. The relatively homogeneous distribution of As in the X-ray maps of both (a) and (b) suggests sorption of As rather than the presence of mixtures containing discrete As mineral species. Electron-microprobe analyses of the rims in Figure 2.8 gave up to 5.3 wt% $\text{As}_2\text{O}_5$ , and analyses of the rims in Figure 2.9 range from 5.6 to 7.1 wt% $\text{As}_2\text{O}_5$ .	33
Figure 3-1: Schematic diagram showing dimensions of squeezer components. All values are in millimetres, and dimensions are for both 5.1 cm (2-in.) and 7.6 cm (3-in.) squeezer parts. Values in brackets correspond to 5.1 cm squeezer components.	42
Figure 3-2: Drawing to the left shows a cross section of a core fitted with squeezer components. Photos show setup of the pore-water squeezing method.	44
Figure 3-3: Depth profiles of the porosity, gravimetric (Wt.), and volumetric moisture content ( $\Theta$ ), saturation (Sat), and bulk and particle density ( $\rho$ ) measured from the Sherridon Tailing. The “sample (mL)” profile refers to the amount of water squeezed from the tailings material. Crosshatched area represents hardpan. The water table is at a 4.3 m depth.	50
Figure 3-4: Profiles of pore-water chemistry at site 1 from the Sherridon tailings. Squeezed porewater is shown in solid circles, and the open circles are from drive-point piezometers. The cross-hatched area represents a hardpan layer, and the dashed line shows the position of the static water table. All concentrations in $\text{mg L}^{-1}$ except where noted. Alk refers to alkalinity in $\text{mg L}^{-1}$ as $\text{CaCO}_3$ .	51
Figure 3-5: Profiles of pore-water chemistry at site 2 through lake-bed sediments. Squeezed pore water is show in solid circles and the open circles are from peepers. Upper plot is below a 0.3 m water column, and the lower plot is below a 1.2 m water column. The solid horizontal line represents the sediment porewater–surface-water interface. Concentrations in $\text{mg L}^{-1}$ except where noted.	53
Figure 4-1: Location of the former Sherritt-Gordon Zn–Cu mine in Sherridon, Manitoba, Canada.	60
Figure 4-2: Aerial photos of Fox Lake and the submerged tailings between 1952 and 2007. Images taken (a) 1952; (b) 1968; (c) 1977; (d) 1983; (e) 2001; (f) 2007. Image (e) shows where samples were collected from the tailings on-land (FX) and submerged under a 100 cm water cover (FXS). Image from 2007 courtesy of Google Earth.	62

Figure 4-3: Depth profile through the on land (FX) and submerged tailings (FXS), top row showing the uniformity coefficient (CU), porosity, and grain-size distribution. The bottom row shows the sulfide alteration index (SAI) and weight percent of total sulfur (S), carbon (C), carbonate minerals (CaCO <sub>3</sub> ), and calculated organic carbon (OC). The water-tailings interface is located at a depth of 0 cm for FXS and the dashed horizontal line represents the water table at FX. ....	70
Figure 4-4: Photomicrographs of tailings thin sections in plane-polarized reflected light (A) 2 cm depth in the sub-aerial tailings (FX) showing a single grains of whitish pyrite (py) and yellow chalcopyrite (cp) which are the only remaining sulfides (B) FX 33 cm depth showing sparse pyrite and chalcopyrite (C) FX 62 cm depth showing unaltered pyrite; the grey grain is sphalerite (sp). Pyrrhotite (po) is variably rimmed by marcasite (mr) and in some grains complete replacement by marcasite. (D) 2 cm depth in the subaqueous tailings (FXS) showing unaltered pyrite with pyrrhotite extensively replaced mainly to complete pseudomorphism by marcasite. Grey magnetite (m), brown biotite (bi) lath and two irregular patches of grey goethite (g) are detectable. (E) FXS at a 6 cm depth showing abundant pyrite, altered pyrrhotite, and a grey Fe oxyhydroxide cement surrounding various gangue minerals. (F) FXS 18 cm depth showing unaltered pyrite, a sphalerite grain with a chalcopyrite inclusion, and cores of pyrrhotite with a thin exterior of marcasite. Two irregular patches of grey goethite are present. Depth and width of view are represented by d and wv, respectively. ....	72
Figure 4-5: Depth profile through the sub-aerial (FX) and sub-aqueous (FXS) tailings showing solid-phase concentrations of major and trace elements. Concentrations are in mg/g. The water-tailings interface is located at a depth of 0 cm for FXS and the dashed horizontal line represents the water table at FX. ....	79
Figure 4-6: Measured (line) and modeled (circles) S K-edge XANES spectra for samples of sub-aerial (FX) and sub-aqueous (FXS) tailings. Vertical shaded areas represent measured S K-edge white line maxima for (a) pyrrhotite, (b) covellite, pyrite and/or marcasite, (c) gypsum and/or jarosite reference materials. ....	81
Figure 4-7: Depth profiles through the land-based (FX) and submerged (FXS) tailings; (A) and (B) showing porewater chemistry and calculated ionic strength; (C) and (D) showing calculated saturation indices. All concentrations are in mg L <sup>-1</sup> except where noted. Dashed horizontal line represents water table location in the FX. The Fox Lake (FL) water-tailings interface of FXS is shown at a depth of 0 cm. ....	85

Figure 4-8: (A) Plot of  $\delta^{34}\text{S}$  versus  $\delta^{18}\text{O}_{\text{SO}_4}$  values of dissolved  $\text{SO}_4$  from sub-aerial tailings (FX), sub-aqueous tailings (FXS), Fox Lake (FL) and Sherlett Lake (SL) surface water. The shaded area represents the range of  $\delta^{34}\text{S}$  values measured from seven primary sulfide minerals. VSMOW – Vienna Standard Mean Ocean Water; VCDT – Vienna Canyon Diablo Troilite. (B) Plot of  $\delta^{13}\text{C}_{\text{DIC}}$  versus  $\delta^{18}\text{O}_{\text{CO}_3}$  values measured in 2009 from FXS and FL. Values in brackets refer to sample depths below water-tailings interface. VPDB – Vienna Pee Dee Belemnite (C) Plot of  $\delta^{18}\text{O}$  versus  $\delta^2\text{H}$  values measured in 2001 and 2009 from FX, FXS, FL and SL. ....89

Figure 4-9: Photomicrographs of sub-aqueous tailings at a 6 cm depth in plain reflected light showing (A) unaltered grains of pyrite with thin rims of secondary marcasite, near center of image. (B) Enlargement of (A) with arrows showing the narrow rims of secondary marcasite on the primary pyrite grains. Width of view is represented by wv.....92

Figure 4-10: Most probable number (MPN) populations of acidophilic S-oxidizing bacteria (aSOB), neutrophilic S-oxidizing bacteria (nSOB), acid-producing (fermentative) bacteria (APB), iron-reducing bacteria (IRB) and  $\text{SO}_4$ -reducing bacteria (SRB) in the land-based (FX) and submerged (FXS) tailings. The water-tailings interface is located at a depth of 0 cm for FXS and the dashed horizontal line represents the water table at FX.....93

Figure 5-1: Location of Sherridon, Manitoba, Canada, and the study area including locations of the Camp and Woods tailings impoundments, and all piezometer nests. Surface water flow is to the north through Camp Lake. ....100

Figure 5-2: Transect of water chemistry and flow across the Woods tailings from piezometer nests S8 to W3 located in Woods Lake (Figure 5.1). Black dots represent discrete sampling locations. Dashed line with inverted triangle represents location of the water table. The cross-hatched area indicates the extent of the hardpan. Solid lines with arrows are the groundwater flow and the dashed lines are equipotential lines. Groundwater flows through the tailings from piezometer S8 to S16 directly into Woods Lake.....103

Figure 5-3: Plot of  $\delta^{34}\text{S}$  versus  $\delta^{18}\text{O}$  values of dissolved  $\text{SO}_4$  from surface waters, groundwater, vadose and seepage zones and sulfate minerals. The shaded area represents the range of  $\delta^{34}\text{S}$  values (0.2 to 1.2 ‰ VCDT) from the primary pyrite.....104

Figure 5-4: Profile through piezometer nest S16 showing groundwater chemistry with depth. Dashed line with inverted triangle represents location of the water table.....105

Figure 5-5: Saturation indices calculated using MINTEQA2, plotted versus depth at piezometer nest S16. Dashed line with inverted triangle represents location of the water table.....	106
Figure 5-6: Groundwater flow and chemistry across the Camp tailings from S4 to S1 located adjacent to Camp Lake. Black dots represent discrete sampling locations. Dashed line with inverted triangle represents location of the water table. The cross-hatched area indicates the extent of the hardpan. Groundwater flows through the tailings from piezometer S4 to S1 directly into Camp Lake. Revised from Moncur et al. (2005). .....	107
Figure 6-1: Site map of the former Sherritt-Gordon mine showing locations of the tailings impoundments and Woods seepage (WS) and Valley Seep (VS). Letters A-E refers to images in Fig. 6.2. The inset shows the location of Sherridon, Manitoba, Canada. ....	113
Figure 6-2: Photographs of the main areas where secondary sulfate minerals occurred. (A) A large block of melanterite-rich hardpan excavated from the Camp tailings; (B) the Seep Pool; note that in this photo the back wall had collapsed filling in the pool; (C) groundwater seepage from the Woods tailings dam along the Valley Seep with melanterite in the foreground; (D) a channel in the Valley Seep that collects all the groundwater seepage. Note the green colour of the water due to high concentrations of dissolved Fe(II). Photos (E) to (G) show Woods Seep (WS) in various seasons; (E) WS shortly after a rain event; (F) WS after a dry period in August with rozenite and melanterite blanketing the surface; (G) WS in October with melanterite precipitating in ATV tracks. ....	116
Figure 6-3: Profile of the Seep Pool area showing the locations of Core A (0.9 m), Core B (0.6 m), Core C (0.3 m) and the Seep Pool (0 m) and XRD and total carbon analyses of the tailings core samples. Height refers to meters above Seep Pool. ....	120
Figure 6-4: Profile of the Seep Pool area showing selected porewater chemistry from Core A (0.9 m), Core B (0.6 m), Core C (0.3 m) and the Seep Pool (0 m). Height refers to meters above Seep Pool. ....	121
Figure 6-5: (A)-(F) show field images of the secondary mineral phases with the corresponding SEM photomicrograph: (A) alpersite; (B) mixture of alpersite and chalcantite; (C) hexahydrite (Hex); (D) mixture of pickeringite (Pkt) and halotricite (Hal); (E) melanterite; and (F) hardpan melanterite. (G) shows an accumulation of copiapite, (H) a mixture of birnessite and gypsum; and (I) an EDS spectra showing a mixture of melanterite and jurbanite. Minerals (A)-(D) and (I) were collected from the wall of the Seep Pool where Core B was extracted and (G) from where Core A was collected; (E) and (H) are from the Valley Seep; and (F) from the Camp Tailings. ....	122



Figure 6-6: Results from the dissolution experiments showing pH and Eh variations over time. ....	130
Figure 6-7: Temporal plots showing (A) discharge from Camp Weir and precipitation; water chemistry from Sherlett Creek and Camp Weir showing (B) pH; dissolved concentrations of (C) SO <sub>4</sub> ; (D) Fe; (E) Zn; and (F) Al. Revised after Moncur et al. (2014). Vertical red lines represent a period of above normal precipitation. Concentrations in mg L <sup>-1</sup> .....	134
Figure 7-1: Map of the study area showing the location of Sherridon (inset), tailings impoundments, lakes, weirs, streams, communities and mine site. Abbreviations represent: MCWS – Manitoba Conservation Weather Station; L – Lodge; SB – South Bay; CB – Camp Bay; CN – Camp Narrows; and NB – North Bay. ....	140
Figure 7-2: Image on the left shows an aerial view of the abandoned mine site with the Woods Tailings in the foreground, the smaller Camp Tailings and the proximity of the community of Cold Lake in the upper left. Image to the right looking SW across Camp Lake with the Camp Tailings in the upper right of the image; note the green density-driven seepage discharging near shore and extending out into Camp Lake along topographic low points in the lake bed. ....	141
Figure 7-3: Water levels from Sherlett Creek, Camp Lake, Camp Weir, and cumulative precipitation. Water levels were measured relative to a local datum, therefore constants were assigned to the Camp Lake (20 cm) and Camp Weir (40 cm) water level data to allow presentation on one graph. ....	147
Figure 7-4: Spatial variations of water chemistry from Fox Lake (FL) to Camp Weir (CW), measured in 2001 (shaded symbols), 2004 (open symbols) and 2006 (crossed symbols). Saturation indices were calculated using MINTEQA2. Abbreviations represent: TL – Trap Lake; TC – Trap Creek; WL – Woods Lake; CB – Camp Bay; CN – Camp Narrows; and NB – North Bay. ....	148
Figure 7-5: Temporal plots from Woods Wier showing (A) discharge and precipitation; (B) pH; (C) dissolved SO <sub>4</sub> and metal concentrations, and; (D, E and F) saturation indices calculated using MINTEQA2. Vertical lines represent November and May, respectively. Water Samples were not collected between November 2001 to April 2002 and August 2002 to March 2003. Other missing data sets represent freeze-up where no discharge was observed over the weir. ....	150
Figure 7-6: Spatial variations of water chemistry from Sherlett Lake (SL) to Camp Weir (CW), measured in 2001 (shaded symbols), 2004 (open symbols) and 2006 (crossed symbols). Saturation indices were calculated using MINTEQA2. Abbreviations represent: SC – Sherlett Creek; L – Lodge; and SB – South Bay. ....	155

Figure 7-7: Temporal plots showing (A) discharge from Camp Weir and precipitation; (B) dissolved SO <sub>4</sub> and metal concentrations from Sherlett Creek; (C and D) pH and alkalinity as CaCO <sub>3</sub> , from Sherlett Creek and Camp Weir; (E) dissolved SO <sub>4</sub> and metal concentrations from Camp Weir; and (F, G and H) saturation indices calculated using MINTEQA2 from Camp Weir. Vertical lines represent November and May, respectively. Water Samples were not collected between November 2001 to April 2002 and August 2002 to March 2003.....	157
Figure 7-8: Discharge and loadings from Camp Weir, Sherlett Creek and Woods Weir, between April, 2003 and September 2006.....	162
Figure 7-9: Maps showing the distribution of Zn and Cu concentrations in the lake-bottom sediments of Cold Lake and Kississing Lake (modified from Moncur et al., 2007). .....	166
Figure 8-1: Maps show (a) distribution of active energy wells, revised after Lemay (2003) and (b) regional groundwater flow and the location of water wells (symbols are differentiated by geological formation) used in this study. Inset shows the extent of the oil sands and location of the Cold Lake-Beaver River Basin in Alberta, Canada. ....	175
Figure 8-2: Cross-section, A–A0 from Figure 8.1b, showing the distribution of stratigraphic units across the Cold Lake-Beaver River Basin (revised after Parks et al. (2005)). .....	178
Figure 8-3: Depth profile of total As concentrations from five bore-holes in the Cold Lake – Beaver River basin. GC – Grand Centre; MC – Marie Creek; BNV – Bonnyville; and LP –Lea Park Formations. Data from Andriashek (2000). .....	183
Figure 8-4: BSE images of representative As-bearing mineral phases observed in sediment samples showing framboidal pyrite at: (a) Site 1, 6 m depth; (b) Site 2, 11.5 m depth. Secondary Fe oxyhydroxide pseudomorphs after framboidal pyrite at: (c) Site 1, 1 m depth; (d) Site 2, 1 m depth. ....	188
Figure 8-5: Normalized As K-edge XANES spectra for sediment samples collected at: (a) Site 1, 5.5 and 6 m depths (c) Site 2, 1 and 11.5 m depths; and derivatives for samples from (b) Site 1 and (c) Site 2. Vertical line is at 11874.7 eV representing the main absorption peak for As(V) and 11868.5 eV in (d) representing As(-I).....	189
Figure 8-6: Spatial distribution of As in groundwater across the CLBR Basin. Arrows show groundwater flow direction in each formation (modified after Parks et al. (2005)). Gray shading indicates the extent of each formation. There was insufficient data to map groundwater flow in the Marie Creek and Bonnyville Formations. Scale bar and north arrow applicable to all submaps.....	191

Figure 8-7: The relationship between As concentrations in groundwater and various other aqueous parameters (top two rows). Plots in the bottom row show calculated SI values for arsenolite, ferrihydrite and siderite (near equilibrium conditions $SI = -0.4$ to $0.4$ , are represented by the horizontal dashed lines). Symbols are representative of the different formations included in the data set. ....	195
Figure 8-8: Depth profiles of groundwater chemistry from the CLBR basin. The vertical dashed lines represent maximum allowable drinking water limits. ....	198
Figure 8-9: Temporal variation of As concentrations in groundwater from wells in eight aquifers within the CLBR basin from 2000 and 2010. Horizontal dashed line represents the As drinking water standard of $10 \mu\text{g L}^{-1}$ . ....	201
Figure 9-1: Depth profile of water chemistry through glacial till and sand aquifers in NE Alberta, showing a similar weathering trend to oxidized mine tailings. Dashed line represents the water table location. ....	212

# **Chapter 1:**

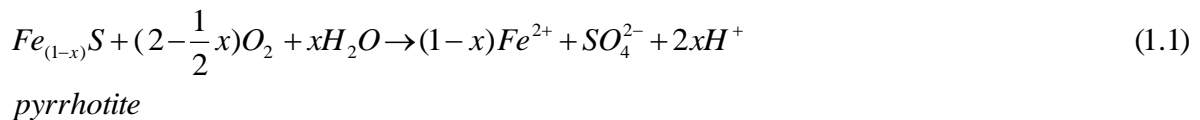
## *Introduction*

## 1.1 Geochemical Processes in Mine Tailings

### 1.1.1 Sulfide Oxidation

When exposed to the atmosphere, sulfide-rich mine wastes oxidize and release acid,  $SO_4$  and metal(oid)s and other toxic elements to the adjacent porewater. Infiltration of rain and snow melt eventually displaces this metal-rich porewater into underlying aquifers and adjacent surface water (Nordstrom and Alpers, 1999; Johnson et al., 2000; Blodau, 2004, Moncur et al., 2006). When groundwater affected by sulfide oxidation discharges to a surface water body, Fe(II) can further oxidize, producing additional acidity, and leading to serious environmental degradation (Dubrovsky et al., 1984). Microbial mediated oxidation of sulfide minerals within mine wastes may continue to release toxic elements to the surrounding environment for decades to millennia (Blowes et al., 1992; Nordstrom and Alpers, 1999; Moncur et al., 2005).

The most common sulfide minerals in mine wastes are pyrite [ $FeS_2$ ] and pyrrhotite [ $Fe_{1-x}S$ ] both of which have little commercial value. The oxidation of pyrrhotite and pyrite by atmospheric oxygen can be represented as:

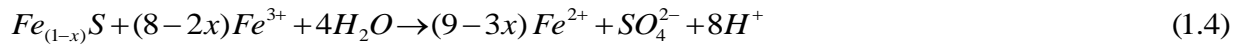


Reactions (1.1) and (1.2) release Fe(II),  $SO_4$  and  $H^+$ . Pyrite and pyrrhotite may contain trace elements that occur as impurities, most commonly arsenic (Savage et al., 2000; Nordstrom, 2002; Paktunc et al., 2006; Paktunc, 2008) and other trace elements such as Pb, Sb, Bi, Cu, Co, Ni, Zn, Au, Ag, Se and Te (Deditius et al., 2011). These trace elements may be liberated through

oxidation. Ferrous iron released in reactions (1.1) and (1.2) can be further oxidized to form Fe(III), which under mildly acidic to near-neutral pH conditions, will precipitate as ferric oxyhydroxide generating additional  $H^+$ , as represented by the reaction:

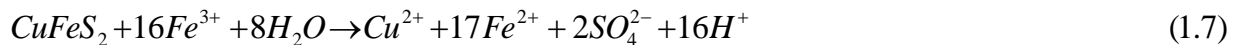
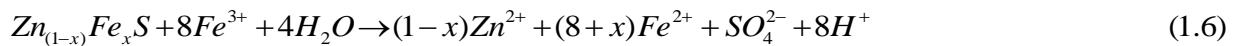


Under very low pH conditions ( $pH < 3$ ), Fe(III) can remain in solution and become the dominant oxidant (Singer and Stumm, 1970):



In this case, Fe(II) becomes the dominant form of Fe in solution. Reactions (1.4) and (1.5) indicate that for every mole of  $Fe_{(1-x)}S$  and  $FeS_2$  oxidized by Fe(III), 8 and 16 moles of  $H^+$  are generated, respectively. The primary mechanism for sulfide oxidation at pH conditions  $< 3$  involves Fe(III) as the main oxidant (Nordstrom, 1982). The presence of Fe(III) in pyrrhotite may increase the rate of Fe(II) oxidation, thereby accelerating the overall oxidation of pyrrhotite (Moncur et al., 2009). Nordstrom (1982) observed that the oxidation of sulfide minerals by aqueous Fe(III) is more rapid than atmospheric  $O_2$  oxidation.

In addition to pyrite and pyrrhotite, other Fe-bearing sulfide minerals can contribute to the generation of low-quality porewater and drainage. For example, the generation of Fe(III) in acidic solutions by the oxidation of pyrite and pyrrhotite can enhance the oxidation of sphalerite [ $Zn_{(1-x)}Fe_xS$ ], chalcopyrite [ $CuFeS_2$ ], and arsenopyrite [ $FeAsS$ ] as represented by (Rimstidt et al., 1994):





The oxidative dissolution of these sulfide minerals in reactions (1.6 – 1.8) release dissolved Zn, Cu, As, Fe(II) and  $H^+$ . In addition to oxidation by  $O_2$  and Fe(III), sulfide oxidation is also catalyzed by sulfur oxidizing bacteria (Gould and Kapoor, 2003). The rate of oxidation can be accelerated by microbial catalysts, however they will not alter the reaction chemistry (Suzuki, 1999). A detailed description of sulfide oxidation reactions in tailings environments is given by Lindsay et al. (2015).

### 1.1.2 Acid Neutralization

Gangue minerals incorporated in the tailings can neutralize  $H^+$  released from bacterial mediated sulfide oxidation. Examples of gangue that can contribute appreciably to acid-neutralizing reactions include carbonates, (oxy)hydroxides and silicate minerals (Jambor et al, 2000; Jambor et al., 2002). Their dissolution typically leads to a distinct sequence of pH plateaus following the successive dissolution of calcite [ $CaCO_3$ ], siderite [ $FeCO_3$ ], Al-oxyhydroxides, Fe(III) oxyhydroxides, and silicates (Dubrovsky et al., 1984; Blowes and Jambor, 1990; Blowes and Ptacek, 1994; Jurjovec et al., 2002; Blowes et al., 2014).

During the early stages of sulfide oxidation, the dissolution of carbonate minerals, such as calcite, results in maintaining the pH of the porewater near neutral (pH 6.5-7.5) through:



In reaction (6) the dissolution of one mole of calcite results in the consumption of one mole of  $H^+$  and release of Ca. Values of pH up to 8.0 have been measured from tailings where dolomite and ankerite dissolution are the principal carbonates in the tailings (Blowes et al., 1998; Lindsay et al., 2009a). The pH of the porewater will remain neutral providing that there is a sufficient mass of primary carbonate minerals remaining in the mine wastes.

During the dissolution of carbonate minerals via sulfide oxidation, secondary siderite [FeCO<sub>3</sub>] can precipitate in the presence of Fe(II) (Al et al., 2000; Jurjovec et al., 2002). The depletion of primary carbonate minerals in the tailings results in an abrupt decline in porewater pH, however the pH may be controlled by the dissolution of secondary siderite:



The dissolution of siderite will buffer the porewater between a pH of 4.8 to 6.3, sequestering one mole of H<sup>+</sup> while releasing Fe(II) and bicarbonate. It should be noted that Fe(II) released in reaction (1.10) can be oxidized upon discharge to oxic environments producing 3 moles of H<sup>+</sup>, therefore siderite dissolution does not provide an overall increase in acid neutralization capacity (Lindsay et al., 2015).

As the dissolution of carbonate minerals occur, the dissolution of the most soluble silicate minerals (*e.g.*, biotite [K(Fe)<sub>3</sub>[AlSi<sub>3</sub>O<sub>10</sub>(OH)<sub>2</sub>]) may release dissolved Al (Murakami et al., 2003) to the porewater which may precipitate as gibbsite [Al(OH)<sub>3</sub>] or another Al oxyhydroxide mineral phase:



When siderite is depleted, the pH declines leading to equilibrium dissolution of gibbsite and a pH plateau of the porewater between 4.0 to 4.3. Upon the dissolution of the Al oxyhydroxide phase, the equilibrium dissolution of Fe(III) oxyhydroxides will be the primary neutralizing mineral maintaining the porewater pH between 2.5 and <3.5 (Blowes et al., 2014):



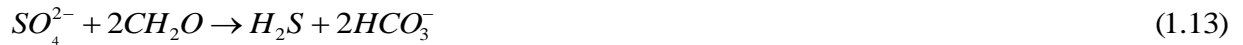
Porewater within zones of oxyhydroxide dissolution is characterized by pH ranging from approximately 2.5 to 4 and high dissolved concentrations of Al and Fe(III) (Lindsay et al., 2015).



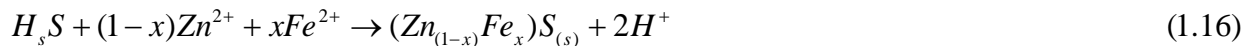
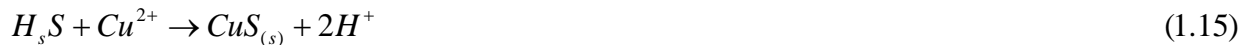
Following the depletion of the carbonate minerals and Al and Fe(III) hydroxides in the tailings, the dissolution of silicate minerals becomes the primary process contributing to acid neutralization (Blowes et al., 2014). The degree of acid neutralization is dependent on the rates of acid production through sulfide oxidation and subsequent silicate dissolution (Lapakko and Antonson, 2012). In addition, the dissolution rate of silicate minerals is slow relative to the rate of groundwater flow, therefore surface water and groundwater at some abandoned mine sites where late stage oxidation is occurring in high-sulfide mine wastes can produce waters with pH <1 and concentrations of dissolved Fe and SO<sub>4</sub> >100 000 mg L<sup>-1</sup> (Nordstrom et al., 2000, Frau, 2000, Moncur et al, 2005).

### 1.1.3 Sulfate Reduction

Dissolved metals and SO<sub>4</sub> released by sulfide oxidation reactions in mine tailings can be attenuated through microbial mediated sulfate reduction (Tuttle et al., 1969; Hulshof et al., 2003, 2006; Blowes et al., 2006; Lindsay et al., 2009b, 2011a). Under anoxic conditions with available nutrients and labile organic carbon (Praharaj and Fortin, 2008; Winch et al., 2009), sulfate reducing bacteria catalyze the oxidation of organic carbon (Berner, 1980):



In reaction (1.13), SO<sub>4</sub> is reduced to H<sub>2</sub>S producing 2 moles of alkalinity. The release of H<sub>2</sub>S in the presence of elevated concentrations of metals such as Fe, Cu and Zn can stimulate the precipitation of secondary sulfide minerals:



Reaction (1.14) to (1.16) result in the production of 2 moles of  $H^+$  and the precipitation of secondary mackinawite  $[FeS]$ , covellite  $[CuS]$ , and sphalerite  $[Zn_{(1-x)}Fe_x]$ . The formation of secondary sulfides are potentially important sinks for other metals within sulfide tailings impoundments, for example, the precipitation of biogenic pyrite has been shown to attenuate Cu, Zn and other metals in tailings and mining-impacted sediments (Ferris et al., 1987).

## 1.2 Research Objectives

The primary objective of this research was to help further our understanding of the long-term effects of sulfide oxidation in sulfide-rich tailings impoundments. This thesis consists of a series of field studies designed to make progress towards this goal, each addressing a knowledge gap surrounding sulfide oxidation with the focus being on long-term effects. The research contributions provided by this thesis will include answering the questions:

- What mineralogical changes will develop during seven decades of sulfide oxidation in high-sulfide tailings?
- How effective is long-term subaqueous storage of tailings in limiting sulfide oxidation over six-decades?
- Can an organic carbon layer act as an effective long-term source of microbial mediated sulfate reduction to inhibit sulfide oxidation?
- What are the seasonal and interannual (measured over 5 years) variations in metal and  $SO_4$  loadings to downstream watersheds?
- Can we apply knowledge learned from sulfide oxidation and metal release in mine tailings to understand weathering processes occurring in other environments such as glacial fluvial sediments?

## 1.3 Thesis Organization

This thesis is organized into nine chapters to address the research objectives identified above, each of which analyzes a component of sulfide oxidation and the subsequent release of dissolved metals and  $SO_4$ . Chapters 1 through 8 were written as individual manuscripts, therefore there is

some repetition of concepts and background information among the different chapters. Organization of the chapters progress from local microscopic detail to watershed scale overviews. Chapter 2 presents a review of sulfide oxidation in the Sherridon tailings and the behavior of pyrite, pyrrhotite, and other important Fe bearing minerals that are frequently overlooked, such as sphalerite, magnetite and to a lesser degree biotite. Chapter 3 describes a method for extracting tailings porewater from the unsaturated zone, although it can be applied to other sediments. This porewater technology described in Chapter 3 is used to extract tailings porewaters during studies in Chapters 4, 5 and 6. Chapter 4 presents mineralogical, geochemical and microbial mechanisms occurring in tailings that have been submerged under a shallow water cover for nearly six decades. Chapter 5 shows naturally established biogeochemical sulfur cycling in a sulfide-rich tailings impoundment that has undergone >50 years of sulfide oxidation. Chapter 6 investigates hyperacidic saline surface seeps discharging from the tailings and examines the association between the secondary salts with the seepage waters from which they formed, and evaluates controls on  $\text{SO}_4$  and metal mobility during dissolution precipitation reactions using field observations and laboratory dissolution experiments. Chapter 7 describes long-term seasonal variations and impacts to a stream receiving groundwater and surface water discharging from the Sherridon tailings, to understand geochemical processes controlling water quality and assess the impact to a down-gradient receiving water body. In Chapter 8, mineralogical and geochemical methods used in the previous chapters were applied to identify the source of elevated arsenic concentrations in groundwater from glaciofluvial sediments. In Chapter 9, conclusions of all chapters are summarized specifying the contributions from this research to improve our current understanding of mine drainage and to make recommendations for future research.

## Chapter 2:

### *Mine drainage from the weathering of sulfide minerals and magnetite*

Reproduced with permission from: Moncur, M.C., Jambor, J.L., Ptacek, C.J., Blowes, D.W., 2009. Mine drainage from the weathering of sulfide minerals and magnetite. *Appl. Geochem.* 24, 2362–2373. Copyright 2015 Elsevier Ltd., License Number 3603470992491. Editorial and formatting changes have been made to accommodate reproduction in this thesis.



## **2.1 Executive Summary**

Pyrite and pyrrhotite are the principal minerals that generate acid drainage in mine wastes. Low-pH conditions derived from Fe-sulfide oxidation result in the mobilization of contaminant metals (such as Zn, Cd, Ni and Cr) and metalloids (such as As) which are of environmental concern. This paper uses data from detailed mineralogical and geochemical studies conducted at two Canadian tailings impoundments to examine the mineralogical changes that pyrite, pyrrhotite, sphalerite and magnetite undergo during and after sulfide oxidation, and the subsequent release and attenuation of associated trace elements. The stability of sphalerite in tailings impoundments generally was greater than that of pyrrhotite, but less than pyrite. Dissolved Ni and Co derived from Fe sulfides, and to a lesser extent, dissolved Zn and Cd from sphalerite, was commonly attenuated by early-formed Fe oxyhydroxides. As oxidation progresses, a recycling occurs due to continued leaching from low-pH pore waters and because the crystallinity of Fe oxyhydroxides gradually increases which decreases their sorptive capacity. Unlike many other elements, such as Cu, Pb and Cr, which form secondary minerals or remain incorporated into mature Fe oxyhydroxides, Zn and Ni become mobile. Magnetite, which is a potential source of Cr, was relatively stable except under extremely low-pH conditions. A conceptual model for the sequence of events that typically occurs in an oxidizing tailings impoundment was developed outlining the progressive oxidation of a unit of mine waste containing a mixed assemblage of pyrrhotite and pyrite.

## **2.2 Introduction**

Pyrite [FeS<sub>2</sub>] is the most abundant metal sulfide associated with the Earth's crust (Rimstidt and Vaughan, 2003; Murphy and Strongin, 2009) and contributes significantly to the world's acid drainage through natural weathering or from anthropogenic activities. However, in many mineral

deposits, pyrrhotite [Fe<sub>1-x</sub>S] is also a significant contributor of acid drainage. The oxidation of Fe-sulfide minerals and the subsequent generation of acidity may lead to destructive impacts to receiving ground and surface waters (Blowes and Jambor, 1990; Nordstrom and Alpers, 1999; Johnson et al., 2000; Levings et al., 2005; Moncur et al., 2006). Low-pH effluent is the primary concern in wastes from sulfide-bearing metalliferous deposits where potentially toxic metals and metalloids are solubilized and become mobile in the low-pH pore waters.

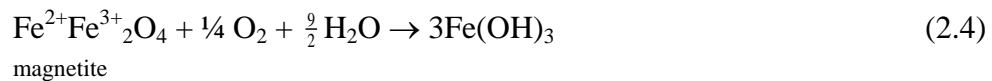
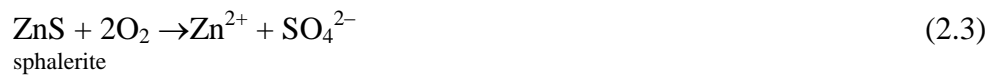
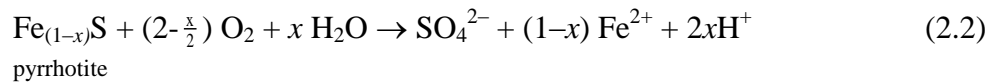
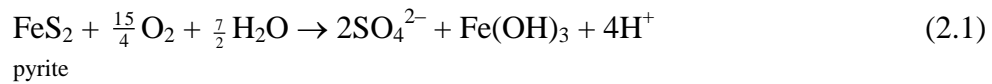
This paper presents a review of the behavior of pyrite, pyrrhotite, sphalerite [ZnS], and magnetite [Fe<sup>2+</sup>Fe<sup>3+</sup><sub>2</sub>O<sub>4</sub>] based on geochemical and mineralogical data from over 30 tailings impoundments studied by the authors worldwide with specific examples from the Sherritt-Gordon tailings in Sherridon, Manitoba, Canada, where detailed mineralogical and geochemical characterization has been conducted (Fig. 2.1). The focus of this paper is primarily on the mineralogical changes that develop during sulfide oxidation, and on the behavior of the principal trace elements that are released by the oxidation of the sulfide minerals.



Figure 2-1: Map of Canada showing the locations of Sherridon, Manitoba, and other mine sites investigated by the authors that contributed to this manuscript.

## 2.3 Oxidation of the Sulfide Minerals

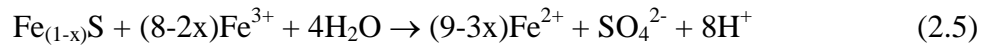
The oxidation of pyrite, pyrrhotite, sphalerite and magnetite may be written as follows:



These simplified equations, where  $\text{Fe}(\text{OH})_3$  is a replacement for ferrihydrite [ $5\text{Fe}_2\text{O}_3 \cdot 9\text{H}_2\text{O}$ ], do not adequately describe the complex reactions that occur in the oxidation process. For example, the oxidation of pyrite involves a series of multiple reactions to achieve the end product in reaction (2.1) (Garrels and Thompson, 1960; Nordstrom and Southam, 1997; Druschel et al., 2004). Reactions involving pyrrhotite in Eq. (2.2) are similarly complex and do not always



express the amount of acid generated by the mineral (Nicholson and Scharer, 1994; Janzen et al., 2000). Crystal-structure vacancies related to the Fe deficiency in pyrrhotite may allow the vacancy-associated Fe<sup>2+</sup> to waiver between Fe<sup>2+</sup> and Fe<sup>3+</sup> valence states, thereby potentially destabilizing defect structures that are more easily broken than those of pyrite and oxidize more rapidly than pyrite (Jambor, 2003; Murphy and Strongin, 2009). The presence of Fe<sup>3+</sup> in pyrrhotite may increase the rate of oxidation of Fe<sup>2+</sup> to Fe<sup>3+</sup> which in turn will accelerate the oxidation of pyrite and pyrrhotite by Fe<sup>3+</sup> through:



The oxidation of pyrite and pyrrhotite in reactions (2.5) and (2.6) is more rapid than oxidation by atmospheric O<sub>2</sub> in reactions (2.1) and (2.2) (Nordstrom, 1982), and with the dissolution of pyrrhotite, Fe<sup>3+</sup> may be released.

Although pyrite and pyrrhotite are the primary concerns with regard to the dissolution of Fe-bearing sulfide minerals, sphalerite, magnetite and other Fe-bearing minerals are commonly overlooked as potential candidates for contributing to mine drainage. Sphalerite is commonly Fe-bearing, magnetite contains both Fe(II) and Fe(III), and other minerals that contain Fe (*e.g.*, siderite [FeCO<sub>3</sub>]; biotite [K(Fe)<sub>3</sub>AlSi<sub>3</sub>O<sub>10</sub>(OH)<sub>2</sub>]), may provide an additional input to acid generation through the oxidation of Fe(II) and hydrolysis of Fe(III) as described by the reactions:



where one mole of acid is consumed in reaction (2.7), but three are released in reaction (2.8).

## 2.4 Trace Element Mineral Associations

Trace elements associated with pyrrhotite are Ni and, to a lesser extent, Co (Gunsinger et al., 2006b). The same association applies to pyrite, however, pyrite may be arsenical (Paktunc, 2008). The association of Au with As-bearing pyrite (Cook and Chryssoulis, 1990; Fleet et al., 1993; Palenik et al., 2004) results in ineffective cyanidation unless the pyrite is artificially oxidized (McCreadie et al., 2000). Following ore processing, the arsenical pyrite and arsenical residues are commonly stored within tailings facilities, and subsequent dissolution and mobilization of the As is an environmental concern.

Sphalerite is the principal source of Zn and Cd in mine tailings. Sphalerite may be present in percentages at sites, where Zn recovery was not included in the concentration process, as was the case in the early years of milling at the former Sherritt–Gordon Mine in Manitoba, Canada (Farley, 1949). Also, Fe typically substitutes partially for Zn in sphalerite (Pring et al., 2008) and can affect the flotation process potentially decreasing recoveries (Walker, 1930; Gigowski et al., 1991; Zieliński et al., 2000). The oxidation and dissolution rates of sphalerite also have been observed to increase with increasing Fe content in the mineral (Perez and Dutrizac, 1991; Weisener, 2002; Blowes et al., 2003). In laboratory studies, both low-Fe and high-Fe sphalerites have been observed to show a rapid initial dissolution rate with release of Zn from the mineral surface, followed by a much slower rate of reaction (Buckley et al., 1989; Giudici et al., 2002; Weisener et al., 2003; Stanton et al., 2008).

The structure of sphalerite can lead to substitution by a wide variety of ions in percentage amounts, such as Cu, Mn, In, Fe and Cd (de Giudici et al., 2002). Up to 13.4 mol% Cd has been incorporated in synthetic sphalerite at 600°C (Maurel, 1978), but in most natural occurrences the Cd content is <1 wt.% (Domènech et al., 2002; Moncur et al., 2005; Koski et al., 2008; Pring et

al., 2008). The larger atomic radius of Cd relative to that of Zn prefers the wurtzite-type structure (hexagonal ZnS) over that of sphalerite (Patrick et al., 1998).

Magnetite in sulfide-bearing mine wastes is of interest because the mineral forms a solid-solution series with chromite [ $\text{Fe}^{2+}\text{Cr}_2\text{O}_4$ ] and other members of the spinel group, and can be Cr-bearing (Kadzialko-Hofmohl et al., 2008). Although the common rock forming minerals such as chlorite, mica, amphibole and pyroxene may contain trace amounts of Cr (Tischendorf et al., 2001; Jambor et al., 2002), in most of the oxidized tailings impoundments investigated by the authors, the presence of dissolved concentrations of Cr have been observed to coincide with the presence of Cr-bearing magnetite in the tailings (*e.g.*, Johnson et al., 2000; Moncur et al., 2005; Gunsinger et al., 2006b).

## **2.5 Mineralogical and Geochemical Behavior**

The relative resistance of various sulfide minerals to oxidation in tailings impoundments has been documented previously (Jambor, 1994; Jambor and Blowes, 1998; Plumlee, 1999; Gunsinger et al., 2006a; Koski et al., 2008). An updated version of the relative resistance, as observed by optical microscopy of field samples from several tailings sites is presented in Table 2.1. The listing serves as a guide to the susceptibility of the sulfide mineral to oxidation where the textures and grain sizes are similar. It is also important to recognize that: (i) a ‘persistence’ effect may be present and (ii) the order applies to primary minerals. An example of the persistence effect would be the opposite behaviors of galena [PbS] and sphalerite during oxidation. Although exceptions are common in carbonate-rich environments, where the replacement of Fe-bearing sphalerite is by Fe oxyhydroxides (Bertorino et al., 1995; Fanfani et al., 1997; Boulet and Larocque, 1998) or Fe oxyhydroxides and sulfur (Jeong and Lee, 2003), in sulfate-rich systems derived from sulfide mine wastes that generate acid drainage, the dissolution

of sphalerite typically occurs without the formation of alteration rims that partly or completely pseudomorph the sphalerite. The solubilization of sphalerite typically occurs by particle-size reduction rather than replacement by secondary minerals. Sphalerite dissolution and the subsequent precipitation of smithsonite [ZnCO<sub>3</sub>] has been suggested as a control for dissolved Zn concentrations (*e.g.*, Nordstrom and Alpers, 1999; Bain et al., 2001; Malmström et al., 2008), however, secondary smithsonite has not been identified in sulfide-containing tailings impoundments. The absence of secondary smithsonite in sulfide tailings could be due to difficulties in identifying minute masses of secondary smithsonite or due to the high solubility of smithsonite in low-pH waters. Alternatively, Zn concentrations could also be controlled by the precipitation of other Zn bearing minerals, such as Fe oxyhydroxides. The behavior of magnetite seems to be similar to that of sphalerite, but because the magnetite content of most non-calcareous sulfide deposits is low, the first appearance of magnetite is typically below the zone of intense oxidation.

Table 2-1: Schematic relative resistance of sulfides and magnetite in oxidized tailings.

pyrrhotite	Fe <sub>1-x</sub> S	low resistance
galena	PbS	↓
sphalerite	(Zn,Fe)S	
bornite	Cu <sub>5</sub> FeS <sub>4</sub>	
pentlandite	(Fe,Ni) <sub>9</sub> S <sub>8</sub>	
arsenopyrite	FeAsS	
marcasite	FeS <sub>2</sub>	
pyrite	FeS <sub>2</sub>	
chalcopyrite	CuFeS <sub>2</sub>	
magnetite	Fe <sub>3</sub> O <sub>4</sub>	
molybdenite	MoS <sub>2</sub>	

The ‘persistence’ effect is demonstrated by galena, when compared to sphalerite, which forms a rim of anglesite [PbSO<sub>4</sub>] during oxidation. Due to the lower solubility of galena, the formation of secondary anglesite rims slows the progress of further replacement but does not

completely retard it. Therefore, although galena and sphalerite are similar in reactivity, galena may persist in a strongly oxidized environment that has removed sphalerite. Similar alteration rim or retardation applies to other minerals, such as pyrrhotite and arsenopyrite, except for enargite [Cu<sub>3</sub>AsS<sub>4</sub>], where the effects are much less pronounced.

The limitation concerning the oxidation of primary minerals is marcasite [FeS<sub>2</sub>]. Laboratory experiments have shown a similar (Wiersma and Rimstidt, 1984) or greater reactivity for marcasite than for pyrite (Rinker et al., 1997; McGuire et al., 2001; Uhlig et al., 2001; Elsetinow et al., 2003) but the reaction rates vary widely. The placement of marcasite in Table 2.1 refers only to primary marcasite of a homogeneous texture and grain size similar to that of the associated pyrite. This condition is stressed because marcasite is commonly a secondary mineral that forms rims and pseudomorphs after pyrrhotite in the early stage of oxidation (Blowes and Jambor, 1990). This type of marcasite is typically heterogeneous on a µm or finer scale, and in this form it seems to be a metastable transitional mineral that very readily alters to goethite (Jambor, 2003).

The stabilities of the various sulfide minerals can be illustrated by the sulfide alteration index (SAI), which is a practical method of mapping the changes observed in the appearance and disappearance of the sulfide minerals through a vertical profile of a tailing impoundment. The SAI was first constructed by Blowes and Jambor (1990) for a series of cores through the Waite Amulet tailings impoundment near Noranda (Quebec, Canada). An example of a SAI for the tailings from the Sherritt–Gordon mine at Sherridon (Manitoba, Canada) is described and illustrated in Table 2.2 and Fig. 2.2. At both sites the ore deposit consisted of volcanogenic massive sulfides and the tailings contain pyrite and pyrrhotite. The Sherridon site is used to illustrate the mineralogical and geochemical changes that typically occur in a sulfide oxidation profile.

Table 2-2: Sulfide alteration index (SAI) of the Sherridon tailings (revised after Blowes and Jambor, 1990; Moncur et al., 2005).

Index	Alteration
10	Almost complete oxidation of sulfides; traces of chalcopyrite ± pyrite
9	Only sparse pyrite and chalcopyrite; no pyrrhotite or sphalerite
8	Pyrite and chalcopyrite common, but chalcopyrite proportion higher than normal possibly because of pyrite dissolution; no pyrrhotite or sphalerite
7	Pyrite and chalcopyrite proportions normal; pyrrhotite absent but sparse sphalerite present
6	Pyrrhotite absent but sphalerite common
5	Pyrrhotite represented by marcasite pseudomorphs
4	First appearance of pyrrhotite, but only as remnant cores
3	Cores of pyrrhotite abundant
2	Well-developed cores of pyrrhotite, with narrower alteration rims; replacement by marcasite decreasing, and pseudomorphs are absent
1	Alteration restricted to narrow rims on pyrrhotite

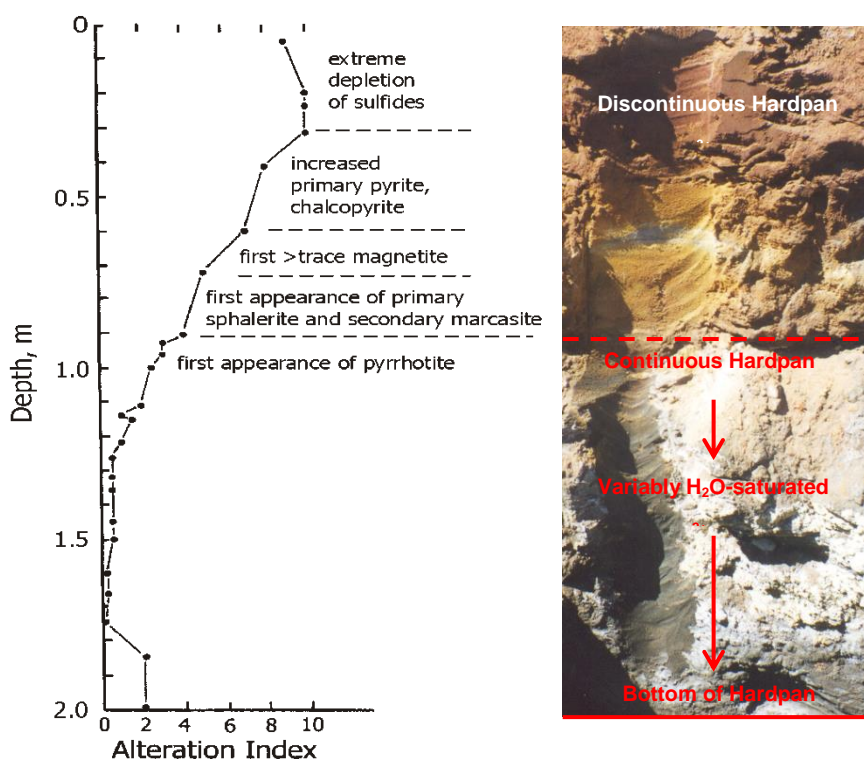


Figure 2-2: Cross-section through the center of the older Sherridon tailings impoundment, showing the mineralogical changes related according to a sulfide alteration index (SAI) (after Moncur et al., 2005), which is a relative scale of alteration intensity. At SAI = 10, the sulfides have been almost completely obliterated (Fig. 2.6); at SAI = 3, remnant cores of pyrrhotite are abundant; at SAI = 1, the alteration occurs only as narrow rims on pyrrhotite (Fig. 2.6e,f). A continuous hardpan extends from 0.9 m to 2 m. The photo to the right of the SAI plot shows fresh exposed tailings on the left adjacent to extensive development of surface blooms of tertiary rozenite (white mineral) that formed shortly after the Fe<sup>2+</sup>-rich continuous hardpan was exposed to O<sub>2</sub> (right half of the photo). Analysis of the rozenite showed that Zn is present in trace amounts. The static water table is at approximately 4 m below ground surface.

The Sherritt–Gordon mine at Sherridon operated from 1931–1932 and from 1937–1951, during which 7.7 Mt of pyritic ore grading 2.45% Cu, 2.97% Zn, 19.9 g tons<sup>-1</sup> Ag and 0.62 g tons<sup>-1</sup> Au were milled, however a Zn concentrate was not produced until 1942 (Farley, 1949). The sulfide assemblage consisted of mainly pyrite and pyrrhotite with lesser amounts of chalcopyrite, sphalerite, and minor amounts of only a few other minerals, including arsenopyrite [FeAsS], cubanite [CuFe<sub>2</sub>S<sub>3</sub>] and local occurrences of galena. The tailings were discharged into

two impoundments, the older of the two is briefly referred to in the following; a more detailed description is in Moncur et al. (2005).

The tailings, with groundwater temperatures ranging from 6.0–15.5°C, have been oxidizing for over 70 years and have formed a continuous ochreous hardpan that is >1 m thick. Near the center of the impoundment the tailings extend to a depth of 7 m and the water table is at a depth of approximately 4 m, however the top of the hardpan located at 0.9 m marks the zone where the tailings are variably water-saturated. The unsaturated zone above the hardpan has a high SAI, is depleted in sulfides and carbonates, and the pore gas-phase O<sub>2</sub> concentrations show a rapid downward decrease to a depth of 0.5 m that reflects O<sub>2</sub> consumption by sulfide oxidation (Fig. 2.3). In contrast to the deeper continuous hardpan that begins at 0.9 m, the unsaturated, near-surface zone contains only thin (1–10 cm) layers of Fe oxyhydroxide precipitates lacking lateral continuity, and which can be categorized as a discontinuous hardpan. The bulk-sample X-ray data indicate that the zone is rich in gypsum [CaSO<sub>4</sub>•2H<sub>2</sub>O], jarosite [(K,Na)(Al,Fe)<sub>3</sub>(SO<sub>4</sub>)<sub>2</sub>(OH)<sub>6</sub>], native sulfur (from the oxidation of pyrrhotite), and goethite [α-FeOOH] (Fig. 2.4). Optical microscopy revealed that phlogopite [K(Mg,Fe)<sub>3</sub>AlSi<sub>3</sub>O<sub>10</sub>(OH)<sub>2</sub>] and plagioclase [(Na,Ca)Al(Si,Al)<sub>3</sub>O<sub>8</sub>] have been substantially altered, and the X-ray data indicate that chlorite and biotite are depleted (Fig. 2.4). Replacement of Al-bearing silicates, mainly albite and biotite, by amorphous silica is common in this near-surface zone of the tailings.



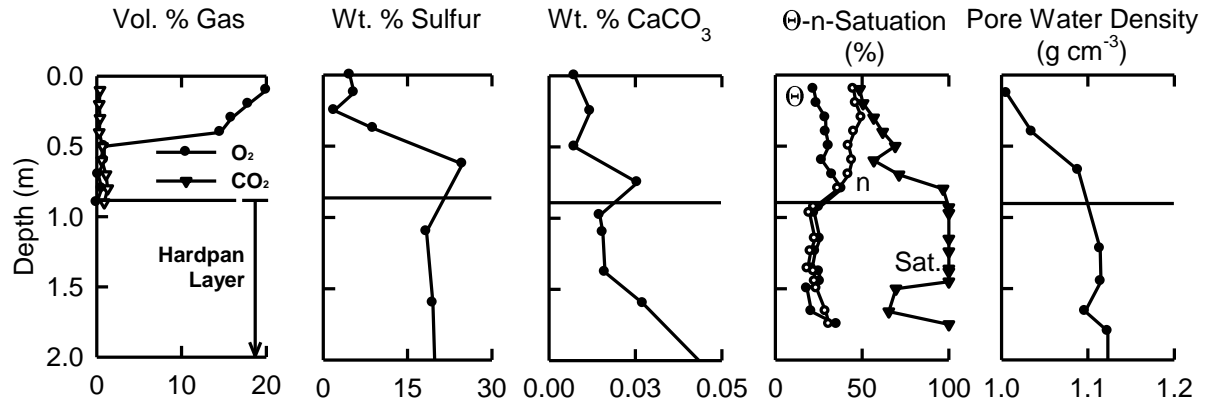


Figure 2-3: Variation in O<sub>2</sub> and CO<sub>2</sub> gas, percent sulfur and calcium carbonate [CaCO<sub>3</sub>], volumetric moisture content [ $\Theta$ : where  $((\text{mass}_{\text{water}}/\text{density}_{\text{water}})/\text{volume}_{\text{total}})$ ], porosity (n), and saturation, and pore water density, in the Sherridon tailings. The solid horizontal line shows the top of the main hardpan. The static water table is at approximately 4 m below ground surface. Data from Moncur et al. (2005).

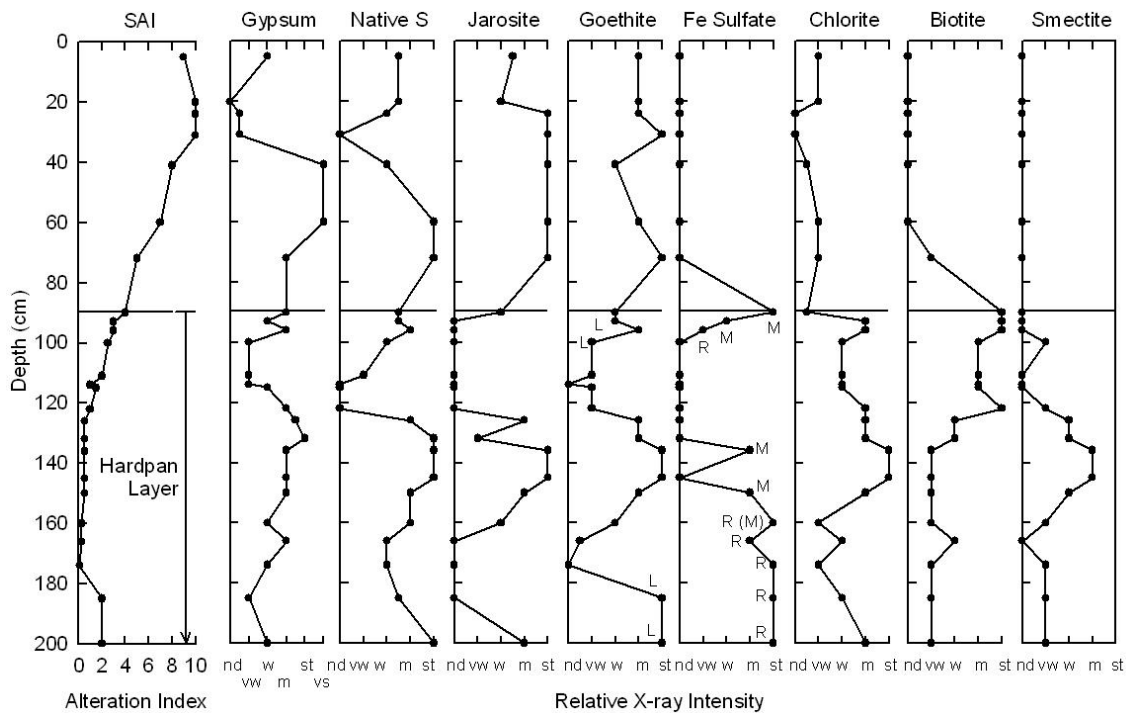


Figure 2-4: Sulfide alteration index (SAI) and bulk-sample X-ray diffractometry data for the Sherridon tailings. Plotted points for the diffractometry data represent the X-ray peak height (generally the highest peak in the diffraction pattern of the mineral) as follows: nd not detected; vw very low (very weak) peak height; w weak; m medium; st strong. In the plot for goethite, L is for lepidocrocite [ $\gamma$ -FeOOH], and in the plot for the Fe sulfates, M is melanterite and R is rozenite. The solid horizontal line shows the top of the main hardpan. The static water table is approximately 4 m below ground surface.

The main continuous hardpan zone extends from 0.9 to 2.0 m. Compared to the ochreous, Fe(III)-rich overlying tailings, the main hardpan is blackish and solidly cemented; although the same secondary minerals that have formed in the near-surface zone are also present. The main hardpan is characterized by an enrichment in Fe(II)-sulfate minerals (melanterite [FeSO<sub>4</sub>•7H<sub>2</sub>O] and rozenite [FeSO<sub>4</sub>•4H<sub>2</sub>O]) (Fig. 2.4), and by decreased porosity (Fig. 2.3) related to the cementation by secondary minerals. Similar enrichments of Fe(II)-sulfate minerals in hardpan layers have been observed in the tailings impoundment at the Heath Steele mine, Newcastle, NB (Blowes et al., 1992), the Renison Bell Tin Mine, Tasmania, Australia (Gilbert et al., 2003) and in mine-waste piles at the Elizabeth Mine, Strafford, VT (Hammarstrom et al., 2005).

## **2.6 Progression of Sulfide Alteration**

The unaltered Sherridon tailings contain up to 60 wt.% of combined pyrite and pyrrhotite, with the relative proportion variable from 1:1 to 1:2, respectively. Mineralogical examination of samples from the oxidized zone above the main hardpan shows that the sulfides have been almost completely replaced in the most oxidized material near the surface (Fig. 2.5). The downward progression is marked by the initial appearance of pyrite, then by the additional appearance of sphalerite and by marcasite pseudomorphs after pyrrhotite (Fig. 2.6a and b). In other tailings impoundments, Fe oxyhydroxide replacement rims on pyrite are common (Jambor, 2003). At the Sherridon tailings, the oxidation of pyrite is marked by depletion of the mineral. Extensively altered pyrrhotite is first observed at the top of the hardpan layer. The thickness of the alteration rims on pyrrhotite gradually decreases toward the bottom of the hardpan (Fig. 2.6c and d). The hardpan is a zone of accumulation of secondary minerals, including small amounts of covellite [CuS]. The accumulation zone forms in advance of the sulfide-oxidation front and appears to be migrating downward. The near-surface, Fe<sup>3+</sup>-rich zone represents a slightly older

and more advanced stage of oxidation which is expected to gradually expand downward approaching the Fe(II)-rich hardpan. Various Fe-sulfate minerals undergo this progression of Fe(II)→Fe(III) transformation as oxidation progresses (Nordstrom and Alpers, 1999; Jambor et al., 2000a).

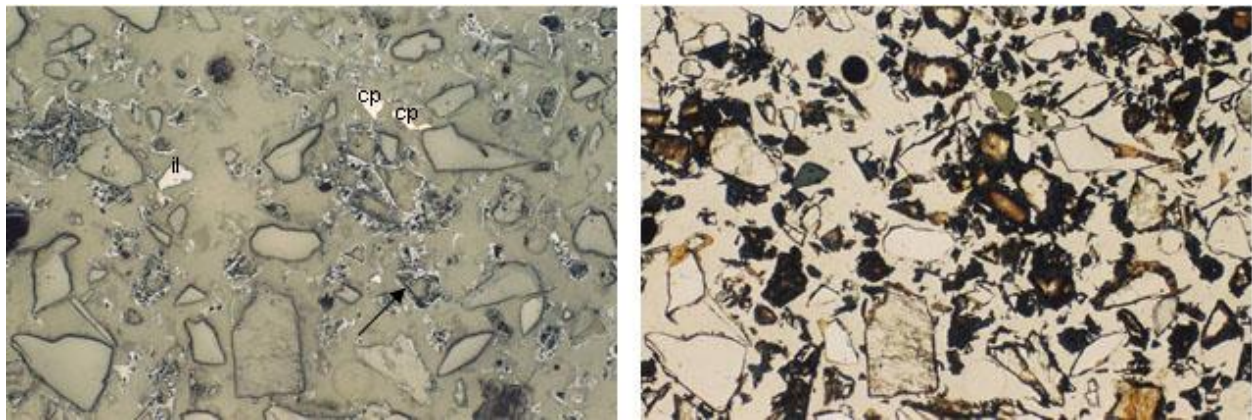


Figure 2-5: Tailings from the Sherridon sulfide-depleted zone at 20 cm depth. Photo to the left, in plain reflected light, width of field 2.6 mm, shows two adjacent residual grains of chalcopyrite (cp), which are the only remaining sulfides (the whitish grain 'il' on the left is ilmenite  $\text{FeTiO}_3$ ). The narrow grey rims, as at the arrow, are Fe oxyhydroxides, mainly goethite. Photo to the right is of the same field, but in plain transmitted light. The black areas are Fe oxyhydroxides that have formed as rims and pseudomorphs after Fe sulfides.

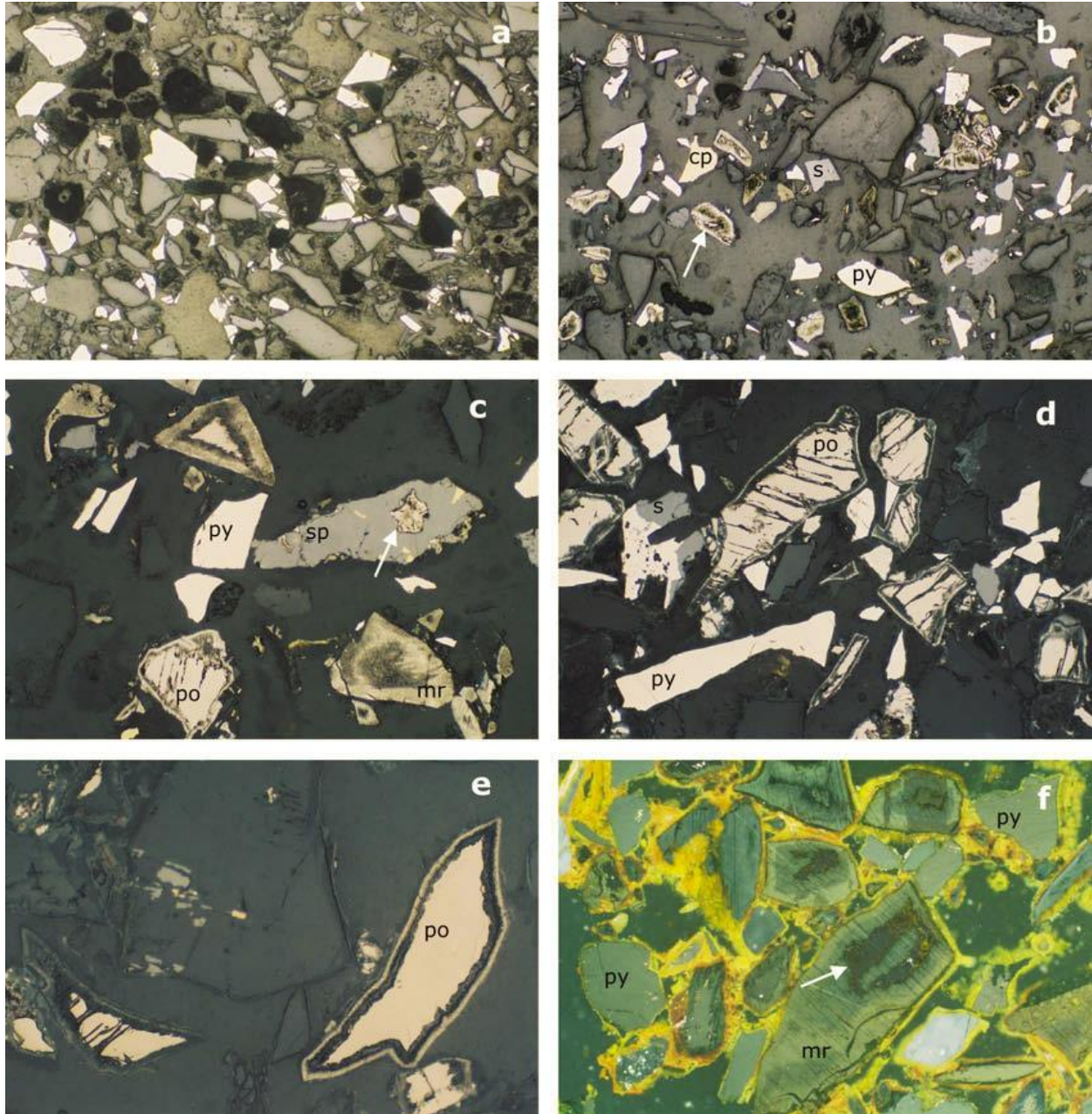


Figure 2-6: Photomicrographs of the Sherridon tailings; (a) to (e) are for plain reflected light. (a) Oxidized zone at 60 cm depth, showing complete replacement of pyrrhotite, now represented by blackish pseudomorphs, but with no alteration evident for the whitish grains of pyrite. Width of field is 2.1 mm. (b) Top of the hardpan contact at 90 cm depth, showing unaltered pyrite (py), sphalerite (s, at center), and a grain of chalcopyrite (cp). The zoned grains, as at the arrow, are pseudomorphs after pyrrhotite, wherein the whitish rims are secondary marcasite. Width of field is 2.1 mm. (c) Hardpan contact at 90 cm depth; width of field is 0.625 mm. The white, homogeneous grains are pyrite (py). Pyrrhotite (po, and at the core of the triangular particle at the top) is variably rimmed by marcasite (mr); in the particle at the bottom right no pyrrhotite remains. The large grey grain is sphalerite (sp) containing, at the arrow, an inclusion of former pyrrhotite, now altered to marcasite. (d) Hardpan zone at 116–126 cm depth, showing white

unaltered pyrite (py) and weak alteration of pyrrhotite (po) along the rim and basal parting, with a narrow outermost rind of marcasite. Width of field is 0.625 mm. (e) Hardpan zone at 112–118 cm depth, showing cores of pyrrhotite with a thin exterior of marcasite; the intermediate zone is a Fe sulfate, as is indicated by its low reflectance and spectrally high S content. Width of field is 0.625 mm. (f) Basal part of the hardpan zone at 185 cm depth; reflected light, internal reflection, polarizers almost crossed, width of field 0.625 mm. The grains showing the basal parting are marcasite after pyrrhotite, a few remnants of which are present, as at the arrow. The cementing material is yellowish in plain light (whitish in the reproduction), and is apparently a mixture of Fe oxyhydroxide and Fe sulfate. The unaltered grains at the top right and lower left are pyrite (py).

## 2.7 Geochemical Variations with Depth

Within the Sherridon tailings, sulfide minerals below the permanent water table do not show signs of alteration (SAI = 0). The unaltered tailings solids average 246 mg g<sup>-1</sup> Fe, 7.7 mg g<sup>-1</sup> Zn, 2.2 mg g<sup>-1</sup> Cu, 0.01 mg g<sup>-1</sup> Ni, 0.08 mg g<sup>-1</sup> Co, 0.005 mg g<sup>-1</sup> Cr and 31 mg g<sup>-1</sup> Al. Pore waters from the unsaturated zone in the Sherridon tailings locally contain up to 280 g L<sup>-1</sup> SO<sub>4</sub>, 129 g L<sup>-1</sup> Fe, 55 g L<sup>-1</sup> Zn, 1.6 g L<sup>-1</sup> Cu, 0.02 g L<sup>-1</sup> Ni, 0.11 g L<sup>-1</sup> Co, 0.003 g L<sup>-1</sup> Cr, 0.01 g L<sup>-1</sup> Cd and 7.2 g L<sup>-1</sup> Al, which in mine-tailings settings are among the highest documented values in the world (Moncur et al., 2005). The pH, Eh and distribution of trace elements in the pore waters above and below the permanent water table are illustrated in Fig. 2.7. High concentrations of Fe, SO<sub>4</sub>, and many of the metals coincide with low-pH conditions above the main hardpan and above the permanent water table.

Dissolved Cu in the pore waters is derived from chalcopyrite. Concentrations are highest at the top of the main hardpan, decreasing rapidly to <1.2 mg L<sup>-1</sup> at depth. The decrease coincides with the appearance of secondary covellite and melanterite (0.25 wt.% Cu), which appear to act as controls on dissolved Cu.

Dissolved concentrations of Zn and Cd, which are attributed to the dissolution of sphalerite, behave differently. Although Zn was commonly detected in electron-microprobe analyses of the secondary Fe oxyhydroxides (0.10–0.33 wt.% Zn in six samples), the high

mobility and only limited attenuation of Zn is reflected by the high concentrations in the pore water beneath the main hardpan, as also observed in other sulfide tailings (Blowes et al., 1991; Gunsinger et al., 2006a). Values for Cd, however, are highest within the hardpan, and the distribution is similar to that of dissolved concentrations of Pb and Cr (Fig. 2.7).

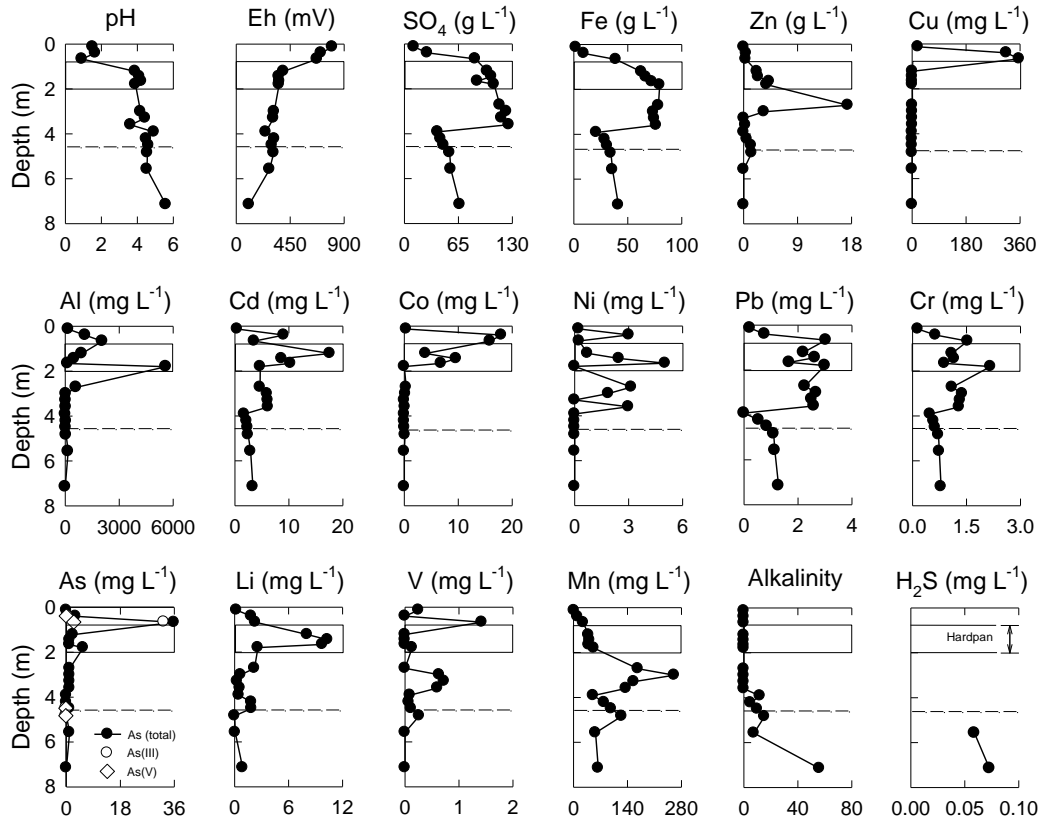


Figure 2-7: Profiles of the water chemistry of the Sherridon tailings from August, 2001. The rectangular enclosure shows the position of the main hardpan, and the dashed horizontal line is the position of the static water table. Data from Moncur et al. (2005).

Dissolved Co and Ni concentrations are derived from the oxidation of pyrite and pyrrhotite. Concentrations of dissolved Co, like those of Cu, are highest near the top of the main hardpan, decrease progressively within the hardpan, and are negligible beneath it. The distribution pattern indicates solid-phase attenuation, most likely by sorption or coprecipitation with the Fe oxyhydroxides. In contrast, dissolved Ni is mobile and largely unattenuated.

Chromium has multiple primary sources as it was detected by electron-microprobe analyses in magnetite, biotite and amphibole. As well, almandine garnet [ $\text{Fe}^{2+}_3\text{Al}_2(\text{SiO}_4)_3$ ] is present in the tailings, and the Cr-dominant species uvarovite [ $\text{Ca}_3\text{Cr}_2(\text{SiO}_4)_3$ ] is known to occur in outcrops near the mine (Froese and Goetz, 1981). Although Cr was detected in the Fe oxyhydroxides within the hardpan, the concentrations of dissolved Cr below the hardpan are not substantially lower than those within it (Fig. 2.7).

Small amounts of arsenopyrite are the principal primary source of As. Speciation of dissolved As concentrations indicates that As(III) is more abundant than As(V), but the distribution of both is similar. The downward profile for  $\text{As}_{\text{total}}$  is like that of Cu, indicating distinct attenuation at the top of the hardpan (Fig. 2.7). Although a discrete secondary As mineral was not identified in the Sherridon tailings, in other impoundments the sorption of As by Fe oxyhydroxides (Figs. 2.8 and 2.9) and substitution in jarosite are of common occurrence (Alpers et al., 1994; Jambor, 1999; Jambor et al., 2000b; Savage et al., 2000; Paktunc and Dutrizac, 2003).

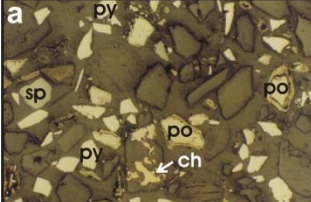
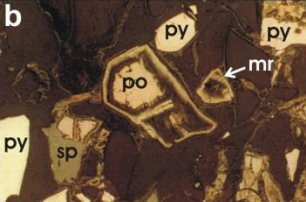
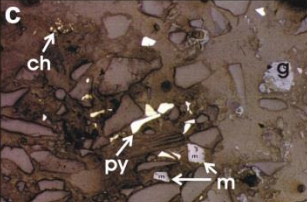
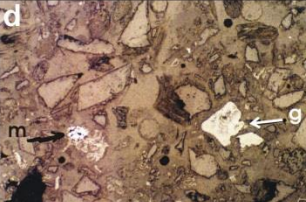
The tailings profile of pore water pH and the downward mobility of dissolved  $\text{SO}_4$  and the metal concentrations is well illustrated in Fig. 2.7. The oxidation front and the hardpan will continue to move downward over time. For example, covellite that currently serves as a solid-phase sink for Cu will be exposed to oxidizing acid conditions, releasing Cu to the pore waters along with the remobilization of other temporarily attenuated species bound in soluble mineral phases. An example of this type of recycling, specifically for As, has been documented by Courtin-Nomade et al. (2003) for As-rich tailings that have oxidized along a sloped topography. Early attenuation of As occurs in association with amorphous and poorly crystalline Fe oxyhydroxides, such as ferrihydrite (Jambor and Dutrizac, 1998), and As decreases in the solid phase through desorption as goethite becomes the dominant Fe oxyhydroxide mineral phase.

## 2.8 Generalized Paragenesis

Table 2.3 shows a simplified sequence of the paragenesis that occurs within a sulfide tailings impoundment. The table shows that most reactions proceed concurrently, however the transformation of some minerals is more distinct than others. For example, laboratory examinations of freshly exposed surfaces of pyrite and other sulfide minerals have shown that the minerals react almost instantaneously to produce secondary mineral phases, however the secondary minerals at that stage are present in minute amounts and are not observable megascopically or by standard optical microscopy (Jambor, 2003). The replacement of pyrrhotite by secondary minerals in Table 2.3 is the first indicator of alteration in the ‘earliest’ stage of the oxidation of a sulfide tailings impoundment. The alteration of pyrrhotite is preceded by the diffusion of S to the grain surface which forms a S-enriched alteration rim where the Fe has departed (Pratt et al., 1994a,b; Mycroft et al., 1995). The released Fe oxidizes to form Fe oxyhydroxide and the S-enriched alteration rim typically forms marcasite (Jambor, 1994). In some cases the boundary between the pyrrhotite core and the marcasite rim is also S-enriched and through microprobe analysis, reveals a mineral that has a composition that is approximately  $\text{Fe}_2\text{S}_3$ , also observed by Murphy and Strongin (2009). This Fe sesquisulfide phase is interpreted by the authors to be less stable than either pyrrhotite or marcasite, and it oxidizes much more rapidly producing an interior zone that is blackish in reflected light as illustrated in Fig. 2.6e. The oxidation of pyrrhotite may also form native sulfur (Fig. 2.4) and Fe(II)-sulfate minerals that may dissolve and crystallize seasonally as  $\text{SO}_4$  containing both Fe(II) and Fe(III), as is the case in the Sherridon tailings.



Table 2-3: Schematic representation of the progressive oxidation of a unit of mine waste containing a mixed assemblage of pyrrhotite (po) and pyrite (py). In the earliest stage of oxidation, the secondary products are formed predominantly from pyrrhotite, with native sulfur and marcasite derived exclusively from pyrrhotite; the Fe oxyhydroxides may include ‘amorphous’ material and ferrihydrite, but typically consist predominantly of very fine-grained goethite with a high sorptive capacity. In the late stage, following consumption of the sulfides, pH will eventually rise and jarosite will therefore also be unstable. Photomicrographs of the Sherridon tailings; (a) earliest to (d) late. (a) Unaltered grains of pyrite, sphalerite (sp) and chalcopyrite (ch) with grains of pyrrhotite rimmed by secondary marcasite (mr). (b) Near the center of the photo is a particle consisting of a core of pyrrhotite, a dark intermediate zone, and a rind of marcasite. The dark zone is vacant, but local areas of Fe sulfate are detectable. Pyrite and sphalerite grains are unaltered. (c) Whitish grains are pyrite and chalcopyrite accompanied by two grains of magnetite (m). On the right is a large particle of goethite. Pyrrhotite is no longer present. (d) On the left is a whitish grain of pitted magnetite and on the right are two particles of compact goethite. Note the absence of sulfide minerals.

EARLIEST	EARLY	MATURING	LATE
<b>oxidation of Fe sulfides</b>	<b>acceleration</b>	<b>slowing</b>	<b>consumed</b>
native sulfur (from po)	_____	_____	_____
marcasite (from po)	_____	_____	_____
Fe oxyhydroxides (fine-grained)	Fe oxyhydroxides (coarsening + recycling)	goethite	goethite
Fe <sup>2+</sup> sulfates (mainly from po)	Fe <sup>2+</sup> sulfates → Fe <sup>2+</sup> - Fe <sup>3+</sup>	Fe <sup>3+</sup> sulfates	_____
_____	jarosite (K <sup>+</sup> mainly from biotite)	jarosite	jarosite
<b>po + py</b>	<b>py &gt; po</b>	<b>py</b>	_____
			

During the ‘early’ oxidation of pyrrhotite, acid and Fe(III) are released which increases the oxidation of other Fe sulfides and decreases the pore water pH. The presence of carbonate minerals within the tailings may neutralize the acidity, however if carbonate minerals are not present or have become consumed, the pH will continue to decrease because most of the common rock-forming minerals have a slow reaction rate and poor neutralizing capacity (Jambor et al., 2000c, 2002; Jurjovec et al., 2002). The silicate minerals observed to be the most

susceptible to low-pH dissolution within oxidized tailings are micas (*e.g.*, biotite) and chlorite (*e.g.*, Sherridon, Fig. 2.4). In low-pH conditions the incongruent early release of K from biotite (Kalinowski and Schweda, 1996; Malmström et al., 1996) provides the main source of K for jarosite precipitation (Jambor, 1994). Although other silicate minerals such as K feldspar, muscovite and illite also release K during weathering, concentrations are much lower due to the low solubility of the minerals (Jambor et al., 2002). As the tailings ‘mature’, pyrrhotite will be depleted long before pyrite is consumed. During the final or ‘late’ stage, the tailings will take on the characteristics of a mature gossan (Blowes et al., 1992) and as the pore water pH rises due to the absence of sulfide minerals, jarosite will become unstable. During this evolution of tailings weathering, there is a continuous recycling of trace elements often resulting in the temporary formation of fine-grained poorly crystalline Fe oxyhydroxides (Figs. 2.8 and 2.9; tailings samples from the Yellowknife Au-producing area, Northwest Territories, Canada) or precipitation of soluble sulfate minerals. However, the high sorptive and retentive capacities of the Fe oxyhydroxides decline as their crystallinity improves by increasing the grain sizes and decreasing their surface areas (Courtin-Nomade et al., 2003), and goethite becomes the dominant Fe oxyhydroxide because it is a stable phase relative to species such as ferrihydrite or lepidocrosite.

The 4 stages of tailings oxidation presented in Table 2.3 are not of equal duration. The initial oxidation ‘earliest’ stage is almost instantaneous upon atmospheric exposure, and the effects become evident in pyrrhotite-rich environments. The progression through the ‘earliest’ and ‘early’ stages may occur within a few months or a few years, whereas, the ‘maturing’ and ‘late’ stages may require many centuries.

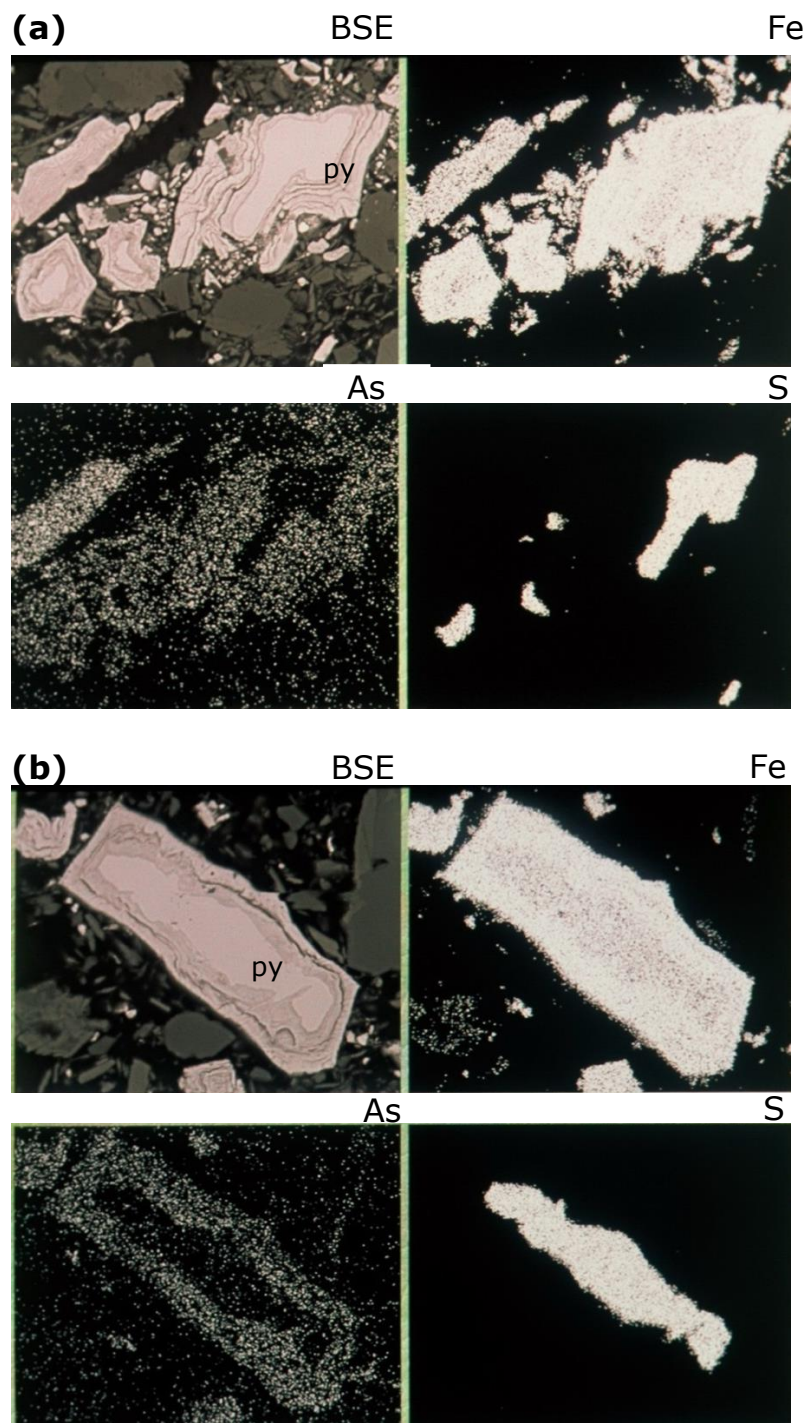


Figure 2-8: Examples of well-developed alteration rims of Fe oxyhydroxide on pyrite in tailings from the Yellowknife gold-producing area, Northwest Territories, Canada. Photos (a) and (b) are backscattered-electron (BSE) images of oxyhydroxide-rimmed pyrite (py) and the corresponding x-ray maps that show the distribution of Fe, As, and S. The residual pyrite is outlined well by the maps for S. Note that As is concentrated in the Fe oxyhydroxides and has been sorbed from the pore waters rather than from the low-As host pyrite. The bar scales are 45  $\mu\text{m}$  for (a) and 35  $\mu\text{m}$  for (b).

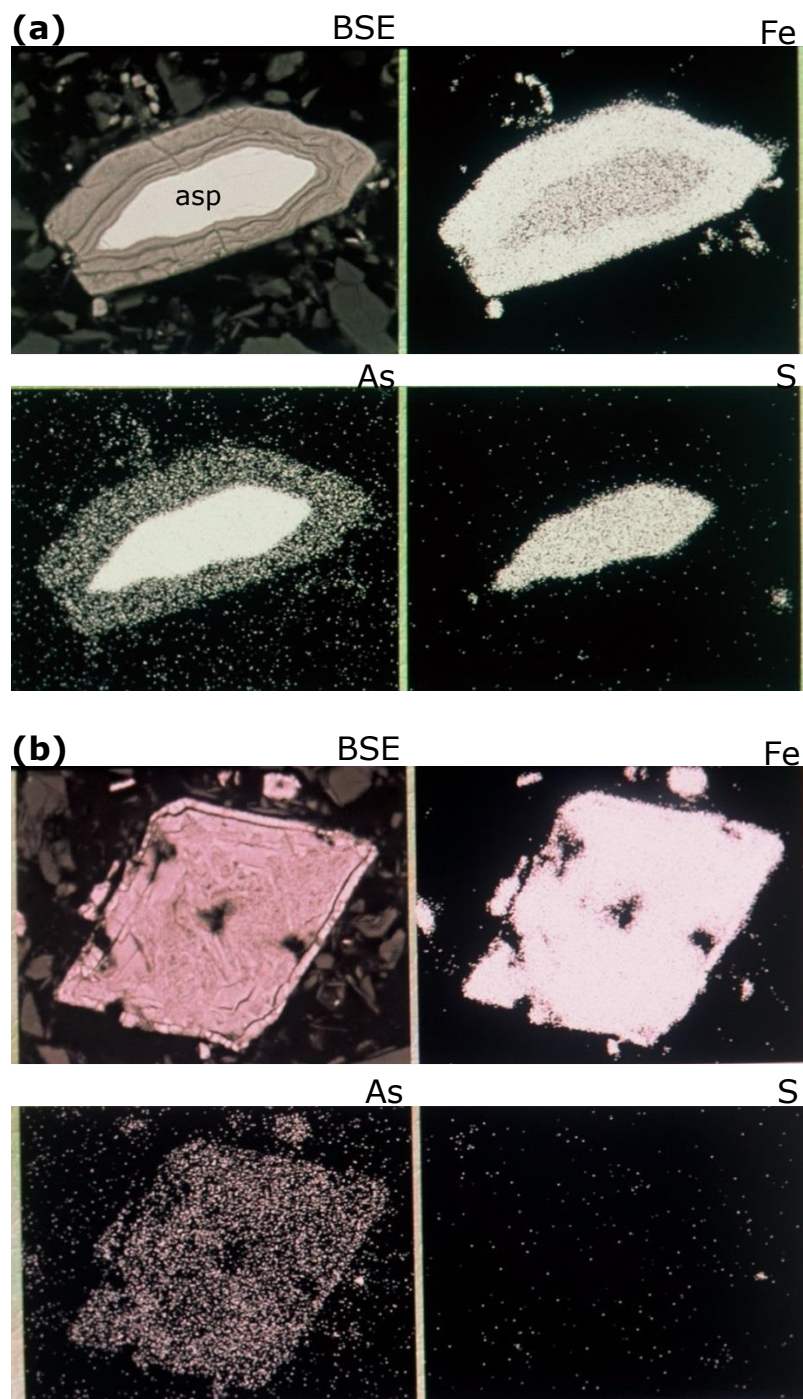


Figure 2-9: (a) BSE image of remnant arsenopyrite (asp) and (b) a pseudomorph of Fe oxyhydroxide after arsenopyrite in tailings from the Yellowknife area, Northwest Territories, Canada. The bar scales are 50  $\mu\text{m}$  and 25  $\mu\text{m}$ , respectively. The black areas within the pseudomorph are voids. The relatively homogeneous distribution of As in the X-ray maps of both (a) and (b) suggests sorption of As rather than the presence of mixtures containing discrete As mineral species. Electron-microprobe analyses of the rims in Figure 2.8 gave up to 5.3 wt%  $\text{As}_2\text{O}_5$ , and analyses of the rims in Figure 2.9 range from 5.6 to 7.1 wt%  $\text{As}_2\text{O}_5$ .

## 2.9 Conclusions

Geochemical and mineralogical data for pore water, primary and secondary minerals from tailings impoundments has provided a great deal of insight into the processes occurring during the oxidation of sulfide-rich tailings. The behavior of pyrite, pyrrhotite, sphalerite and magnetite are particularly important in controlling the release and attenuation of metals. In the earliest stage of oxidation, secondary products are formed predominantly from the alteration of pyrrhotite, with native sulfur, marcasite, Fe sulfate and Fe oxyhydroxides derived from pyrrhotite during which pyrite shows little or no evidence of alteration. Iron oxyhydroxides may include amorphous material and ferrihydrite, but typically consist of very fine-grained goethite with a high sorptive capacity. The relative stability of sphalerite is greater than that of pyrrhotite but is less than that of pyrite. Dissolved Ni and Co derived from solid solution in the Fe sulfides, and to a much lesser extent, dissolved Zn and Cd from sphalerite, commonly co-precipitate or absorb into early formed Fe oxyhydroxides, however, as the tailings system matures, a recycling occurs due to continued leaching from low-pH pore water and because the gradually increased crystallinity of the Fe oxyhydroxides decreases their sorptive capacity. Unlike many other elements, such as Cu, Pb, and Cr, which either form secondary minerals or are readily incorporated as solid solutions, Zn and Ni remain mobile. During the late stage of oxidation within a tailings impoundment following consumption of the sulfide minerals, the pore water pH will eventually rise and jarosite will therefore be unstable leaving goethite as the dominate secondary mineral.

## Chapter 3:

### *Pore-water extraction from the unsaturated and saturated zones*

Reproduced with permission from: Moncur, M.C., Blowes, D.W., Ptacek, C.J., 2013. Pore-water extraction from the unsaturated and saturated zones. *Can. J. Earth Sci.* 50(10), 1051-1058. © 2008 Canadian Science Publishing, NRC Research Press, License Number 3603480239559. Editorial and formatting changes have been made to accommodate reproduction in this thesis.

### **3.1 Executive Summary**

A simple, inexpensive method for extracting pore water from unsaturated soils, which uses a combination of immiscible fluid displacement, suction, and mechanical compression, is described. This method uses a squeezing chamber to contain the unsaturated sediments in aluminum core tubing to prevent exposure of the sediments and porewater to atmospheric O<sub>2</sub> and subsequent oxidation reactions. Geochemical artifacts resulting from high-compression squeezing are prevented by maintaining the pressure applied during the squeezing at a minimum. Comparison of squeezed profiles with field measured profiles of pH, Eh (oxidation–reduction potential), alkalinity, and metal speciation indicates good agreement between these parameters using this method. Depending on the water content of the sediments, a range of water volumes (several millilitres to excess of 100 mL) can be extracted from a single core section 7.6 cm in diameter by 20 cm long. Porewater was produced immediately from sediments at near-saturated conditions, whereas several hours were required to obtain pore water from sediment with low moisture contents. Porewater was extracted from unsaturated sediments with as little as 6% volumetric moisture content. The squeezing technique provided water samples from both unsaturated and saturated sediments ranging from silt- to sand-sized particles. The method was applied successfully to collect porewaters from unsaturated sediments in neutral and acidic mine tailings; processed sands from oil sand operations, septic beds, agriculturally impacted sediments; and saturated soils from peat bogs, from wetlands, and at groundwater–surface interfaces.

### **3.2 Introduction**

Understanding geochemical processes in the unsaturated zone (vadose zone) is a fundamental aspect of hydrogeology studies. The vadose zone is an important component of many aspects of

hydrogeology, including oxidation–reduction reactions, infiltration, evaporation, soil moisture, and groundwater recharge (Nielsen et al. 1986). Contaminated pore water from the vadose zone is also thought to be a major route of contamination to terrestrial invertebrates (Lock et al. 2002) and indirectly to benthic and pelagic organisms (Knezovich et al. 1987; Eggleton and Thomas 2004).

The disposal of industrial solid and liquid waste such as metals and  $\text{SO}_4$  from mine wastes (Blowes et al. 1991; Moncur et al. 2005; Abolfazlzadehdoshanbehbazari et al. 2013), application of agricultural products such as nitrogen (Robertson et al. 1996) and pesticides (Close et al. 2003), and discharge of pharmaceutical and phosphate from septic systems (Ptacek 1998; Carrara et al. 2008) in or on unsaturated soils can eventually lead to aquifer contamination. Therefore, it is of great importance to have a method of extracting representative porewater samples from the vadose zone to enhance the understanding of transport processes, dissolved ion concentrations, redox conditions, and possible degradation and transformation of pollutants.

Methods most commonly used to extract porewater from the vadose zone include centrifuging (Edmunds and Bath 1976; Kinniburgh and Trafford 1996; Gooddy et al. 2002), suction lysimetry (Peters and Healy 1988; Rollo and Jamieson 2006; Lindsay et al. 2009; Curley et al. 2011; Smith et al. 2012), and high-pressure squeezing (Heinrichs et al. 1996). A detailed review of vadose zone pore-water sampling techniques is presented by Kelln et al. (2001) and Fares et al. (2009). The primary concern during porewater extraction is the introduction of oxygen, which has been shown to significantly alter redox conditions and sample speciation (Bufflap and Allen 1995). Centrifuging requires handling of the sediment sample during placement into tubes or bottles, and the primary method to minimize exposure to oxygen is to process samples in an anoxic chamber to prevent oxidation artifacts. The low volumes of water typically present in unsaturated sediment samples often require multiple samples to be



centrifuged to obtain sufficient volumes of water for some geochemical analyses, thus requiring extensive operating and processing time (Koehler et al. 2000). Porous ceramic cups are typically used to extract unsaturated zone pore water by suction lysimetry. Installation of lysimeters requires a pre-bored hole, emplacement of the lysimeter, and backfilling to surface. The porous cup is backfilled with silica flour, and the annulus of the lysimeter is backfilled with the parent material or grout to surface. A vacuum is applied inside the porous cup to pull water from the sediment pore space into a collection vessel. Three purge volumes of water must be extracted and expelled before samples are collected, to ensure possible oxidation artifacts introduced during the lysimeter emplacement are purged (Lindsay et al. 2009). Studies have shown that anion, cation, and pH measurements using porous cups are representative of the natural pore water for non-dilute solutions (Winger et al. 1998), but trace metal concentrations can be significantly altered at low concentrations (Peters and Healy 1988). Under low-pH conditions, as found in many high-sulfide mine wastes, dissolution of the silica flour and possibly the ceramic cup could lead to buffering of the pore waters and a decrease in the concentrations of dissolved metals and  $\text{SO}_4$ .

High-pressure pore-water squeezing methods are used to compress the pore space of the sediment to displace the pore water. A disadvantage of this method is that high-pressure conditions can modify the solubility of minerals and alter porewater chemical compositions (Manheim 1966; Sayles et al. 1973; Toole et al. 1984; Fares et al. 2009). This method also requires disturbance of the sediments during placement into the compression chamber, which may allow oxygen to enter the samples. To minimize the effects of oxidation reactions on water chemistry, the sediment samples may require preparation in an anoxic environment.

Squeezing techniques have been used extensively for the collection of pore water from bottom sediments in oceans (*e.g.*, de Lange et al. 1992; Huerta-Diaz et al. 2007), estuaries (*e.g.*,

Carr and Chapman 1995), lakes (*e.g.*, Patterson et al. 1978; Azcue and Rosa 1996), and saturated clay (*e.g.*, Kelln et al. 2001; Birks et al. 2007). The purpose of this study is to describe an innovative method for extracting porewater from unsaturated soils using a squeezing technique that utilizes a combination of immiscible fluid displacement, suction, and minimal mechanical compression. This method limits the exposure of pore water to oxygen during extraction procedures, therefore preserving redox conditions. The squeezing apparatus is inexpensive, is simple to construct and operate, and can produce porewater samples quickly with minimal labour. This squeezing method was adapted from a lake sediment porewater squeezing method described by Patterson et al. (1978) and later modified for porewater extraction for unsaturated sediments by Smyth (1981); Blowes et al. (1991), and Moncur et al. (2005). Although this method has been used extensively by the authors, previous publications have not described the method in detail. As part of this study, this modified technique was also applied to the saturated zone to provide direct comparisons with traditional lake-sediment dialysis arrays (peepers).

### **3.3 Methods and Materials**

#### **3.3.1 Core Collection**

Sediment core collection for this pore-water squeezing technique uses the piston core-barrel method described by Starr and Ingleton (1992). This piston-coring method allows for the collection of sediment samples ranging from clay to sand-sized particles and does not use drilling fluids, in order to prevent sample contamination. The core is collected in thin-walled (0.127 cm; 0.05-in.) aluminum irrigation tubes of 5.1 cm (2-in.) or 7.6 cm (3-in.) diameter, which are readily available and inexpensive. A possible limitation of using Al tubing is that under acidic conditions, Al could be mobilized from the tubing to the porewater. To overcome possible Al

contamination of the pore water, stainless steel can be used as an alternative core casing. Drilling apparatus, described in detail by Starr and Ingleton (1992), is driven into the sediments at 1.52 m (5-ft) intervals using a gas- or electric-powered jackhammer. (Pneumatically powered jackhammers had been used in past applications but were found to be destructive with respect to the drilling equipment). Continuous undisturbed core using this method with a jackhammer have been collected to depths of 14 m (Moncur et al. 2005) and to 18m (Starr and Ingleton 1992). The core sample is removed from the ground by use of a chain hoist supported by scaffolding or a tripod. Upon recovery, ends of the core interval are cut to length with a tubing cutter to remove any headspace, then sealed with low-density polyethylene caps and wrapped with duct or electrical tape. Core is immediately transported to the field laboratory for porewater extraction or frozen for future analysis.

A limitation of this coring method is compaction of the core sample. Compaction was mainly observed in core collected from the unsaturated zone. Driving the core barrel through sediments can create frictional stress between the Al tubing and sediments, which may modify the porosity and structure of the sample. The samples are compressed in response to even application along the length of the core. To compensate for this compaction, a correction factor must be applied to the core section. For example, when a 0.80 m core is recovered from a 1 m sediment profile and the residual bore hole is open to a 1 m depth, 0.20 m of compaction occurred during core collection. If the core is sectioned into 0.20 m intervals for pore-water squeezing, then a 0.05 m correction factor is added to each interval to account for compaction.

The drilling and accessory equipment can easily fit into a pick-up truck or van, making it ideal and inexpensive for collecting samples from remote locations. In addition to using trucks, the authors have transported the piston-coring equipment to remote locations using helicopters, float planes, small aircraft, small boats with outboard motors, barges, all-terrain vehicles, and a

golf cart. Once at the site, the equipment can easily be carried several kilometres by hand to the desired locations.

Alternatively, for shallow core collection <3 m, a length of Al core tubing fitted with a core collector may be driven into soft sediments without using the piston-coring method.

### **3.3.2 Squeezer Construction**

The squeezer consists of three main parts: a piston, a filter disk, and a collection base. A scale drawing is shown in Fig. 3.1, and a detailed list of components is provided in Table 3.1.

Squeezer parts are constructed from solid nylon rod, which is relatively soft for rapid machining yet durable over numerous extractions. Nylon is also used because it is easy to clean and resistant to dilute acids (10% HCl or HNO<sub>3</sub>). Squeezer pieces are machined to a diameter that can be inserted into the Al core tubing and fitted with sealing O-rings to prevent any gas or water exchange between sediments contained within the core and the outside environment. It should be noted that squeezer parts are not limited to dimensions provided in this manuscript and can be constructed to fit any core tubing.

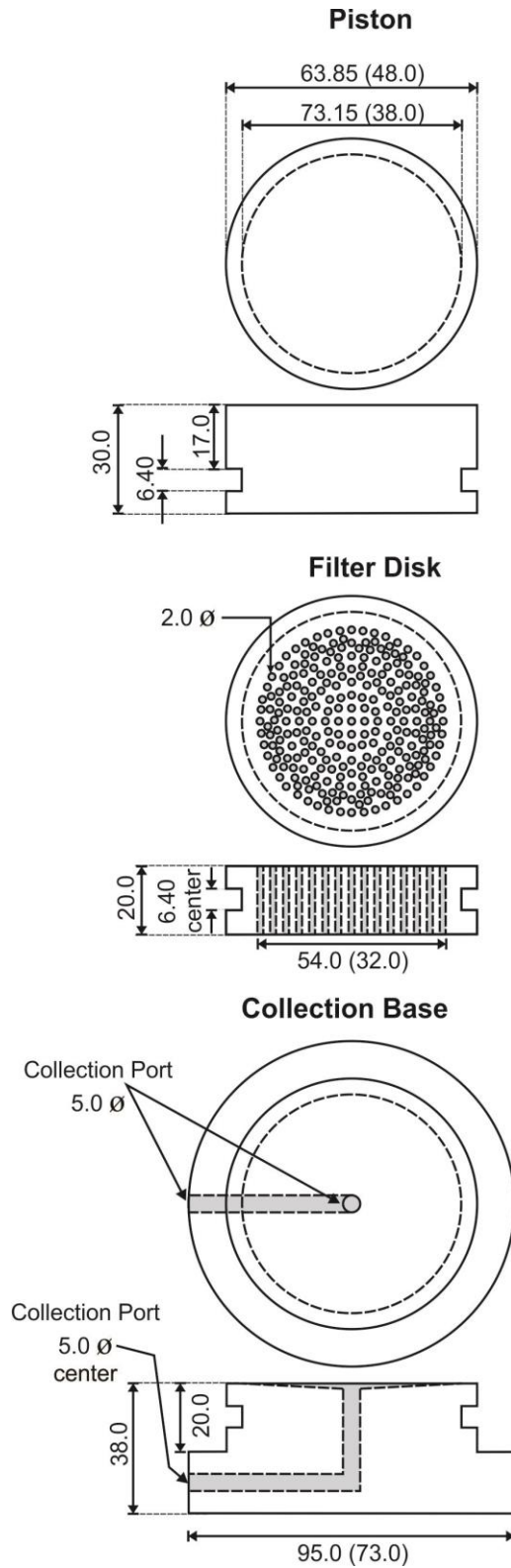


Figure 3-1: Schematic diagram showing dimensions of squeezer components. All values are in millimetres, and dimensions are for both 5.1 cm (2-in.) and 7.6 cm (3-in.) squeezer parts. Values in brackets correspond to 5.1 cm squeezer components.

Table 3-1: Materials and dimensions for 5.1 cm (2-in.) and 7.6 cm (3-in.) squeezer components.

Al Core Tubing	<u>2-inch Diameter</u>		<u>3-inch Diameter</u>		<u>Material</u>
	(mm)	(inches)	(mm)	(inches)	
<i><u>Piston</u></i>					Nylon
Height	30	1.18	30	1.18	
O.D.	48	1.89	73.15	2.88	
<i><u>Filter Disk</u></i>					Nylon
Height	20	0.79	20	0.79	
O.D.	48	1.89	73.15	2.88	
Perforation Diameter	32	1.26	54	2.13	
Perforations	2 $\phi$	0.08 $\phi$	2 $\phi$	0.08 $\phi$	
<i><u>Collection Base</u></i>					Nylon
Base Height I.D.	20	0.79	20	0.79	
Base Height O.D.	18	0.71	18	0.71	
Base I.D.	48	1.89	73.15	2.88	
Base O.D.	73	2.87	95	3.74	
Collection Port Diameter	5 $\phi$	0.2	5 $\phi$	0.2	
O-Ring Groove Height	6.4	0.25	6.4	0.25	
O-Ring Groove O.D.	38	1.50	63.85	2.51	
O-Ring Filter	Whatman Grades 1 and 40; 42.5 mm $\phi$		Whatman Grades 1 and 40; 70 mm $\phi$		Nitrile
					Paper

Squeezer frames are constructed from three 25.4 cm  $\times$  25.4 cm (10-in.  $\times$  10-in.) square aluminum plates with a thickness of 2.54 cm (1-in.) (Fig. 3.2). Holes are drilled in each plate corner 3.18 cm (1¼-in.) from the corner edge. The bottom plate requires 16.67 mm (21/32-in.) tapped holes; the centre and top plate requires 19.45 mm (49/64-in.) clearance holes.

Alternatively the middle plate can be fitted with brass or copper bushings to prevent wear on the plate. Four 1.91 cm (¾-in.) diameter factory threaded (10 threads per inch) steel rods in 91.44 cm (3-ft) lengths are used to support the three plates. The four rods are screwed into the base plate and secured with washers and nuts. A hydraulic bottle jack (1–4 t capacity) is placed on the bottom plate. Holes in the middle plate are aligned and glided along the four threaded rods until

supported on the hydraulic jack. The middle plate is “floating” and used as the compression plate. Four nuts and washers are placed from the top along each threaded rod to match the height of the core to be squeezed. The upper plate is placed on the four washers and nuts, levelled horizontally, and then fastened with washers and nuts. The upper plate is stationary and used as the pressure plate.

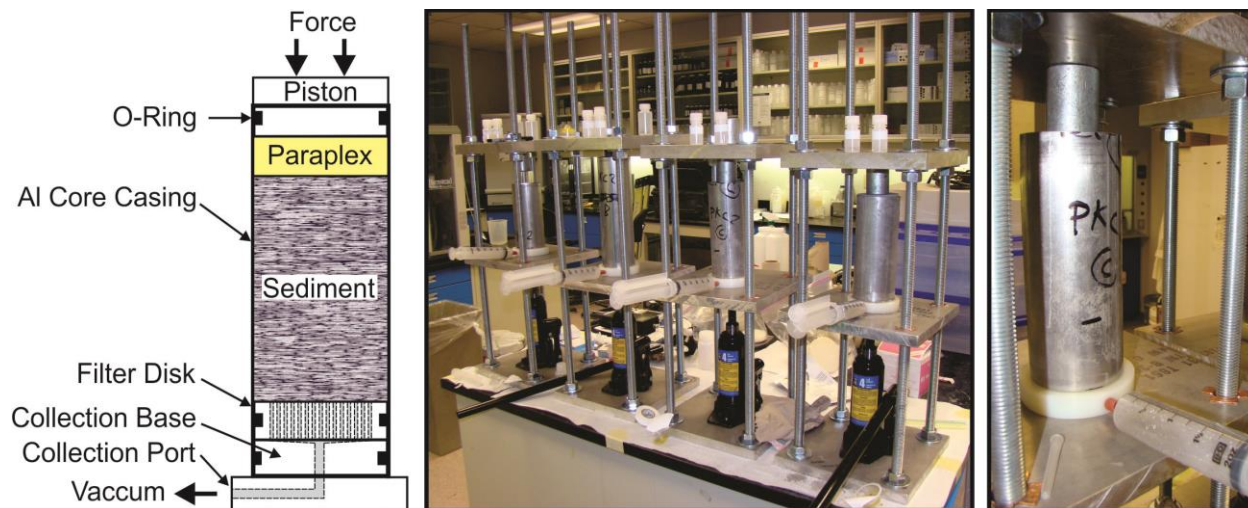


Figure 3-2: Drawing to the left shows a cross section of a core fitted with squeezer components. Photos show setup of the pore-water squeezing method.

### 3.3.3 Squeezing Procedure

Collected cores are typically cut into lengths of 15–25 cm. The Al core tubing containing the sediment samples is used as the squeezing chamber to minimize any disturbance or contact with oxygen that would otherwise occur if samples were extruded following other squeezing methods. It is important to section the Al core tubing with a proper pipe cutter to make an even cut to properly fit squeezer pieces. Sections of sediment 4 cm in length (3.5 cm for 5.1 cm (2 in.) core) is removed from the bottom end of the core section to accommodate the squeezer pieces. Burs along the cut surface of the core tube should be removed with a deburring tool, and any sediment on inside of the exposed core tubing must be removed. A Whatman no. 1 filter paper is

placed on the exposed sediments, followed by the insertion of the filter disk, which is covered by a second Whatman no. 40 filter paper. The bottom of the core tubing is then fitted with the protrusion end of the collection base. The core is inverted to the upright position, and a rubber septa (5 mm diameter by 11 mm length) is inserted into the collection port of the collection plate. Approximately 6 cm of sediment is removed from the top of the core section, followed by deburring and removal of excess sediment. About 4.5 cm of the void area is replaced with Paraplex G62 (Rohm and Haas Inc.), an immiscible hydrophobic fluid, used in this method to displace pore water downward through the sediments. The final step is to insert the piston in the top of the core. If sediments are fine and saturated, Paraplex may not be necessary, in which case only the upper 1.5–2 cm of the sediments require removal to fit the piston.

After the assembled core and squeezers are positioned in the squeezer frames, the hydraulic jack is pressurized until the core is stabilized and cannot be shifted. At this time a 60 mL syringe affixed with a needle is used to pierce the septum in the collection base. Air from the core is expelled into the syringe until a maximum vacuum of 165 kPa (24 psi) is achieved. A stopper is placed between the syringe plunger and syringe barrel to create a constant vacuum. Little pressure is required for displacement; therefore, pressure is gently applied in small increments, typically one to two pumps of the 4 t jack. Both pressure and syringe vacuum must be applied to the core section at all times. If after 5–10 min no water has arrived to the syringe, vacuum in the syringe should be reset and pressure increased by pumping the jack once or twice. Once pore water is discharging into the syringe, the pressure is increased only when water no longer flows; however, it is important to maintain a steady pressure and vacuum. Rapidly applying pressure will force Paraplex through larger pore spaces or can create channelling between the sample and core tubing, leading to premature breakthrough of the Paraplex before sufficient water has collected in the syringe. Applying too much pressure can also force



sediments to break through the paper filters and into the syringe portal, making it difficult to obtain water. Using minimum pressure will also provide maximum water yields and prevent the alteration of porewater chemistry that can occur during high-pressure squeezing (Manheim 1966; Sayles et al. 1973; Toole et al. 1984).

The first few millilitres of water collected is typically discarded, as this water has likely been oxidized during placement of the squeezer parts. As water is collected in the syringe, it should be expelled frequently into sample bottles before Paraplex breaks through into the syringe. Once the breakthrough of Paraplex has occurred, little water is produced. Collected waters are filtered through 0.45 m disposable button filters to minimize the water volume used in the filtering process. Each syringe containing sample is split into the desired aliquot. It is important to split samples during collection rather than fill each bottle sequentially because water collected should be an average over the entire squeezed interval to obtain reproducible values. When determining pH, Eh, and alkalinity, measurements should be collected at least two to three times over the duration of squeezing. Examples of parameters collected using this squeezing method include pH; alkalinity; cations; anions (*e.g.*, Blowes et al. 1991; Moncur et al. 2005; Gunsinger et al. 2006); Fe speciation (Johnson et al. 2000); As speciation (McCreadie et al. 2000; Moncur et al. 2005); dissolved organic carbon (Dold et al. 2005); stable isotopes  $\delta^{18}\text{O}$ ,  $\delta^2\text{H}$ ,  $\delta^{34}\text{S}\text{-SO}_4$ ,  $\delta^{18}\text{O}\text{-SO}_4$  (Moncur et al. 2009, 2012; Moncur and Smith 2012); and nutrients (Zanini et al. 1998).

The length of time required to extract water depends on saturation of the soil and sediment type. A saturated silty material can produce water immediately, whereas the same material with low moisture content may require several hours before any water is expelled from the core. Depending on the water content, several millilitres to volumes in excess of 100 mL can

be extracted from a single core section. The authors have successfully extracted water from core with volumetric moisture content as low as 6%.

### **3.3.4 Case Study Field Methods**

Core was collected from two locations (site 1 and site 2) at an abandoned mine site in Sherridon, Manitoba, Canada, approximately 700 km northwest of Winnipeg, Manitoba. At site 1, continuous core of the tailings was collected from surface to a depth of 4.3 m at the water table. Core was collected in thin-walled aluminum tubes of 7.6 cm (3-in.) diameter. At a depth of 1 m, hardpan was encountered, and a backhoe was required to excavate a pit through to the underlying unconsolidated tailings. At the bottom of the excavated pit, approximately 2m from surface, tailings samples were collected using the piston core-barrel method described by Starr and Ingleton (1992). Samples of hardpan were collected from the walls of the excavated pit by a horizontal coring method using 7.6 cm diameter aluminum tubing. Cores were cut into 25 cm lengths, then immediately squeezed using Paraplex to displace porewater to measure porewater composition. At each site, an additional 5.1 cm (2-in.) diameter core was collected to a depth of 1.5 m for solid analyses. Physical properties of the tailings were determined through measurements of gravimetric and volumetric moisture content, bulk density, and particle density. The particle density was measured with an air comparison pycnometer, Beckman model 930. The porosity was calculated from the measured bulk density and particle density. In the bottom of the excavated pit, two ¾-in.-diameter stainless steel drive-point piezometers were installed to depths of 5.8 and 6.5 m using a gasoline-powered jackhammer.

At site 2, porewater was collected from bottom sediments of an acidic lake in two areas using both the squeezing method without Paraplex and dialysis arrays (peepers) following the design and method of Hesslein (1976). Peepers consist of a Plexiglas plate (120 cm × 20 cm × 2.3

cm) with two vertical rows of horizontal cells 6.5 cm long by 0.9 cm wide and 1 cm in depth. From centre to centre the cells are spaced at 1.25 cm intervals. Prior to deployment, the peepers were assembled while submerged in Ar-purged distilled water, and chambers were fitted with a 0.45 µm cellulose nitrate filter membrane and conditioned with continuous Ar-bubbling for approximately 24 h. From a boat, one peeper was installed to a depth of 35 cm below the water sediment interface, near the shore of the lake where the overlying water column was 30 cm. The second peeper was installed to a depth of 60 cm below the water sediment interface, approximately 65 m out from the first peeper. The lake water column above the second peeper was 1.2 m. Peepers were allowed to approach diffusive equilibrium with the adjacent pore water over a 14-day period. After extracting peepers from the lake sediments, they were immediately rinsed with distilled water to remove any adhered sediments. There were two vertical rows of chambers at an equivalent depth. Water was promptly collected from each sample chamber using a dedicated sterile 5 mL syringe and then transferred to 4 mL Nalgene bottles. Water collected from one sample chamber was acidified with 12 N (N referring to normality) trace-metal-grade HNO<sub>3</sub> to a pH of <1 for cation analysis and water from the other sample chamber was unacidified for anion analysis. All samples were refrigerated at 4°C during shipping and storage prior to analysis. After peeper sampling, 5.1 cm (2-in.) diameter cores were collected adjacent to each peeper location. Cores of 60 and 70 cm length were collected near peepers 1 and 2, respectively. Core was sectioned into 15 cm intervals and immediately squeezed in the field to determine the pore-water composition.

Measurements of Eh and pH were made at least three times during pore-water squeezing to obtain representative results. The Eh was measured using an Orion platinum redox electrode (model 96-78BN), checked against Zobell's solution (Nordstrom 1977) and Light's solution (Light 1972). The pH was measured using an Orion Ross combination electrode (model 815600)

calibrated with standard buffer solutions at pH 7, 4, and 1. Measurements of alkalinity were made on filtered samples using a Hach digital titrator and bromcresol green – methyl red indicator and with 0.16 N H<sub>2</sub>SO<sub>4</sub>. Extracted pore water was collected in sterile 60 mL syringes and filtered through 0.45 µm cellulose-nitrate filters before being split into two aliquots. One aliquot of water was acidified with 12 N trace-metal-grade HNO<sub>3</sub> to a pH of <1 for cation analysis, and another aliquot was left unacidified to use for anion analysis. All samples were immediately refrigerated until analysis. Cations were analyzed by inductively coupled plasma atomic emission spectroscopy, and anions were determined using ion chromatography.

Groundwater from piezometers at site 1 was collected using a peristaltic pump and polyethylene tubing. All piezometers were bailed dry and allowed to recover prior to sampling. Measurements of Eh and pH were made in a sealed flow-through cell, maintained at groundwater temperature (8–10 °C). Calibration of the Eh and pH probes was checked before and after each sampling point. Temperature and alkalinity were measured at each location. Samples were filtered with 0.45 µm cellulose-nitrate filters and split into two aliquots for anion and cation analysis. All samples were stored and analyzed following the same methods as for samples collected from pore-water squeezing.

### **3.4 Progression of Sulfide Alteration**

Two sites from the abandoned Sherritt Gordon mine site are presented to demonstrate the applicability of the squeezing technique to unsaturated and saturated high-sulfide mine tailings. At site 1, core was collected through a 4.3 m thick unsaturated zone to the water table (Figs. 3.3, 3.4). At site 2, two peepers were installed into the bottom sediments of an acidic lake. Core was collected adjacent to each peeper to compare pore-water concentrations (Fig. 3.5).

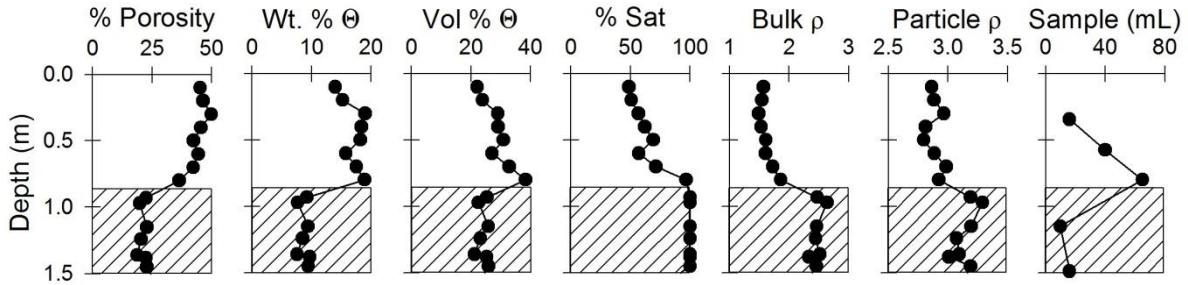


Figure 3-3: Depth profiles of the porosity, gravimetric (Wt.), and volumetric moisture content ( $\Theta$ ), saturation (Sat), and bulk and particle density ( $\rho$ ) measured from the Sherridon Tailing. The “sample (mL)” profile refers to the amount of water squeezed from the tailings material. Crosshatched area represents hardpan. The water table is at a 4.3 m depth.

### 3.4.1 Unsaturated Profile

The gravimetric moisture content increased from 14% near the tailings surface to 19% at the top of the massive hardpan and then sharply decreased to an average of 9% within the hardpan layer (Fig. 3.3). The porosity of the tailings showed a decrease from the tailings surface to the top of the hardpan and then an abrupt decrease within the hardpan layer. The decrease in porosity within the hardpan is attributed to precipitation of secondary minerals, which infill pore spaces. Saturation of the tailings was 50% at the surface, increased with depth, and was 100% within the hardpan. Although the tailings were 100% saturated within the hardpan, the volume of water expelled through squeezing was less than the water available from the overlying unconsolidated materials owing to the decrease in porosity. The amount of water squeezed from the tailings corresponded to the water content, increasing from 16 mL near surface to 65 mL at the top of the hardpan. Below the hardpan, the amount of water squeezed sharply dropped to 10 and 15 mL, respectively. The results in Fig. 3.3 show that the low permeability of the hardpan limited the amount of recharge, causing water to pool above the hardpan.

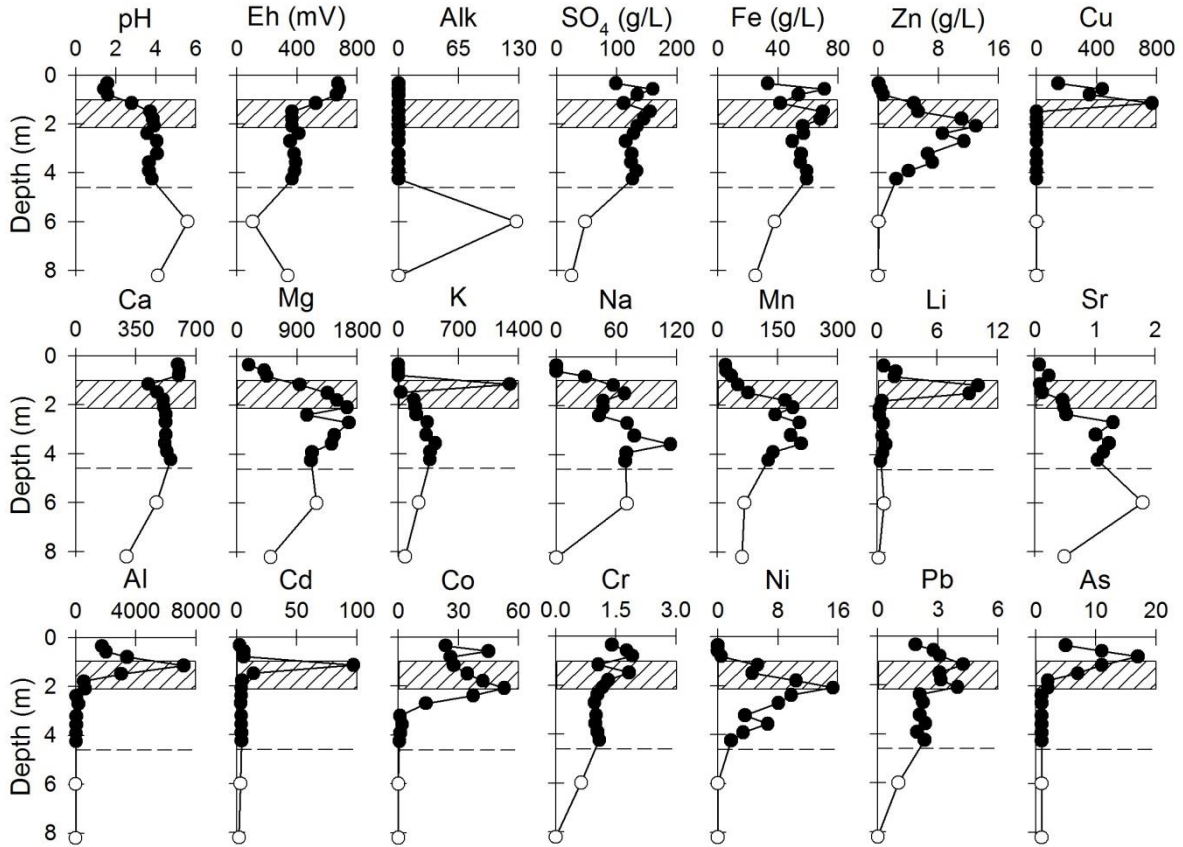


Figure 3-4: Profiles of pore-water chemistry at site 1 from the Sherridon tailings. Squeezed porewater is shown in solid circles, and the open circles are from drive-point piezometers. The cross-hatched area represents a hardpan layer, and the dashed line shows the position of the static water table. All concentrations in  $\text{mg L}^{-1}$  except where noted. Alk refers to alkalinity in  $\text{mg L}^{-1}$  as  $\text{CaCO}_3$ .

Figure 4 shows a depth profile of porewater squeezed from mine tailings at site 1 from surface to the water table. Water chemistry below the water table is represented by two drive-point piezometers. Above the hardpan layer, the pH of the tailings pore water was as low as 1.42, and the Eh was approximately 650 mV. The pH increased abruptly where the hardpan was first encountered, gradually increasing with depth. The Eh decreased at the hardpan layer and continued to decrease with depth. Extremely high concentrations of Fe ( $70\,000\ \text{mg L}^{-1}$ ),  $\text{SO}_4$  ( $160\,000\ \text{mg L}^{-1}$ ), Zn ( $13\,000\ \text{mg L}^{-1}$ ), Al ( $7\,190\ \text{mg L}^{-1}$ ), Cd ( $97\ \text{mg L}^{-1}$ ), Co ( $45\ \text{mg L}^{-1}$ ), Cu ( $770\ \text{mg L}^{-1}$ ), Cr ( $1.9\ \text{mg L}^{-1}$ ), Mn ( $209\ \text{mg L}^{-1}$ ), Ni ( $15.3\ \text{mg L}^{-1}$ ), Pb ( $4.3\ \text{mg L}^{-1}$ ), and As ( $17$

mg L<sup>-1</sup>) were observed in the vadose zone at site 1. Measurable alkalinity was not detected at any location in the unsaturated zone.

Below the water table, most metals and SO<sub>4</sub> decreased in concentration. Below this depth, concentrations measured in the piezometer are lower but still remain well above regulatory standards. This concentration front likely represents a peak period of sulfide oxidation reactions when very high concentrations of oxidation products were released to the vadose zone pore waters. Although dissolved concentrations of metals and SO<sub>4</sub> decreased below the water table, the concentrations remained elevated, with Fe and SO<sub>4</sub> values up to 37 900 and 57 800 mg L<sup>-1</sup>, respectively, in the groundwater.

Results in Fig. 3.4 demonstrate the importance of understanding porewater chemistry in the unsaturated zone in terms of mechanisms controlling the concentrations of dissolved major ions and dissolved metals and the acid-neutralization reactions that affect the mobility of dissolved metals. Retrieving water samples from above the water table is essential, because this is the zone of active gas transport and interactions between pore waters and atmospheric gases.

The extraction of pore water from the unsaturated zone using this squeezing method is qualitative. To limit possible uncertainties, we plan, in the near future, to implement an independent validation of this squeezing method under controlled conditions using a physical unsaturated model in the laboratory. This model will also include access ports to measure pressures within the squeezing chamber to ensure pressure exerted on the sample is not exceeding the solubility of discrete mineral phases, potentially altering pore-water concentration.

### **3.4.2 Surface Water – Groundwater Interface**

Performance and consistency of sediment squeezing has previously been compared with peepers, and no significant differences were found between the methods (Manson et al. 1998; Huerta-

Diaz et al. 2007). Depth profiles in Fig. 3.5 show peeper and porewater squeezing results from site 2, confirming consistency between the two methods. Porewater results from below the 0.30 m water column showed a strong correlation between the measured parameters, except dissolved Cu concentration. Dissolved ions measured from pore water below the 1.2 m water column correlate fairly well, except that peeper concentrations for Ca, Mg, Na, and Mn are lower than squeezed pore-water values. Lower dissolved concentrations observed from the peepers could be due to an inefficient diffusive equilibrium time. Despite the fact the peepers underwent 14 days to equilibrate with the lake-sediment pore water, Berg and McGlathery (2001) found that it may take up to a month for peepers to fully reach diffusive equilibrium.

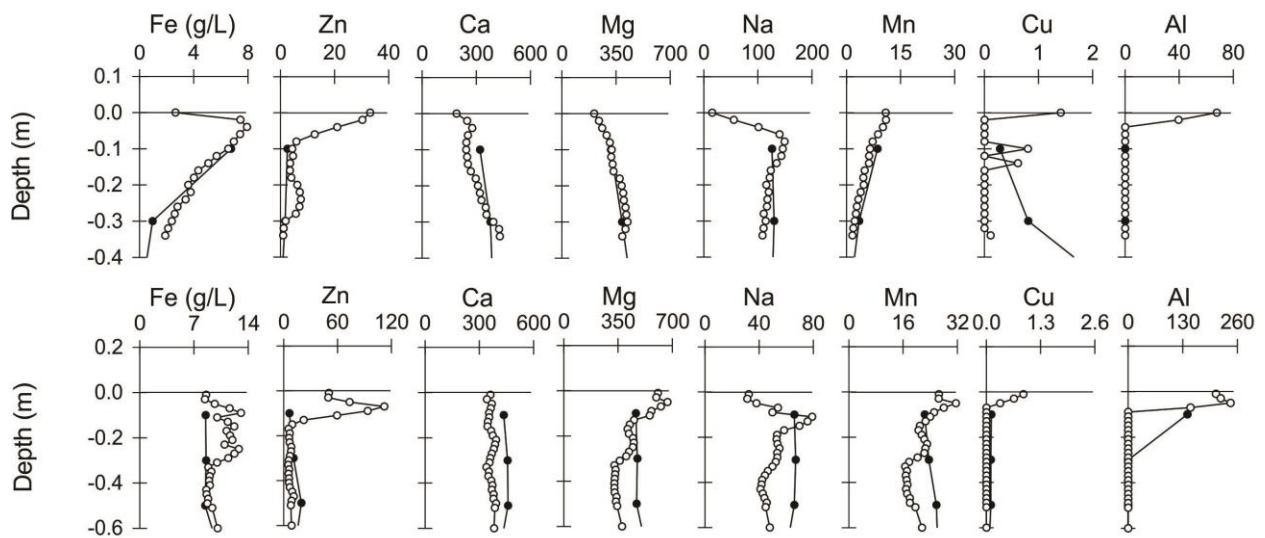


Figure 3-5: Profiles of pore-water chemistry at site 2 through lake-bed sediments. Squeezed pore water is show in solid circles and the open circles are from peepers. Upper plot is below a 0.3 m water column, and the lower plot is below a 1.2 m water column. The solid horizontal line represents the sediment porewater–surface-water interface. Concentrations in  $\text{mg L}^{-1}$  except where noted.

A limitation of using this squeezing method to study lake or saturated sediment pore waters is that it does not provide the detailed resolution of peepers. Installation of the squeezer parts requires 2–4 cm of sediment to be removed from each end of the core tube. This loss of



resolution is clearly shown in Fig. 3.4, where sediment pore water in the upper 4 cm of the profile is not represented by squeezing but is shown by the peepers. A further disadvantage of this method is that applying maximum pressure to the core section using the 4 t jacks could alter the pore-water chemistry (Fares et al. 2009).

Although peepers can recover samples free of temperature, pressure, and oxidation artifacts, they require significant preparation and long equilibrium times, which may not be practical at remote locations. For instance, in Fig. 3.5, the time required to collect core and produce water through squeezing was approximately 3 h, whereas the peepers required 24 h of gas purging followed by 14 days to equilibrate.

### **3.5 Conclusions**

This squeezing method is an effective low-cost technique for recovering porewater from unsaturated soils using a combination of immiscible fluid displacement, suction, and minimal mechanical compression. An advantage of this method is that redox-sensitive parameters in the porewater are not exposed to O<sub>2</sub> during extraction, and therefore the need for sample preparation in an anoxic environment is excluded. Porewater can be successfully squeezed from silt- to sand-sized sediments with volumetric moisture contents as low as 6%. A further advantage of this method is that the porewater chemistry is not altered by compression, as can be the case in high-pressure squeezing. Limitations of this method include compaction of sediments during core collection, modification of the porewater if the core section is subjected to high pressure, and loss of some material due to removal of sediments to fit squeezer parts. Aluminum tubing was used to collect samples and used in the squeezing chamber because it is readily available and inexpensive; however, in low-pH environments, potential leaching of Al from the casing could occur. To overcome possible Al contamination to the porewater, stainless steel could be used as

an alternative core casing. This squeezing method is applicable to unsaturated sediments in environments such as mining, oil sand operations, septic beds, agriculturally impacted sediments, and saturated soils from peat bogs and wetlands and at groundwater–surface interfaces.

## Chapter 4:

# *Long-term mineralogical and geochemical evolution of sulfide mine tailings under a shallow water cover*

Reproduced with permission from: Moncur, M.C., Ptacek, C.J., Lindsay, M.B.J., Blowes, D.W., Jambor, J.L., 2015. Long-term mineralogical and geochemical evolution of sulfide mine tailings under a shallow water cover. *Appl. Geochem.* 41, 176-188. Copyright 2015 Elsevier Ltd., License Number 3604610427487. Editorial and formatting changes have been made to accommodate reproduction in this thesis.

## 4.1 Executive Summary

The long-term influence of a shallow water cover limiting sulfide-mineral oxidation was examined in tailings deposited near the end of operation in 1951 of the former Sherritt-Gordon Zn–Cu mine (Sherridon, Manitoba, Canada). Surface-water, porewater and core samples were collected in 2001 and 2009 from above and within tailings deposited into a natural lake.

Mineralogical and geochemical characterization focused on two contrasting areas of this deposit: (i) sub-aerial tailings with the water table positioned at a depth of approximately 50 cm; and (ii) sub-aqueous tailings stored under a 100 cm water cover. Mineralogical analyses of the sub-aerial tailings showed a zone of extensive sulfide-mineral alteration extending 40 cm below the tailings surface. Moderate alteration was observed at depths ranging from 40 to 60 cm and was limited to depths >60 cm. In contrast, sulfide-mineral alteration within the submerged tailings was confined to a <6 cm thick zone located immediately below the water-tailings interface. This narrow zone exhibited minimal sulfide-mineral alteration relative to the sub-aerial tailings. Sulfur K-edge X-ray absorption near edge structure (XANES) spectroscopy showed results that were consistent with the mineralogical investigation. Porewater within the upper 40 cm of the sub-aerial tailings was characterized by low pH (1.9–4.2), depleted alkalinity, and elevated  $\text{SO}_4$  and metal concentrations. Most-probable number (MPN) enumerations revealed abundant populations of acidophilic sulfur-oxidizing bacteria within these tailings. Conversely, porewater in the sub-aqueous tailings was characterized by near-neutral pH, moderate alkalinity, and relatively low concentrations of dissolved  $\text{SO}_4$  and metals. These tailings exhibited signs of dissimilatory sulfate reduction (DSR) including elevated populations of sulfate reducing bacteria (SRB), elevated porewater  $\text{H}_2\text{S}$  concentrations, and strong  $\delta^{34}\text{S}\text{-SO}_4$  and  $\delta^{13}\text{C}\text{-DIC}$  fractionation. Additionally, mineralogical investigation revealed the presence of secondary coatings on primary

sulfide minerals, which may serve as a control on metal mobility within the sub-aqueous tailings. Results from this study provide critical long-term information on the viability of sub-aqueous tailings disposal as a long-term approach for managing sulfide-mineral oxidation.

## **4.2 Introduction**

Extraction and processing of base and precious metals from sulfide- ore deposits generates large volumes of sulfide tailings. When tailings are exposed to oxygen, sulfide minerals within the tailings will oxidize generating acidity, releasing elevated concentrations of dissolved  $\text{SO}_4$ , metals and metalloids to the porewater (Nordstrom and Alpers, 1999; Blowes et al., 2013). The rate of sulfide oxidation is greatest immediately after mine tailings are deposited because at this time, sulfide mineral surfaces are fresh and the  $\text{O}_2$ -diffusion path is shortest (Gunsinger et al., 2006). Therefore, following deposition, it may be desirable to control atmospheric  $\text{O}_2$  entry into the tailings through the addition of a barrier or cover over the mine wastes. Physical barriers that have been applied or proposed include dry covers composed of fine grained materials to maintain high water contents (Rasmuson and Collin, 1988; Nicholson et al., 1989; Yanful et al., 1994; Ouangrawa et al., 2009; Dobchuk et al., 2013; Lu et al., 2013); covers composed of geosynthetic materials (Sodermark and Lundgren, 1988; Lewis and Gallinger, 1999; Rowe and Hosney, 2013); and covers containing  $\text{O}_2$ -consuming materials (Reardon and Moddle, 1985; Broman et al., 1991; Tassé et al., 1994). In addition to limiting  $\text{O}_2$  diffusion, covers also contain the tailings and protect them from wind and water erosion (Kossoff et al., 2014).

Water covers offer an alternative approach to dry covers for managing sulfide-mineral oxidation. Sub-aqueous tailings deposition has potential to limit sulfide-mineral oxidation and associated environmental impacts (*e.g.*, Hamilton and Fraser, 1978; Pedersen et al., 1993; Yanful and Simms, 1997; Jacob and Otte, 2004; Vigneault, 2007). The  $\text{O}_2$  ingress into tailings is limited

by the low diffusion coefficient of the water cover. For example, the diffusive flux of O<sub>2</sub> to water covered tailings may decrease by up to 10,000 times relative to sub-aerial tailings (Robertson et al., 1997; Awoh et al., 2013). Suppression of sulfide-mineral oxidation therefore may be accomplished by disposal of tailings into lakes or deep marine environments (Pedersen, 1985; Pedersen et al., 1993; Poling et al., 2002), or by the construction of wet covers on existing tailings impoundments (Robertson, 1992). A number of laboratory and field studies have investigated the short-term storage of tailings under shallow water covers (Davé et al., 1997; Li et al., 1997; Holmström and Öhlander, 1999; Vigneault et al., 2001; Elberling and Damgaard, 2001; Samad and Yanful, 2005), but only a few studies have considered the reactivity of tailings that have been submerged over long time periods (*e.g.*, Jacob and Otte, 2004; Vigneault et al., 2007).

The objective of this study was to understand the biogeochemical processes that have occurred within sulfide mine tailings subjected to over 60 years of storage under a 100 cm water cover. This study involved detailed analyses of mineralogy of powder and thin section samples, geochemical analyses of tailings porewater and solids, stable isotope analyses of porewater, and enumerations to identify active microbial populations within the tailings.

### **4.3 Study Site**

The former Sherritt-Gordon Zn–Cu Mine is located in Sherridon, approximately 700 km northwest of Winnipeg, MB, Canada (Fig. 4.1). The site is situated near the southern edge of the Precambrian Shield in a region characterized by long, cold winters and cool summers. Monthly mean temperatures range from -21 °C in January to 18 °C in July and the mean annual temperature is 0.5 °C (Environment Canada, 2012). The long-term mean precipitation for Flin Flon, which is 60 km SW of the site, is 488 mm year<sup>-1</sup>, which is fairly similar to the total

precipitation in Sherridon (Moncur et al., 2014). Evapotranspiration losses in the Sherridon area are approximately 350 mm annually (Hydrological Atlas of Canada, 1978).



Figure 4-1: Location of the former Sherritt-Gordon Zn–Cu mine in Sherridon, Manitoba, Canada.

Two Precambrian Zn–Cu volcanogenic massive sulfide ore bodies were exploited to produce Zn and Cu concentrates with minor amounts of Au and Ag. Each ore body was approximately 5m thick and occurred as lenticular layers of massive and disseminated sulfides, and as irregular remobilized masses (Goetz and Froese, 1982). The ore averaged 2.5 wt.% Cu, 3.0 wt.% Zn,  $0.62 \text{ g t}^{-1}$  Au and  $20 \text{ g t}^{-1}$  Ag (Farley, 1949). Ore-zone sulfides were, in decreasing order of abundance, pyrite [FeS<sub>2</sub>] and pyrrhotite [Fe<sub>(1-x)</sub>S] (2:1 ratio), chalcopyrite [CuFeS<sub>2</sub>], sphalerite [ZnS], and accessory cubanite [CuFe<sub>2</sub>S<sub>3</sub>]. Farley (1949) reported trace arsenopyrite [FeAsS] occurring as small grains within pyrrhotite, native gold, and irregular occurrences of galena [PbS] in veinlets and disseminations within hanging-wall shear zones in the gneiss host rock. From 1931 to 1951, a total of 7.7 Mt of pyritic ore was milled to produce 0.17 Mt of Cu, 0.14 Mt of 50 percent Zn concentrate, and minor amounts of Ag (91,000 kg) and Au (2900 kg) (Mineral Resources Branch, 1978).

Sulfide tailings from the mining operations were discharged into three separate tailings impoundments containing a combined 7.4 Mt and occupying an area of 47 ha. The Camp tailings were deposited between 1931 and 1932 and the Woods tailings were deposited between 1937 and 1951. Tailings were deposited into Fox Lake at the end of mining in 1951. Extensive sulfide-mineral oxidation within the Camp and Woods tailings has generated porewaters with low pH values and extremely elevated concentrations of dissolved SO<sub>4</sub> and metals (Moncur et al., 2005; 2009a). Discharge of surface water and groundwater from the tailings deposits into adjacent Camp Lake has severely degraded water quality (Moncur et al., 2006). Effluent from Camp Lake flows into Kississing Lake where concentrations of Zn and Cu in the bottom sediments were elevated well above background concentrations in an area covering 9.5 km<sup>2</sup> (Moncur et al., 2014).

Fox Lake is a small (700 m by 300 m) lake situated in a semi-closed basin with one outflow. The lake overlies Precambrian Shield rock of the Sherridon Group, consisting of both metasedimentary and metavolcanic rocks (Froese and Goetz, 1981). The Fox tailings were slurried and discharged into Fox Lake from a number of spigot lines. This deposit extends from the shoreline outward into Fox Lake where the majority of tailings were submerged as several lobes that form small exposed islands (Fig. 4.2). The exposed tailings were visually oxidized and did not support vegetation. In contrast, much of the submerged tailings were overlain by a layer of naturally established vegetation and detritus.



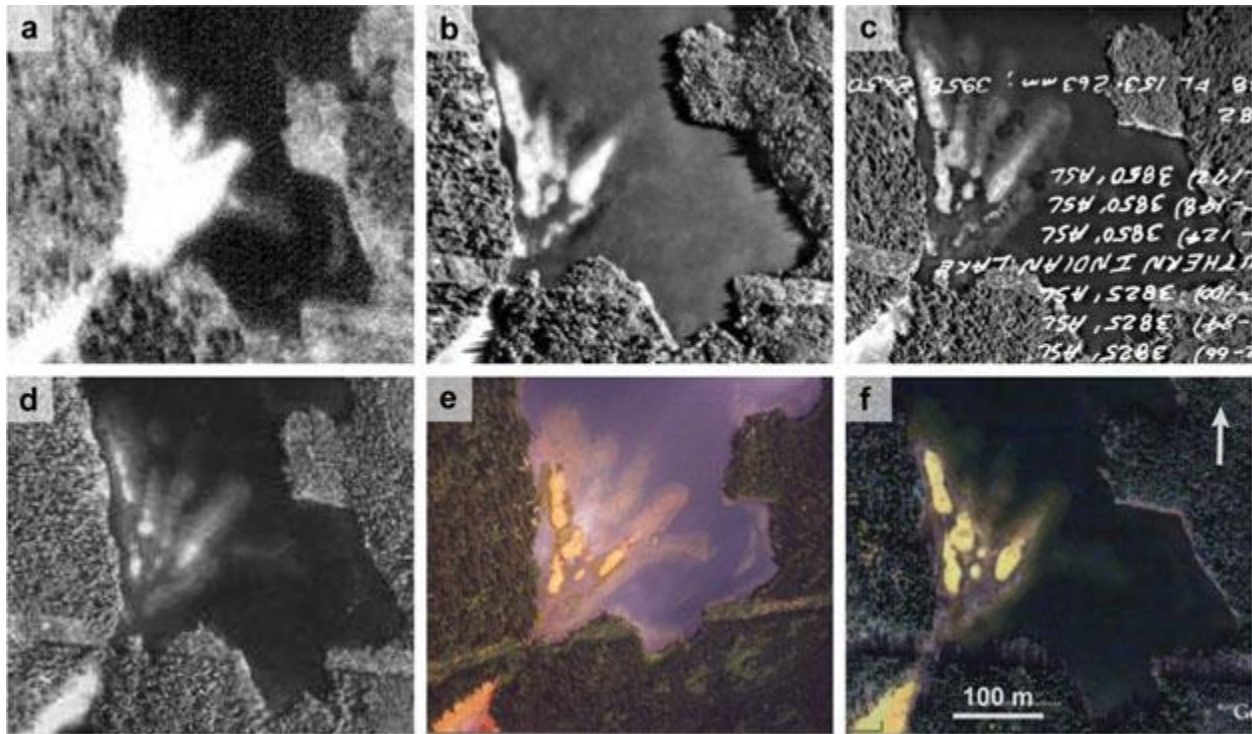


Figure 4-2: Aerial photos of Fox Lake and the submerged tailings between 1952 and 2007. Images taken (a) 1952; (b) 1968; (c) 1977; (d) 1983; (e) 2001; (f) 2007. Image (e) shows where samples were collected from the tailings on-land (FX) and submerged under a 100 cm water cover (FXS). Image from 2007 courtesy of Google Earth.

## 4.4 Methods

### 4.4.1 Core Collection and Piezometer Installation

Air photos and satellite images were used to identify areas within the Fox tailings where samples representative of sub-aqueous and sub-aerial tailings could be collected. Core samples were collected in August 2001 and August 2009, at two locations from the Fox tailings; an exposed sub-aerial tailings location (FX), and a sub-aqueous tailings location characterized by an approximately 100 cm water cover (FXS) (Fig. 4.2). Two cores extending from the tailings surface to a depth of 100 cm were collected from each location. One core was used to obtain porewater samples and the other to obtain samples of tailings solids. Core samples were cut into 25 cm sections, capped and sealed, and immediately stored in a freezer at -20 °C until analysis.

Additional core samples were collected in August 2006 at each location and stored at 4 °C for microbial enumerations. Drive-point piezometers measuring 1.3 cm in diameter and screened over the bottom 5 cm were installed into the submerged tailings in August, 2009, to depths of 12, 38, 63 and 88 cm below the water-tailings interface. These piezometers facilitated collection of larger porewater volumes than could be obtained by squeezing porewater from 2001 core samples.

#### **4.4.2 Solid Phase Analyses and Mineralogy**

Core collected for solid analyses was split by sawing cores while frozen, and one half was analyzed for total metals, sulfur, carbon and grain-size distribution, and the other half for mineralogy. Discrete samples were collected along the length of core where visual changes were observed. Samples of tailings solids from FX and FXS were analyzed for total metal concentrations using a HF/HNO<sub>3</sub> extraction followed by inductively coupled plasma–optical emission spectrometry (ICP–OES) detection. Total extractable carbonate was measured using the method of Barker and Chatten (1982), and total sulfur (S) and carbon (C) were determined by combustion and infrared detection using a C and S analyzer (LECO Corporation, USA). Physical properties of the FX and FXS tailings collected in 2001 were determined through grain-size analysis using standard sieve sizes. The porosity ( $n$ ) of the tailings was calculated using the method of Istomina (1957), where  $n = 0.225(1 + 0.83CU)$ . The uniformity coefficient is represented by CU, where  $CU = D_{60}/D_{10}$ .

Primary crystalline phases in the tailings, collected in 2001, were identified through X-ray diffractometry (XRD) using a Siemens rotating-anode instrument. Polished thin sections of the core samples were prepared without the use of water, thereby minimizing the dissolution of readily soluble minerals. These sections were examined by optical microscopy, using both

transmitted and reflected light. Areas of interest were marked on the section and photos were taken to assist in location of the relevant grains during examination by scanning electron microscopy–energy dispersive spectrometry (SEM–EDS). The SEM–EDS utilized a Phillips XL-30 instrument with a coupled energy-dispersion analyzer. Using a fully-automated Cameca SX50 scanning electron-microprobe, thin sections were analysed to provide an indication of compositional variation of select minerals.

Bulk S K-edge X-ray absorption near edge structure (XANES) spectra were collected from tailings on the SXRMB beamline (06B1-1) at the Canadian Light Source (Saskatoon, SK, Canada) to identify oxidized and reduced sulfur species. Frozen core samples obtained in 2009 were freeze-dried under vacuum at -45 °C and pulverized in an agate mill. The powdered samples were then mounted with carbon tape on a copper plate and transferred into the vacuum chamber on the SXRMB end station. The monochromator used a Si (111) crystal and replicate spectra were collected in total electron yield (TEY) mode for samples (n = 3) and reference materials (n = 2) including pyrite, pyrrhotite, chalcopyrite, sphalerite, galena, elemental sulfur [S<sub>8</sub>], gypsum [CaSO<sub>4</sub>•2H<sub>2</sub>O], and jarosite [KFe<sub>3</sub>(OH)<sub>6</sub>(SO<sub>4</sub>)<sub>2</sub>]. Additional spectra for chalcocite [Cu<sub>2</sub>S] and covellite [CuS] were obtained from SXRMB beamline scientists. Data processing and analysis was performed using ATHENA, which is part of the IFEFFIT software suite (Ravel and Newville, 2005). All spectra were calibrated to the theoretical S8 K-edge energy (E<sub>0</sub>; 2472.0 eV) according to first derivative maxima. Linear combination fitting (LCF) of normalized spectra was constrained by fixing E<sub>0</sub> values to calibrated energies and limiting total reference spectra to four, except when additional phases were identified by XRD and/or petrographic examination.

### 4.4.3 Aqueous Geochemistry

The squeezing method described by Moncur et al. (2013) was used to extract porewater from cores collected in 2001 and 2009 from FX and in 2001 from FXS. From each location a continuous 100 cm core was collected for squeezing and cut into 25 cm sections. Each core-section top was fitted with a sealed plunger and the bottom was fitted with a sealed base with an outlet port to collect expelled water. Pressure was applied to the plunger to displace the porewater downward through the core. Resulting water was collected into 60 mL polyethylene (PE) syringes, filtered through 0.45  $\mu\text{m}$  surfactant free cellulose acetate membranes, and transferred to prewashed PE bottles. One aliquot was acidified with 12 N trace-metal grade  $\text{HNO}_3$  to a pH of less than 2 for cation analysis, and other aliquots were left unacidified for analyses of inorganic anions and stable isotope ratios of  $\delta^{34}\text{S}$ ,  $\delta^{18}\text{O}_{\text{SO}_4}$ ,  $\delta^{18}\text{O}$  and  $\delta^2\text{H}$ .

Determinations of porewater Eh and pH were made at least three times during squeezing to ensure results were representative. The Eh was measured using a platinum combination redox electrode (96-78BN; Thermo Scientific, USA), which was checked against ZoBell's (Nordstrom, 1977) and Light's solution (Light, 1972). The pH was measured using a Ross combination electrode (815600; Thermo Scientific, USA) calibrated with standard buffer solutions at pH 7, 4, and 1. Measurements of alkalinity were made on filtered samples by titrating with 0.16 N  $\text{H}_2\text{SO}_4$  to the bromcresol green–methyl red endpoint (pH 4.5).

Porewater from piezometers installed in the submerged tailings was collected with a peristaltic pump using 0.64 cm diameter PE tubing. The piezometers were pumped dry and allowed to recover prior to sampling. Measurements of Eh and pH were made in the field using a sealed flow-through cell that was maintained near groundwater temperature. The pH electrode was calibrated and the performance of the Eh electrode was checked before each measurement.

The temperature was measured from each piezometer in situ using a down-hole temperature probe. Water samples were collected following methods as described above with additional samples collected for the analyses of dissolved organic carbon (DOC) and hydrogen sulfide ( $\text{H}_2\text{S}$ ). To prevent atmospheric contamination, samples for  $\delta^{13}\text{C}_{\text{DIC}}$  and  $\delta^{18}\text{O}_{\text{CO}_3}$  determination were collected by filling a 60 mL syringe with water directly from the peristaltic pump tubing. Water from the syringe was then injected into 100 mL vacuum-sealed glass bottles fitted with Teflon-lined septa. Surface water samples were collected near the shore of Fox Lake using a 60 mL PE syringe held approximately 5 cm below the lake surface annually between 2001 and 2009 following the same procedures as above.

All water samples were immediately refrigerated at 4 °C until analysis. Water samples were analyzed using ICP-OES for major cations, inductively coupled plasma-mass spectrometry (ICP-MS) for trace elements, and ion chromatography (IC) for anions. Combustion and infrared detection were used for DOC analysis. Dissolved  $\text{H}_2\text{S}$  was determined using the methylene blue procedure (SMEWW, 2005). Sulfur-isotope ratios of dissolved  $\text{SO}_4$  were determined by adding  $\text{BaCl}_2$  to precipitate  $\text{BaSO}_4$ , which was then converted into  $\text{SO}_2$  in an elemental analyzer coupled to a mass spectrometer in continuous flow mode (Giesemann et al., 1994). Sulfur-isotope measurements are reported in delta notation ( $\delta^{34}\text{S}$ ) relative to the Vienna Canyon Diablo Troilite (V-CDT) standard. Oxygen-isotope analysis on  $\text{BaSO}_4$  samples was carried out by pyrolysis in a high temperature conversion/elemental analyzer-interfaced to an isotope-ratio mass spectrometer. Values of  $\delta^{34}\text{S}$  and  $\delta^{18}\text{O}$  in  $\text{SO}_4$  were measured to identify reactions affecting  $\text{SO}_4$  concentrations including oxidation of pyrite and bacterially mediated sulfate reduction. The oxygen isotopic composition of water samples was determined by the  $\text{H}_2\text{O}$ – $\text{CO}_2$  equilibration method (Nelson, 2000). Hydrogen (deuterium) isotopic composition in water was measured on an isotope ratio mass spectrometer determined by reduction of water to  $\text{H}_2$  gas using chromium

metal as an active reducing agent. The results of oxygen and deuterium isotope measurements are expressed in delta notation ( $\delta^{18}\text{O}$  and  $\delta^2\text{H}$ ) relative to Vienna Standard Mean Ocean Water (V-SMOW) standard. The  $\delta^{18}\text{O}$  and  $\delta^2\text{H}$  composition of surface and porewater was measured to identify the degree of evaporative enrichment and groundwater surface water interactions. The method of Assayag et al. (2006) was used to determine  $\delta^{13}\text{C}$  on dissolved inorganic carbon, reported relative to Vienna Pee Dee Belemnite (V-PDB) standard. The  $\delta^{13}\text{C}$  of dissolved inorganic carbon (DIC) was used to identify processes such as carbonate dissolution and bacterial sulfate reduction.

#### **4.4.4 Microbial Enumerations**

To identify bacterial populations that could be catalyzing oxidation and reduction reactions in the tailings, enumerations of neutrophilic sulfur-oxidizing bacteria (nSOB), acidophilic sulfuroxidizing bacteria (aSOB), acid-producing (fermentative) bacteria (APB), sulfate-reducing bacteria (SRB), and iron-reducing bacteria (IRB) were performed using a five-tube most probable number (MPN) approach (Cochran, 1950). Methods for preparation, inoculation, and enumeration of nSOB and aSOB are described in detail by Blowes et al. (1996). Briefly, the nSOB and aSOB media contained  $\text{Na}_2\text{S}_2\text{O}_3 \cdot 5\text{H}_2\text{O}$  as the electron donor and the final pH was adjusted to 7.0 and 4.2, respectively. Media were filter sterilized and 9 mL aliquots were dispensed into sterile culture tubes. As described by Lindsay et al. (2011), APB were grown in a saccharide and peptide medium (Hulshof et al., 2003), whereas IRB and SRB were grown in Fe(III) EDTA (Gould et al., 2003) and modified Postgate C (Blowes et al., 1996) media, respectively. Culture tubes were filled with 9 mL aliquots of the APB medium, capped, and sterilized. Media for IRB and SRB enumerations were dispensed in 9 mL aliquots into 20 mL serum vials, which were then crimp-sealed and sterilized. All growth media were inoculated with

1.0 g of sample from refrigerated core samples within 30 days of collection. Sample handling and inoculation for the SRB and IRB enumerations were performed in an anaerobic chamber. Enumeration of positive results was performed after 48 h for APB and after four weeks for nSOB, aSOB, IRB, and SRB.

#### **4.4.5 Geochemical Modeling**

Porewater chemistry data were interpreted with the assistance of the equilibrium chemical-speciation/mass-transfer model MINTEQA2 (Allison et al., 1990). The MINTEQA2 database was modified for consistency with the WATEQ4F database (Ball and Nordstrom, 1991). Additional solubility data were incorporated for siderite (Ptacek and Blowes, 1994) and Co (Papelis et al., 1988). Saturation indices were calculated for discrete minerals that may control concentrations of dissolved ions in porewaters.

### **4.5 Results and Discussion**

#### **4.5.1 Fox Lake Water Level**

Information on methods of tailings deposition into Fox Lake is limited. Water levels in Fox Lake were not recorded during or after tailings deposition; therefore, it remains unclear if there were periods during the past 60 years when the tailings may have been exposed to oxygen. In the absence of water level data, air photos of the Fox tailings taken between 1952 and 2008 were used to gain some information about the history of the tailings (Fig. 4.2). Due to the poor resolution and high reflectance of the 1952 image, it is difficult to determine the extent of water cover over the tailings; however, subsequent images of the tailings from 1968 to 2008 show that the majority of the tailings remained submerged. Minimal water level fluctuations of Fox Lake were observed during annual visits between 2000 and 2009. The water table elevation in the

land-based tailings was 50 cm below the ground surface in 2001 and 2009. Hydraulic head data from piezometers installed in the submerged tailings at FXS combined with water level data from Fox Lake showed the absence of a vertical hydraulic gradient, suggesting that there was no advective flow between the water cover and underlying porewater. The hydraulic gradient between FX and FXS was not determined.

#### **4.5.2 Physical Tailings Characteristics**

Grain-size distributions were measured on samples extracted at various depths from the FX and FXS tailings showing a well sorted, fine- to medium-grained sand (Fig. 4.3). Average calculated CU values from the FX and FXS tailings were similar at 2.6 and 2.9, respectively, representative of a uniform grain-size distribution (Fig. 4.3). A perfectly uniform sediment such as dune sand has a  $CU = 1$ , whereas a poorly sorted glacial till has a  $CU = 30$ . The uniform sorting and relatively low silt content in both tailings profiles suggest deposition was near the spigot point (Robertson, 1994). The  $D_{10}$  (mm) of the tailings, which is the grain-size diameter at which 10% by weight of the particles are finer, showed that values from both profiles were almost identical below a 40 cm depth, however, the grain size was much coarser in the FX tailings above 40 cm. The coarser nature of the FX tailings above 40 cm is not due to a physically larger grain-size, but a result of sulfide oxidation followed by Fe oxyhydroxide precipitation causing formation of cemented grain-clusters and coatings to form on primary mineral surfaces. The calculated porosities of both tailings profiles were similar, ranging from 0.40 and 0.42, typical of sand (Freeze and Cherry, 1979). Grain size distributions measured from the FXS tailings and the FX tailings below a 40 cm depth were similar to those measured in the unoxidized Camp tailings (Moncur et al., 2005).



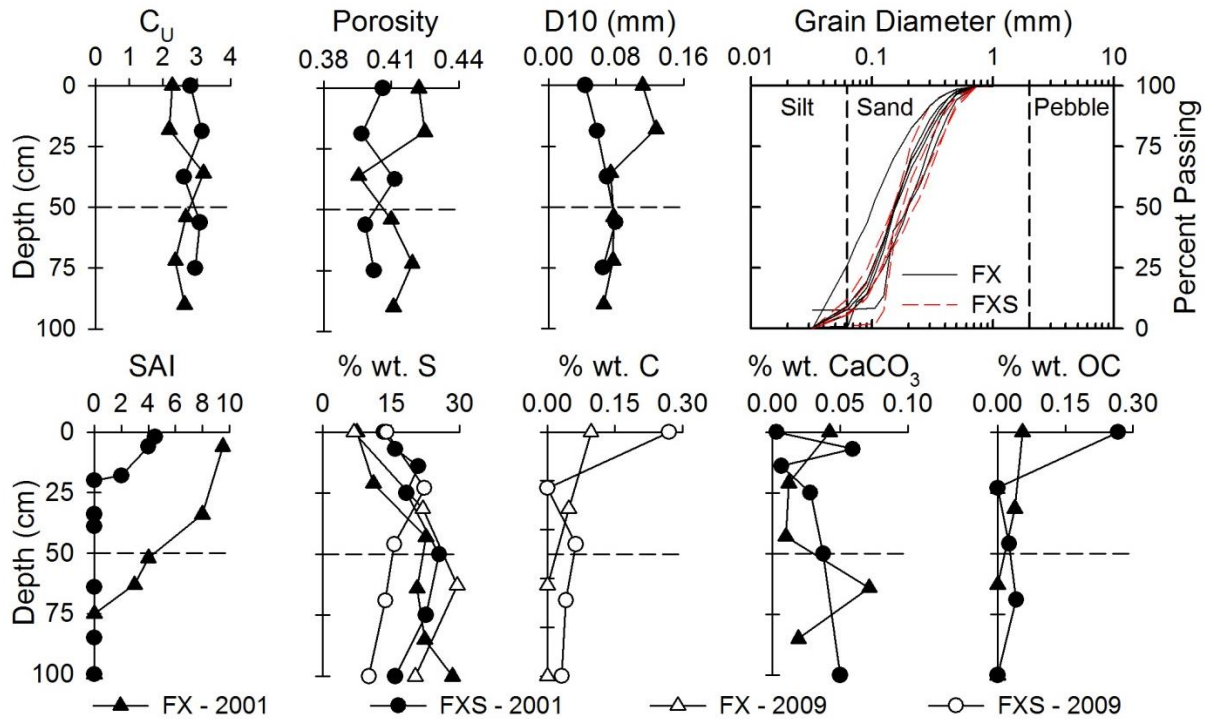


Figure 4-3: Depth profile through the on land (FX) and submerged tailings (FXS), top row showing the uniformity coefficient (CU), porosity, and grain-size distribution. The bottom row shows the sulfide alteration index (SAI) and weight percent of total sulfur (S), carbon (C), carbonate minerals ( $\text{CaCO}_3$ ), and calculated organic carbon (OC). The water-tailings interface is located at a depth of 0 cm for FXS and the dashed horizontal line represents the water table at FX.

### 4.5.3 Mineralogy

Optical microscopy and XRD analysis of the non-opaque assemblage in the unaltered tailings indicate the presence of quartz, albite, and microcline, with smaller amounts of amphibole, muscovite and biotite. Accessory amounts of sillimanite and chlorite were detected. Carbonate minerals were not observed during this study; however, Moncur et al. (2005) reported trace amounts of primary siderite in the Camp tailings. Sulfide minerals comprised up to 28 wt.% of the unaltered Fox tailings. The principal sulfides were pyrite and pyrrhotite with minor amounts of sphalerite and trace chalcopyrite also observed. Secondary Fe oxyhydroxides were abundant

in the ochreous zone of both the on-land and submerged tailings, with goethite being the only Fe oxyhydroxide detected in the X-ray diffractograms in all samples examined.

#### **4.5.4 Sub-Aerial Tailings**

Extensive sulfide oxidation of the sub-aerial tailings was observed in the tailings likely exposed for six decades to atmospheric oxidation. The tailings were characterized by an ochreous zone of extensive oxidation that extended from the surface to a depth of 40 cm. This zone was underlain by a transitional zone of weaker oxidation and unaltered tailings beginning at a 60 cm depth.

Optical microscopy was used to assess the sulfide alteration intensity (SAI), which is classified on a scale of 1–10 developed by Blowes and Jambor (1990) and refined by Moncur et al. (2005, 2009a,b). For example, at a SAI = 10, the sulfides have been almost completely obliterated; at SAI = 3, remnant cores of pyrrhotite are abundant; and at SAI = 1, the alteration occurs only as narrow rims on pyrrhotite. The SAI was determined on tailings samples collected from FX and FXS in 2001 (Fig. 4.3).

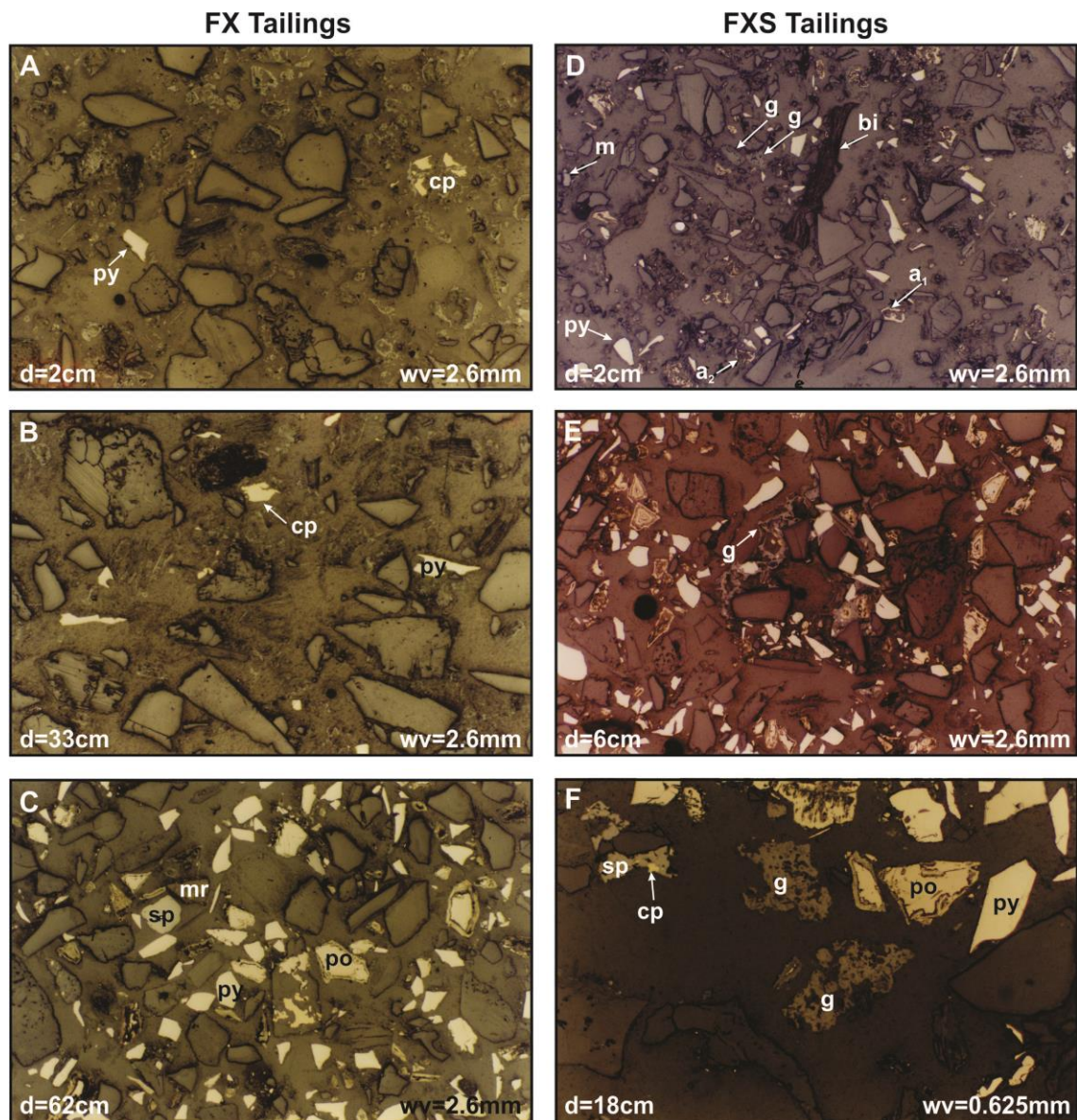


Figure 4-4: Photomicrographs of tailings thin sections in plane-polarized reflected light (A) 2 cm depth in the sub-aerial tailings (FX) showing a single grains of whitish pyrite (py) and yellow chalcopyrite (cp) which are the only remaining sulfides (B) FX 33 cm depth showing sparse pyrite and chalcopyrite (C) FX 62 cm depth showing unaltered pyrite; the grey grain is sphalerite (sp). Pyrrhotite (po) is variably rimmed by marcasite (mr) and in some grains complete replacement by marcasite. (D) 2 cm depth in the subaqueous tailings (FXS) showing unaltered pyrite with pyrrhotite extensively replaced mainly to complete pseudomorphism by marcasite. Grey magnetite (m), brown biotite (bi) lath and two irregular patches of grey goethite (g) are detectable. (E) FXS at a 6 cm depth showing abundant pyrite, altered pyrrhotite, and a grey Fe oxyhydroxide cement surrounding various gangue minerals. (F) FXS 18 cm depth showing unaltered pyrite, a sphalerite grain with a chalcopyrite inclusion, and cores of pyrrhotite with a thin exterior of marcasite. Two irregular patches of grey goethite are present. Depth and width of view are represented by d and wv, respectively.

Samples from the uppermost 6 cm of the ochreous zone contained numerous grains of pyrite and chalcopyrite, but pyrrhotite and sphalerite were not observed (Fig. 4.4A). The proportion of chalcopyrite to pyrite was higher than observed in the unaltered tailings with some of the chalcopyrite grains showing irregular margins possibly due to leaching. Pyrite lacked alteration rims but many of the grains had smooth margins bounding a shard-like habit that was not observed in unaltered tailings. Furthermore, pyrite was noticeably sparse relative to its abundance in the deeper unaltered tailings and Fe oxyhydroxides were abundant. A majority of sulfide minerals had been consumed by oxidation; therefore, an SAI of 9 was assigned to these samples (Fig. 4.3). Unlike the older Camp tailings where extensive near-surface sulfide oxidation had resulted in almost complete destruction of soluble Al-silicate minerals (*e.g.*, biotite, chlorite) and extensive alteration to albite and amphibole (Moncur et al., 2005), Al-silicate alteration in these sub-aerial tailings was limited to minor biotite replacement by Fe oxyhydroxides and minimal replacement of muscovite by Fe oxyhydroxide along the basal cleavage planes. Other than the presence of Fe oxyhydroxides, which are associated with all minerals, no other evidence of secondary replacement of Al-silicate minerals was observed.

The pyrite content was greater at a depth of 33–35 cm, but remained approximately 25% of that typical of unaltered samples. The SAI from 33–35 cm was 8 (Fig. 4.3). A few grains of chalcopyrite were present, but pyrrhotite and sphalerite were not observed. Similar to the upper 6 cm zone, samples at a 33–35 cm depth were strongly ochreous, however at both depths, Fe oxyhydroxides did not cement the particles into large aggregates, and in both zones, the greatest concentration of the Fe oxyhydroxides was associated with the smaller particles. The oxidation intensity declined at a depth of 51–54 cm, which corresponded to the water table depth. Abundances of pyrite and pyrrhotite at this depth were typical of those found in unaltered tailings. Several grains of sphalerite were also observed, marking the first appearance of this

sulfide within the tailings profile. Although pyrrhotite alteration was observed throughout the profile, the variation of alteration was predominantly from narrow to thick rims of marcasite, surrounding residual cores of unaltered pyrrhotite. Complete pseudomorphs after pyrrhotite were present, but they were much less common than particles containing residual pyrrhotite. The SAI at this depth is assigned to be 4 (Fig. 4.3). Polished thin sections did not exhibit megascopic ochreous particles, but particles observed microscopically with transmitted light had exteriors stained by Fe oxyhydroxides that were too sparse to appear as discrete rims in reflected light. Samples observed at depths of 62–65 and 72–75 cm were similar in that both contained abundant pyrite and pyrrhotite, with accessory amounts of sphalerite > chalcopyrite. At a depth of 62–65 cm, some pyrrhotite grains exhibited alteration rims of marcasite and a SAI of 4 was assigned (Fig. 4.4C). The pyrrhotite was fresh at a depth below 72 cm and the SAI assigned was 0 (Fig. 4.3).

#### **4.5.5 Sub-Aqueous Tailings**

In contrast to the observed oxidation zone in the sub-aerial tailings, the equivalent ochreous zone in the submerged tailings extended only 6 cm below the water-tailings interface. The SAI value assigned to these shallow tailings is 4.5 (Fig. 4.3). Petrographic examination of tailings collected from a depth of 2 cm revealed major amounts of pyrite with no visible alteration. At this depth, pyrrhotite exhibited similar to greater abundance than pyrite, and occurred sparingly as residual cores. More than 95 percent of the pyrrhotite at this depth had been pseudomorphically replaced as a rim of marcasite surrounding a hollow core (Fig. 4.4D). Unaltered chalcopyrite was present in trace quantities and sphalerite was absent with the exception of a single grain that occurred as an intergrowth with chalcopyrite.

Goethite was common as irregular patches, but rims on individual particles were poorly developed and incomplete. Cementation of groups of particles by goethite occurred only locally where clots and patches of goethite form a matrix rather than inter-particle binding agent. Over 20 particles in the polished thin section were examined by SEM–EDS analyses to determine the compositions and their variations among different areas and textures of Fe oxyhydroxide. All spectra were similar with small amounts of S, Al, and Si consistently present. Several of the centers within the marcasite pseudomorphs were also examined using SEM–EDS. All except one of the centers were devoid of minerals. The ratio of the peak heights for Fe and S resembled those of pyrrhotite (i.e., Fe:S = 1:1); however, the reflectance of the mineral was characteristic of a  $\text{SO}_4$  rather than sulfide phase. Therefore, the former mineral in the dark centers of the pseudomorphs was presumably melanterite, which was abundant in the X-ray diffractogram of the underlying sample from 6 cm. The rapid dissolution of melanterite in water (Chou et al., 2013) would explain its absence.

Mica observed was predominantly muscovite, but biotite was formerly the more abundant of the two prior to its extensive replacement by Fe oxyhydroxides and lesser amounts of hydrobiotite. Replacement of muscovite has been minimal and was restricted to Fe oxyhydroxide occurrences along the basal cleavage, as observed in the on land-tailings.

The ochreous zone at the top of the FXS core was less than 6 cm thick and was megascopically distinctive due to the orange color. Samples collected at a 6 cm depth consisted of blackish tailings that were directly below the ochreous zone. Optical microscopic examination revealed that the principal non-opaque gangue assemblage at 6 cm was similar to that in the overlying ochreous tailings, and a bulk XRD confirmed that the similarity extended to the presence of detectable hydrobiotite and a small amount of kaolinite (~2%). One of the main differences between 6 cm depth and the overlying ochreous tailings is that goethite was less

abundant and did not occur as coatings on primary sulfides. Petrographic examination revealed that goethite occurred only in small areas as an intergranular fill and as rims observed on the adjoining gangue minerals (Fig 4E).

The opaque minerals present at a 6 cm depth consisted of abundant unaltered pyrite and abundant pseudomorphs after pyrrhotite (Fig. 4.4E). A few grains of unaltered chalcopyrite were observed and sphalerite was largely absent. Therefore the SAI was rated to be 4 (Fig. 4.3). The pseudomorphs after pyrrhotite, as observed at a 2 cm depth, consisted predominantly of marcasite. In contrast to the sub-aerial tailings, Fe oxyhydroxides were not associated with these pseudomorphs. Similar to the overlying ochreous tailings, melanterite likely was previously infilling voids associated with pyrrhotite. Although melanterite was abundant in bulk XRD analysis, it was not observed in the polished thin section. Despite the fact that samples were prepared with the use of a non-aqueous lubricant, melanterite was likely dissolved or abraded during section preparation.

Energy-dispersive spectroscopic analyses of several areas of Fe oxyhydroxide solids gave results similar to those obtained at shallower depths, for example S, Si, and Al were consistently present. Samples from the 6 cm zone are the only ones in which jarosite was detected in the XRD analyses. This mineral was sparse (~1%) and was associated with the Fe oxyhydroxides.

Optical microscopy showed that the principal minerals at a depth of 18 cm in the submerged tailings were quartz, microcline, and albite, with amphibole and mica common. Both muscovite and biotite were present, with a small amount of the biotite replaced by chlorite or hydrobiotite, or in some cases both of these phases. Chlorite was also present as extremely fine-grained aggregates, which are interpreted to be part of the primary assemblage.

Iron oxyhydroxide phases were relatively sparse at a depth of 18 cm. Two areas of cementation were observed, but most of the oxyhydroxides occurred as isolated, irregular

patches (Fig. 4.4F). Sulfide minerals consisted mainly of unaltered pyrite and pyrrhotite that exhibited varying degrees of alteration. Narrow marcasite rims surrounding preserved pyrrhotite cores were the most common form of pyrrhotite alteration. However, minor amounts of altered pyrrhotite exhibited marcasite rims and hollow cores. Numerous sphalerite grains were also observed at this depth and a relatively low SAI of 2 was assigned (Fig. 4.3).

The non-opaque assemblage at a depth from 20–100 cm was similar to that at 18 cm. Differences were that hydrobiotite and goethite were not detected by XRD and Fe oxyhydroxides were not observed by optical microscopy. Major amounts of pyrite and pyrrhotite were present and neither mineral exhibited signs of alteration. Sphalerite was common as were lesser amounts of chalcopyrite; however, these phases comprised less than 1 vol.% of total sulfides. The SAI below 20 cm was 0 (Fig. 4.3).

#### **4.5.6 Solid-Phase Geochemistry**

Total sulfur ( $S_{\text{tot}}$ ) concentrations from both the FX and FXS tailings exhibited similar depth dependent trends (Fig. 4.3). Sub-aerial tailings exhibited the greatest  $S_{\text{tot}}$  depletion above the water table, whereas  $S_{\text{tot}}$  depletion was limited to the upper 20 cm of the subaqueous tailings. These  $S_{\text{tot}}$  profiles are generally in agreement with the SAI profiles. Sub-aqueous tailings showed similar  $S_{\text{tot}}$  concentrations in the upper 25 cm of the core between 2001 and 2009, but showed lower concentrations with depth in 2009. Lower  $S_{\text{tot}}$  concentrations in the 2009 core could be attributed to heterogeneities in mineral distribution during deposition. Total-S within unaltered tailings ranged from 16 to 28 wt.%; these values are attributed to sulfide S because primary sulfate minerals were not identified in the Fox tailings or observed in the Camp or Woods tailings impoundments (Moncur et al., 2005, 2009a, 2009b).



Total carbon (C) content was consistently low, averaging 0.04 and 0.08 wt.% for the FX and FXS tailings, respectively (Fig. 4.3). Total extractable carbonate contents were also low with a maximum of 0.07 wt.% in the unaltered tailings, consistent with observations in the Camp tailings. During mineralogical investigations carbonate or other carbon-bearing minerals such as graphite were not identified; therefore, it is assumed that the majority of the total C is organic carbon, which was calculated as the difference between total C and carbonate-C (Fig. 4.3). The highest organic C concentration was observed near the surface of both locations. The FXS tailings were vegetated, and although the organic matter was removed prior to total C analysis, roots and other fragments of organic matter likely remained. Although the FX tailings were not vegetated, decaying organic matter (i.e., leaf litter, plant materials) was observed on the exposed tailings surface that could have contributed to the organic C content.

The order of abundance of major elements in the unaltered tailings solids, as determined by total metal concentrations, was Fe > Al > Ca > Na > Mg, on a mass basis. This order agrees with the tailings mineralogy consisting of pyrite and pyrrhotite, albite

$[(\text{Na}_{0.71}\text{Ca}_{0.28}\text{K}_{0.01})_{\Sigma 1.00}(\text{Si}_{2.69}\text{Al}_{1.33})_{\Sigma 4.02}\text{O}_8]$ , microcline  $[\text{KAlSi}_3\text{O}_8]$ , amphibole

$[(\text{Na}_{0.48}\text{Ca}_{0.15}\text{K}_{0.06})\text{R}_{0.69}(\text{Ca}_{1.58}\text{Fe}_{0.39}\text{Mn}_{0.03})_{\Sigma 2.00}(\text{Mg}_{2.51}\text{Fe}_{1.73}\text{Al}_{0.63}\text{Ti}_{0.13})_{\Sigma 5.00}(\text{Si}_{6.33}\text{Al}_{1.67})_{\Sigma 8.00}\text{O}_{22.93}\text{F}_{0.07}]$ , and biotite

$[(\text{K}_{0.91}\text{Na}_{0.02})_{\Sigma 0.93}(\text{Mg}_{2.24}\text{Fe}_{0.46}\text{Mn}_{0.01}\text{Al}_{0.32}\text{Ti}_{0.03})_{\Sigma 3.06}\text{Al}_{1.00}(\text{Si}_{2.80}\text{Al}_{0.20})_{\Sigma 3.00}\text{O}_{10.76}\text{F}_{0.24}]$ . Potassium concentrations were not measured during analyses. In general, depth dependent trends of major elements were not evident within either the FX or FXS tailings. Because sulfide oxidation reactions were not extensive enough to significantly alter Al-silicate minerals, there was minimal depletion of major elements in the ochreous zones (Fig. 4.5).

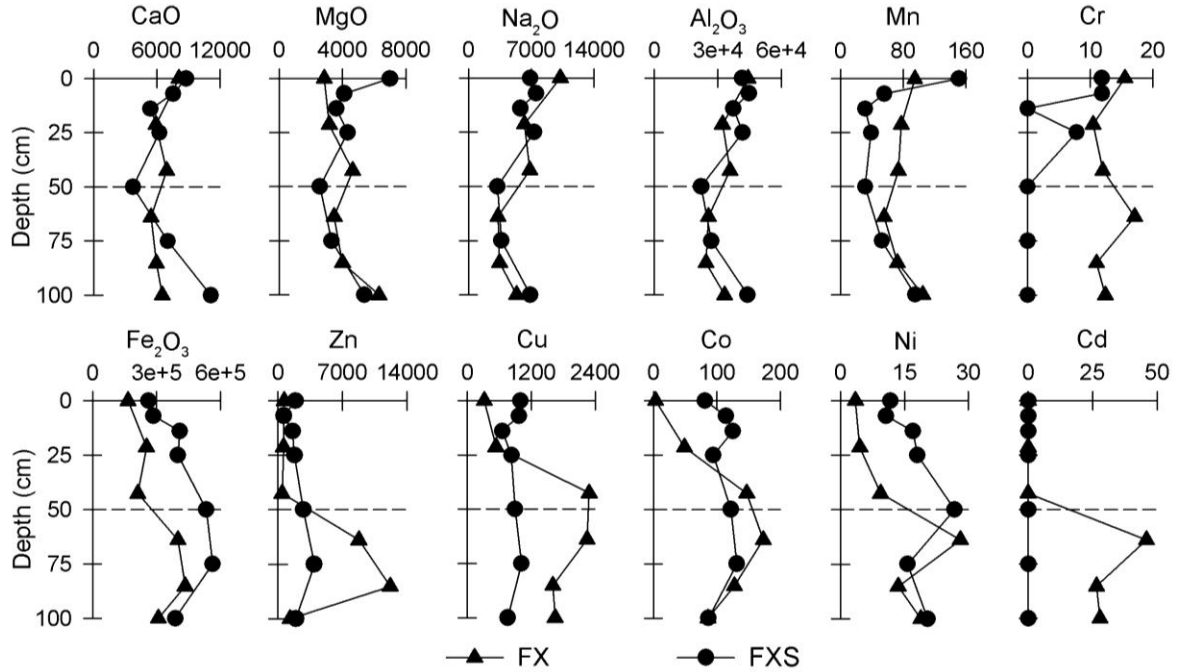


Figure 4-5: Depth profile through the sub-aerial (FX) and sub-aqueous (FXS) tailings showing solid-phase concentrations of major and trace elements. Concentrations are in mg/g. The water-tailings interface is located at a depth of 0 cm for FXS and the dashed horizontal line represents the water table at FX.

The relative mass abundance of trace metals in the unaltered tailings follows the order:  $Zn > Cu > Mn > Co > Pb > Ni > Cr > Cd$ . Unlike the major elements, there is a strong depth dependent trend with Zn, Cu, Co Ni and Cd, which is consistent with assigned SAI values (Fig. 4.3). Within the ochreous zone of the FX tailings, Cu is depleted with concentrations increasing just above the water table, whereas the concentrations of Zn, Cd, Co and Ni have their greatest concentrations at or below the water table. This trend is consistent with the relative resistance of sulfide minerals in oxidized tailings where chalcopyrite  $[CuFeS_2]$  has the highest resistance to oxidation followed by pyrite  $[(Fe,Co)S_2]$ , sphalerite  $[(Zn,Cd)S]$ , and pyrrhotite  $[(Fe,Co)_{1-x}S]$  having the least residence (Moncur et al., 2009b). The increase of Co occurred slightly higher in the profile than Zn and Cd, consistent with Co associated with pyrite, and its greater resistance to oxidation relative to sphalerite and pyrrhotite. Microprobe analysis of sphalerite grains found

that Cd concentrations were consistently detected (Moncur et al., 2009b). Chromium and Mn, were not depleted in the ochreous zones because these elements were likely associated with more stable Al-silicate minerals.

#### **4.5.7 X-ray Absorption Spectroscopy**

Sulfur K-edge measurements for sub-aerial tailings (FX) collected from depths of 0, 20, and 40 cm exhibited a dominant peak positioned at 2472.2 eV (Fig. 4.6). These spectra also featured a broad hump spanning 2474–2480 eV and a minor peak at 2482.6 eV. Results of the LCF indicated that pyrite comprised a maximum of 8% of the S K-edge spectrum measured for unsaturated sub-aerial tailings (Table 4.1). Minor chalcopyrite (4% of S K-edge spectrum) was present in the uppermost FX sample, whereas pyrrhotite and sphalerite were not detected. The relatively low abundance of pyrite and chalcopyrite within these highly altered tailings is consistent with optical examination and XRD analyses. Fitting using pyrite and marcasite provided statistically similar results; therefore, LCF analysis could not distinguish between these FeS<sub>2</sub>(s) polymorphs. Nonetheless, these results revealed that pyrite and/or marcasite were a minor component of S K-edge spectra obtained for unsaturated tailings from the FX profile. The absence of S associated with pyrrhotite and sphalerite is indicative of extensive sulfide-mineral alteration, and is consistent with the assigned SAI of 9.

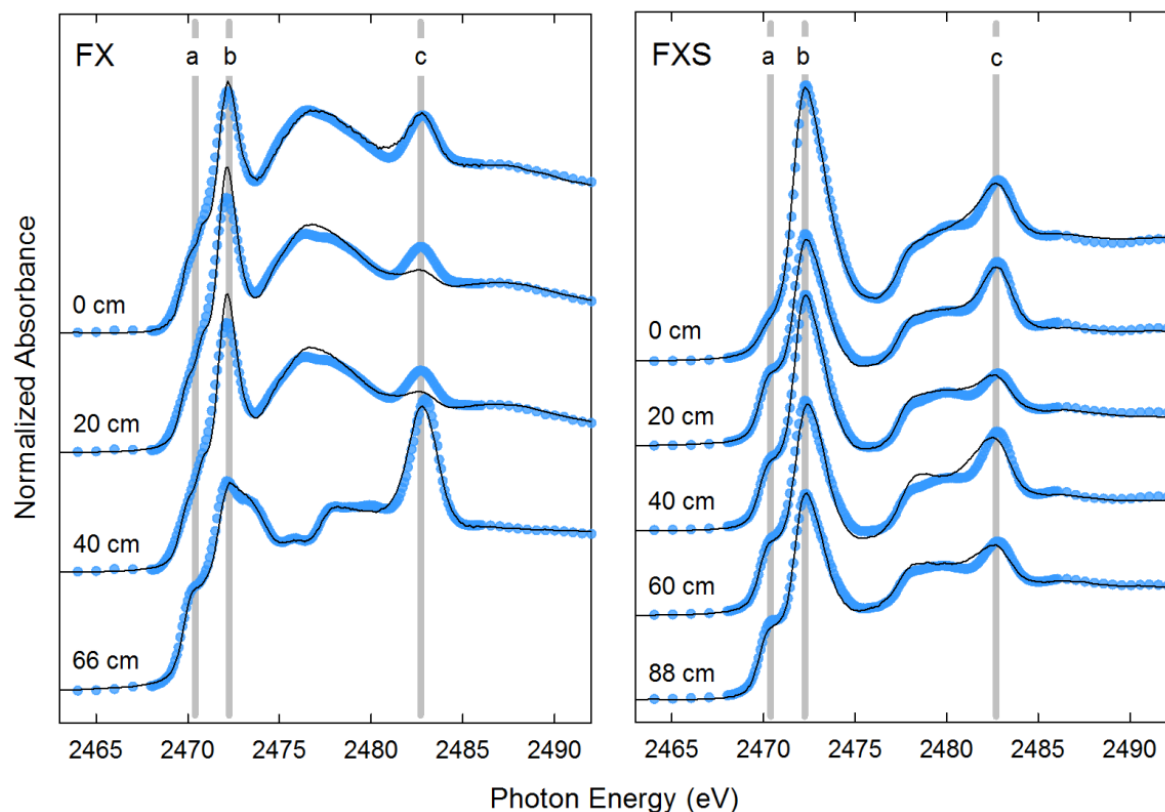


Figure 4-6: Measured (line) and modeled (circles) S K-edge XANES spectra for samples of sub-aerial (FX) and sub-aqueous (FXS) tailings. Vertical shaded areas represent measured S K-edge white line maxima for (a) pyrrhotite, (b) covellite, pyrite and/or marcasite, (c) gypsum and/or jarosite reference materials.

Covellite was the dominant component of S K-edge spectra within this zone. The covellite reference spectrum comprised 89–92% of the fitted S K-edge spectra for samples obtained from depths of 0, 20, and 40 cm. Although not detected by XRD, these LCF results suggest that covellite was likely a common phase at the sulfide grain surfaces in the unsaturated sub-aerial tailings. These apparently disparate results are attributed to methodological differences between XRD, which detects only abundant (commonly >1 wt.% of bulk mineral assemblage) crystalline phases, and XAS, which is an element-specific method that detects both crystalline and non-crystalline phases. Moreover, the S K-edge XANES spectra were collected using TEY detection, which is highly sensitive to grain surfaces. These results therefore suggest that

covellite occurred as thin surface coatings on remnant sulfides. Under oxic conditions, covellite formation may result from Cu(II) replacement of Fe(II) in pyrrhotite or pyrite (Boorman and Watson, 1976; Blowes and Jambor, 1990; Holmström et al., 1999) and/or Fe(III) leaching of chalcopyrite (Córdoba et al., 2008) under acidic pH conditions. The occurrence of covellite coatings at grain surfaces suggests that these processes have occurred in unsaturated FX tailings. The bulk ratio of pyrite and/or marcasite to covellite is likely much greater than apparent values derived from these surface sensitive S K-edge XANES analyses. Covellite is therefore interpreted as a trace phase in the bulk mineral assemblage.

Table 4-1: Results of LCF analysis of S K-edge XANES spectra for sub-aerial (FX) and sub-aqueous (FXS) tailings. Fitted reference spectra included pyrite (py) and marcasite (mr), pyrrhotite (po), chalcopyrite (cp), sphalerite (sp), gypsum (gp), jarosite (ja), and covellite (cv). The R factor is the mean-square misfit between the measured and modeled spectra.

Location	Depth (cm)	py/mr	Po	cp	sp	gp	ja	cv	Sum	R factor
FX	0	0.06		0.04				0.89	1.00	0.0021
	20	0.08						0.92	1.00	0.0030
	40	0.08						0.92	1.00	0.0029
	66	0.49	0.20	0.24	0.05		0.02		1.00	0.0020
FXS	0	0.74	0.19		0.02	0.05			1.00	0.0007
	20	0.50	0.30	0.11	0.04	0.05			1.01	0.0011
	40	0.58	0.29	0.10	0.04	0.01			1.02	0.0010
	60	0.50	0.38	0.04	0.04	0.05			1.01	0.0033
	88	0.48	0.20	0.23	0.05	0.03			1.00	0.0013

The S-K-edge XANES spectrum for the 66 cm sample differed substantially from the shallower FX sample. A peak positioned at 2472.2 eV exhibited a shoulder at approximately 2470.4 eV and an additional peak was located at 2482.8 eV. Results of LCF indicated that pyrite and/or marcasite comprised approximately 50% of the S K-edge spectrum for this sample. Pyrrhotite, chalcopyrite, and sphalerite accounted for 20%, 24%, and 5% of the S-K-edge spectrum, respectively. These results also indicate that below the water table, which was

positioned 50 cm below surface, tailings have undergone considerably less oxidation than the overlying unsaturated tailings.

Sulfur K-edge XANES spectra for the sub-aqueous tailings (FXS) exhibited a dominant peak at 2473 eV (Fig. 4.6). Similar to the 66 cm FX sample, spectra for all FXS samples exhibited a shoulder at 2470.4 eV on the dominant peak, and a minor peak at 2482.7 eV. The LCF indicated that gypsum accounted for up to 5% of S in the sub-aqueous tailings (Table 4.1). The sample obtained from the tailings-water interface (i.e., 0 cm) exhibited the smallest shoulder at 2470.4 eV, which corresponds to the S K-edge white line maximum for pyrrhotite. Pyrite plus marcasite accounted for 74% of the S Kedge spectrum for this sample, whereas pyrrhotite and sphalerite comprised 19%. The high ratio of pyrite-S and/or marcasite-S to pyrrhotite-S is attributed to the formation of secondary marcasite rims at pyrrhotite surfaces. Additionally, the relatively low abundance of sphalerite is consistent with optical mineralogy.

All deeper FXS samples (i.e., 20, 40, 60 and 88 cm) were characterized by similar S K-edge spectra. Results of LCF revealed that 48–58% of the S K-edge spectra were contributed by pyrite and/or marcasite. Pyrrhotite and chalcopyrite accounted for an additional 20–38% and 4–23% of the S K-edge spectra, respectively. Minor amounts of sphalerite and gypsum were also present in these samples. These results are generally consistent with results of XRD analysis and optical examination of unaltered tailings.

## **4.5.8 Porewater Chemistry**

### ***4.5.8.1 Sub-Aerial Tailings***

Porewater was squeezed from core at 25 cm intervals from surface to a 100 cm depth from the land-based tailings in 2001 and 2009. The oxidation of sulfide minerals within the vadose zone of the tailings has resulted in generation of low pH conditions (pH 1.9–3.7) and elevated

concentrations of dissolved  $\text{SO}_4$  (up to  $59,000 \text{ mg L}^{-1}$ ), Fe (up to  $28,000 \text{ mg L}^{-1}$ ) and trace metals (Fig. 4.7). The highest concentrations of dissolved metals were observed near the tailings surface although elevated concentrations of dissolved Fe,  $\text{SO}_4$  and other metals persisted through the water table to a depth of 100 cm (Table 4.2).

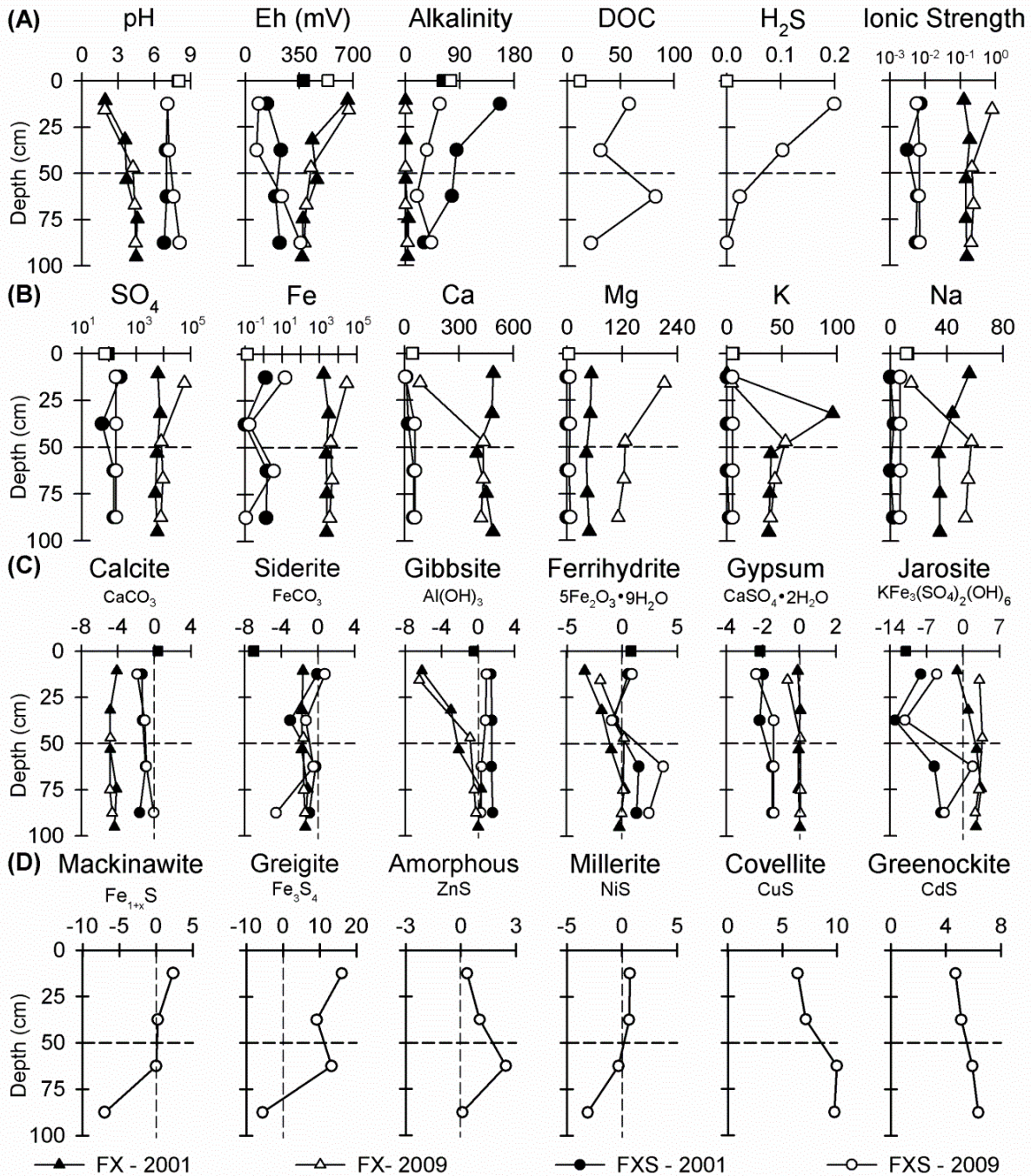


Figure 4-7: Depth profiles through the land-based (FX) and submerged (FXS) tailings; (A) and (B) showing porewater chemistry and calculated ionic strength; (C) and (D) showing calculated saturation indices. All concentrations are in mg L<sup>-1</sup> except where noted. Dashed horizontal line represents water table location in the FX. The Fox Lake (FL) water-tailings interface of FXS is shown at a depth of 0 cm.



Depth profiles of pH and Eh values were consistent over the eight year period between 2001 and 2009. However, an order of magnitude increase of SO<sub>4</sub>, chloride and most dissolved metals occurred at a depth of 15 cm in 2009 (Fig. 4.7). For example, between 2001 and 2009, SO<sub>4</sub> and Fe increased from 6000 to 59,000 mg L<sup>-1</sup> and 2000 and 28,000 mg L<sup>-1</sup>, respectively (Table 4.2). The elevated concentrations of dissolved SO<sub>4</sub> and metals at a depth of 15 cm in 2009 resulted in much higher calculated ionic strength values. This increase of dissolved elements is a result of continuing sulfide oxidation reactions occurring in the near-surface tailings over the eight-year period. Alkalinity was not detected in porewater in the vadose zone of the land-based tailings. In 2001, alkalinity values were minimal; 5 mg L<sup>-1</sup> (as CaCO<sub>3</sub>) at 75 cm and 3 mg L<sup>-1</sup> (as CaCO<sub>3</sub>) at 95 cm below the surface. By 2009, the only measureable alkalinity was 3 mg L<sup>-1</sup>, at a depth of 90 cm below surface. At and below the water table, concentrations of dissolved ions were relatively similar. Modeled saturation indices indicated that tailings porewaters were undersaturated with respect to carbonate minerals (Fig. 4.7). Porewater was undersaturated with respect to Al hydroxide and Fe(III) oxyhydroxide mineral phases, but become supersaturated with respect these phases near the water table. The porewater was supersaturated with respect to goethite throughout the depth profile. Low temperature mine waters are typically supersaturated with respect to goethite when other Fe(III) oxyhydroxide are also at saturation. As a result, this observation is not necessarily indicative of goethite precipitation (Alpers and Nordstrom, 1999). However, goethite was the only Fe oxyhydroxide consistently detected in all X-ray diffractograms examined from the FX tailings samples, in agreement with modeling results. The porewater was also at saturation with respect to gypsum and jarosite suggesting that these secondary mineral phases could be controlling dissolved concentrations of SO<sub>4</sub>, Fe and K.

Table 4-2: Porewater chemistry measured from the land-based (FX) and submerged (FXS) tailings in 2001 and 2009.

Location	pH	SO <sub>4</sub> mg L <sup>-1</sup>	Fe mg L <sup>-1</sup>	Al mg L <sup>-1</sup>	Zn mg L <sup>-1</sup>	Cu mg L <sup>-1</sup>	Cr mg L <sup>-1</sup>	Co mg L <sup>-1</sup>	Cd mg L <sup>-1</sup>
<u>0.13 m depth</u>									
FX-2001	1.93	6200	1600	190	9.3	6.4	0.21	0.36	0.13
FX-2009	1.90	59000	28000	1500	170	170	0.63	33	3.3
FXS-2001	7.09	260	1.26	<dl	<dl	0.01	<dl	<dl	<dl
FXS-2009	7.05	1600	1.33	0.01	0.07	2.2	<dl	0.0006	0.0006
<u>0.62 m depth</u>									
FX-2001	3.71	5800	2200	14	7.0	0.08	0.09	<dl	0.16
FX-2009	4.38	9400	4500	68	7.0	19	0.05	0.1	0.39
FXS-2001	7.04	150	1.54	<dl	0.01	0.01	<dl	0.006	<dl
FXS-2009	7.15	1700	0.16	0.04	0.07	0.9	<dl	0.0003	<dl
<u>0.89 m depth</u>									
FX-2001	4.49	5900	2400	8.3	2.2	<dl	0.08	0.05	0.16
FX-2009	4.43	7900	3500	68	15	16	0.02	0.3	0.02
FXS-2001	6.81	150	1.34	<dl	0.01	0.01	<dl	<dl	<dl
FXS-2009	7.00	1700	1.35	0.01	0.06	<dl	<dl	0.0003	<dl
dl	0.01	<0.01	<0.0002	< 0.01	<0.0005	<0.0005	<0.0005	<0.0005	<0.0005

#### 4.5.8.2 Sub-Aqueous Tailings

In contrast to the sub-aerial tailings, porewater from the subaqueous tailings was at circumneutral pH and mildly reducing, containing low concentrations of SO<sub>4</sub> and Fe. Most dissolved metal concentrations were near or below analytical detection limits (Table 4.2). Concentrations of dissolved ions, pH, Eh and calculated ionic strength exhibited minimal variability between 2001 and 2009 (Fig. 4.7). However, alkalinity concentrations measured in 2009 were almost twice as high as those measured in 2001. Speciation modeling results show that porewaters approached or attained saturation with respect to calcite and siderite, suggesting that equilibrium with respect to these carbonate minerals may be maintaining circumneutral pH conditions (Blowes et al., 2013). Other minerals at saturation or supersaturation in porewaters that might be controlling dissolved ions include gibbsite, ferrihydrite, goethite, gypsum and jarosite (Fig. 4.7).

### 4.5.9 Sulfate Reduction

Values of  $\delta^{34}\text{S}$  and  $\delta^{18}\text{O}$  for dissolved  $\text{SO}_4$  were determined for porewater from the sub-aerial and sub-aqueous tailings, and for surface water from Fox Lake. Values of  $\delta^{34}\text{S}_{\text{SO}_4}$  for the sub-aerial tailings exhibited little variation (1.8–3.3‰) and were consistent with  $\delta^{34}\text{S}$  values of the primary sulfide minerals, which ranged from 0.2 to 2.6‰ (n = 7; Moncur et al., 2009a).

Fractionation between  $\delta^{34}\text{S}$  in the primary sulfide and associated dissolved  $\text{SO}_4$  was less than 2‰ (Taylor et al., 1984a; Krouse et al., 1991; Rye et al., 1992).

Values of  $\delta^{34}\text{S}$  and  $\delta^{18}\text{O}$  for dissolved  $\text{SO}_4$  for the sub-aqueous tailings were generally more positive than the primary sulfide minerals, which is consistent with the fractionation associated with bacterial (dissimilatory)  $\text{SO}_4$  reduction (Fig. 4.8A). The  $\delta^{34}\text{S}_{\text{SO}_4}$  values in the sub-aqueous tailings ranged from 18‰ (13 cm depth) to 7.6‰ (63 cm depth). Similarly,  $\delta^{18}\text{O}_{\text{SO}_4}$  values ranged from 4.1‰ (13 cm depth) to 0.2‰ (63 cm depth). Decreases in  $\text{SO}_4$  concentrations resulting from dissimilatory sulfate reduction (DSR) can generate significant sulfur isotope fractionation where the remaining  $\text{SO}_4$  becomes enriched in  $^{34}\text{S}$  (Harrison and Thode, 1958; Kaplan and Rittenberg, 1964; Fritz et al., 1989; Habicht and Canfield, 1997; Knöller et al., 2004). Sulfate reduction was also apparent from other geochemical parameters measured for the submerged tailings and for Fox Lake. As sulfate-reducing bacteria catalyze the oxidation of organic carbon, the reduction of  $\text{SO}_4$  to  $\text{H}_2\text{S}$  (Berner, 1980) occurs through the reaction:



where  $\text{CH}_2\text{O}$  represents a generic organic compound. The organic carbon source in Fox Lake and the submerged tailings likely originated from overlying vegetation and DOC in the surface waters. (Fig. 4.4). The precipitation of sparingly-soluble metal-sulfides occurs when  $\text{H}_2\text{S}$  is produced in the presence of dissolved metals:



where  $\text{Me}^{2+}$  denotes a divalent metal such as Fe, Cd, Ni, Cu, Co and Zn; and MeS represents the corresponding metal sulfide precipitate (Berner, 1985; Seal, 2003). The sequence of reactions in equations (4.1) and (4.2) decreases the concentrations of dissolved  $\text{SO}_4$ , Fe, and other metals, and increases porewater alkalinity and pH (Tuttle et al., 1969; Benner et al., 1999; Lindsay et al., 2009b). The reduction of  $\text{SO}_4$  described in reaction (1) is consistent with the trends of increased pH, alkalinity, and  $\text{H}_2\text{S}$ , and with the decreased Eh observed in the sub-aqueous tailings porewater (Fig. 4.7). Studies on acid neutralization of lakes (Cook et al., 1986), tailings (Benner et al., 2000), tailings amended with organic substrate (Lindsay et al., 2011) and for the treatment of acid rock drainage (Benner et al., 1999) have shown that DSR coupled with secondary metal-sulfide precipitation can promote increased concentrations of alkalinity, pH buffering, and the formation of secondary metal-sulfide phases.

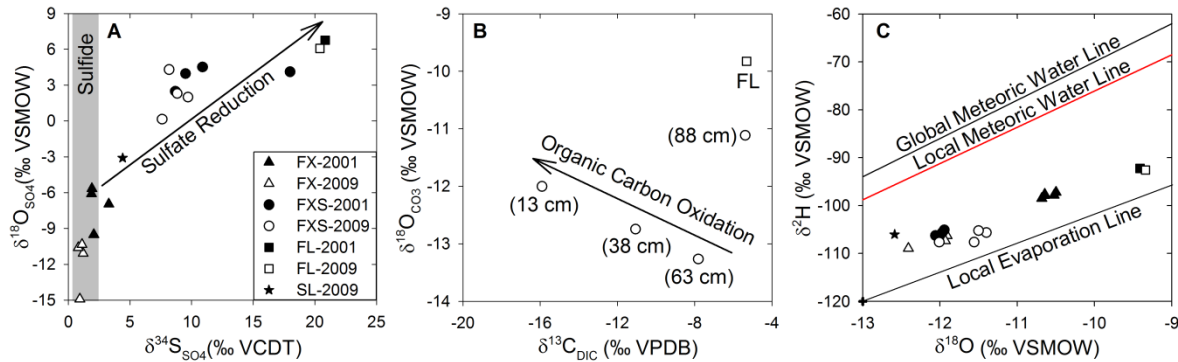


Figure 4-8: (A) Plot of  $\delta^{34}\text{S}$  versus  $\delta^{18}\text{O}_{\text{SO}_4}$  values of dissolved  $\text{SO}_4$  from sub-aerial tailings (FX), sub-aqueous tailings (FXS), Fox Lake (FL) and Sherlett Lake (SL) surface water. The shaded area represents the range of  $\delta^{34}\text{S}$  values measured from seven primary sulfide minerals. VSMOW – Vienna Standard Mean Ocean Water; VCDT – Vienna Canyon Diablo Troilite. (B) Plot of  $\delta^{13}\text{C}_{\text{DIC}}$  versus  $\delta^{18}\text{O}_{\text{CO}_3}$  values measured in 2009 from FXS and FL. Values in brackets refer to sample depths below water-tailings interface. VPDB – Vienna Pee Dee Belemnite (C) Plot of  $\delta^{18}\text{O}$  versus  $\delta^2\text{H}$  values measured in 2001 and 2009 from FX, FXS, FL and SL.

Values of  $\delta^{13}\text{C}_{\text{DIC}}$  became more negative toward the tailings surface while, with the exception of the 88 cm sample, values of  $\delta^{18}\text{O}_{\text{CO}_3}$  became more positive (Fig. 4.8B). These

trends in  $\delta^{13}\text{C}_{\text{DIC}}$  and  $\delta^{18}\text{O}_{\text{CO}_3}$  are generally consistent with DSR coupled with oxidation of organic carbon. The porewater sample with highest concentrations of  $\text{H}_2\text{S}$ , alkalinity and most enriched  $\delta^{34}\text{S}_{\text{SO}_4}$ ,  $\delta^{18}\text{O}_{\text{SO}_4}$  and  $\delta^{18}\text{O}_{\text{CO}_3}$  and depleted  $\delta^{13}\text{C}_{\text{DIC}}$  is near the interface with the overlying water column, where the highest concentrations of organic carbon occurred in the sediments (Fig. 4.3). Depth profiles of alkalinity for the sub-aqueous tailings (FXS, Fig. 4.7) generally decrease from the tailings surface, with the shallowest depths having alkalinity concentrations that are similar to the values measured in Fox Lake. However, mixing of Fox Lake water and tailings porewater (13 cm depth) cannot account for observed differences in the  $\delta^{13}\text{C}_{\text{DIC}}$  and  $\delta^{18}\text{O}_{\text{CO}_3}$  (Fig. 4.8B). These observations are consistent with the interpretation that DSR occurred within the sub-aqueous tailings and that rates may have been greatest immediately below the water-tailings interface.

The  $\delta^{18}\text{O}$  and  $\delta^2\text{H}$  composition of porewater in the sub-aerial and sub-aqueous tailings reveal temporal and spatial differences in water sources. In 2001, porewater from the sub-aerial and sub-aqueous tailings, and from the Fox Lake were all distinct and plotted along a local evaporation line (Gibson et al., 2010). Porewater from the sub-aqueous tailings exhibited the most negative  $\delta^{18}\text{O}$  and  $\delta^2\text{H}$  values, whereas porewater from the sub-aerial tailings was characterized by slightly enriched  $\delta^{18}\text{O}$  and  $\delta^2\text{H}$  values. The sub-aerial tailings porewater exhibited more negative  $\delta^{18}\text{O}$  and  $\delta^2\text{H}$  values in 2009 compared to 2001. These values were also more negative relative to sub-aqueous tailings porewater collected in 2009. Variations in  $\delta^{18}\text{O}$  and  $\delta^2\text{H}$  values between the sampling events were relatively small for the submerged tailings, indicating a fairly consistent stable hydrological setting. The subaerial tailings porewater exhibited a larger range in  $\delta^{18}\text{O}$  and  $\delta^2\text{H}$  compositions between the two sampling events, indicating variations in the source of water or in the degree of evaporation. Porewater collected in 2001 from the sub-aerial tailings exhibited more enriched isotopic signatures than in 2009,

suggesting greater evaporation, or mixing with summer precipitation or enriched surface water. The apparent lack of hydrological variability in the sub-aqueous tailings is consistent with observed stability of the geochemical profiles over time. In contrast, the sub-aerial tailings exhibited greater geochemical variability, which may be attributed, at least in part, to greater hydrological variability as suggested by these  $\delta^{18}\text{O}$  and  $\delta^2\text{H}$  values. The weighted mean annual composition of local precipitation for the areas was -17‰ for  $\delta^{18}\text{O}$  and -130‰ for  $\delta^2\text{H}$ , measured in The Pas, MB, the nearest long-term precipitation monitoring station, 150 km south of Sherridon. Local groundwater is typically similar to the weighted mean annual composition of local precipitation, with Canada being more biased toward winter precipitation (Jasechko et al., 2014). The LEL of the area is from a survey of 151 lakes in northwestern Manitoba (Gibson et al., 2010) and the intercept of the LEL for NW Manitoba and the GMWL (Fritz et al., 1987) is about -17‰. Mixing of groundwater ( $\delta^{18}\text{O}$  of -17‰) with Fox Lake water ( $\delta^{18}\text{O}$  of -9.5) suggests that porewater from the FXS tailings ( $\delta^{18}\text{O}$  of -11.5) was comprised of more than 50% surface water.

Modeled saturation indices indicate that porewater from the sub-aqueous tailings approached saturation or became supersaturated with respect to secondary sulfide minerals (Fig. 4.7). Speciation modeling results were consistent with the presence of secondary sulfides observed in the submerged tailings at a depth of 6 cm. Secondary grains of covellite, each no more than 15  $\mu\text{m}$  across, occur within the pyrrhotite pseudomorphs. In addition, rims of secondary marcasite on unaltered primary pyrite were also identified at a depth of 6 cm in the submerged tailings. The rims occurred on a few grains and were extremely thin (Fig. 4.9). The optical identification of the rims as marcasite was consistent with EDS analysis. Secondary metal-sulfide phases were not detected in the S K-edge XANES spectra from the sub-aqueous tailings. However, similar to the XRD results, these phases were likely below method detection

limits in the presence of abundant pyrite and pyrrhotite (Table 4.1). Furthermore, despite the textural difference between the host pyrite and the fine-grained marcasite rim, the two were difficult to distinguish in backscattered-electron images because both minerals had the same composition. Other studies (*e.g.*, Pedersen et al., 1993; Paktunc and Davé, 2002; Lindsay et al., 2011) have also reported the presence of secondary sulfide minerals, which control metal and SO<sub>4</sub> concentrations in sulfate-reducing zones at mining-impacted sites.

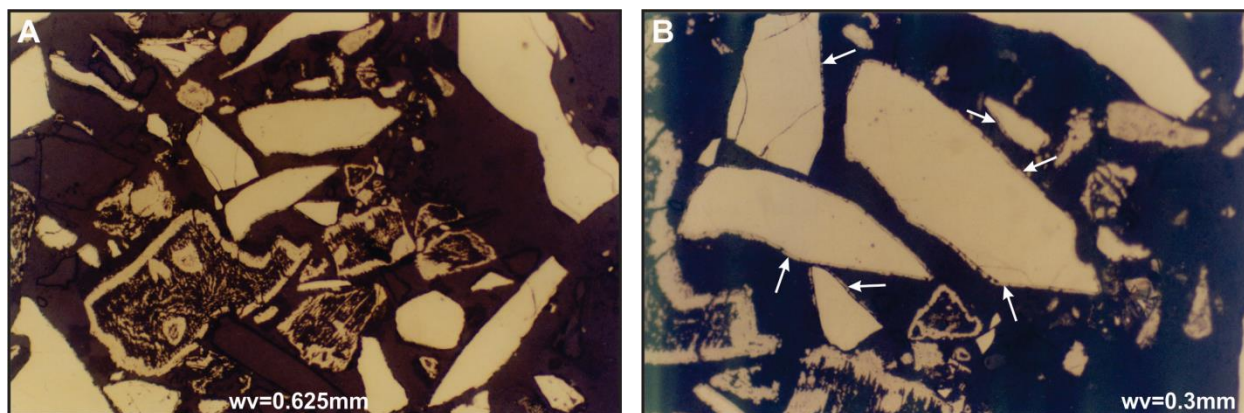


Figure 4-9: Photomicrographs of sub-aqueous tailings at a 6 cm depth in plain reflected light showing (A) unaltered grains of pyrite with thin rims of secondary marcasite, near center of image. (B) Enlargement of (A) with arrows showing the narrow rims of secondary marcasite on the primary pyrite grains. Width of view is represented by wv.

#### 4.5.10 Microbial Enumerations

Most-probable number populations of IRB and SRB were low within the ochreous zone of the sub-aerial tailings, which was dominated by aSOB. Populations of nSOB were consistently low throughout the sub-aerial tailings profile. Decreasing populations of aSOB with depth in the sub-aerial tailings corresponded to an increase in SRB numbers below the ochreous zone. This trend is indicative of O<sub>2</sub> consumption due to sulfide-mineral oxidation above the water table and DSR in the underlying saturated anoxic zone. Fermenters (APB) were not detected in the FX profile and IRB numbers above the detection limit were attributed to false positives associated with high dissolved Fe(II) concentrations (Fig. 4.10).

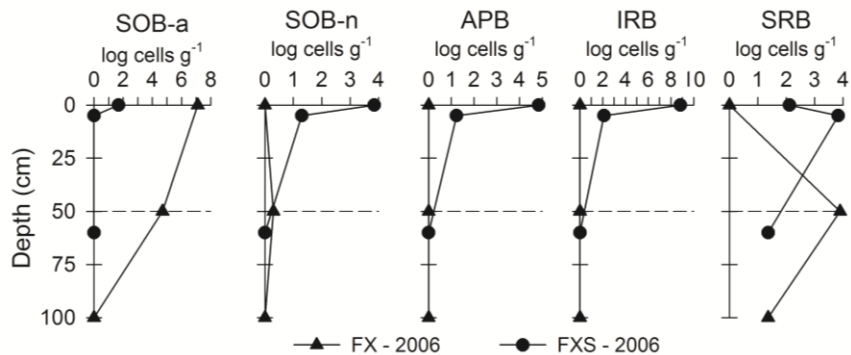


Figure 4-10: Most probable number (MPN) populations of acidophilic S-oxidizing bacteria (aSOB), neutrophilic S-oxidizing bacteria (nSOB), acid-producing (fermentative) bacteria (APB), iron-reducing bacteria (IRB) and SO<sub>4</sub>-reducing bacteria (SRB) in the land-based (FX) and submerged (FXS) tailings. The water-tailings interface is located at a depth of 0 cm for FXS and the dashed horizontal line represents the water table at FX.

In contrast to the sub-aerial tailings, nSOB exhibited higher MPN populations than aSOB in the sub-aqueous tailings. Nonetheless, populations of both nSOB and aSOB were low at depths greater than 13 cm below the tailings surface. The largest populations of SRB and IRB within the sub-aqueous tailings occurred near the water-tailings interface. These values also corresponded to the highest APB numbers, which suggests that the production of organic acids via fermentation supported SRB and IRB activity at this depth (Lindsay et al., 2011; McDonald et al., 2013). Rapid consumption of these organic acids by SRB and IRB could explain why DOC concentrations (Fig. 4.10) were not substantially higher near the water-tailings interface, where active DSR may have been occurring (McDonald et al., 2013). Populations of SRB and IRB generally decreased with depth, yet viable populations of these heterotrophic bacteria persisted throughout the sub-aqueous tailings profile. The large shift in the  $\delta^{34}\text{S}_{\text{SO}_4}$  values and an increase of H<sub>2</sub>S concentration and SRB population indicate that active DSR was occurring in the sub-aqueous tailings.



#### 4.5.11 Fox Lake Water Quality

Comparison of water quality parameters for the submerged tailings, land-based tailings and Fox Lake (Fig. 4.7) shows the importance of limiting oxidation to minimize the generation of low pH waters with high dissolved metal concentrations. Despite low pH, high SO<sub>4</sub> and metal concentrations present in porewater of the land-based tailings, the water quality of Fox Lake remained circumneutral, likely due to the ameliorating influence of DSR (Table 4.3). The lake surface water was at equilibrium with respect to calcite suggesting this phase may be controlling the porewater pH (Fig. 4.7). The δ<sup>18</sup>O and δ<sup>2</sup>H composition of Fox Lake is indicative of evaporative enrichment in a surface water body, and suggests hydrological changes were minimal between sampling campaigns. The δ<sup>34</sup>S<sub>SO4</sub> and δ<sup>18</sup>O<sub>SO4</sub> values were consistent with the dissolved SO<sub>4</sub> being strongly influenced by DSR. Water-quality data are sparse prior to 2001, but the limited data available seems to indicate a general improvement in water quality over the 25-year period (Table 4.3).

Table 4-3: Water chemistry measured from Fox Lake (FL) surface water between 1983 and 2009. Median calculations for FL and Sherlett Lake (SL) were determined from 2002 to 2009 data. GPAL refers to the Canadian guidelines for the protection of aquatic life (CCME, 2007). Historical values from Beck<sup>a</sup> (1983) and Beck<sup>b</sup> (1988). Detection limit represented by dl. Hyphens indicate that parameter was not determined.

Date	pH	Alkalinity mgL <sup>-1</sup> CaCO <sub>3</sub>	SO <sub>4</sub> mg L <sup>-1</sup>	Fe mg L <sup>-1</sup>	Zn mg L <sup>-1</sup>	Cu mg L <sup>-1</sup>	Ca mg L <sup>-1</sup>	Mg mg L <sup>-1</sup>
1983 <sup>a</sup>	7.3	-	-	-	0.26	0.56	-	-
1988 <sup>b</sup>	7.2	48	-	1	0.5	0.01	64	5.7
2001	7.97	62	93	0.09	<dl	0.005	45	4.5
2002	8.44	57	33	<dl	<dl	<dl	47	4.6
2003	7.79	68	81	0.38	<dl	0.003	42	4.4
2004	7.34	88	84	0.19	<dl	0.006	52	4.9
2005	7.53	86	70	1.0	0.005	<dl	47	4.6
2006	8.56	70	-	-	-	-	-	-
2008	7.90	58	72	0.06	0.002	0.003	41	4.2
2009	8.05	75	70	0.13	0.002	<dl	44	4.6
FL Median	7.9	72	70	0.16	0.002	0.003	45	4.6
SL Median	7.6	25	4.5	0.10	0.10	0.002	7.6	2.8
GPAL	6.5-9.0	-	-	0.3	0.03	0.002	-	-
dl	0.01	<1	<0.01	<0.0002	<0.0005	<0.0005	<0.005	<0.0001

Sherlett Lake is a shield lake located up-stream of the former mining site and is therefore considered representative of background water quality (Beck, 1983; Moncur et al., 2014). Sherlett Lake was sampled annually between 2002 and 2009. A comparison of water quality between Fox Lake and Sherlett Lake indicated that dissolved Fe and Cu concentrations were similar; however, Fox Lake exhibited much lower dissolved Zn concentrations (Table 4.3). Elevated dissolved Zn concentrations observed in Sherlett Lake are related to weathering of sulfide-bearing waste rock from the mine that was used for construction along the shore (Moncur et al., 2014). Conversely, dissolved SO<sub>4</sub>, Ca and Mg concentrations were an order of magnitude higher in Fox Lake than Sherlett Lake, likely a result of (sulfide) mineral weathering products from the sub-aerial tailings. The  $\delta^{18}\text{O}$  and  $\delta^2\text{H}$  composition of Sherlett Lake, -12.59 ‰ and -106.1‰, respectively, shows less evaporative enrichment than Fox Lake ( $\delta^{18}\text{O}$ : -9.34‰ and  $\delta^2\text{H}$ : -92.6‰), typical of a flow-through surface-water body as described by Moncur et al. (2014). The  $\delta^{34}\text{S}_{\text{SO}_4}$  value measured for Fox Lake in 2009 (20.4‰) was indicative of strong fractionation via DSR, whereas the  $\delta^{34}\text{S}_{\text{SO}_4}$  value for Sherlett Lake (4.4‰) was more representative of sulfide-mineral oxidation (Fig. 4.8). Strong reducing conditions in Fox Lake are likely controlling dissolved metal concentrations in the surface waters, nevertheless weathering of the sub-aerial tailings is evident from the elevated dissolved concentrations of SO<sub>4</sub>, Ca, and Mg. Dissolved Fe, Zn, and Cu concentrations remained below Canadian maximum concentrations for the protection of aquatic life (CCME, 2007).

## 4.6 Conclusions

Sulfide mine tailings were deposited into Fox Lake more than 60 years ago. This deposit included sub-aerial tailings (FX) exposed to atmospheric oxygen since deposition and sub-aqueous tailings (FXS) positioned below a continuous 100 cm water cover. The sub-aerial

tailings exhibited a well-defined, ochreous oxidation zone with extensive sulfide mineral depletion that extended from surface to about 40 cm depth. A transitional zone of much weaker oxidation extended from 40 to 60 cm below the tailings surface, and the sulfide mineral assemblage remained unaltered at depths >60 cm. In contrast to the sub-aerial tailings, the oxidation zone observed in the sub-aqueous tailings was thin, extending <6 cm below the water-tailings interface.

Porewater collected from the sub-aerial tailings exhibited low pH, depleted alkalinity, and elevated concentrations of dissolved  $\text{SO}_4$  and metals (i.e., Fe, Zn, Cu). The sub-aerial tailings contained elevated populations of acidophilic sulfur oxidizing bacteria (aSOB), which catalyze sulfide-mineral oxidation at low pH in the presence of  $\text{O}_2$  and water. Increased populations of sulfate-reducing bacteria (SRB) below the ochreous zone were indicative of  $\text{O}_2$  consumption via sulfide-mineral oxidation in the overlying tailings. Conversely, the sub-aqueous tailings exhibited strong reducing conditions with porewater characterized by circumneutral pH and low concentrations of dissolved  $\text{SO}_4$  and metals. This porewater also exhibited elevated  $\text{H}_2\text{S}$  concentrations and strong  $\delta^{34}\text{S}_{\text{SO}_4}$  enrichment indicative of dissimilatory sulfate reduction (DSR) whereas the subaerial tailings porewater had depleted  $\delta^{34}\text{S}_{\text{SO}_4}$  values similar to the signature of sulfide minerals in the tailings. Marcasite occurred as secondary coatings on primary minerals within 2 cm of sub-aqueous tailings surface. Secondary covellite was also observed in this zone. These findings further emphasize the influence of reducing conditions and microbial activity on metal mobility within sub-aqueous mine tailings. Results from this study suggest that the use of sub-aqueous tailings deposition as an approach to limiting oxidation may be effective over extended time periods.

## Chapter 5:

### *Tracing the sulfur cycle at an abandoned high-sulfide tailings impoundment using chemical and isotopic techniques*

Reproduced with permission from: Moncur, M.C., Ptacek, C.J., Mayer, B., Blowes, D.W., Birks, S.J., 2009. Tracing the sulfur cycle at an abandoned high-sulfide tailings impoundment using chemical and isotopic techniques. In: A. Mehrotra, G. Hao (Eds.) 11<sup>th</sup> International Symposium on Environmental Issues and Waste Management in Energy and Mineral Production. Banff, AB. November 16-19, pp. 316-324. Editorial and formatting changes have been made to accommodate reproduction in this thesis.

## **5.1 Executive Summary**

The former Sherritt-Gordon Mine located in Sherridon, Manitoba, Canada, deposited sulfide tailing into the Woods tailings impoundment from 1937 to 1951. Since closure, microbially mediated sulfide oxidation reactions have lead to the depletion of sulfides in the near surface of the tailings. Consequently, concentrations of sulfide oxidation products were elevated in the unsaturated tailings porewater with highest concentrations of metals and lowest pH conditions present in the zone of active oxidation. Concentrations of dissolved metals and  $\text{SO}_4$  decrease below the water table, but remain elevated in deeper groundwater. At the border between the tailings and Woods Lake, concentrations of metals and  $\text{SO}_4$  decrease coinciding with significant sulfur isotope fractionation with depth indicating that bacterial (dissimilatory) sulfate reduction is responsible for this trend rather than dilution. Presently, bacterial sulfate reduction occurring at the tailings edge appears to lead to a substantial decrease in loading of dissolved metals,  $\text{SO}_4$  and low pH groundwater to Woods Lake.

## **5.2 Introduction**

When exposed to the atmosphere, sulfide-rich mine wastes oxidize and release acid,  $\text{SO}_4$  and metals to the adjacent porewater. Infiltration of rain and snow melt eventually displaces this metal-rich porewater into underlying aquifers and adjacent surface water (Nordstrom and Alpers, 1999; Johnson et al., 2000; Blodau 2004, Moncur et al., 2006). When groundwater affected by sulfide oxidation discharges to a surface water body, Fe(II) can further oxidize, producing additional acidity, and leading to serious environmental degradation (Dubrovsky et al., 1984).

The purpose of this study was to investigate the biogeochemical sulfur cycling at a high-sulfide tailings impoundment that has undergone >50 years of oxidation using sulfur isotope ratios along with other geochemical parameters. Other goals were to identify the source of  $\text{SO}_4$

and determine if  $\delta^{34}\text{S-SO}_4$  values can be used to trace the extent of mine drainage out into the receiving aquatic environment.

### **5.3 Site Background**

The former Sherritt-Gordon Mine, located in Sherridon, Manitoba (Canada), 700 km northwest of Winnipeg (Fig.5.1), processed approximately 7.7 Mt of pyritic ore between 1931 and 1951. The Zn-Cu massive-sulfide ore body produced Zn and Cu concentrates with minor amounts of Au and Ag. The 7.4 Mt of tailings (60 wt% as sulfide) were discharged into two separate tailings impoundments covering a total area of 47 ha (Fig. 5.1). The Camp tailings are 7 ha and have been oxidizing for over 70 years. The Woods tailings have been oxidizing for over 50 years and encompass an area of 40 ha and completely infill Trap Lake and about half of Woods Lake. Core extracted from piezometer nest S5 indicates that the Woods tailings were deposited on organic-bearing detrital sediments which contain vegetation fragments and diatoms indicative of a lacustrine depositional environment. Groundwater and surface water from the Woods tailings flows into Woods Lake then enters Camp Lake through Woods Weir (Fig. 5.1). Groundwater and surface water derived from both tailings impoundments flows directly into Camp Lake that discharges into Kississing Lake which has been seriously impacted by acid and metal loading (Moncur et al., 2007).

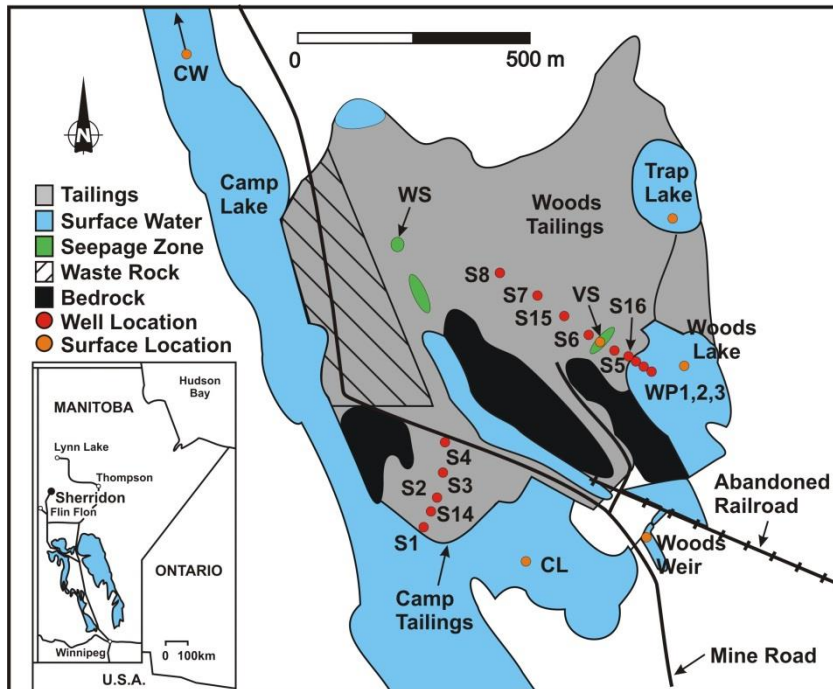


Figure 5-1: Location of Sherridon, Manitoba, Canada, and the study area including locations of the Camp and Woods tailings impoundments, and all piezometer nests. Surface water flow is to the north through Camp Lake.

## 5.4 Methods

The Woods tailings impoundment was instrumented with 9 piezometer nests, with each nest consisting of 1 to 4 drive-point and (or) bundle piezometers. At all piezometer-nest locations, continuous cores of the tailings were collected from the tailings surface to the water table or refusal, using the method of Starr and Ingleton (1992). All cores were cut into 20 to 25 cm lengths, and then sampled to determine porewater composition using a squeezing technique described by Moncur et al. (2013). Methods of piezometer installation, groundwater sampling, squeezing and water analyses used at the Woods tailings were identical to those used at the Camp tailings, described by Moncur et al. (2005). Hydraulic conductivity were measured from all piezometers using bail-tests and interpreted using the method of Hvorslev (1951)

The  $\delta^{34}\text{S}$  and  $\delta^{18}\text{O}$  values of dissolved  $\text{SO}_4$  were measured from seven porewater samples in the unsaturated zone and 12 groundwater samples from Woods tailings, and 13 surface water

samples. In addition, four secondary sulfate minerals and two primary pyrite samples were analyzed for  $\delta^{34}\text{S}$ . Soluble sulfate minerals were dissolved in distilled water followed by filtering.  $\text{BaCl}_2$  was added to all water samples to precipitate  $\text{BaSO}_4$ . The  $\text{BaSO}_4$  precipitates were washed, filtered with  $0.45\ \mu\text{m}$   $\text{NH}_4$ -acetate filters, dried and analyzed for their  $^{34}\text{S}/^{32}\text{S}$  ratios as described by Knöller et al. (2004). All isotope ratios are reported in the delta notation ( $\delta^{34}\text{S}$ ,  $\delta^{18}\text{O}$ ) as parts per thousand (‰) relative to the Vienna Cañon Diablo Triolite (VCDT) standard.

Groundwater chemistry was interpreted with the assistance of the equilibrium chemical-speciation/mass-transfer model MINTEQA2 (Allison et al., 1990). The MINTEQA2 data base was modified to make it consistent with that of WATEQ4F (Ball and Nordstrom, 1991). Field measurements of  $\text{H}_2\text{S}$  were input to calculate sulfide-mineral saturation indices at piezometer nest S16.

## 5.5 Results and Discussion

Depth to the water-table in the Woods tailings was 7.8 m below the tailings surface at S8, and intersects the tailings surface adjacent to Woods Lake near S16 (Fig. 5.2). During spring melt and storm events, seepage zones formed along the flanks of the tailings between S6 and S5. The hydraulic conductivity measured from 18 piezometers had an arithmetic average of  $1.6 \times 10^{-6}\ \text{m s}^{-1}$ . The horizontal hydraulic gradient was 0.01 between S8 and S16. There was a strong upward vertical gradient between the underlying organic-rich lake sediments and the overlying tailings. The average porosity of the tailings was 0.44, measured from eight tailings samples extracted from S6 and S15 core. Calculated groundwater velocity across the woods tailings was estimated to be  $1.2\ \text{m a}^{-1}$ .

The unoxidized Woods tailings contained nearly equal proportions of pyrite and pyrrhotite with minor amounts of sphalerite, chalcopyrite, and traces of galena, arsenopyrite



and cubanite. In the near surface oxidation zone, these sulfides were completely obliterated as the result of sulfide mineral oxidation reactions. At piezometer nest S8, the oxidized zone extends from surface to a depth of 2 m at which location a dense ferrous hardpan has formed. The hardpan extends horizontally from S8 to near S6 (Fig. 5.2). The oxidation of sulfide minerals within the Woods tailings unsaturated zone has resulted in extremely elevated concentrations of dissolved  $\text{SO}_4$  (up to  $244,000 \text{ mg L}^{-1}$ ), Fe (up to  $107,000 \text{ mg L}^{-1}$ ), elevated concentrations of trace metals and the generation of low pH conditions  $< 1$  (Fig. 5.2). The highest concentrations of dissolved metals were observed within the unsaturated zone. Near the water-table most dissolved metals and  $\text{SO}_4$  show a decline in concentrations. Although concentrations of dissolved metals and  $\text{SO}_4$  decrease below the water table, these concentrations remained elevated throughout the Woods tailings ( $\text{SO}_4$  up to  $55,000 \text{ mg L}^{-1}$ ; Fe up to  $33,000 \text{ mg L}^{-1}$ ) except near Woods Lake where concentrations of dissolved metals and  $\text{SO}_4$  showed a sharp decrease ( $\text{SO}_4$   $327 \text{ mg L}^{-1}$ ; Fe  $0.14 \text{ mg L}^{-1}$ ) coinciding with an increase in pH and alkalinity.

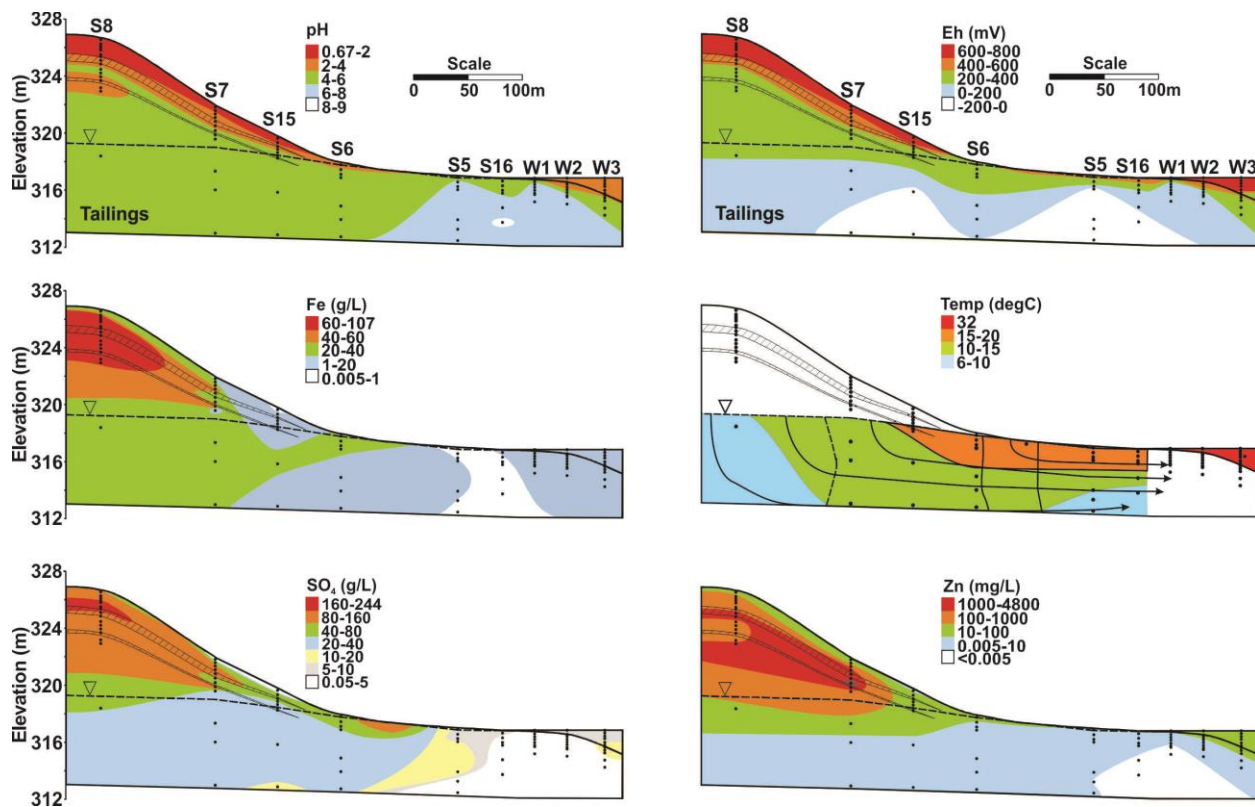


Figure 5-2: Transect of water chemistry and flow across the Woods tailings from piezometer nests S8 to W3 located in Woods Lake (Figure 5.1). Black dots represent discrete sampling locations. Dashed line with inverted triangle represents location of the water table. The cross-hatched area indicates the extent of the hardpan. Solid lines with arrows are the groundwater flow and the dashed lines are equipotential lines. Groundwater flows through the tailings from piezometer S8 to S16 directly into Woods Lake.

Values of  $\delta^{34}\text{S}$  and  $\delta^{18}\text{O}$  for dissolved  $\text{SO}_4$  obtained from the unsaturated zone porewaters, groundwaters and surface waters are presented in Fig. 5.3. Overall the  $\delta^{34}\text{S}$  values from the different water types show little variation (-1.2 to 2.1 ‰) and are similar to the  $\delta^{34}\text{S}$  values of the primary pyrite (0.2 to 1.2‰). Hydrogen sulfide was measured from all piezometers installed in the Woods tailings but the concentrations were negligible. For example, the concentration of dissolved  $\text{SO}_4$  and  $\text{H}_2\text{S}$  measured from S8 was 40,100  $\text{mg L}^{-1}$  and 0.047  $\text{mg L}^{-1}$ , respectively. The negligible concentration of  $\text{H}_2\text{S}$  is not unique to the Woods tailings, having

been observed in other studies (*e.g.* Taylor et al., 1984 a,b; Edraki et al., 2005; Dold and Spangenberg, 2005; Balci et al., 2007).

Secondary SO<sub>4</sub> precipitates have formed at groundwater seepage zones with δ<sup>34</sup>S values ranging from -0.5 to 1.3 ‰, similar to those of the adjacent seepage waters with δ<sup>34</sup>S values between -0.4 and 0.7 ‰, indicating that the secondary SO<sub>4</sub> minerals precipitated from the porewater. Previous studies have shown that sulfur isotope fractionation is minimal during the precipitation of soluble SO<sub>4</sub> minerals, typically <2‰ (Thode and Monster, 1965; Prietzel and Mayer, 2005; Edraki et al., 2005).

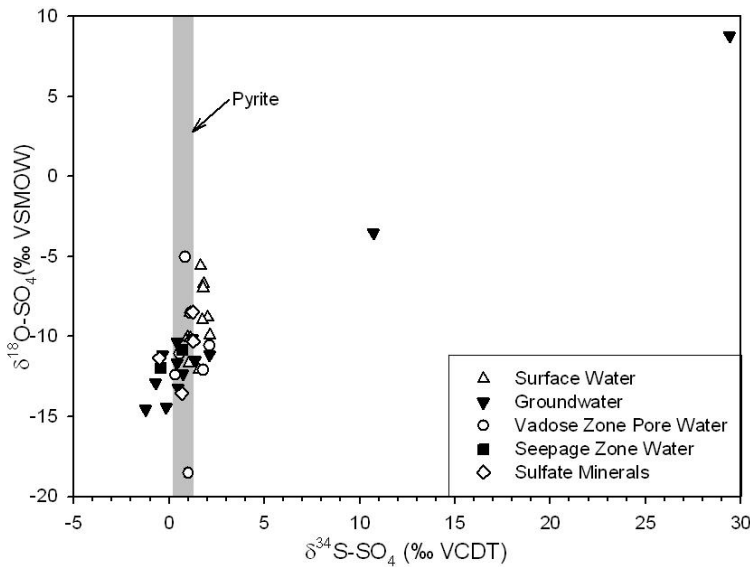


Figure 5-3: Plot of δ<sup>34</sup>S versus δ<sup>18</sup>O values of dissolved SO<sub>4</sub> from surface waters, groundwater, vadose and seepage zones and sulfate minerals. The shaded area represents the range of δ<sup>34</sup>S values (0.2 to 1.2 ‰ VCDT) from the primary pyrite.

Because δ<sup>34</sup>S values of dissolved SO<sub>4</sub> were similar to those of sulfide in the tailings, sulfur isotope ratios are a useful tool for tracing the extent of contamination to the receiving aquatic environment. There is, however, one process that is accompanied by significant sulfur isotope fractionation. At S16 the δ<sup>34</sup>S values of dissolved SO<sub>4</sub> were 1.3‰ near the tailings surface and increased to 29.4‰ with depth, suggesting that bacterial sulfate reduction was

occurring (Fig. 5.4.). Bacterial sulfate reduction is characterized by significant sulfur isotope fractionation with the remaining  $\text{SO}_4$  becoming enriched in  $^{34}\text{S}$  as the  $\text{SO}_4$  concentration decreases during the reduction process (Harrison and Thode, 1958; Kaplan and Rittenberg, 1964; Fritz et al., 1989; Habicht and Canfield, 1997; Habicht et al., 1998, Knöller et al, 2004).

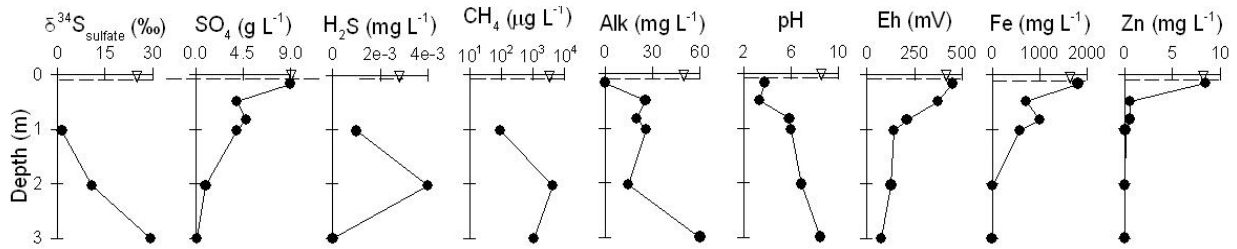


Figure 5-4: Profile through piezometer nest S16 showing groundwater chemistry with depth. Dashed line with inverted triangle represents location of the water table.

Additional evidence that bacterial sulfate reduction was occurring at S16 can be found from examination of the other geochemical parameters measured at this location. As sulfate-reducing bacteria catalyze the oxidation of organic carbon, the reduction of  $\text{SO}_4$  to  $\text{H}_2\text{S}$  (Berner, 1980) occurs through the reaction:



where  $\text{CH}_2\text{O}$  represents a generic organic compound. The organic carbon source at piezometer nest S16 likely originated from the underlying lacustrine sediments. The release of  $\text{H}_2\text{S}$  in the presence of elevated concentrations of  $\text{Fe}^{2+}$  can result in the precipitation of sulfide minerals:



where  $\text{Me}^{2+}$  denotes a divalent metal such as Fe, Cd, Ni, Cu, Co and Zn; and MeS represents an amorphous or poorly crystalline metal sulfide. The sequence of reactions in equations (5.1) and (5.2) decreases the concentrations of dissolved  $\text{SO}_4$ , Fe, and other metals, and increases alkalinity and pH (Tuttle et al., 1969; Walton-Day et al., 1990; Peine and Peiffer, 1998; Benner et al., 1999; Lindsay et al., 2009). The reduction of  $\text{SO}_4$  described in reaction (5.1) is consistent

with the trends of increased pH, alkalinity, and H<sub>2</sub>S, production of methane and with the decreased Eh with depth (Fig. 5.4). Saturation indices calculated using MINTEQA2 indicate that groundwater at piezometer nest S16 approaches saturation or becomes supersaturated with respect to Fe and Zn secondary sulfide minerals (Fig. 5.5). Although mineralogical analyses of the tailings at piezometer nest S16 were not conducted, the occurrence of secondary pyrite was observed in reducing zones of the Fox tailings (Moncur et al., 2015). Other studies (*e.g.*, Pedersen et al., 1993; Paktunc and Davé, 2002) have also reported the presence of secondary sulfide minerals in sulfate-reducing zones at mining-impacted sites which control metal and SO<sub>4</sub> concentrations. The large shift in the δ<sup>34</sup>S-SO<sub>4</sub> values and increase of H<sub>2</sub>S and CH<sub>4</sub> indicates that bacterial sulfate reduction was occurring at piezometer nest S16, limiting the loading of dissolved metals, SO<sub>4</sub> and low pH groundwater to Woods Lake. However as the organic carbon source becomes depleted, metal loading will likely increase.

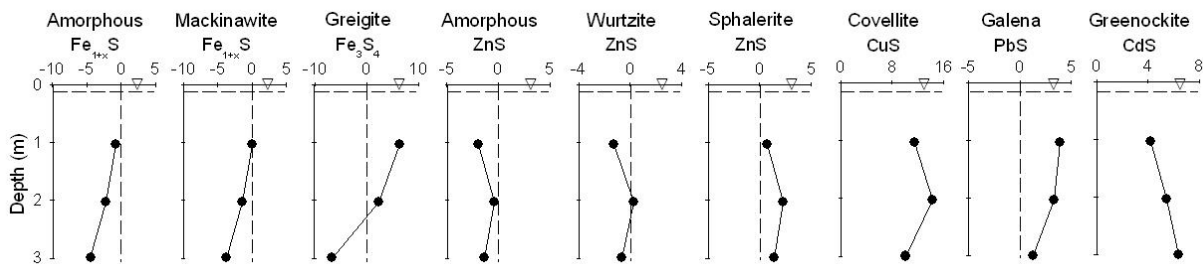


Figure 5-5: Saturation indices calculated using MINTEQA2, plotted versus depth at piezometer nest S16. Dashed line with inverted triangle represents location of the water table.

The deposition of the Woods tailings directly over native organic-rich lake sediments was likely entirely fortuitous and not intended as means to promote natural attenuation of dissolved metals and SO<sub>4</sub> through bacterial sulfate reduction. However, the geochemical and isotopic profiles through the tailings demonstrate that this organic-rich layer has promoted significant bacterial sulfate reduction resulting in decreased metal loadings, near neutral pH values and

increased alkalinity. Sediment cores from the Woods and Camp tailings impoundments showed that both tailings areas were originally deposited on top of organic-rich lake deposits. The organic layer beneath the Woods tailings is still generating sufficient dissolved organic carbon (DOC) to promote bacterial sulfate reduction, however, at the more mature Camp tailings, the production of DOC from the underlying lake sediments appears to be exhausted. In the Camp tailings, where bacterial sulfate reduction was not observed, concentrations of dissolved  $\text{SO}_4$  (up to  $58,000 \text{ mg L}^{-1}$ ), Fe (up to  $46,000 \text{ mg L}^{-1}$ ) and other metals are discharging directly to Camp Lake seriously degrading the water quality of the lake (Fig. 5.6) (Moncur et al., 2006).

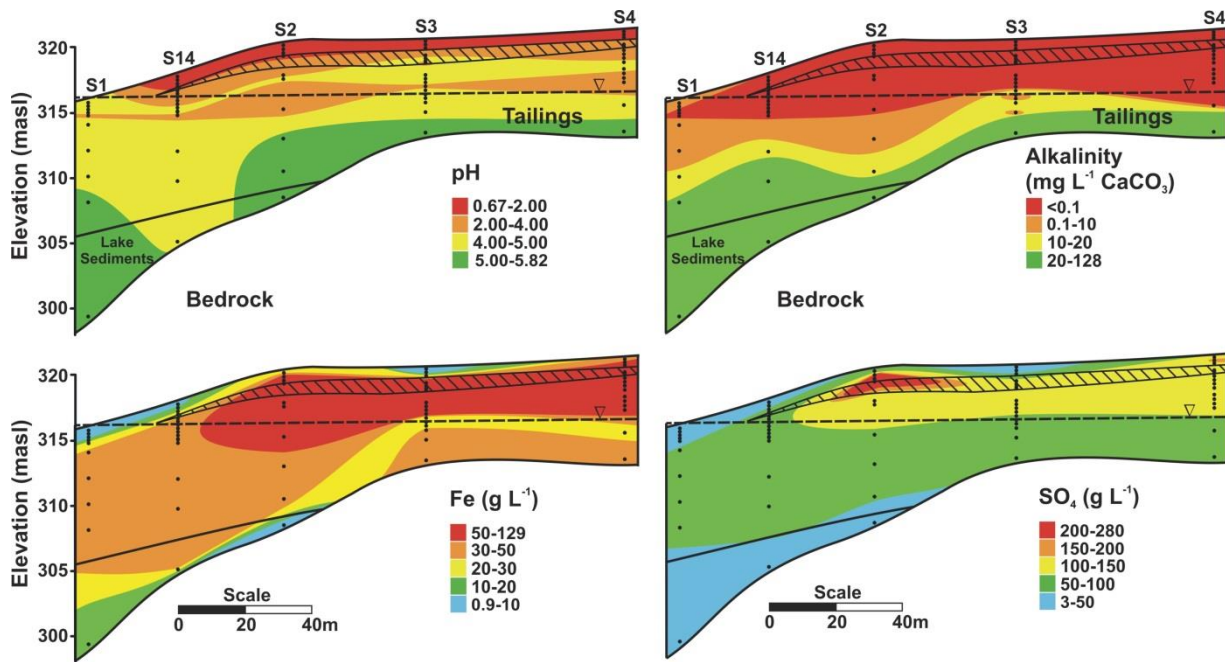


Figure 5-6: Groundwater flow and chemistry across the Camp tailings from S4 to S1 located adjacent to Camp Lake. Black dots represent discrete sampling locations. Dashed line with inverted triangle represents location of the water table. The cross-hatched area indicates the extent of the hardpan. Groundwater flows through the tailings from piezometer S4 to S1 directly into Camp Lake. Revised from Moncur et al. (2005).

## 5.6 Conclusions

The oxidation of sulfide minerals in the Woods tailings has resulted in the release of extremely elevated concentrations of dissolved  $\text{SO}_4$ , metals and acid to the groundwater and receiving

surface waters. With the exception of piezometer nest S16,  $\delta^{34}\text{S-SO}_4$  values from unsaturated zone porewater, groundwater, surface water and soluble sulfate minerals showed little variation (-1.2 to 2.1 ‰) and were similar to the  $\delta^{34}\text{S}$  values of the primary pyrite (0.2 to 1.2‰) suggesting that  $\delta^{34}\text{S}$  of  $\text{SO}_4$  constitutes a useful environmental tracer for pollutant tracing at the site. At S16,  $\delta^{34}\text{S-SO}_4$  values were 1.3‰ near the surface of the tailings and increased to 29.4‰ with depth, indicating that bacterial sulfate reduction was occurring. Bacterial sulfate reduction was further confirmed by increased pH, alkalinity,  $\text{H}_2\text{S}$ , production of methane and reducing conditions with depth. Saturation indices calculated with MINTEQA2 suggested that secondary sulfide minerals were precipitating in the zone of bacterial sulfate reduction. Bacterial sulfate reduction occurring at piezometer nest S16 was significantly limiting the loading of dissolved metals,  $\text{SO}_4$  and low pH groundwater to Woods Lake, but metal loading is expected to increase when the organic carbon source is depleted. This study demonstrates that depositing sulfide tailings over organic-rich sediments may induce bacterial (dissimilatory) sulfate reduction within the tailings leading to the attenuation of dissolved metals and  $\text{SO}_4$ .

## **Chapter 6:**

### *Occurrence and implications of efflorescent sulfate minerals from the former Sherritt-Gordon Zn-Cu mine*

Statement of Contributions for Chapter 6: Michael Moncur designed the study, conducted the field work, compiled the data, performed the modeling, assisted with the mineralogy, and wrote the manuscript.



## 6.1 Executive Summary

The former Sherritt-Gordon sulfide deposit in Sherridon, Manitoba, was mined for zinc, copper, silver and gold between 1930 and 1951. Since mine closure, two high-sulfide tailings impoundments underwent extensive oxidation resulting in the release of very high concentrations of dissolved  $\text{SO}_4$  and metals to the tailings porewater. During precipitation events and spring freshet, surface seeps develop along the flanks of the impoundments discharging groundwater with a pH as low as 0.39 and dissolved concentrations of  $\text{SO}_4$  and iron up to  $203 \text{ g L}^{-1}$  and  $68 \text{ g L}^{-1}$ , respectively, along with other metals at elevated concentrations. A number of efflorescent minerals were observed within groundwater seepage areas. Using a combination of powder X-ray diffraction and energy dispersive spectroscopy, secondary efflorescent sulfate minerals at seepage zones were identified, including melanterite, rozenite, halotrichite, chalcantinite, alpersite, copiapite, hexahydrite, jurbanite, pickeringite, jarosite and gypsum. Geochemical modeling of seepage waters using a modified WATEQ4F database for ferrous and ferric-sulfate minerals indicated the occurrence of most of the observed sulfate salts was favoured. The geochemical modelling used data available for seepage waters that were representative of discharging water after mineral precipitation had already occurred. Discrepancies between some of the observed and modeled results likely reflect the use of water compositions representative of the later stages in the reaction sequence rather than the composition during actual mineral formation. The formation of these secondary efflorescent minerals resulted in a temporary removal of  $\text{SO}_4$  and metals from solution, however these minerals rapidly dissolved during laboratory dissolution tests which would result in increased loading to receiving surface waters during precipitation events and spring freshet.

## 6.2 Introduction

Pyrite [ $\text{FeS}_2$ ] and pyrrhotite [ $\text{Fe}_{1-x}\text{S}$ ] are the primary sulfide minerals found in mine wastes. Oxidation of these minerals results in the generation of acid and elevated concentrations of dissolved  $\text{SO}_4$  and metals. Acid-sulfate water produced from sulfide oxidation reactions can lead to the precipitation of efflorescent hydrated-metal salts. During dry periods, efflorescent minerals can form by evaporative processes (Hammarstrom et al., 2005). These processes occur when the weathering products in solution exceed the mineral saturation state, allowing precipitation of secondary mineral (Alpers et al., 1994). Efflorescent minerals typically precipitate in low-temperature settings at groundwater seeps, pore spaces in the vadose zone of tailings and waste rock, mineral deposits, sulfidic shales and coalbeds (Jambor et al., 2000b; Hammarstrom et al., 2005; Chou et al., 2013). The precipitation and dissolution of efflorescent minerals are important with respect to the cycling of metals. During precipitation, efflorescent salts will temporarily sequester acid,  $\text{SO}_4$ , metals, and metalloids from solution, reducing these loadings to groundwater and surface water (Alpers et al., 1994; Jambor et al., 2000b). However, most efflorescent minerals are highly soluble and dissolve rapidly during rain events and spring freshet (Bayless and Olyphant, 1993; Alpers et al., 2000; Frau, 2000, Jerz and Rimstidt, 2003, Chou et al., 2013). The rapid dissolution of these minerals releases acid and metals which can have devastating short-term impacts to receiving aquatic environments (Nordstrom, 1977; 2009). Comprehensive reviews on secondary  $\text{SO}_4$  minerals are provided by Jambor et al. (2000b) and Chou et al. (2013).

Numerous field studies have described the occurrence of secondary sulfate minerals from mine drainage and their role in the cycling of  $\text{SO}_4$  and metals in the environment. Most of these studies have been carried out in areas where annual temperatures are well above freezing. Some

of these areas with notable occurrences of sulfate salts include Iron Mountain, California (Nordstrom and Alpers, 1999; Nordstrom et al., 2000; Jamieson et al., 2005; Sobron and Alpers, 2013), Iberian Peninsula, Spain (Buckby et al., 2003; Romero, et al., 2006; Valente et al., 2013; Parviainen et al, 2015), Sardinia and eastern Liguria, Italy (Frau, 2000; Carbone et al, 2013), Queensland, Australia (Harris et al., 2003), southeastern, USA (Jerz and Rimstidt, 2003; Hammarstrom et al., 2005) and Nevada (Peterson et al., 2006), to name a few. Limited field studies on secondary sulfate salts from mine drainage have been conducted in regions where the annual temperature is near or below 0°C (*e.g.* Wilson et al., 2009). The purpose of this study was to describe the occurrence of secondary sulfate minerals at an abandoned mine in northern Canada where the average annual temperature is near freezing with minimum temperatures below -40°C. We examine the association between the secondary salts with the seepage waters from which they formed, and evaluate controls on SO<sub>4</sub> and metal mobility during dissolution precipitation reactions using field observations and laboratory dissolution experiments.

### **6.3 Site Background**

The former Sherritt-Gordon Zn-Cu mine is located in Sherridon Manitoba, Canada, in a high-boreal region, approximately 700 km NW of Winnipeg (lat: 55.124226°, long: -101.085818°) (Fig. 6.1). Sherridon has a climate that borders between humid continental and subarctic. The mean annual temperature of the region is 0.2°C, with a minimum monthly average of -19.8°C in January and a maximum of 18.2 in July (Environment Canada, 2012). Minimum monthly relative humidity occurs in May at 64 % with maximum monthly values in November at 80 %. Average annual precipitation for the area is 488 mm, of which 150 mm occurs as snowfall. The mean annual lake evaporation in the region is 487 mm.

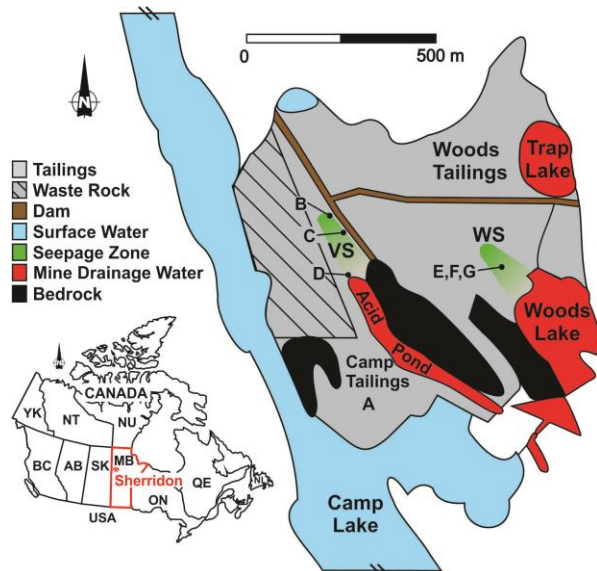


Figure 6-1: Site map of the former Sherritt-Gordon mine showing locations of the tailings impoundments and Woods seepage (WS) and Valley Seep (VS). Letters A-E refers to images in Fig. 6.2. The inset shows the location of Sherridon, Manitoba, Canada.

Sherridon is situated on Precambrian Shield of the Sherridon Group, consisting of both metasedimentary and metavolcanic rock (Froese and Goetz, 1981). Two stratiform ore bodies, each about 5 m thick, and their remobilized offshoots, are interlayered with quartz-rich gneiss. The ore consisted mainly of pyrite and pyrrhotite with minor amounts of sphalerite and chalcopyrite (Goetz and Froese, 1982) (Table 6.1). Trace amounts of galena, exsolution laths of cubanite in chalcopyrite, arsenopyrite within pyrrhotite, and native gold were also observed in the ore (Farley, 1949).

Table 6-1: Primary sulfide minerals observed in the ore (O) by Farley (1949) and the tailings (T) by Moncur et al. (2005).

Mineral	Ideal Formula	Occurrence
Pyrite	$\text{FeS}_2$	O,T
Pyrrhotite	$\text{Fe}_{(1-x)}\text{S}$	O,T
Sphalerite	$(\text{Zn,Fe})\text{S}$	O,T
Chalcopyrite	$\text{CuFeS}_2$	O,T
Cubanite	$\text{CuFe}_2\text{S}_3$	O
Galena	$\text{PbS}$	O
Arsenopyrite	$\text{FeAsS}$	O,T

Ore bodies were mined between 1930 to 1932 and 1937 to 1951, producing 0.17 Mt of Cu, 0.14 Mt of 50 percent Zn concentrate, and minor amounts of Ag (91,000 kg) and Au (2900 kg) (Moncur et al., 2005). Sulfide tailings from the mining operation were slurried into three separate impoundments covering a combined area of 47 ha (Fig. 6.1). The earlier produced tailings were discharged into the Camp tailings impoundment covering an area of 7 ha, and the Woods tailings was deposited in a 47 ha area between 1937 and 1951. A small volume of tailings, less than 1 ha, were deposited directly into Fox Lake near the end of mining in 1951.

Detailed mineralogical studies have been done on the Camp (Moncur et al., 2005; 2009) and Fox Lake (Moncur et al., 2015) tailings. In summary, sulfide minerals make up to 60 wt% of the tailings, mainly as pyrrhotite and pyrite, with minor amounts of sphalerite, chalcopyrite, marcasite, and traces of arsenopyrite (Table 6.1). Non-sulfide primary minerals in the tailings include quartz, K-feldspar, albite and biotite, with other accessory and trace silicate minerals (Moncur et al., 2005). The tailings are carbonate deficient, containing <1 % siderite. No other carbonate minerals were observed.

Since deposition, extensive sulfide oxidation has occurred in the upper 0.5 to 1 m of the Camp and Woods tailings. The lack of buffering minerals in the tailings has resulting in the generation of low pH porewaters with extremely high concentrations of dissolved SO<sub>4</sub>, Fe and metals (Moncur et al., 2005). Groundwater and surface water discharging from the tailings has seriously degraded the water quality of Camp Lake (Moncur et al., 2006). Impacted surface water flowing from Camp Lake to downstream Kississing Lake has led to elevated concentrations of metals in bottom sediment over a 10 km<sup>2</sup> area and a decline in macroinvertebrate populations (Moncur et al., 2014).

The oxidation of pyrite and pyrrhotite in the tailings has resulted in the formation of secondary minerals. Within the Camp and Woods tailings, two distinct zones of secondary

mineral precipitation have been observed in the unsaturated zone (Moncur et al., 2005; 2009b). In the active oxidation zone, a discontinuous, platy Fe(III)-rich hardpan, typically <0.1m thick was present. This ferric hardpan was composed mainly of goethite with some ferrihydrite and lepidocrocite (Table 6.2). Secondary sulfate minerals included gypsum, jarosite and trace amounts of alunite. Secondary Fe(II) mineral phases were absent. Below the active oxidation zone was a continuous Fe(II) hardpan up to 1 m thick, found at depths between 0.5 to 2 m (Fig. 6.2A). Cements in this hardpan were mainly composed of the Fe(II) minerals melanterite and rozenite, with gypsum and lesser amounts of goethite, lepidocrocite and ferrihydrite (Moncur et al., 2005). A similar melanterite-rich hardpan was observed at the Heath Steele mine by Blowes et al. (1991). During and after rain events, seepage zones formed along the flanks of the Camp tailings where the Fe(II) hardpan terminated. The seep water contained elevated concentrations of dissolved Fe up to 68 g L<sup>-1</sup>, SO<sub>4</sub> up to 150 g L<sup>-1</sup> and metals (Moncur et al., 2005). Melanterite was observed to form at these seepage zones. These seepage areas were not extensive and only produced water for a short time following precipitation events.

Table 6-2: Secondary sulfate and Fe(III)-oxyhydroxide minerals observed in the hardpan layers (Moncur et al., 2005).

Mineral	Ideal Formula
Melanterite	Fe <sup>II</sup> SO <sub>4</sub> •7H <sub>2</sub> O
Rozenite	Fe <sup>II</sup> SO <sub>4</sub> •4H <sub>2</sub> O
Jarosite	KFe <sup>III</sup> <sub>3</sub> (SO <sub>4</sub> ) <sub>2</sub> (OH) <sub>6</sub>
Alunite	KAl <sub>3</sub> (SO <sub>4</sub> ) <sub>2</sub> (OH) <sub>6</sub>
Gypsum	CaSO <sub>4</sub> •2H <sub>2</sub> O
Jurbanite	AlSO <sub>4</sub> (OH)•5H <sub>2</sub> O
Native Sulfur	S
Ferrihydrite	Fe <sup>III</sup> <sub>2</sub> O <sub>3</sub> •9H <sub>2</sub> O
Lepidocrocite	γ-Fe <sup>III</sup> O(OH)
Goethite	α-Fe <sup>III</sup> O(OH)



Figure 6-2: Photographs of the main areas where secondary sulfate minerals occurred. (A) A large block of melanterite-rich hardpan excavated from the Camp tailings; (B) the Seep Pool; note that in this photo the back wall had collapsed filling in the pool; (C) groundwater seepage from the Woods tailings dam along the Valley Seep with melanterite in the foreground; (D) a channel in the Valley Seep that collects all the groundwater seepage. Note the green colour of the water due to high concentrations of dissolved Fe(II). Photos (E) to (G) show Woods Seep (WS) in various seasons; (E) WS shortly after a rain event; (F) WS after a dry period in August with rozenite and melanterite blanketing the surface; (G) WS in October with melanterite precipitating in ATV tracks.

## 6.4 Methods

### 6.4.1 Mineral Sampling and Analyses

Sulfate salts were collected using stainless steel tweezers or a spatula. Larger samples were collected by hand wearing Nalgene gloves. Collected samples were stored using two methods. One method involved submerging the salts in mineral oil stored in sealed glass jars. For the second method, salts were tightly packed in sealed plastic containers with limited headspace and store at 4°C. In the laboratory, salts stowed in plastic containers were purged with argon gas for approximately 30 s, resealed, then stored in a freezer at -20°C. During sample collection in late

October, the air temperature was 2°C with temperatures falling to a minimum of -5°C the previous night. Relative humidity was not measured.

Three duplicate cores were collected from the wall of the SP. A 7.6 cm diameter Al core tube was driven 30 cm into the wall at heights of 0.9 m (Core A), 0.6 (Core B) and 0.3 m (Core c) above the SP. Core ends were sealed with polyethylene (PE) caps and immediately frozen. One core was collected for porewater extraction and the other used for mineralogical analyses. Minerals were identified using a combination of powder X-ray diffraction (XRD) using a Panalytical X'pert Pro diffractometer Co (K $\alpha$ ) radiation, scanning electron microscopy (SEM) and energy dispersive spectroscopy (EDS). For the XRD analyses, samples were removed from their storage containers, ground in an agate mortar, back-packed into sample holders and the diffraction data were collected immediately. Total sulfur (S) and carbon (C) were determined from core samples by combustion and infrared detection using a S and C ELTRA analyzer.

#### **6.4.2 Seep Water Chemistry**

Water was collected from seepage zones using a 60 mL polyethylene (PE) syringe, passed through a 0.45  $\mu$ m surfactant free cellulose acetate filter, then divided into separate polypropylene bottles for anion and cation analyses. Cations were preserved in the field to a pH <2 using trace-grade HNO<sub>3</sub> and analyzed using ICP-OES for major cations and inductively coupled plasma-mass spectrometry (ICP-MS) for trace elements. Anions were analyzed using ion chromatography. Water samples were stored at 4°C until analyses. In situ measurements of Eh, pH, electrical conductivity (EC), and temperature were made in the field by inserting the probes in the seep water zones. Measurements of Eh were determined using a platinum combination redox electrode, checked against ZoBell's (Nordstrom, 1977) and Light's solution (Light, 1972). The pH was measured using a Ross combination electrode calibrated with



standard pH 7, 4, and 1 buffer solutions. A combination EC-temperature probe was used to measure water EC and temperatures. Alkalinity measurements were made on filtered samples by titrating with 0.16N H<sub>2</sub>SO<sub>4</sub> to the bromocresol green–methyl red endpoint. Water sampling was conducted at the same time as the secondary sulfate salts were collected.

A squeezing method (Moncur et al., 2013) was used to remove porewater from Cores A, B and C. A viscous immiscible fluid (Paraplex™) was added to the top of each core to displace porewater downward through the core during squeezing. Expelled porewater was analyzed for anions, cations and alkalinity. Porewater Eh and pH on unfiltered samples were measured at least three times during squeezing to obtain representative values.

### **6.4.3 Speciation Modeling**

Seep water chemistry data was interpreted with the geochemical model PHREEQC version 3 (Parkhurst and Appelo, 2013) using the WATEQ4F (Ball and Nordstrom, 1991) database. The WATEQ4 database was modified to include thermodynamic data for schwertmannite (Bigham et al., 1996; Kawano and Tomita, 2001). An application of PHREEQC is to calculate saturation indices (SI) of discrete mineral phase, where a SI = 0 represents equilibrium conditions, SI > 0 supersaturated conditions, and a SI < 0 represents undersaturated condition. Saturation indices were computed from seep waters to compare calculated saturation states for various mineral phases to observed secondary minerals in the field. The Pitzer database was used to calculate the SI's of hexahydrite and gypsum and to determine the density and ionic strength of seep waters.

### **6.4.4 Laboratory Dissolution Experiments**

Batch leaching experiments were simulated using seven efflorescent minerals stored frozen in argon gas and three tailings samples from cores A, B and C. (Fig. 6.2A). Experiments were done aerobically at room temperature and involved adding 10 g of sample to a beaker containing 50

mL of ultra-pure water. A stir rod was used to continuously agitate the sample. Measurements of pH and Eh were recorded every 30 s until they stabilized, typically for 30 to 45 minutes. At the end of the experiment, the solution was collected using a 60 mL PE syringe and passed through a 0.45  $\mu\text{m}$  filter. Water samples were analyzed for dissolved anions, cations, and alkalinity.

## **6.5 Results and Discussion**

### **6.5.1 Woods Seep**

During rain events and spring freshet, groundwater seeps developed at the WS (Fig. 6.2E). This seep water was analyzed on three occasions and had an average pH of 3.4 with high concentrations of dissolved  $\text{SO}_4$  ( $118,000 \text{ mg L}^{-1}$ ), Fe ( $59,200 \text{ mg L}^{-1}$ ), Al ( $1,280 \text{ mg L}^{-1}$ ), Zn ( $160 \text{ mg L}^{-1}$ ), Pb ( $3.3 \text{ mg L}^{-1}$ ), and Cd ( $3.1 \text{ mg L}^{-1}$ ). After rain events in the summer months when temperatures were warm, efflorescent minerals would form rapidly, blanketing the surface of the WS (Fig. 6.2F). The efflorescent mineral assemblage was a mixture of mostly rozenite with melanterite. Melanterite was likely the first mineral to precipitate, but under warm, dry conditions and decreasing water activity during mineral precipitation, melanterite tends to dehydrate to rozenite (Jambor and Trail, 1963; Chou et al., 2002). During late fall and early spring when temperatures were low and relative humidity was high, melanterite was observed to accumulate in pools and along the fringes of the seepage zones (Fig. 6.2G).

### **6.5.2 Seepage Valley**

Initial seeps along the SV started at the SP where groundwater was observed to up-well into a pool approximately 2 m x 1.5 m. The walls above the pool were composed of tailings that extended to a height of about 2.5 m. The tailings that form the wall were extensively oxidized with a crust of jarosite covering the surface and intermittent Fe(III) hardpan layers. At a height of

1 m above the pool, there was an overhang supported by a hardpan shelf that sheltered the lower area from continuous direct sunlight and rain (Fig. 6.2B). Directly below the shelf were two zones of efflorescent minerals at heights of approximately 0.9 m and 0.6 m above the pool.

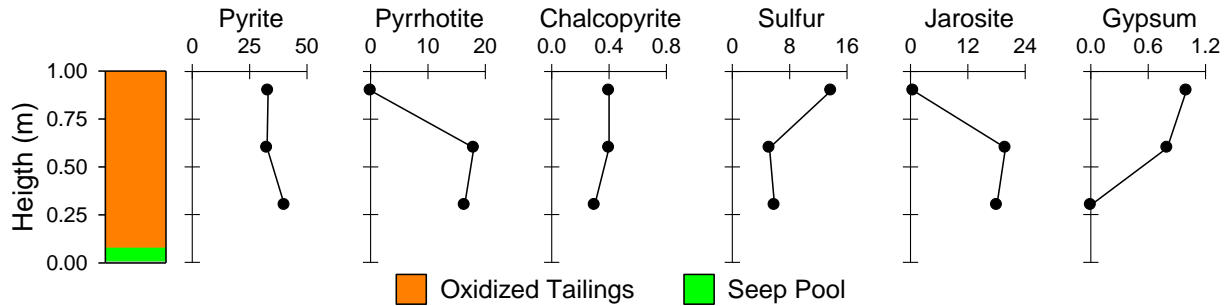


Figure 6-3: Profile of the Seep Pool area showing the locations of Core A (0.9 m), Core B (0.6 m), Core C (0.3 m) and the Seep Pool (0 m) XRD analyses of the tailings core samples are in wt. %.. Height refers to meters above Seep Pool.

At a height of 0.9 m above the pool, XRD analysis of the tailings found that sulfide minerals were extensively oxidized. In this zone, pyrrhotite was completely oxidized, resulting in the generation of elemental S (14 wt.%), a product of pyrrhotite oxidation (Fig. 6.3). In the Camp and Fox tailings, pyrrhotite typically equaled or exceeded pyrite in the unoxidized tailings (Moncur et al., 2005). Although pyrrhotite was consumed, a significant amount of pyrite (33 wt.%) was still present in the tailings. The oxidation of sulfide minerals in this zone resulted in a very low porewater pH of 0.38 and extremely elevated concentrations of dissolved  $\text{SO}_4$ , Fe, and metals (Fig. 6.4). Porewater was tacky with a blood-red color and a density of  $1.26 \text{ g mL}^{-1}$ . Redox conditions were oxidizing at +730 mV and the alkalinity was completely consumed. The main efflorescent mineral that precipitated from this acid-sulfate porewater was copiapite (Fig. 6.5; Table 6.3), a relatively common ferrous-ferric sulfate mineral found in oxidized sulfide mine wastes and ore deposits (Jambor et al., 2000b). Copiapite was observed to form as aggregates of yellow to orange clusters on the wall of the tailings. It has been proposed that the first efflorescent mineral phase to form after pyrite oxidation is melanterite, followed by the

dehydration of rozenite and finally copiapite (Nordstrom and Alpers, 1999; Jerz and Rimstidt, 2003). Neither melanterite or rozenite were identified in this zone suggesting the salts had matured, and most of the Fe(II) in the associated porewater and mineral structure had oxidized to Fe(III).

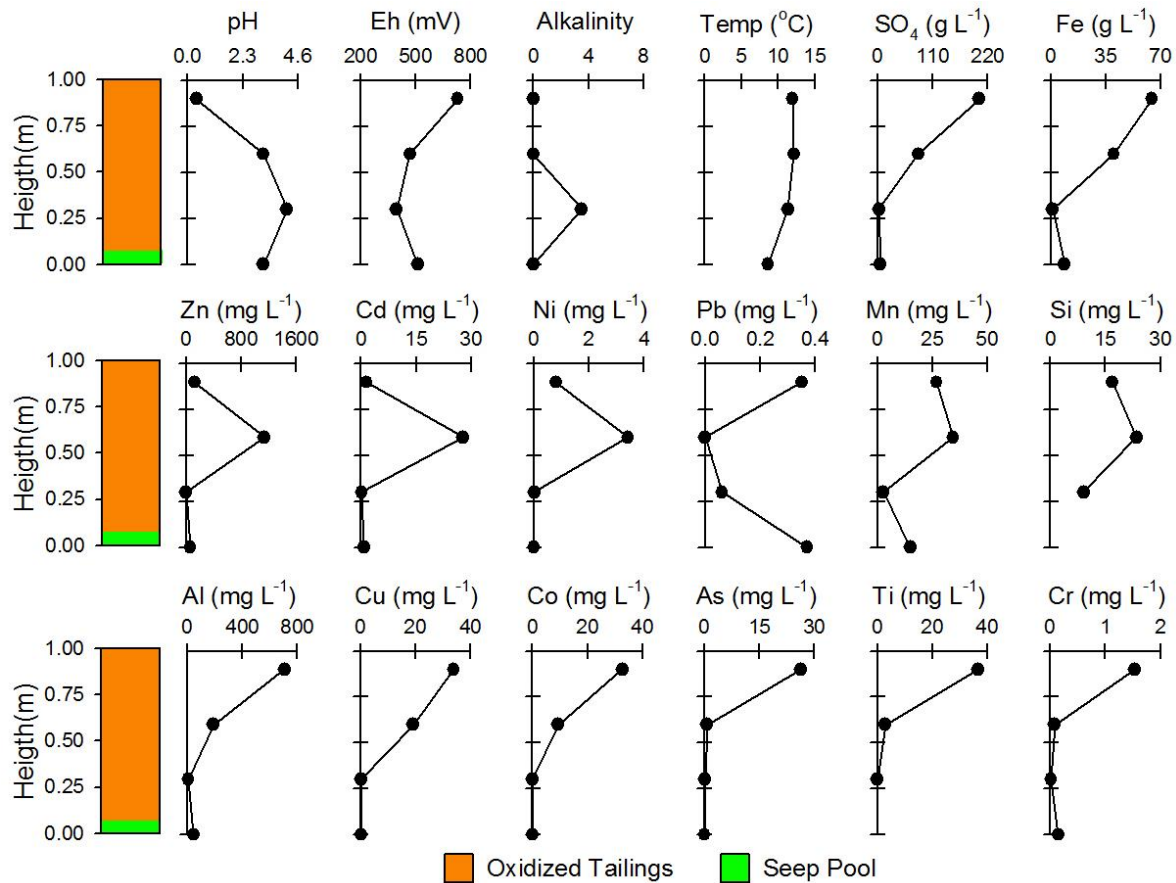


Figure 6-4: Profile of the Seep Pool area showing selected porewater chemistry from Core A (0.9 m), Core B (0.6 m), Core C (0.3 m) and the Seep Pool (0 m). Height refers to meters above Seep Pool.

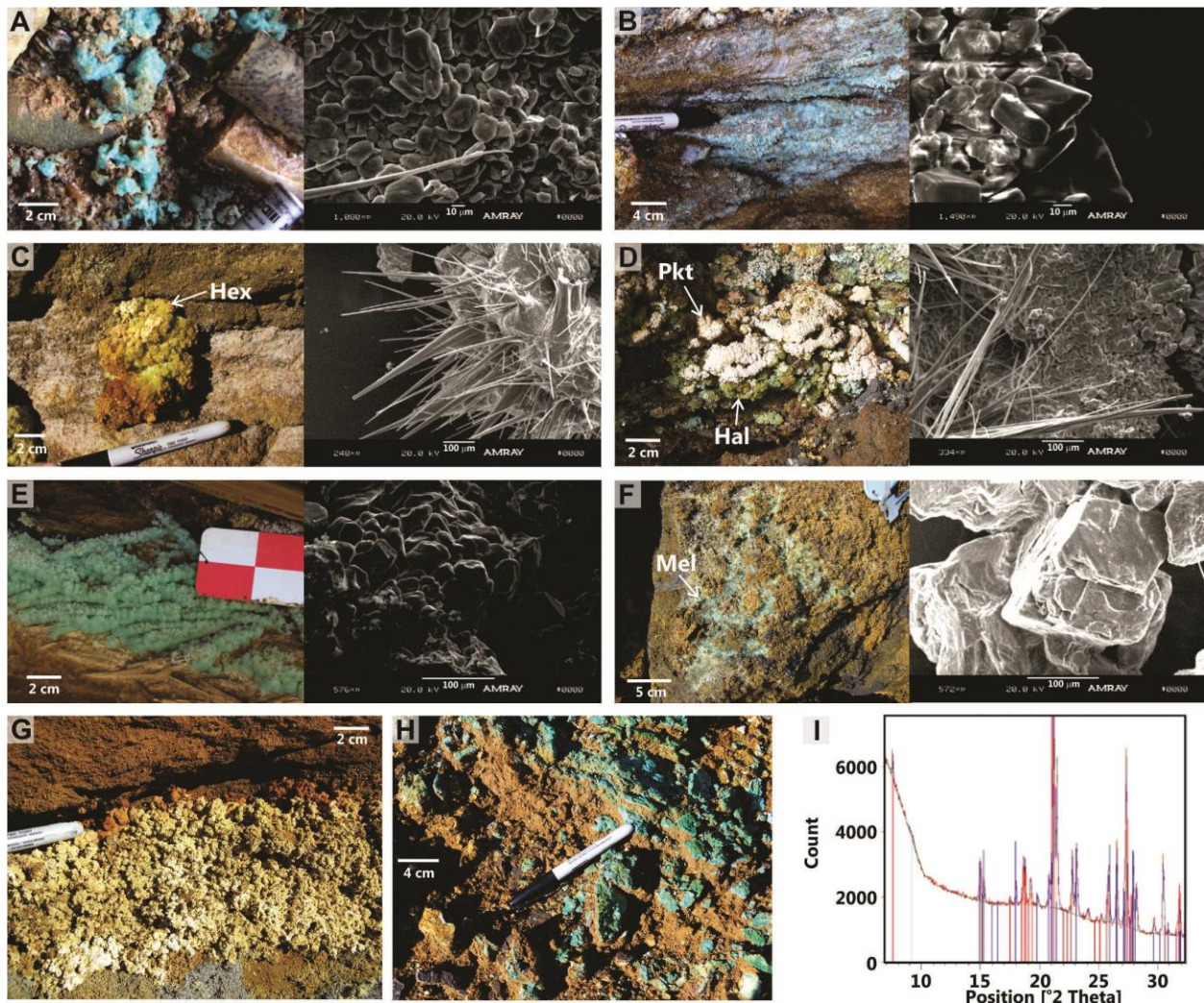


Figure 6-5: (A)-(F) show field images of the secondary mineral phases with the corresponding SEM photomicrograph: (A) alpersite; (B) mixture of alpersite and chalcantinite; (C) hexahydrite (Hex); (D) mixture of pickeringite (Pkt) and halotricite (Hal); (E) melanterite; and (F) hardpan melanterite. (G) shows an accumulation of copiapite, (H) a mixture of birnessite and gypsum; and (I) an XRD spectra showing a mixture of melanterite and jurbanite. Minerals (A)-(D) and (I) were collected from the wall of the Seep Pool where Core B was extracted and (G) from where Core A was collected; (E) and (H) are from the Valley Seep; and (F) from the Camp Tailings.

At a height of 0.6 m above the SP, pyrrhotite content in the tailings increased to 18 wt.% and concentration of elemental S decreased 5 wt.%, showing a decline in the intensity of sulfide oxidation (Fig. 6.3). The pyrite concentration in the tailings remained constant. Porewater extracted from the 0.6 m zone had a density of  $1.11 \text{ g mL}^{-1}$  with a green color, suggesting that Fe(II) was the dominant species. Although there was a decrease in dissolved  $\text{SO}_4$  and Fe by 122,000 and  $24,000 \text{ mg L}^{-1}$ , respectively, concentrations were still elevated (Fig. 6.4). Dissolved

Zn, Cd, and Ni showed increased concentrations, whereas concentrations of all other metals decreased (Fig. 6.4). The increase of Zn and Cd in porewaters is due to the oxidation of pyrrhotite, which is the main host of these metals in the tailings, whereas elevated Ni concentrations are due to pyrrhotite oxidation (Moncur et al., 2009a). The obliteration of pyrrhotite above the 0.6 m zone explains the absence of these metals, having likely been displaced downward over time. Porewater pH increased to 3.16 which corresponded to a decrease in Eh. A number of efflorescent salts were observed to precipitate in this zone (Table 6.3). The main phases identified included divalent Fe(II) minerals melanterite, rozenite, and halotrichite, and divalent Mg minerals hexahydrite and pickeringite. These efflorescent salts had precipitated on the wall below the zone of copiapite occurrence, covering the surface of the tailings as coarse granular aggregates, botryoidal blooms and globules (Fig. 6.5). Most of the salts were observed as assemblages of two mineral phases. Halotrichite and pickeringite typically coexisted (Fig. 6.5D) as did alpersite and chalcantinite (Fig. 6.5B). EDS analysis of melanterite found that it consistently contained concentrations of Zn and Cu, similar to the composition of melanterite from the Camp seeps and tailings (Moncur et al., 2005; 2009b) and Iron Mountain (Nordstrom and Alpers, 1999). One sample collected from the 0.6 m zone contained a mixture of melanterite and needles of jurbanite [ $\text{AlSO}_4(\text{OH}) \cdot 5\text{H}_2\text{O}$  (Sabelli, 1985)] (Fig. 6.4I). During EDS analysis, the jurbanite sample charged therefore it was not possible to capture a SEM image.

Table 6-3: Secondary sulfate minerals observed at seepage zones.

Mineral	Ideal Formula
Copiapite	$\text{Fe}^{\text{II}}\text{Fe}^{\text{III}}_4(\text{SO}_4)_6(\text{OH})_2 \cdot 20\text{H}_2\text{O}$
Jarosite	$\text{KFe}^{\text{III}}_3(\text{SO}_4)_2(\text{OH})_6$
Melanterite	$\text{Fe}^{\text{II}}\text{SO}_4 \cdot 7\text{H}_2\text{O}$
Rozenite	$\text{Fe}^{\text{II}}\text{SO}_4 \cdot 4\text{H}_2\text{O}$
Halotrichite	$\text{Fe}^{\text{II}}\text{Al}_2(\text{SO}_4)_4 \cdot 22(\text{H}_2\text{O})$
Alpersite	$\text{CuSO}_4 \cdot 7\text{H}_2\text{O}$
Chalcanthite	$\text{CuSO}_4 \cdot 5\text{H}_2\text{O}$
Hexahydrite	$\text{MgSO}_4 \cdot 6\text{H}_2\text{O}$
Jurbanite	$\text{Al}(\text{SO}_4)(\text{OH}) \cdot 5(\text{H}_2\text{O})$
Pickeringite	$\text{MgAl}_2(\text{SO}_4)_4 \cdot 22(\text{H}_2\text{O})$
Gypsum	$\text{CaSO}_4 \cdot 2\text{H}_2\text{O}$
Birnessite	$(\text{Na}, \text{Ca})_{0.5}(\text{Mn}^{\text{IV}}, \text{Mn}^{\text{III}})_2\text{O}_4 \cdot 1.5\text{H}_2\text{O}$
Native Sulfur	S

Melanterite was the primary mineral phase observed at the 0.6 m zone. Since melanterite is the first efflorescent mineral to precipitate (Chou et al., 2013), it may dissolved Fe(II) from the porewaters near the vicinity of the mineral. The Fe(II) depleted porewater would allow Mg and Al salts to precipitate, accordant with the paragenetic sequence observed by Jerz and Rimstidt (2003). This scenario would account for the presence of Fe(II), Mg and Al salts co-existing in the same zone (Table 6.3; Fig. 6.5). Laboratory experiments by Peterson et al. (2006) found if a solution contained concentrations of Mg that exceeded Cu then epsomite [ $\text{MgSO}_4 \cdot 7\text{H}_2\text{O}$ ] will precipitate with alpersite, however if Cu concentrations exceed Mg concentration then chalcanthite will precipitate. Epsomite was not identified during the mineralogical investigation but assemblages of alpersite and chalcanthite were observed.

Alpersite is a relatively rare efflorescent mineral typically associated with mine waste. The mineral was first described by Peterson et al. (2006) from the Big Mike mine in Nevada, with other occurrences identified from mine waters in Spain (Romero et al., 2006), Australia (Leverett and Williams, 2007) and India (Equeenuddin, 2014). Outside of mine wastes, alpersite

has been identified near active acidic volcanic systems in Nicaragua (Hynek et al., 2013) and Iceland (Hynek et al., 2014). Alpersite identified at the SP was a sugary pale blue sometimes with white needles and darker blue laths of chalcantite. Unlike melanterite, no Zn concentrations were observed in the alpersite or chalcantite during EDS analysis. Following the initial examination of alpersite, the mineral was left on the laboratory bench at room temperature. Overnight it evolved from alpersite to a siderotil/alpersite mix. After 4 months, the alpersite completely altered to siderotil with no detection of szomolnokite.

Below the 0.6 m zone, no visible secondary efflorescent minerals were present although XRD analysis indicated the presence of 18 wt.% of jarosite. At a height of 0.3 m above the pool, the outer <1 mm of the tailings were oxidized. Beneath the oxidized layer, the tailings appeared unoxidized. XRD analysis of the tailings determined there was 40 wt.% pyrite and 43 wt.% pyrrhotite, with with 6 wt.% elemental S (Fig. 6.3). This zone of the tailings contained a very high sulfide content of 57 wt.%, similar to the maximum sulfide content of 60 wt.% measured from the Camp tailings (Moncur et al., 2005). Porewater collected from this zone had a slightly acidic pH of 4.14 compared to upper acidic zones, with relatively low concentrations of dissolved  $\text{SO}_4$  ( $3,300 \text{ mg L}^{-1}$ ), Fe ( $1,400 \text{ mg L}^{-1}$ ), and dissolved metals (Fig. 6.4). This zone had the only measurable alkalinity of  $3.5 \text{ mg L}^{-1}$  of  $\text{CaCO}_3$ .

Water in the seep pool had a pH of 3.16 with concentrations of dissolved  $\text{SO}_4$  and Fe at 8800 and 5800  $\text{mg L}^{-1}$ , respectively (Fig. 6.4). No secondary efflorescent minerals were observed around the pool. The lack of efflorescent minerals below a height of 0.6 m is likely due to exposure to precipitation events and increasing moisture within the tailings. Although the moisture content of the tailings was not measured, visually the tailings became increasingly saturated towards the pool. In addition, during squeezing approximately 20 mL of water was extracted from Core-A whereas close to 100 mL was collected from Core-C. Higher moisture



contents inhibit O<sub>2</sub> diffusion, slowing sulfide oxidation reactions, resulting in porewater with lower concentrations of dissolved solids (Blowes et al., 2013). The area below 0.4 m was not sheltered from precipitation and direct sunlight, therefore the stability of efflorescent minerals would be limited (Chou et al, 2013). The air temperature was 2°C during sampling and well below freezing the previous night, however the temperatures in the pool and tailings wall porewater were around 10°C (Fig. 6.4).

Seeps along the east dam of the VS discharged groundwater with elevated dissolved SO<sub>4</sub> (25,000 mg L<sup>-1</sup>), Fe (14,000 mg L<sup>-1</sup>) and metals. Similar to observations at the WS, during early spring and late fall, melanterite precipitated in the seepage areas (Fig. 6.2B), whereas rozenite was observed in the warmer and drier summer months. Along the west wall of the VS, a turquoise material was observed on oxidized waste rock (Figure 5H). XRD analysis showed spectra for this material that was consistent with a mixture of poorly-crystalline gypsum and birnessite. Birnessite was not observed elsewhere on site.

### **6.5.3 Speciation Modeling**

Geochemical modeling was performed to calculate saturation indices (SI) of the seep waters to compare identified SO<sub>4</sub> minerals with SI values predicted with PHREEQC using the WATEQA2 database (Table 6.4). PHREEQC uses the extended Debye-Hückel equations to calculate activity coefficients of aqueous species where the ionic strength of the solution is typically limited to a maximum value of 0.7 (Ptacek and Blowes, 2000). The ionic strengths of the seep waters range from 0.13 to 8.38, beyond the optimal range of activity corrections calculated using PHREEQC. Application of the Pitzer equation (1973) is the preferred model for saline solutions with high ionic strengths (Nordstrom and Campbell, 2014), however availability of proper thermodynamic data limits calculation of discrete minerals phases in the Pitzer database. Nevertheless, Blowes et

al., (1991), Frau (2000) and Moncur et al. (2005) applied both the ion-association (IA) model used by the extended Debye-Hückel equation and the specific ion-interaction (SII) model used by the Pitzer equation, to hyperacid waters and found that both models predicted similar results for melanterite equilibrium, consistent with mineralogical observations. For example, groundwater sampled at a 3 m depth from the Camp tailings had an ionic strength of 2.8. Both the IA and the SII models calculated similar SI values of -0.21 and -0.36, respectively. For groundwater in the Camp tailings with a lower ionic strength of 0.2, IA and the SII modeling results were almost identical with melanterite SI's of -1.8 and -1.9, respectively (Moncur et al., 2005).

Table 6-4: Speciation modeling results of the seep waters from Woods Seep (WS), Valley Seep (VS) and Seep Pool (SP). The density and ionic strength of the waters were calculated using the Pitzer database. Mineral compositions are listed in Table 6.3 except schwertmannite  $[\text{Fe}_8\text{O}_8(\text{OH})_6(\text{SO}_4)\cdot n\text{H}_2\text{O}]$ .

Phase	WS-0 m	WS-40 m	VS1-0 m	VS2-50 m	SP	Core-A	Core-B	Core-C
Melanterite	0.24	-0.09	-0.81	-0.05	-1.40	-1.51	-0.07	-1.81
Schwertmannite	-9.60	-6.10	-3.80	2.00	-2.40	-34.90	-3.80	-4.10
Jarosite	0.66	2.60	2.31	5.75	0.99	-5.45	1.32	-0.23
Chalcanthite	-4.66	-4.88	-3.49	-3.90	-5.45	-2.85	-3.21	-5.49
Hexahydrite	-1.40	0.17	-2.67	-2.13	0.30	-2.08	0.38	-3.58
Jurbanite	1.12	0.84	-0.59	0.22	-0.26	-1.59	0.33	0.14
Gypsum	0.20	0.20	0.05	-0.05	-0.38	-0.16	0.31	-0.65
Ferrihydrite	-2.25	-1.88	-1.75	-0.89	-1.19	-6.31	-1.51	-0.99
Lepidocrocite	4.03	4.4	4.52	5.38	5.08	-0.20	4.77	5.28
Goethite	3.17	3.63	3.60	4.48	4.43	-0.89	3.92	4.39
Density	1.12	1.14	1.04	1.11	1.01	1.26	1.11	1.00
Ionic Strength (M)	7.46	4.50	1.10	3.50	4.71	8.38	3.64	0.13

Geochemical modeling using the IA model was consistent with field observations for melanterite. At the SP location, porewater extracted from the tailings wall was at saturation with respect to melanterite at Core-B, but undersaturated at location Core-A, Core-C and SP, consistent with melanterite identification at Core-B. Similarly, freshly-formed melanterite was

observed at locations WS-0, WS-40, VS2, but was not observed at the groundwater discharge point VS-0, also consistent with modeling results (Table 6.4; Fig. 6.2C). The absence of jarosite at Core-A and presence in Cores B and C was consistent with modeling results (Fig. 6-3; Table 6-4). Also consistent with modeling results was the observation of gypsum at locations Core A and B but absence in Core-C. Schwertmannite was not identified during the mineralogical investigation consistent with the waters being undersaturated with respect to this mineral phase. At VS2 where the waters are at saturation with respect to schwertmannite, mineralogical examination of  $\text{SO}_4$  minerals was not conducted, therefore presence of this phase was not confirmed. All seep waters were undersaturated with respect to chalcantite even though an accumulation of the mineral was observed at location Core-B. Seep geochemistry used for the speciation geochemical modelling was representative of discharging water after mineral precipitation had occurred. Discrepancies between the presence of chalcantite and modeled prediction likely reflect the use of water compositions representative of the later stages in the reaction sequence rather than the composition during actual mineral formation. There was an abundance of dissolved Fe in solution compared to dissolved Cu, therefore the speciation modeling accurately predicted secondary Fe mineral phases.

#### **6.5.4 Dissolution Experiments**

Efflorescent salts identified during this study were subjected to batch leaching experiments to evaluate whether low pH and metal-rich waters could be produced upon dissolution during rain events. Efflorescent salts used for the experiments included two melanterite samples from the SP and Camp tailings hardpan, copiapite, hexahydrate, and assemblages of halotrichite-pickeringite, and alpersite-chalcantite. The  $\text{SO}_4$  mineral assemblage of birnessite-gypsum was also used in the experiments, as well as tailings from Cores A, B, and C. Similar batch experiments to

evaluate the dissolution of efflorescent salts were described by Frau (2000), Chou et al. (2002), Hammarstrom et al. (2005), Valente et al. (2013), and Carbone et al. (2013).

The pH of all solutions containing the Fe(II), Fe(III), Mg and Cu salts rapidly declined within the first 30 s and stabilized after several minutes (Fig. 6.6), similar to observations by Frau (2000), Hammarstrom et al. (2005) and Valente et al. (2013). Nevertheless, different behaviors were observed between the soluble salts. All of the salts completely dissolved within two minutes. The batch containing the Fe(II)-Fe(III) salt copiapite showed the greatest decrease in pH to a value of 2.02, with the most oxidizing conditions, suggesting a high Fe(III)/Fe(II) ratio, suggesting the material is ferri copiapite. The batch containing tailings from Core A, the area where copiapite was collected, had a similar decline in pH and oxidizing redox conditions. The batches containing the two melanterite samples, hexahydrite and the assemblage of alpersite-chalcanthite, had a similar pH drop ranging from 3.8 and 4.08, however the batch with the hardpan-melanterite and hexahydrite solids were slightly more reduced and the batch with alpersite-chalcanthite was more oxidized (Fig. 6.6). The leachate pH for the halotrichite-pickeringite assemblage was 3.1 comparable to Core B, from where it was sampled. No efflorescent salts were observed at the location of Core C, but the pH of the batch leachate was comparable to the measured porewater pH and both had similar alkalinities of 3.5 and 4.0 mg L<sup>-1</sup> of CaCO<sub>3</sub>, respectively.

The primary mechanism leading to the decrease in pH from the dissolution of Fe-rich efflorescent salts was Fe(II) oxidation. The presence of Fe(III) may promote an additional decrease in pH (Frau, 2000). Furthermore, dissolution of phases containing trivalent ions such as Al(III), present in pickeringite, halotrichite and jurbanite will produce additional H<sup>+</sup> (Valente, et al., 2013). The alpersite-chalcanthite assemblage had the highest pH compared to the other SO<sub>4</sub> salts, consistent with deficiencies of Fe and Al in their structures.

Unlike the efflorescent minerals, dissolution of the birnessite-gypsum assemblage increased the leachate to a pH of 8.15 and produced 19 mg L<sup>-1</sup> of alkalinity. After 45 min reaction time, only 1.79 mg of the 10.0 mg of the birnessite-gypsum assemblage had dissolved. Birnessite is relatively insoluble in water therefore it is assumed that mostly gypsum dissolved during the dissolution batch tests.

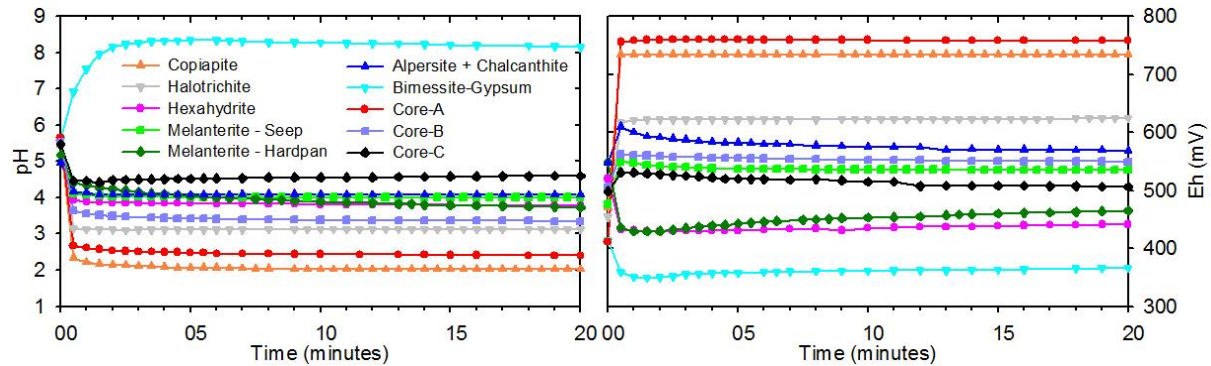


Figure 6-6: Results from the dissolution experiments showing pH and Eh variations over time.

Following a 20 to 45 minute reaction time, leachate samples were collected for anion and cation analyses. No secondary precipitates were observed in the leachate. Dissolution of these salts showed a variety of dissolved metal(oid)s released to solution (Table 6.5). Upon dissolution of the efflorescent salts, leachate waters were dominated by dissolved SO<sub>4</sub> and Fe, except in the alpersite-chalcantinite and halotrichite-pickeringite phases, which were relatively Fe deficient, as expected. Although Zn and Cu were not detected in alpersite or chalcantite during EDS analyses, the leachate contained the highest concentration of these metals, in addition to Ni, Cd and Co, suggesting that there were likely impurities associated with the mineral phases. Dissolution of the halotrichite-pickeringite assemblage released the highest concentration of dissolved Al, consistent with its elemental composition. Dissolution of hexahyrite released the highest concentration of dissolved Zn, Cd and Co, whereas copiapite dissolution released elevated Co and As concentrations (Table 6.5). The highest Cd concentrations were associated with elevated

Zn concentrations, consistent with Hammarstrom et al. (2005) who observed the release of Cd from Zn-rich efflorescent salts. The source of Cd is from the oxidation of sphalerite (Moncur et al., 2009a). Dissolution of the hard pan and surficial seep melanterite samples released almost identical concentrations of dissolved SO<sub>4</sub>, Fe and metal(oid)s even though they formed under different redox conditions (Table 6.5). For example, the Eh of seep water during collection of the melanterite ranged from 410 to 570 mV, whereas the Eh of porewater in the melanterite-rich hardpan ranged from 360 to 410 mV. This observation suggests that uptake of ions during melanterite formation may be consistent in differing redox condition. The main ion released during the dissolution of birnessite-gypsum was SO<sub>4</sub>, with only minor amounts of Fe and metal(oid)s in the leachate, compared to the efflorescent salts.

Table 6-5: Results from the dissolution experiments showing concentrations of dissolved SO<sub>4</sub> and metal(oid)s. Abbreviations refer to melanterite (Mel), alpersite (Alp), chalcantinite (Chl), halotrichite (Hal), pickeringite (Pkt), hexahydrate (Hex), birnessite (Bir) and gypsum (Gyp).

Mineral	SO <sub>4</sub> mg L <sup>-1</sup>	Fe mg L <sup>-1</sup>	Zn mg L <sup>-1</sup>	Cu mg L <sup>-1</sup>	Al mg L <sup>-1</sup>	Ni µg L <sup>-1</sup>	Cd µg L <sup>-1</sup>	Co µg L <sup>-1</sup>	Cr µg L <sup>-1</sup>	As µg L <sup>-1</sup>
Copiapite	18,000	6,400	19	43	250	64	75	7,100	59	1,700
Mel-HP	13,000	6,900	47	137	1.4	154	83	5,000	2.3	1.3
Mel-SP	12,100	6,100	44	141	1.8	150	78	6,500	1.9	1.8
Alp-Chl	13,100	2.9	1,300	2,700	87	10,700	3,000	9,300	4.1	11
Hal-Pkt	16,500	16	410	540	2,000	4,000	3,100	2,800	61	49
Hex	12,900	4,900	1,300	24	170	1500	41,400	12,900	1.8	5.3
Bir-Gyp	1,100	1.3	0.65	0.10	0.13	21	14	9.4	3.3	< 0.3
Core-A	1,200	430	4.20	2.8	26	7.6	18	300	12	200
Core-B	400	160	21	8.9	7.9	23	200	200	1.1	2.3
Core-C	31	2.7	6.9	3.7	0.37	5.2	91	21	0.94	1.5

### 6.5.5 Environmental implication

To assess the influence efflorescent salts had on sequestering SO<sub>4</sub> and metals from waters in seepage zones, water samples were collected at the seepage point and downstream from the WS and VS areas. During sampling, melanterite was observed along the seepage zones at both locations. Seep water sampled in late October from the initial discharge point at WS had a pH of

3.20 with extremely elevated concentrations of SO<sub>4</sub> (151,000 mg L<sup>-1</sup>), Fe (67,800 mg L<sup>-1</sup>) and some metals (Table 6.6). Seepage water collected approximately 40 m downstream from the discharge point had a decrease of about 30 % for dissolved SO<sub>4</sub> and Fe. This near 1:1 ratio of SO<sub>4</sub> and Fe is consistent with the stoichiometry of melanterite [FeSO<sub>4</sub>•7H<sub>2</sub>O]. In addition to SO<sub>4</sub> and Fe uptake, metals including Zn, Cu, Al, Cd and As decreased in concentration, however Co and Cr increased. At the VS where water samples were collected approximately 50 m downstream from the seep discharge point, dissolved SO<sub>4</sub> and Fe also had a 1:1 decrease in concentration, although only a 16 % reduction (Table 6.6). Concentrations of Zn and Cu in the VS water increased over distance, unlike downstream waters at the WS that showed a decrease.

Seepage waters along the VS eventually flow into a drainage channel (Fig. 6.2D).

Concentrations of SO<sub>4</sub> and Fe in the channel decreased by 70% relative to the initial seepage water concentrations. The ratio of dissolved SO<sub>4</sub> to Fe remained at about 1:1, suggesting that removal of these constituents through the formation of melanterite likely was a major control on water composition, also evident from the accumulation of this phase throughout the seepage areas. Within the channel water, Al, Ni and Cd decreased in concentration, but Zn, Cu, Co and Cr all increased, suggesting melanterite may have reached its maximum capacity for sorption or co-precipitation of these metals.

Table 6-6: Selected water chemistry from the Woods Seep (WS) and Valley Seep (VS). All concentrations are in mg L<sup>-1</sup>. A negative % change refers to a decrease in concentration. Concentrations in mg L<sup>-1</sup>.

Seep	pH	SO <sub>4</sub>	Fe	Zn	Cu	Al	Ni	Cd	Co	Cr	As
WS-0 m	3.20	151,000	67,800	164	0.57	1,130	<0.01	3.92	0.03	<0.005	1.8
WS-40 m	3.06	102,000	43,100	107	0.43	876	<0.01	3.12	0.06	0.050	1.5
% Change	-4	-32	-36	-35	-25	-22	-	-20	+100	+900	-17
VS1-0 m	3.47	80,200	54,300	28	0.40	219	0.541	3.7	0.32	< 0.005	< 0.1
VS2-50 m	2.68	68,000	45,500	70	4.0	329	0.54	3.2	0.30	< 0.005	<0.1
VS3-Channel	2.30	24,900	14,000	33	15	130	0.404	1.2	0.65	0.030	< 0.1
% ChangeV1-V2	-23	-15	-16	+150	+900	-50	-0.2	-14	-6	-	-
% ChangeV1-V3	-34	-70	-75	+18	+3700	-41	-25	-68	+103	+500	-

Groundwater and surface water runoff from the Camp and Woods tailings discharge directly into Camp Lake (Fig. 6.1). Camp Lake is a small Precambrian shield lake approximately 2.75 km long that receives freshwater inflow from Sherrlet Creek in the south, with the only outflow to the north through Camp Weir. Water chemistry from Sherrlet Creek and Camp Weir were sampled weekly during the spring and biweekly for the remainder of the year, from 2001 to 2006, to assess the seasonality of  $\text{SO}_4$  and metal loadings (Moncur et al., 2014). Results from this study showed that a spike in dissolved  $\text{SO}_4$  and metal concentrations occurred during spring freshet, decreased after peak discharge, then loadings gradually increased over the summer months until freeze-up at which time concentrations declined rapidly (Fig. 6.7). The initial abrupt surge in dissolved  $\text{SO}_4$ , metals and acid is known as the “first flush” (Younger and Blachere, 2004), where an accumulation of soluble oxidation products are flushed from mine wastes. The gradual increase of dissolved  $\text{SO}_4$  and metals over the summer months in 2003 and 2004 likely represented periods of lower surface run-off with greater input of saline groundwater (Nordstrom, 2009). In late fall, a sudden decrease in acid,  $\text{SO}_4$  and metal concentrations is correlated to the first appearance of ice over Camp Lake (Moncur et al., 2014). During the study, no water sampling was conducted to evaluate short-term loading of  $\text{SO}_4$  and metals during or after a precipitation event. However, from June 23-24, and July 7-15, 2005, the area received heavy rainfall of 49 and 106 mm, respectively. This heavy rainfall did not cause a significant rise in discharge but resulted in an abrupt peak of acid, dissolved  $\text{SO}_4$ , Fe, Zn, Al and other metals discharging over Camp Weir (Fig. 6.7). For example, the pH dropped from 5.0 to 3.1, with significant rises in  $\text{SO}_4$  (64 to 200  $\text{mg L}^{-1}$ ), Fe (8 to 570  $\text{mg L}^{-1}$ ), Al (0.8 to 31  $\text{mg L}^{-1}$ ), Zn (0.5 to 13  $\text{mg L}^{-1}$ ) and Cu (0.05 to 1.0  $\text{mg L}^{-1}$ ). Concentrations remained elevated until the rainfall subsided. The dissolved concentration of Fe, Zn, and Al exceeded values observed at any other time during the study, as did the precipitation, resulting in the highest loadings of these metals



over Camp Weir (Moncur et al., 2014). No abnormal peaks of dissolved ions were observed in Sherlett Creek waters during these heavy rain events. The dissolution of efflorescent salts and flushing of metal-laden porewater from the unsaturated zone was the likely cause of the abrupt increase in  $\text{SO}_4$  and dissolved metal concentrations. This peak-loading due to efflorescent salt dissolution response to large precipitation events has also been reported at other mine sites (*e.g.* Bayless and Olyphant, 1993; Keith et al., 2001; Hammarstrom et al., 2005; Cánovas et al., 2008; 2010, Nordstrom, 2009; Sarmiento et al., 2009, and Chou et al., 2013).

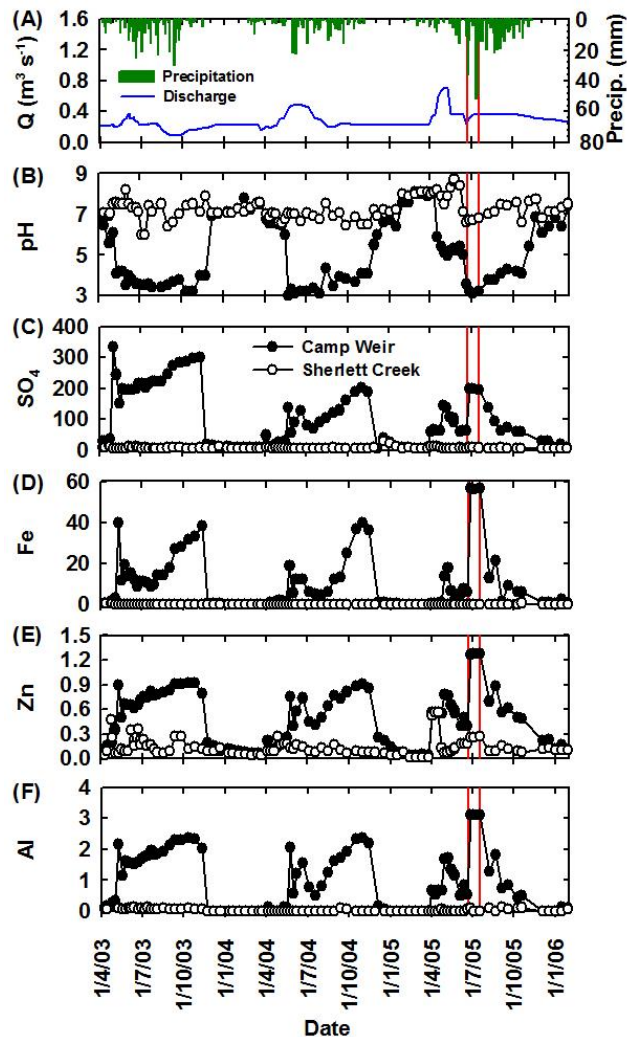


Figure 6-7: Temporal plots showing (A) discharge from Camp Weir and precipitation; water chemistry from Sherlett Creek and Camp Weir showing (B) pH; dissolved concentrations of (C)  $\text{SO}_4$ ; (D) Fe; (E) Zn; and (F) Al. Revised after Moncur et al. (2014). Vertical red lines represent a period of above normal precipitation. Concentrations in  $\text{mg L}^{-1}$ .

## 6.6 Conclusions

Extensive sulfide oxidation in the Woods tailings has resulted in the generation of groundwater seeps with low pH and elevated concentrations of dissolved  $\text{SO}_4$  and metals. During rain events and spring freshet, seeps formed at the toe of slopes discharging this hyperacidic saline groundwater. In early spring and late fall when temperatures were near freezing and the relative humidity was high, formation of melanterite was common at seepage zones. During the summer months melanterite rapidly dehydrated to rozenite. At a seepage pool that was observed to continuously flow during the thawed seasons, a sheltered area of tailings above the pool contained an abundance of efflorescent salts. Copiapite was associated with water containing a low pH of 0.38, oxidizing Eh of 730 mV and the highest dissolved concentrations of  $\text{SO}_4$  and Fe, whereas Fe(II) and Mg salts precipitated in a zone where the pH was 3.2, with a Eh of 470 mV and lower concentration of  $\text{SO}_4$  and Fe. Water sampled downstream from the seepage discharge points revealed that dissolved Fe and  $\text{SO}_4$  were removed from solution at a 1:1 ratio, consistent with the stoichiometry of melanterite. Acid and metals were also sequestered from solution, limiting their concentrations.

Dissolution experiments of the efflorescent salts showed that these minerals rapidly dissolved, resulting in leachate with a low pH and high dissolved  $\text{SO}_4$ , Fe and metals, similar to seep waters. The abundance of metals in the leachate such as Al, Zn, Cu, Co, Cd, Co, and As indicates that the efflorescent salts scavenge metal(oid)s during precipitation acting as a transient sink. Although a number of salts were collected from the same seepage area, differing chemical composition of each salt resulted in leachate with a distinct pH and dissolved metal concentrations.

## Chapter 7:

### *Seasonal cycling and mass-loading of dissolved metals and sulfate discharging from an abandoned mine site in northern Canada*

Reproduced with permission from: Moncur, M.C., Ptacek, C.J., Hayashi, M., Blowes, D.W., Birks, S.J., 2014. Seasonal cycling and mass-loading of dissolved metals and sulfate discharging from an abandoned mine site in northern Canada. *Appl. Geochem.* 41, 176–188. Copyright 2015 Elsevier Ltd., License Number 3603470605805. Editorial and formatting changes have been made to accommodate reproduction in this thesis.

## 7.1 Executive Summary

Drainage from sulfide-rich mine waste can contaminate surface waters directly by surface runoff and indirectly through groundwater discharge. The Camp Lake watershed, located in northern Manitoba, receives both direct and indirect drainage from an abandoned tailings impoundment which has resulted in severely degraded water quality. Sulfide oxidation has been occurring for over 70 years at an abandoned mine site in this watershed, resulting in high concentrations of oxidation products in the surface water and groundwater discharging from the two tailings impoundments, both of which flow into the adjacent Camp Lake. A 5-year hydrological and geochemical sampling program was conducted at this small Precambrian shield lake prior to the initiation of remedial actions, to identify the seasonal distribution and mass-loading of dissolved metals and  $\text{SO}_4$  discharging from Camp Lake to the downstream Kississing Lake. Weekly and biweekly sampling of outflow from the lake clearly showed a seasonal cycle of dissolved metals,  $\text{SO}_4$  and pH. During months when the lake was ice-covered, the discharge water had a neutral pH with low concentrations of dissolved metals and  $\text{SO}_4$  similar to background concentrations. At spring melt the discharge sampled at Camp Weir revealed abrupt increases in dissolved metal and  $\text{SO}_4$  concentrations and decreases in pH to values that remained relatively constant until fall freeze-up, when dissolved metal concentrations and pH returned to winter values. The annual and interannual variations in loadings measured at Camp Weir are different from those measured at the two streams feeding Camp Lake showing the contribution of groundwater flow through the tailings to  $\text{SO}_4$  and metal loadings to the lake during dry years and the potential for significant loadings due to flushing of the thick unsaturated zone in the tailings during relatively wet years. The abrupt changes in pH, metal and  $\text{SO}_4$  concentrations and the timing of these changes with the appearance and disappearance of ice-cover on the lakes suggests a combination of physical

and geochemical controls related to shifts in sources of water, mixing and changes in solubility. Despite fairly low average annual metal concentrations measured in Camp Lake discharge, concentrations of Zn and Cu were elevated above background in bottom sediments of Kississing Lake in a zone extending 9.5 km<sup>2</sup> from the location of Camp Lake inflow. These results show the importance of the open-water period in controlling metal discharge from mine-impacted areas, and demonstrate that even when average annual concentrations are only slightly elevated, long-term metal loadings can have a significant impact on the receiving aquatic systems.

## **7.2 Introduction**

When exposed to the atmosphere sulfide-rich mine wastes oxidize and release acid, SO<sub>4</sub> and metals to the environment. Discharge of this metal-rich water can lead to severe degradation of water quality in receiving waters (Nordstrom and Alpers, 1999; Moncur et al., 2006; Nordstrom, 2011; Maia et al., 2012; Walton-Day and Mills, 2015). The impacts of acid rock drainage (ARD) can be observed at a variety of scales ranging from small tributaries to entire watersheds downstream from active or abandoned mine operations (Kimball et al., 2002).

Seasonal variations in water quality measured in streams impacted by ARD have been reported in a number of studies (McKnight and Bencala, 1990; Alpers et al., 1992; Brooks et al., 2001; August et al., 2002; Stillings et al., 2008; Butler et al., 2008; Sarmiento et al., 2009, 2012; Gozzard et al., 2011), however the majority of these studies were limited to short-term monitoring (1–2 years), with reported seasonal variations in water chemistry limited to monitoring during a couple of spring freshets. The goal of the current study is to better understand long-term seasonal variations and impacts to a stream receiving ARD. A mining impacted lake that has been receiving mine effluent for over 70 years was selected, and detailed weekly and biweekly monitoring of the fluxes of water and metals was conducted over a 5 year

period. The specific research objectives were to: (1) understand geochemical processes controlling seasonal variations in water quality in three streams, (2) quantify mass-loading during ice-covered and ice-free periods and (3) assess the impact to a down-gradient water body receiving the mine drainage.

### 7.3 Study Area

The former Sherritt-Gordon Mine, located in Sherridon Manitoba, 800 km northwest of Winnipeg (Fig. 7.1), processed approximately 7.7 Mt of pyritic ore between 1931 and 1951. Zinc and Cu concentrates with minor amounts of Au and Ag were produced from a Zn–Cu volcanic massive-sulfide ore body. The tailings contain up to 60 wt.% as sulfide, mainly as pyrrhotite  $[\text{Fe}_{(1-x)}\text{S}]$  and pyrite  $[\text{FeS}_2]$ , with pyrrhotite equaling or exceeding pyrite in all samples. Other primary sulfide minerals in the tailings are sphalerite  $[(\text{Zn},\text{Fe})\text{S}]$ , chalcopyrite  $[\text{CuFeS}_2]$ , marcasite  $[\text{FeS}_2]$ , and trace amounts of arsenopyrite  $[\text{FeAsS}]$  and galena  $[\text{PbS}]$  (Moncur et al., 2005; 2009). Tailings were discharged into two separate tailings impoundments covering a total area of 47 ha. The Camp tailings are 7 ha in area and were deposited between 1931 and 1932 whereas the Woods tailings are 40 ha in area and were deposited between 1937 and 1951 (Fig. 7.2). The current study was conducted between 2001 and 2006, prior to the initiation of remedial activities in 2008.

Extensive oxidation in the upper 50 cm of the Camp tailings resulted in the generation of tailings porewater with extremely high concentrations of dissolved  $\text{SO}_4$  and metals (pH < 1, 129  $\text{g L}^{-1}$  Fe, 280  $\text{g L}^{-1}$   $\text{SO}_4$ , 55  $\text{g L}^{-1}$  Zn, 7.2  $\text{g L}^{-1}$  Cu, and other metals (Moncur et al., 2005).

Although concentrations of dissolved metals and  $\text{SO}_4$  decreased below the water table, these concentrations remained elevated throughout the Camp tailings impoundment with up to 61  $\text{g L}^{-1}$  Fe and 92  $\text{g L}^{-1}$   $\text{SO}_4$  observed in the deeper groundwater (Moncur et al., 2005). Detailed profiles

of  $^3\text{H}$  and hydraulic head distributions across the tailings indicate that groundwater from the Camp tailings discharged directly to Camp Lake (Moncur et al., 2005; 2006).

Camp Lake is a small, narrow, Precambrian shield lake 2.75 km in length that remains ice covered for 6–7 months of the year. Camp Lake consists of two basins and a semi-isolated bay and has an area of  $1.2 \text{ km}^2$ , a mean depth of 4.3 m, a maximum depth of 10.5 m, and a total volume of  $2.7 \times 10^6 \text{ m}^3$ . Approximately 85% of the shoreline consists of gneissic bedrock that is stained rusty red along the high waterline. The remaining 15% of the shoreline is comprised of mine tailings and waste rock (Moncur et al., 2006).

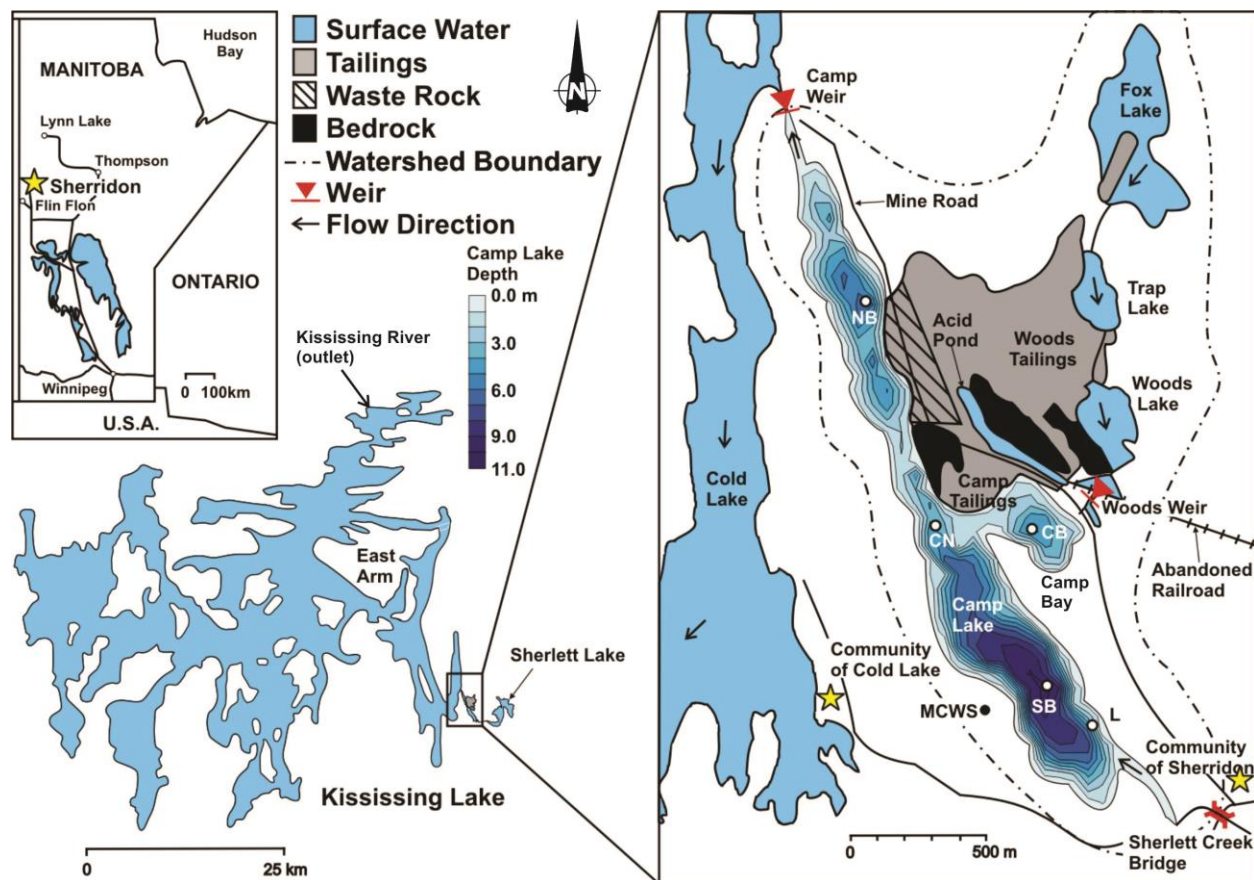


Figure 7-1: Map of the study area showing the location of Sherridon (inset), tailings impoundments, lakes, weirs, streams, communities and mine site. Abbreviations represent: MCWS – Manitoba Conservation Weather Station; L – Lodge; SB – South Bay; CB – Camp Bay; CN – Camp Narrows; and NB – North Bay.

Camp Lake has a local watershed of 6 km<sup>2</sup> with the two tailings impoundments making up 20% of this area. There are only two surface inflows to the lake: inflow from Sherlett Creek bringing water from the unimpacted upstream watershed and inflow from the Fox Lake watershed which enters the lake over Woods Weir (Fig. 7.1). Over 95% of the water input to Camp Lake is from Sherlett Creek (Beck, 1983; Moncur et al., 2006). The only surface-water outflow from the lake is through Camp Weir, a rectangular concrete weir constructed in 1989 at the north end of the lake with removable timber stoppers to control outflow. The total watershed area drained by Camp Lake, including the Sherlett Creek watershed, is 107 km<sup>2</sup>.

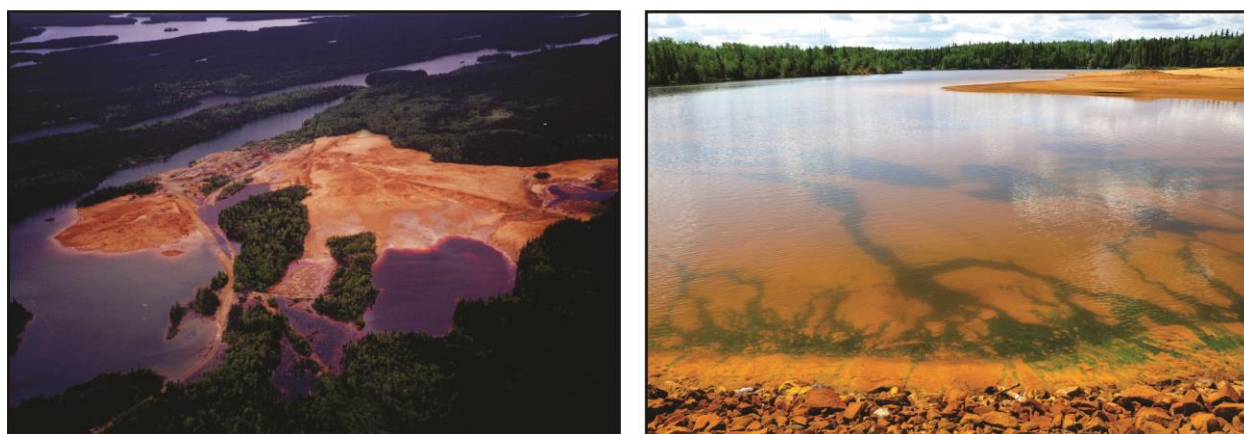


Figure 7-2: Image on the left shows an aerial view of the abandoned mine site with the Woods tailings in the foreground, the smaller Camp tailings and the proximity of the community of Cold Lake in the upper left. Image to the right looking SW across Camp Lake with the Camp tailings in the upper right of the image; note the green density-driven seepage discharging near shore and extending out into Camp Lake along topographic low points in the lake bed.

Discharge of surface water and groundwater from the tailings impoundments into Camp Lake has seriously degraded the water quality. Effluent from the Camp tailings discharges directly into Camp Lake Bay. This aqueous effluent has altered the composition of Camp Lake water, which in turn has modified the physical limnology of the lake. Geochemical profiles of the water column indicate that, despite its shallow depth (6 m), Camp Lake Bay is stratified throughout the year. The greatest accumulation of dissolved metals and SO<sub>4</sub> is in the lower portion of the water column, with observed concentrations including up to 20 g L<sup>-1</sup> SO<sub>4</sub>, 8.5 g L<sup>-1</sup>



Fe, and  $0.3 \text{ g L}^{-1}$  Zn (Moncur et al., 2006). Meromictic conditions and very high solute concentrations are not limited to Camp Lake Bay. Even though solute concentrations are lower outside of the bay, chemical stratification of the water column has been observed throughout the lake. Mineralogical analysis of lake bottom sediments indicates that the formation of secondary ferric oxyhydroxides, gypsum [ $\text{CaSO}_4 \cdot 2\text{H}_2\text{O}$ ] and secondary-sulfides are limiting the concentrations of dissolved Fe and  $\text{SO}_4$  and possibly other metals (Moncur et al., 2006).

Discharge from Camp Lake flows directly into Cold Lake, an easternmost arm of Kississing Lake (Kississing Lake surface area:  $179 \text{ km}^2$ ). Cold Lake is 8.2 km in length and has a  $172 \text{ km}^2$  drainage basin, with 66% of the inflow coming via Camp Lake (Beck, 1983). Drainage from Kississing Lake discharges at the north end of the lake. A prominent feature of Cold Lake is the rusty red discoloration above the high waterline between the Camp Lake outlet and the Cold Lake outlet to Kississing Lake, a further indication of the impact from the mine site.

## **7.4 Methods**

### **7.4.1 Hydrology**

A sharp-crested, 90-deg V-notch weir, referred to here as Woods Weir (WW), was constructed to measure the discharge from Woods Lake into Camp Lake. Outflow from Camp Lake discharges through a broad-crested rectangular concrete weir at the north end of the lake referred to as Camp Weir (CW). Stage-discharge rating curves measured at CW and WW had a relative root-mean-squared error of 6% or less. Water levels were measured continuously at Camp Weir and Woods Weir from July 2001 to August 2003 using a chart recorder (Stevens Chart A-71). From September 2003 to September, 2006, the height of water flowing over the weirs was measured manually when water samples were collected on a weekly or bi-weekly schedule. Water levels also were measured manually where the stream flows through a well confined channel at the

Sherlett Creek Bridge (SC) when water samples were collected. During the period when water levels were measured manually at discrete time intervals, it is possible that peak flow events may have been missed leading to an underestimate in discharge. A pressure transducer (Druck PDCR930) was installed into Camp Lake near location L (Fig. 7.1) between July 12, 2001 and October 4, 2001. Water level data was not measured at any of the locations between April 10, 2002 and June 4, 2002 due to technical difficulties.

Discharge was measured at SC and CW in July 2001, August 2001, October 2001, and June 2002, with the velocity-area method (Dingman, 2002, p.609) using a vertical-axis current meter (Price 1205 Mini Velocity Meter). Error in spot flow measurements using the velocity-area method is expected to be on the order of 5% (Turnipseed and Sauer, 2010). A calibrated bucket was used to measure the volume of flow over WW on the same dates as above. Monthly mass loading from each gauged station was calculated using the discharge-weighted average of dissolved concentrations. This calculation was achieved by multiplying the measured discharge by the ion concentration at the time of sampling. The weekly or biweekly measurements were averaged for the month.

Manitoba Conservation operates an automated weather station that measured daily cumulative rainfall using a tipping bucket rain gauge on the southwest shore of Camp Lake (Fig. 7.1). Precipitation, temperature, relative humidity and wind speed and direction were recorded at this station at 13:00 daily. Snowfall data was measured at the Flin Flon airport, located 60 km SW from the mine site.

#### **7.4.2 Surface Water Quality**

Water samples were collected from SC, WW and CW between July 2001 and September 2006 (Fig. 7.1). There were two brief hiatuses in sampling, occurring from November 2001 to April

2002 and August 2002 to March 2003, when it was not possible to have samples collected. Samples were collected weekly during spring runoff and biweekly over the remainder of the year using sterile 60 mL syringes. Water samples were then filtered through 0.45  $\mu\text{m}$  membranes and stored in prewashed 60 mL Nalgene bottles. One aliquot from each location was acidified to a  $\text{pH} < 1$  with 12 N trace-metal grade  $\text{HNO}_3$  for cation analysis and a second aliquot was left unacidified for anion analysis. All samples were refrigerated until analysis. Concentrations of cations were determined by inductively coupled plasma optical emission spectrometry (ICP–OES), and anion concentrations were determined using an automatic colorimetric procedure or ion chromatography. Values of pH, Eh and temperature were determined at each site during sample collection. The pH electrode was calibrated with standard buffer solutions at pH 7, 4, and 1. The Eh was measured using an Orion platinum redox electrode (model 96-78BN), calibrated in Zobell's solution (Nordstrom, 1977) and Light's solution (Light, 1972) and reported relative to the Standard Hydrogen Electrode. Measurements of alkalinity were made on filtered samples using a Hach digital titrator and bromcresol green/methyl red indicator and with 0.16 N  $\text{H}_2\text{SO}_4$ . Quality control and accuracy for the cation and anion analyses were evaluated by analyzing several standards covering a range of concentration, by analyzing field replicates and splits, and by addition of standards to unknown samples to assess for matrix effects.

Surface water samples also were collected from Sherlett Lake, Fox Lake, Trap Lake, Woods Lake and Acid Pond on July 19, 2001, August 29, 2004 and September 30, 2006. Samples were collected from approximately 5 cm below the water surface using sterile 60 mL syringes, filtered through 0.45  $\mu\text{m}$  membranes and stored in prewashed 60 mL Nalgene bottles. Measurements of pH, Eh, temperature and alkalinity were measured in the field following the methods described above.

### **7.4.3 Geochemical Modeling**

Water chemistry was interpreted with the assistance of the equilibrium chemical-speciation/mass-transfer model MINTEQA2 (Allison et al., 1990). The MINTEQA2 database was modified to make it consistent with that of WATEQ4F (Ball and Nordstrom, 1991), with additional solubility data incorporated for siderite (Ptacek and Blowes, 1994) and Co (Papelis et al., 1988). MINTEQA2 was used to calculate the saturation indices for discrete minerals that may be controlling the concentrations of dissolved ions in surface waters.

### **7.4.4 Lakebed Sediments and Secondary Precipitates**

A total of 54 sediment samples were collected in 2003 and 2004 from the lakebeds of Kississing Lake, Cold Lake, Camp Lake, Woods Lake and Trap Lake using a stainless steel Petite Ponar grab sampler or a gravity corer. The top 2 cm of the sediment samples collected from Kississing Lake and Cold Lake using the grab sampler were transferred into sealed 250 mL prewashed amber glass jars. Core samples collected from Camp Lake, Trap Lake and Woods Lake using the gravity corer were sealed with caps and immediately frozen. Lake bed sediments were analyzed for total metal content by using HF/HNO<sub>3</sub> extraction followed by inductively coupled plasma-optical emission spectrometry (ICP-OES) analysis. Field observations were recorded for the sediment texture, color, and the presence of macrofauna or other visually noticeable features. Sediment sampling in 2003 was carried out by personnel from AECOM in Winnipeg, MB, Canada.

Secondary precipitate samples were collected in October 2005 from the surface of Camp Weir and Woods Weir in sealed plastic containers and immediately frozen. Samples were not purged with nitrogen or argon gas before freezing. Samples were thawed and dried at room temperature in an anoxic glove box for mineralogical examination. Portions of the dried sample

were selected for polished thin-sections prepared without the use of water in order to minimize the dissolution of readily soluble minerals. The polished thin-sections were examined by optical microscopy, using both transmitted and reflected light. In addition, the weir precipitate materials were examined by X-ray diffractometry (XRD) and Rietveld refinement, using a Siemens D5000 powder diffractometer. Precipitates were also analyzed for total metal content by using HF/HNO<sub>3</sub> extraction followed by ICP-OES analysis.

## **7.5 Results and Discussion**

### **7.5.1 Camp Lake Hydrology**

Water-level variations measured at Sherlett Creek, Camp Lake, and Camp Weir and cumulative precipitation over the period July 14 and October 4, 2001 show the strong relationship between water levels at Camp Lake and rainfall amount (Fig. 7.3). For example, between July 29 and July 30, 2001, the area received 25 mm of precipitation, during which time Camp Lake water levels increased by 30 mm then began to decline immediately after the precipitation event. The next storm event consisted of almost the same amount of precipitation, but caused a greater rise in water levels, indicating antecedent moisture conditions played an important role in determining the runoff response. After the second storm event (between August 8 and August 21, 2001) water levels in Sherlett Creek were higher than the water levels at Camp Lake and Camp Weir showing the significance of watershed runoff to flow at Sherlett Creek. The study period (July 16, 2001–September 1, 2006) included variations in the total amounts and distribution of precipitation (Table 7.1). The long-term average precipitation for Flin Flon is 488 mm year<sup>-1</sup>, which is fairly similar to the total precipitation for the first three years of the study period (Environment Canada, 2012). In contrast, 2005 and 2006 were characterized by anomalously high precipitation amounts, and 2004 had fairly low total precipitation, but unusually high amounts of snow.

Table 7-1: Annual precipitation during the study period for the Sherridon area. Total snowfall was measured in Flin Flon, 60 km SW of Sherridon.

Annual Precipitation (January 1 to December 31)	2001 (mm)	2002 (mm)	2003 (mm)	2004 (mm)	2005 (mm)	2006 (mm)
Total Rain Fall	378	324	398	283	588	492
Total Snow Fall (water equivalent)	107	99	74	160	113	157
Total Precipitation	485	423	472	443	701	649

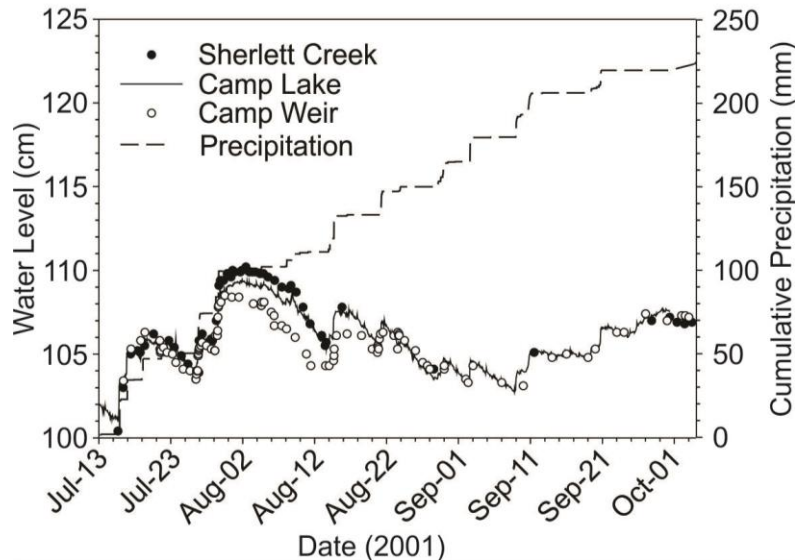


Figure 7-3: Water levels from Sherlett Creek, Camp Lake, Camp Weir, and cumulative precipitation. Water levels were measured relative to a local datum, therefore constants were assigned to the Camp Lake (20 cm) and Camp Weir (40 cm) water level data to allow presentation on one graph.

## 7.5.2 Woods Weir Watershed

The Woods Weir Watershed is a small sub-basin encompassing Fox Lake, the majority of the Woods tailings, Trap Lake and Woods Lake. Headwaters of this watershed originate at Fox Lake, a small Precambrian Shield lake with only one outlet. Even though Fox Lake contains tailings deposited subaqueously prior to 1951, water quality of this lake showed little impact from ARD, with an average pH of 7.94, alkalinity of 72 mg L<sup>-1</sup> as CaCO<sub>3</sub> and low concentrations of dissolved metals and SO<sub>4</sub>. Surface water from Fox Lake flowed through the eastern edge of the Woods tailings into Trap Lake where the pH dropped abruptly to 2.5, then

decreased to 2.3 upon entering Woods Lake (Fig. 7.4). Both Trap Lake and Woods Lake contained elevated concentrations of metals and  $\text{SO}_4$ . The majority of groundwater and surface water from the Woods tailings discharged into Woods Lake. Surface seeps along the flanks of the Woods tailings impoundment discharged porewater with extremely elevated concentrations of  $\text{SO}_4$  ( $85 \text{ g L}^{-1}$ ), Fe ( $51 \text{ g L}^{-1}$ ), Zn ( $0.16 \text{ g L}^{-1}$ ), Al ( $1.4 \text{ g L}^{-1}$ ), Mn ( $34 \text{ mg L}^{-1}$ ), Pb ( $4.9 \text{ mg L}^{-1}$ ) and Ni ( $0.6 \text{ mg L}^{-1}$ ) into Woods Lake. Water flowed from Woods Lake over the Woods Weir directly into Camp Lake, resulting in the appearance of a distinct red plume that dispersed 20 to 30 m from the shore of Camp Lake.

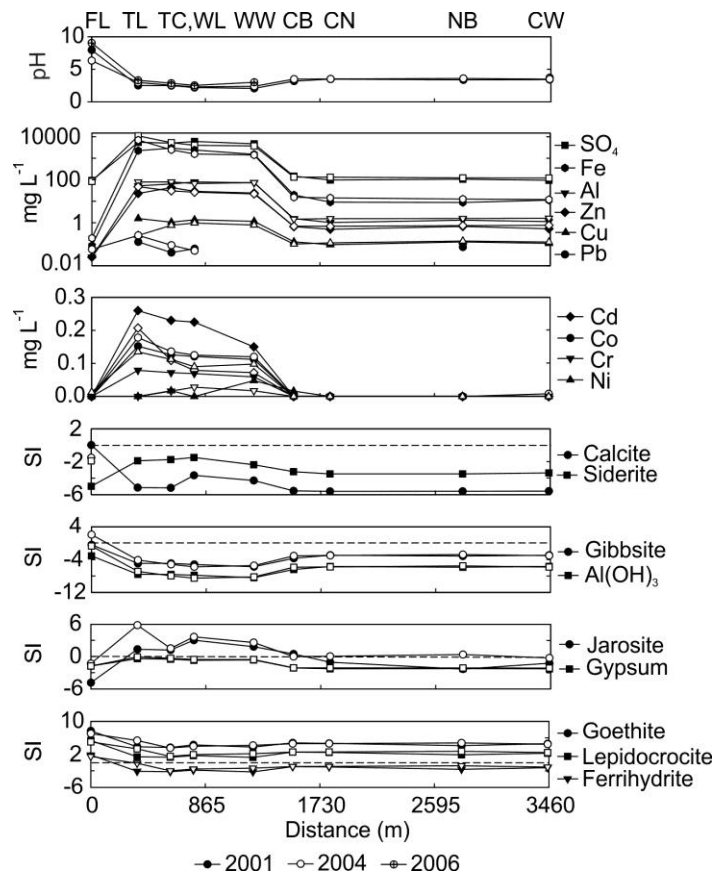


Figure 7-4: Spatial variations of water chemistry from Fox Lake (FL) to Camp Weir (CW), measured in 2001 (shaded symbols), 2004 (open symbols) and 2006 (crossed symbols). Saturation indices were calculated using MINTEQA2. Abbreviations represent: TL – Trap Lake; TC – Trap Creek; WL – Woods Lake; CB – Camp Bay; CN – Camp Narrows; and NB – North Bay.

The hydrograph for discharge over Woods Weir (Fig. 7.5) shows the importance of both snowmelt and precipitation, with spring snowmelt resulting in peak discharges of up to  $0.03 \text{ m}^3 \text{ s}^{-1}$ . During the study period, Woods Weir was observed to be frozen solid by mid-November until spring melt in mid-April. The annual cycle of discharge measured in 2005 and 2006 differed from the previous years in that in addition to the high discharge rates that occurred during the spring freshet, there were also periods of high discharge measured during the summer months in response to high precipitation events. These storm events resulted in abrupt spikes in discharge followed by rapid declines to values ranging from  $0.0004 \text{ m}^3 \text{ s}^{-1}$  to  $0.002 \text{ m}^3 \text{ s}^{-1}$ . During periods of little or no precipitation, base-flow over Woods Weir was minimal, showing the importance of precipitation for maintaining streamflow. For example, during the period from June 22, 2002 and June 28, 2002, when there was no precipitation, discharge was only  $2 \times 10^{-5} \text{ m}^3 \text{ s}^{-1}$ .

Water discharging over Woods Weir had a mean pH value of 3.02,  $\text{SO}_4$  and Fe concentrations of up to  $12.5 \text{ g L}^{-1}$  and  $3 \text{ g L}^{-1}$  respectively, and very elevated concentrations of dissolved Al, Zn, Cu and other metals (Table 7.2). During the spring freshet concentrations of dissolved  $\text{SO}_4$  and metals decreased abruptly with minima that corresponded with peak discharge (Fig. 7.5). Following spring melt, concentrations of dissolved  $\text{SO}_4$  and metals increased during the ice-free months until freeze-up, at which time flow over the weir ceased. During 2005 and 2006 when the total annual precipitation exceeded the average annual precipitation by 100–200 mm, pH values increased and concentrations of some metals were lower, likely due to dilution.



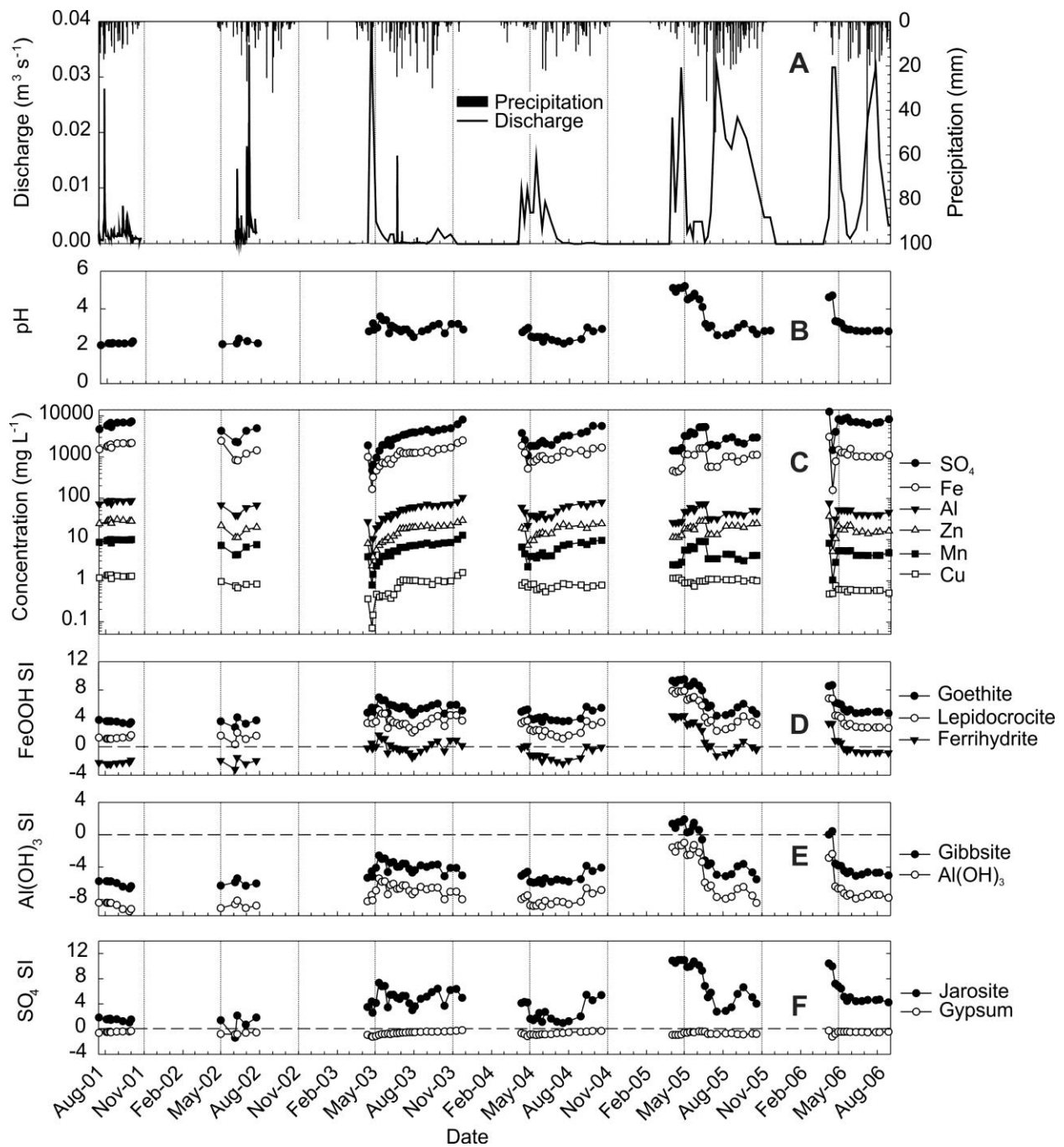


Figure 7-5: Temporal plots from Woods Wier showing (A) discharge and precipitation; (B) pH; (C) dissolved  $\text{SO}_4$  and metal concentrations, and; (D, E and F) saturation indices calculated using MINTEQA2. Vertical lines represent November and May, respectively. Water Samples were not collected between November 2001 to April 2002 and August 2002 to March 2003. Other missing data sets represent freeze-up where no discharge was observed over the weir.

Table 7-2: Average and median concentration of pH, SO<sub>4</sub> and metals from Sherlett Creek, Woods Weir and Camp Lake from July 2001 to September 2006. n refers to the number of samples analyzed; CDWS is the Canadian drinking water standards and GPAL is the Canadian guidelines for the protection of aquatic life. All concentrations in mg L<sup>-1</sup>, except pH which is unitless. Exceeding refers to percentage of average concentrations that exceed regulatory guidelines.

Location	Date (2001-2006)	n	pH	SO <sub>4</sub>	Fe	Al	Zn	Cu	Mn
Sherlett Creek	average	129	7.24	7.8	0.1	0.08	0.13	0.01	0.02
Sherlett Creek	median	129	7.11	6.4	0.1	0.07	0.10	0.01	0.02
Sherlett Creek	exceeding CDWS	129	7%	0%	7%	36%	0%	0%	4%
Sherlett Creek	exceeding GPAL	129	7%	-	7%	36%	3%	38%	-
Woods Weir	average	93	3.02	4080	1210	52	18	0.83	5.7
Woods Weir	median	93	2.52	3700	1250	59	19	0.83	6.5
Woods Weir	exceeding CDWS	93	100%	100%	100%	100%	98%	70%	100%
Woods Weir	exceeding GPAL	93	100%	-	100%	100%	100%	100%	-
Camp Weir	average	128	4.94	95	22	2.0	0.75	0.11	0.22
Camp Weir	median	128	4.25	67	5.9	1.2	0.52	0.01	0.15
Camp Weir	exceeding CDWS	128	76%	0	88%	78%	98%	68%	98%
Camp Weir	exceeding GPAL	128	76%	-	88%	88%	100	98%	-
Camp Weir	ice covered average	53	6.70	37	1.1	0.30	0.18	0.03	0.05
Camp Weir	ice covered median	53	6.60	11	0.3	0.16	0.11	0.02	0.04
Camp Weir	ice-free average	75	3.72	119	39	2.7	1.2	0.15	0.34
Camp Weir	ice-free median	75	3.59	100	11	1.2	0.65	0.12	0.18
CDWS	(Health Canada, 2003)		<sup>2</sup> 6.5-8.5	<sup>3</sup> 500	<sup>3</sup> 0.3	<sup>2</sup> 0.01	<sup>3</sup> 5.0	<sup>3</sup> 1.0	<sup>3</sup> 0.05
GPAL	(CCME, 2007)		6.5-9.0		0.3	0.005	0.03	0.002-0.004	

<sup>1</sup>MAC - Maximum Acceptable Concentrations that are known or suspected to cause adverse effects on health.

<sup>2</sup>IMAC - Interim Maximum Acceptable Concentration for those substances which there are insufficient data to derive MAC, but employ a larger safety factor to compensate for the additional uncertainties involved.

<sup>3</sup>AO - Aesthetic Objectives apply to certain substances or characteristics of drinking water that can affect its acceptance by consumers or interfere with practices for supplying good quality water.

The streambed and side walls of Woods Weir were coated with orange precipitates, characteristic of Fe oxyhydroxide phases (McKnight and Bencala, 1988). There were also localized deposits of a white secondary precipitate along the streambed and weir. Geochemical speciation modeling suggests that water discharging over the Woods Weir was saturated or supersaturated with respect to ferrihydrite [5Fe<sub>2</sub>O<sub>3</sub>•9H<sub>2</sub>O], lepidocrocite [γ-FeO(OH)], goethite

[ $\alpha$ -FeO(OH)], jarosite [KFe<sub>3</sub>(SO<sub>4</sub>)<sub>2</sub>(OH)<sub>6</sub>] and gypsum (Fig. 7.5). XRD analyses of the orange precipitate confirmed that it was composed of 94% goethite with the remaining 6% as a SiO<sub>2</sub> mineral phase. The SiO<sub>2</sub> likely consisted of a secondary silicate mineral phase and/or traces of primary aluminosilicate minerals which were observed during the optical mineralogical examination. No other secondary minerals were observed. The precipitation of Fe oxyhydroxides may result in the co-precipitation or adsorption of metals, including Al, Zn, Cu, Pb, Ni, Co and Cd (Thornber and Wildman, 1984; Bowell and Bruce, 1995; Holmstrom and Ohlander, 2001; Moncur et al., 2009; Frau et al., 2012). Total digestion of the orange secondary precipitates collected from Woods Weir showed that Fe was the dominant ion, however concentrations of Al, Zn, Cu, Cr, Pb and major cations were present indicating that these metals were co-precipitating with or adsorbing to the goethite (Table 7.3). XRD analyses of the white precipitate collected from Woods Weir indicate that it was composed of 33% gypsum and 64% quartz. A smectite-group clay mineral was present in significant amount but could not be fitted with Rietveld analysis and the mineral phase also had planar disorder. It was not possible to identify the smectite- group clay mineral through its optical properties. The aluminum concentration was moderately low, therefore it is possible to narrow the number of smectite-group clay minerals by eliminating minerals such as beidellite [(1/2Ca,Na)<sub>0.3</sub>Al<sub>2</sub>(Si,Al)<sub>4</sub>O<sub>10</sub>(OH)<sub>2</sub>•n(H<sub>2</sub>O)] and possibly saponite [(1/2Ca,Na)<sub>0.3</sub>(Mg,Fe<sup>2+</sup>)<sub>3</sub>(Si,Al)<sub>4</sub>O<sub>10</sub>(OH)<sub>2</sub>•4(H<sub>2</sub>O)]. The absence of Na further indicates that it was not nontronite [Na<sub>0.3</sub>Fe<sub>2</sub><sup>3+</sup>(Si,Al)<sub>4</sub>O<sub>10</sub>(OH)<sub>2</sub>•n(H<sub>2</sub>O)], hectorite [Na<sub>0.3</sub>(Mg,Li)<sub>3</sub>Si<sub>4</sub>O<sub>10</sub>(OH)<sub>2</sub>] or sauconite [Na<sub>0.3</sub>Zn<sub>3</sub>(Si,Al)<sub>4</sub>O<sub>10</sub>(OH)<sub>2</sub>•4(H<sub>2</sub>O)]. Because Al substitutes for Si in some smectite group minerals, it would be difficult to further narrow down the list of potential minerals without Si analysis.

Table 7-3: Whole-rock analyses ( $\text{mg kg}^{-1}$ ) of secondary precipitates collected from Woods Weir ( $\text{WW}_{\text{OR}}$ ) and Camp Weir ( $\text{CW}_{\text{OR}}$ ). Each location is an average of three analyses except for  $\text{WW}_{\text{WHT}}$ , which is for one sample. Subscript OR refers to orange precipitates and WHT refers to a white precipitate.

Location	Fe	Al	Ca	Mg	Na	Zn	Cu	Cr	Pb	Ni	Co	Mn	Cd
$\text{WW}_{\text{OR}}$	5,910,000	9400	3200	1400	710	440	220	11	<5	3.1	1.4	<1	<3.4
$\text{WW}_{\text{WHT}}$	601,000	1100	2800	980	<10	220	40	4.6	25	<2	<1	<1	<3.4
$\text{CW}_{\text{OR}}$	620,000	1500	1500	200	<10	310	440	5.8	14.5	<2	<1	<1	<3.4

### 7.5.3 Acid Pond

Groundwater and surface water discharging from the northwest portion of the Woods tailings and waste rock/abandoned-mine-workings collected in the Acid Pond, adjacent to Camp Lake. The Acid Pond had a pH of 2.45 and dissolved concentrations of up to  $16.7 \text{ g L}^{-1} \text{ SO}_4$ ,  $6.7 \text{ g L}^{-1} \text{ Fe}$ ,  $32 \text{ mg L}^{-1} \text{ Zn}$  (see Moncur et al., 2006). Distinct, green seepage was observed accumulating in topographic lows in the lake bed of Camp Lake about 0.5 m from shore along the mine road that separates the Acid Pond from Camp Lake (Fig. 7.2). The distribution of this seepage (present in lows in the sediment) suggests that flow was density driven and the green color was likely due to the formation of a secondary ferrous sulfate complex (Davis and Ashenberg, 1987) or a secondary Fe or Cu precipitate. Similar groundwater seeps were observed discharging offshore from the Camp tailings.

### 7.5.4 Sherlett Creek Watershed

Sherlett Lake is located upstream of mining activities, at the headwaters of Sherlett Creek, approximately 1 km upstream from Camp Lake. Water in Sherlett Lake had a mean pH of 7.69 and very low concentrations of most dissolved metals (below detection limits), and a mean dissolved  $\text{SO}_4$  concentration of  $5.5 \text{ mg L}^{-1}$ . As water flowed from Sherlett Lake towards Sherlett Creek Bridge (Fig. 7.1), the water quality changed with a slight decrease in the mean pH to 7.24 and increases in the concentrations of dissolved Cu, Zn, Al and  $\text{SO}_4$  to 0.01, 0.13, 0.07 and  $7.8$

mg L<sup>-1</sup>, respectively (Fig. 7.6). Water samples collected on July 19, 2001, August 29, 2004 and September 30, 2006 had pH, SO<sub>4</sub> and dissolved metal concentrations that remained relatively constant at both Sherlett Lake and the Sherlett Creek Bridge (Fig. 7.6). The changes in pH and dissolved metal concentrations that were measured between Sherlett Lake and the bridge were likely related to weathering of sulfide-bearing waste rock from the mine that was used as construction material in contact with Sherlett Creek. Visible sulfide minerals showing extensive oxidation were observed on some waste rock surfaces along the stream banks, which likely represents a source of metals, SO<sub>4</sub>, and acid released to Sherlett Creek.

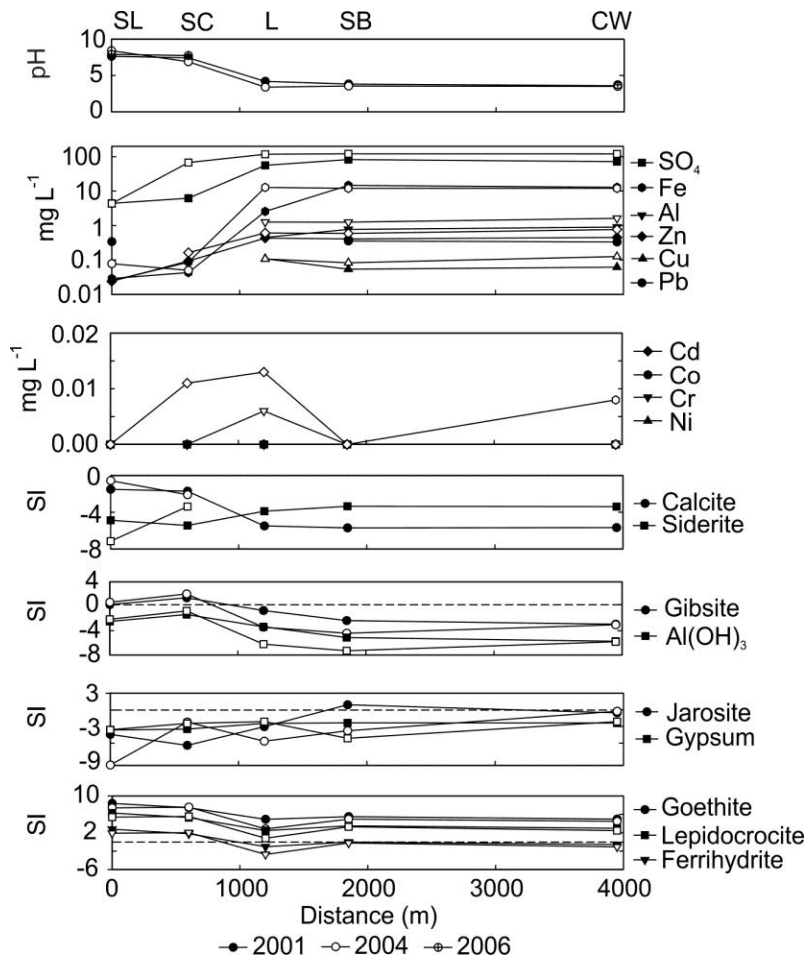


Figure 7-6: Spatial variations of water chemistry from Sherlett Lake (SL) to Camp Weir (CW), measured in 2001 (shaded symbols), 2004 (open symbols) and 2006 (crossed symbols). Saturation indices were calculated using MINTEQA2. Abbreviations represent: SC – Sherlett Creek; L – Lodge; and SB – South Bay.

Unlike the hydrograph for Woods Weir, the hydrograph for Camp Weir was dominated by the effects of snowmelt, with little influence of individual precipitation events. The peak discharge measured at Camp Weir occurred in June (average  $0.65 \text{ m}^3 \text{ s}^{-1}$ ), during the spring freshet after which discharge remained at fairly low rates over the summer and fall months (Fig. 7.7). The average discharge over the weir during the study was  $0.32 \text{ m}^3 \text{ s}^{-1}$  (standard deviation  $0.10 \text{ m}^3 \text{ s}^{-1}$ ). During the study period Sherlett Creek and Camp Weir were ice covered from November to April. During this time base flow discharge over the weir averaged  $0.23 \text{ m}^3 \text{ s}^{-1}$ . The

hydrograph for Camp Weir showed interannual variations in discharge in this part of the basin (Fig. 7.7). The relatively low discharge measured for the spring freshet for 2003 was consistent with the low total snow amounts for that year. The spring freshet for 2004, the year with the unusually high amounts of precipitation received as snow, showed an extended melt period compared to other years. The higher discharge for the spring freshet and for the summer periods for 2005 and 2006 was consistent with the above average precipitation for those years. Temporal water sampling from Sherlett Creek showed that the pH, alkalinity, and concentrations of dissolved  $\text{SO}_4$  and metal remained relatively constant during the study period (Fig. 7.7B–D). There did not appear to be any major shifts in dissolved ion concentrations during the summer and winter seasons or in response to precipitation events.

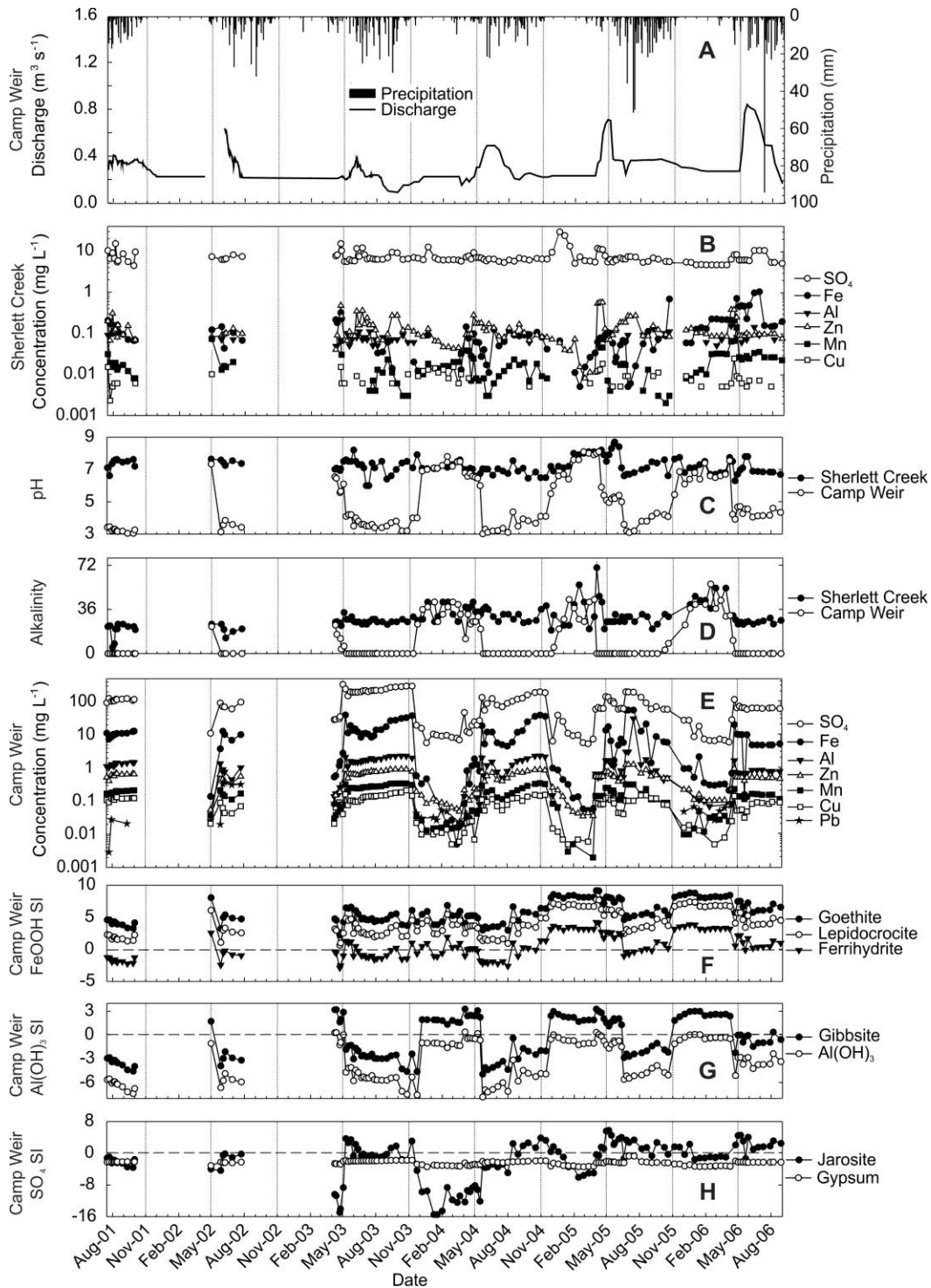


Figure 7-7: Temporal plots showing (A) discharge from Camp Weir and precipitation; (B) dissolved  $\text{SO}_4$  and metal concentrations from Sherlett Creek; (C and D) pH and alkalinity as  $\text{CaCO}_3$ , from Sherlett Creek and Camp Weir; (E) dissolved  $\text{SO}_4$  and metal concentrations from Camp Weir; and (F, G and H) saturation indices calculated using MINTEQA2 from Camp Weir. Vertical lines represent November and May, respectively. Water Samples were not collected between November 2001 to April 2002 and August 2002 to March 2003.



### 7.5.5 Camp Weir

As discussed in the previous section, the hydrograph for Camp Weir (Fig. 7.7A) showed the dominance of discharge generated during the spring freshet. Even though Sherlett Creek and Camp Weir had similar hydrographs, the seasonal cycles of water-quality parameters showed the influence of the adjacent tailings on Camp Lake water quality that are absent from water entering from the Sherlett Creek watershed. The water exiting Camp Lake measured at Camp Weir showed a distinct cycle in quality parameters that included very low pH (3.3) and elevated dissolved metal concentrations when discharge was highest in the spring and early summer (Fig. 7.7C–E). This cycle was not observed at Sherlett Creek where concentrations of dissolved constituents showed no seasonal trends (Fig. 7.7B–D). At Camp Weir the lowest pH values and highest concentrations of dissolved  $\text{SO}_4$  and metals coincided with peak flows. During the late fall and winter months these water-quality parameters returned to values more similar to background, as those measured at Sherlett Creek, with pH values increasing to neutral and concentrations of dissolved metals and  $\text{SO}_4$  decreasing by an order of magnitude (Table 7.2). This annual cycle was likely due to a combination of physical and geochemical controls.

The abruptness of the shifts in pH, metal and  $\text{SO}_4$  concentrations and the timing of these changes with the appearance and disappearance of ice-cover on the lakes suggest that physical factors related to shifts in sources of water and mixing may be responsible for some of these changes. The pH values at Camp Weir began to deviate from the Sherlett Creek inflow water at spring melt when there was increased recharge through the tailings, flushing the unsaturated and saturated zones of the tailings and bringing low pH waters with high metal concentrations to the lake. Reductions in the volume of low-pH water with high metal concentrations entering Camp Lake from Camp Bay, Woods Weir and the Acid Pond during the winter likely contributed to the

observed seasonal trends. During the winter Camp Lake was covered with over 1 m of ice, protecting it from wind, wave fetch, and temperature fluctuations that can lead to mixing of the water column (Klapper and Schultze, 1997). Without these mixing processes, the upper portion of the water column was stratified resulting in near neutral pH values in the top 2 m of the water column (Moncur et al., 2006). A bathymetric survey of Camp Lake in August 2001 found that the maximum water depth over a ridge separating Camp Bay from the main lake was 1.5 m, thus during winter months when there is a >1 m ice cover and stratified, discharge of low quality water entering the lake would be limited.

In addition to these physical controls, there are geochemical controls related to mineral solubility that can explain some of the annual cycles in pH,  $\text{SO}_4$ , and metal concentrations observed in discharge over Camp Weir. During the ice-covered months when there was very little discharge over Camp Weir, the pH increased, resulting in an increase in tendency for precipitation of Fe- and Al-bearing secondary minerals, and the accumulation of Fe and Al oxyhydroxide and  $\text{SO}_4$  minerals (Kimball and Wetherbee, 1989; Alpers et al., 1992; Bowell and Bruce, 1995; Moncur et al., 2009). Saturation with respect to other metal phases was also approached as pH increased, leading to precipitation of these phases. The tendency for metals to co-precipitate or adsorb to Fe and Al precipitates also increases at a near neutral pH (Kimball et al., 1992). Geochemical modeling of the water flowing over Camp Weir indicated that during the summer and fall, the water was saturated or supersaturated with respect to goethite and lepidocrocite and undersaturated with respect to gypsum, ferrihydrite, jarosite, and gibbsite [ $\text{Al}(\text{OH})_3$ ] (Fig. 7.7). During the winter and early spring runoff, when the pH was near neutral, the water also was supersaturated with respect to ferrihydrite and gibbsite, possibly attenuating Fe, Al,  $\text{SO}_4$ , and other metals. Melting of the ice-cover over Camp Lake in Mid-April corresponded to an abrupt decrease in pH to between 3 and 4. Coincident with the decrease in

pH, water flowing over Camp Weir became undersaturated with respect to gibbsite and ferrihydrite. Minerals such as ferrihydrite have a high sorption capacity potentially leading to metal uptake, however under low-pH conditions, these metals are released due to a decrease in sorptive capacity from the ferrihydrite (Moncur et al., 2009). The decrease in pH corresponds to peak concentrations of dissolved metals and  $\text{SO}_4$ , suggesting that the dissolution of Fe and Al mineral phases could be releasing additional metals to surface waters.

The surface of Camp Weir was covered with a 1–2 cm accumulation of an orange poorly crystalline secondary precipitate. The precipitate samples from Camp Weir were collected in October when the pH was <4. XRD analysis using Rietveld refinement indicated that it was composed of 99% goethite, however it is more likely ferrihydrite. Rietveld refinement does not properly identify poorly crystalline phases such as ferrihydrite. Ferrihydrite is also metastable and tends to transform to goethite or hematite (Combes et al., 1989; Blowes et al., 2013). During sample collection and preparation, ferrihydrite may have transformed to goethite due to its metastability. Optical microscopy indicated the absence of any other secondary minerals except for a few small grains of primary aluminosilicate minerals interpreted to be deposited by wind or water. Total digestion of these secondary precipitates collected from Camp Weir showed that Fe was the dominant ion, however significant concentrations of Al, Zn, Cu, Cr, Pb and major cations were present suggesting that these metals were co-precipitating with or adsorbing to goethite (Table 7.3). The low-pH of waters flowing over the weir during ice-free periods likely increased the solubility of metal oxyhydroxides (Theobald et al., 1963; Munk et al., 2002) thereby releasing associated metals. When Camp Lake was ice-covered, the pH of water flowing over the weir was near neutral and the discharge waters were at saturation with respect to Al hydroxides. At this time, precipitation of Al hydroxides may have controlled dissolved Al concentrations.

The absence of secondary Al minerals during the October sampling event might have been because Al-minerals were not stable at the pH ranges observed in waters during that period (Brookins, 1988). Another mineralogical control on dissolved Al concentrations also could be the precipitation of Al-sulfate mineral phases, which have been observed in mine impacted streams (Furrer et al., 2002; Munk et al., 2002).

### **7.5.6 Metal and SO<sub>4</sub> Loading**

Average monthly flux-weighted concentrations of H<sup>+</sup>, and dissolved metals and SO<sub>4</sub> measured during the study period (Fig. 7.8) indicate that the period of lowest water quality occurred between May and November. Water quality during this period was still well above Canadian guidelines for the protection of aquatic life, and only exceeded the Canadian maximum acceptable drinking water aesthetic objectives in June and July (Table 7.2).

Comparison of the annual and interannual variations in discharge data for Camp Weir, Sherlett Creek and Woods Weir illustrates the relatively small flux of water received from Woods Weir (Fig. 7.8, Table 7.4). Despite the small volumes of water entering Camp Lake from Woods Weir, the monthly average concentrations of metals and SO<sub>4</sub> show the loading from this watershed is a significant proportion of the total loading to the lake. In contrast, the upstream Sherlett Creek watershed was a significant source of water to Camp Lake, but contributed very little to the loading of metals or SO<sub>4</sub>.

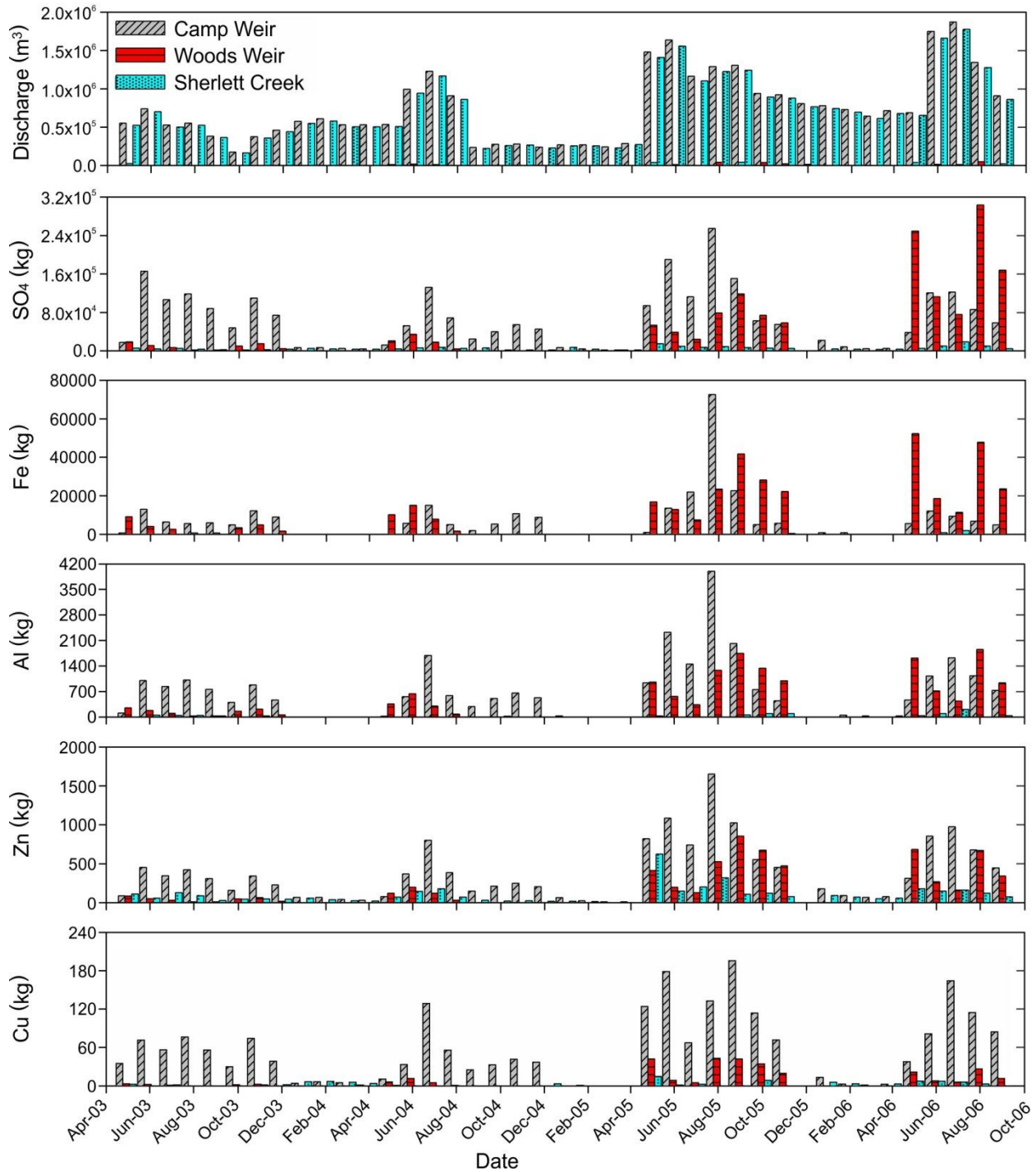








Figure 7-8: Discharge and loadings from Camp Weir, Sherlett Creek and Woods Weir, between April, 2003 and September 2006.

Comparisons of the loadings measured at Camp Weir and Woods Weir over the study period show the importance of groundwater to SO<sub>4</sub> and metal loadings of the system during dry

years and the potential for significant loadings due to flushing of the unsaturated zone during relatively wet years. If flow from the Woods tailings were the only source of SO<sub>4</sub> and dissolved metals to Camp Lake, one would expect the loadings from Woods Weir to be a significant component of the net loadings measured at Camp Weir. During the drier years in the study period (2003 and 2004) loadings from Woods Weir represent a very small portion of the total loadings exiting over Camp Weir, indicating significant inputs of SO<sub>4</sub> and metals between these two measuring points. Groundwater flow through the Camp tailings into Camp Lake has been observed (Moncur et al., 2005) and is likely the main source of these inputs.

Table 7.4: Average annual loading of metals between April 2003 to August 2006 from Sherlett Creek (SC), Woods Weir (WW) and Camp Weir (CW).

Location	Discharge (m <sup>3</sup> a <sup>-1</sup> )	SO <sub>4</sub> (kg a <sup>-1</sup> )		Fe (kg a <sup>-1</sup> )		Al (kg a <sup>-1</sup> )		Zn (kg a <sup>-1</sup> )		Cu (kg a <sup>-1</sup> )		Mn (kg a <sup>-1</sup> )	
SC	5,700,000	41,000	113	170	0.5	210	1	680	2	34	0.1	63	0.2
WW	39,000	68,000	187	26,000	72	1,000	3	310	1	14	0.04	130	0.4
CW	6,000,000	750,000	2067	57,000	157	5,400	15	2,500	7	460	1	890	2.5

The loadings from Camp Weir were higher than any of the other measuring locations for most months. Exceptions included brief periods when the loadings from Woods Weir were larger for some metals; in 2006 for Fe and in 2005 and 2006 for SO<sub>4</sub>, Al and Zn. Anomalously high summer precipitation occurred in 2005 and 2006 (Table 7.1) resulting in much higher discharge volumes over Woods Weir. The high metal and SO<sub>4</sub> loadings from Woods Weir for these years suggest that when there is sufficient water available in the watershed, large quantities of metals can be mobilized from the watershed. The thick unsaturated zone of the Camp tailings contains porewaters with extremely high concentrations of SO<sub>4</sub> and metals (*e.g.* maximum concentrations: SO<sub>4</sub> = 280 g L<sup>-1</sup>; Fe = 129 g L<sup>-1</sup>; Al = 7.2 g L<sup>-1</sup>; Cu = 1.6 g L<sup>-1</sup>), low pH values, and secondary precipitates that include highly soluble salts (*e.g.* melanterite) (Moncur et al., 2005). In areas of

the Woods tailings the unsaturated zone was greater than 6 m thick, and also contained concentrations of dissolved metals similar to the Camp tailings (Moncur et al., 2009b). Flushing of these porewaters and the dissolution of soluble salts during the spring melt, or periodic flushing during wet years would result in peak-loadings that occur annually during the spring freshet and periodically during wet years (*e.g.* 2005 and 2006). This type of temporal pattern in peak-loading due to dissolution of secondary precipitates has been reported in response to large precipitation events at similar mine sites (*e.g.* Nordstrom, 2009; Sarmiento et al., 2009).

Loadings of Cu were consistently highest at the Camp Weir sampling location, and only small increases in loadings occurred during the anomalously wet years of 2005 and 2006. The differences between the relatively small increases in Cu loading observed in the wet years versus the dry years and the large increases in metal and SO<sub>4</sub> loadings observed in the wet years versus dry years were likely due to the higher concentrations of SO<sub>4</sub>, Fe, Al and Zn in the porewater and the presence of soluble sulfate minerals in the secondary precipitates in the tailings.

To put the large SO<sub>4</sub> and metal loadings presented graphically in Figure 7.8 in perspective, the annual average metal loadings were converted to hypothetical cattle units using an average cattle weight of 363 kg (Curtis et al., 2008) (Table 7.4). The average annual SO<sub>4</sub> and metal loadings during the study period included large fluxes of SO<sub>4</sub> and Fe out of the Camp Lake system into the downstream Kississing Lake.

### **7.5.7 Down-Stream Impact to Cold Lake**

The annual loadings of Zn and Cu over Camp Weir are fairly low (Zn = 2500 kg a<sup>-1</sup>, Cu = 460 kg a<sup>-1</sup>) when compared with the annual loadings from other severely impacted mine sites (*e.g.* Odiel River, Zn = 2,612,000 kg a<sup>-1</sup>, Cu = 1,252,000 kg a<sup>-1</sup>, described in Olías et al., 2006; Iron Mountain Zn + Cu + Cd = 300,000 kg a<sup>-1</sup>, described in Nordstrom and Alpers, 1999; Britannia

Mine, Zn = 10–160 kg d<sup>-1</sup>, Cu = 10–425 kg d<sup>-1</sup>, described in Barry et al., 2000). However, despite the relatively low annual loading, concentrations of Zn and Cu are elevated in lake bed sediments from Cold Lake and Kississing Lake, impacting an area of over 9.5 km<sup>2</sup> (950 ha) (Fig. 7.9). Orange Fe oxyhydroxide precipitates were observed covering native sediments throughout the impacted area in the Cold Lake and Kississing Lake benthic sediments. Concentrations of Zn in sediment samples collected from Cold Lake were in the range of 820 mg kg<sup>-1</sup> to 4380 mg kg<sup>-1</sup>, exceeding the CCME (2002) recommended probable effect level (PEL) of 315 mg kg<sup>-1</sup>. The PEL is defined as the level above which adverse biological effects are expected to occur frequently (CCME, 2002). Sediment samples collected from Cold Lake also had elevated Cu concentrations ranging from 388 mg kg<sup>-1</sup> and 1190 mg kg<sup>-1</sup>. The recommended PEL for Cu in fresh water sediments is 197 mg kg<sup>-1</sup>. The lowest concentrations of Zn and Cu in the sediments from Cold Lake were at the outlet from Camp Lake and the most elevated concentrations were at location A13. Sediment samples collected from a depth of 29 m in Kississing Lake at location A19 contained 1700 mg kg<sup>-1</sup> and 220 mg kg<sup>-1</sup> of Zn and Cu, respectively. Similar concentrations of Zn and Cu in the sediments from Kississing Lake were observed in all samples collected south of A19 to the Cold Lake outlet (Fig. 7.9). Average background concentrations of Zn and Cu measured in lake sediment samples collected from Sherlett Lake were 190 mg kg<sup>-1</sup> and 50 mg kg<sup>-1</sup> respectively, well below concentrations measured in sediments from Cold Lake and Kississing Lake (Beck, 1983).

Macroinvertebrates were found to be absent or present in very limited numbers during visual inspection of lake bed sediment during sediment sampling campaigns at Camp Lake, Cold Lake and Kississing Lake. Molluscs, including piisid and sphaerid clams, amphipods, chironomids larvae, larger oligochaetes, and other commonly encountered benthic fauna were absent in sediment samples from Cold Lake and the lower portion of the eastern arm of



Kississing Lake to the outlet to Cold Lake (UMA, 2004). Benthic invertebrates also were not found in near shore areas in Cold Lake and Kississing Lake to location A19 and beyond. Aquatic invertebrates were not observed in near shore areas of Camp Lake, Cold Lake or Kississing Lake within the 950 ha impacted area during this study. In contrast, lakes upstream of the impacted area are characterized by an abundance of bivalves including unionids, at least three gastropod species, crayfish, larval insects, leaches, and juvenile and small fish (UMA, 2004).

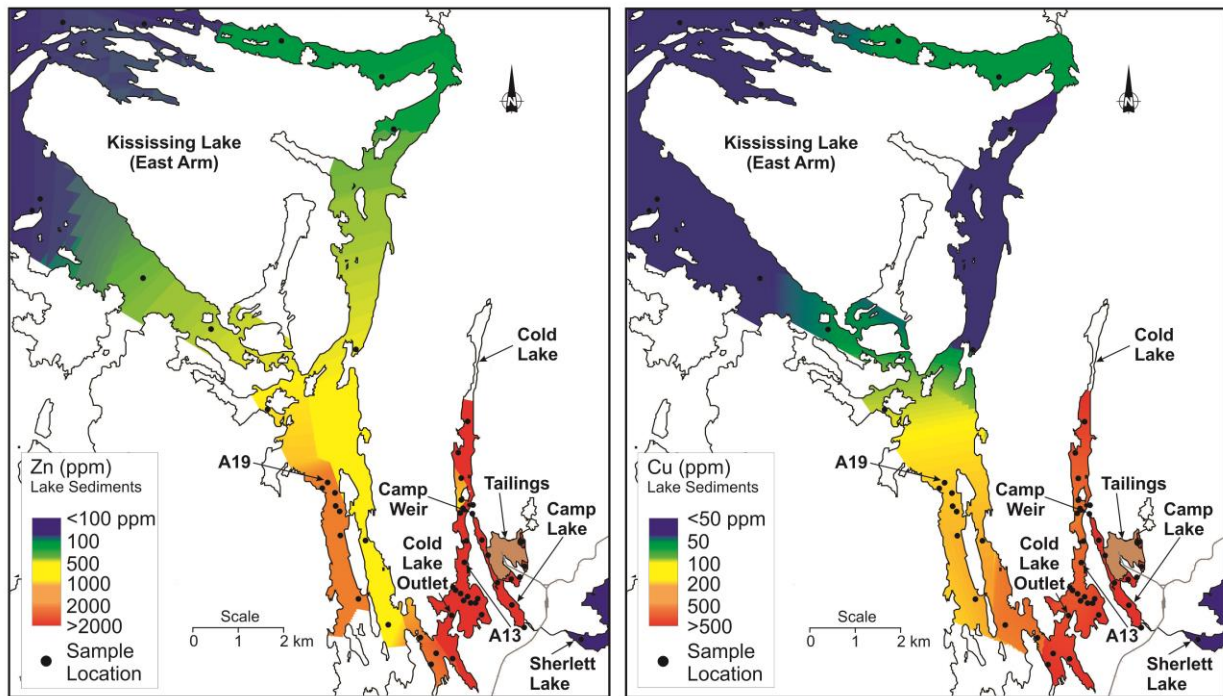


Figure 7-9: Maps showing the distribution of Zn and Cu concentrations in the lake-bottom sediments of Cold Lake and Kississing Lake (modified from Moncur et al., 2007).

Even though benthic macroinvertebrates were absent within the area of lake sediments containing elevated concentrations Zn and Cu, fish studies by Beck (1983) and UMA (2004) concluded that adult fish appeared healthy. Analysis of muscle tissue from adult fish netted in Sherlett Lake, Cold Lake near the Camp Weir outlet and adjacent to the community of Cold Lake, and in Kississing Lake near location A19, found that tissues contained no bioaccumulation of metals. Gill net results, however, provide evidence of impact on fish population. The catch per unit effort averaged 0.71 fish per meter of net in Sherlett Lake and only 0.15 fish per meter net in

Cold Lake. Further indication of impact of the mine effluent to fish populations in Cold Lake is reported by Saquet et al. (2002). This study found that fish sampled near the Camp Weir outlet contained otoliths with elevated abundances of Zn, Mn, Fe, Cu and Sr. Concentrations of Sr were amongst the highest reported for any freshwater fish and Zn concentration were the highest observed in any fish studied by the authors (Saquet et al., 2002).

## **7.6 Conclusions**

Long-term weathering of sulfide minerals at the Sherridon mine site has led to release of metals,  $\text{SO}_4$  and acid to groundwater and surface waters for more than five decades after mining has ceased. Comparison of the annual and interannual loadings measured at the unimpacted basin (Sherlett Creek) with the loadings measured at Camp Weir and Woods Weir Creek showed the importance of groundwater flow through the tailings to  $\text{SO}_4$  and metal loadings to the lake during dry years and the potential for significant loadings due to flushing of the thick unsaturated zone in the tailings during relatively wet years. At Sherlett Creek, low concentrations of metals and high pH values coincided with times of peak discharge, whereas at Woods Weir and Camp Weir, neutral pH and low concentrations of dissolved metals and  $\text{SO}_4$  were measured during the winter months when discharge volumes were low and the lake was ice-covered. Winter freeze-up limited infiltration of meteoric water through the tailings and Woods Weir remained frozen from mid-November to mid-April. In addition, Camp Bay was potentially isolated due to winter ice buildup over a ridge that separated the bay from the main basin of Camp Lake. During spring melt the discharge sampled at Camp Weir revealed abrupt increases in dissolved metal and  $\text{SO}_4$  concentrations and decreases in pH to values that remained relatively constant until fall freeze-up, when dissolved metal concentrations and pH returned to winter values. The abrupt changes in pH, metal and  $\text{SO}_4$  concentrations and the timing of these changes with the appearance and

disappearance of ice-cover on the lakes suggests a combination of physical and geochemical controls related to shifts in sources of water and mixing and changes in solubility. During years with above average precipitation, the loading of metals was greater when compared to dryer years, suggesting that the application of a low-permeable cover over the tailings may limit infiltration rates and decrease loadings. The long-term release of metals has led to elevated concentrations of metals in sediment over a 10 km<sup>2</sup> area in Kississing Lake and a decline in the macroinvertebrate population. Even though the average annual concentrations of dissolved metals and SO<sub>4</sub> discharging over the Camp Weir to Cold Lake seem to be within or very near regulatory guidelines, this study demonstrates the importance of seasonal variations in water quality, metal loadings and the potential for long-term impacts to downstream water bodies. These results suggest that in northern regions the ice-free period is critical in controlling metal discharge from mine-impacted areas, and demonstrate that even when average annual concentrations are only slightly elevated, long-term metal loadings can have a significant impact on the receiving aquatic systems.

## Chapter 8:

### *Source and distribution of naturally occurring arsenic in groundwater from Alberta's Southern Oil Sands Regions*

Reproduced with permission from: Moncur, M.C., Paktunc, D., Birks, S.J., Ptacek, C.J., Welsh, B., Thibault, Y., 2015. Source and distribution of naturally occurring arsenic in groundwater from Alberta's Southern Oil Sands Regions. *Appl. Geochem.* <http://dx.doi.org/10.1016/j.apgeochem.2015.02.015>. Copyright 2015 Elsevier Ltd., License Number 3604620370105. Editorial and formatting changes have been made to accommodate reproduction in this thesis.

## 8.1 Executive Summary

Arsenic (As) concentrations as high as  $179 \mu\text{g L}^{-1}$  have been observed in shallow groundwater in Alberta's Southern Oil Sand Regions. The geology of this area of Alberta includes a thick cover (up to 200 m) of unconsolidated glacial deposits, with a number of regional interglacial sand and gravel aquifers, underlain by marine shale. Arsenic concentrations observed in 216 unconsolidated sediment samples ranged from 1 to 17 ppm. A survey of over 800 water wells sampled for As in the area found that 50% of the wells contained As concentrations exceeding drinking water guidelines of  $10 \mu\text{g L}^{-1}$ . Higher As concentrations in groundwater were associated with reducing conditions. Measurements of As speciation from 175 groundwater samples indicate that As(III) was the dominant species in 74% of the wells. Speciation model calculations showed that the majority of groundwater samples were undersaturated with respect to ferrihydrite, suggesting that reductive dissolution of Fe oxyhydroxides may be the source of some As in groundwater. Detailed mineralogical characterization of sediment samples collected from two formations revealed the presence of fresh framboidal pyrite in the deeper unoxidized sediments. Electron microprobe analysis employing wavelength dispersive spectrometry indicated that the framboidal pyrite had variable As content with an average As concentration of 530 ppm, reaching up to 1840 ppm. In contrast, the oxidized sediments did not contain framboidal pyrite, but exhibited spheroidal Fe oxyhydroxide grains with elevated As concentrations. The habit and composition suggest that these Fe oxyhydroxide grains in the oxidized sediment were an alteration product of former framboidal pyrite grains. X-ray absorption near edge spectroscopy (XANES) indicated that the oxidized sediments are dominated by As(V) species having spectral features similar to those of goethite or ferrihydrite with adsorbed As, suggesting that Fe oxyhydroxides are the dominant As carriers. XANES

spectra collected on unoxidized sediment samples, in contrast, indicated the presence of a reduced As species (As(-I)) characteristic of arsenopyrite and arsenian pyrite. The results of the mineralogical analyses indicate that the oxidation of framboidal pyrite during weathering may be the source of As released to shallow aquifers in this region.

## 8.2 Introduction

Arsenic occurs in the environment in oxidation states of -III, -I, 0, III and V. In sulfide minerals such as arsenian pyrite [FeS<sub>2</sub>] and arsenopyrite [FeAsS], As is in the As(-I) oxidation state (Campbell and Nordstrom, 2014). In natural groundwater, the most prevalent oxidation states of As are oxyanions of arsenite [As(III)] and arsenate [As(V)]. Aerobic waters are dominated by As(V) species whereas As(III) is the principal species in anaerobic environments (Nordstrom, 2002). Under circumneutral pH, both species have an affinity for Fe oxyhydroxide surfaces, but because As(III) is not as strongly adsorbed, it is more mobile in reducing aqueous environments than As(V) (Dixit and Hering, 2003). Both As(III) and As(V) are toxic (Amend et al., 2014; Leybourne et al., 2014), with As(III) being 25-60 times more toxic than As(V) (Korte and Fernando, 1991).

After contamination of drinking water by pathogenic organisms, elevated As concentrations in groundwater is the second most recognized global health hazard in drinking water (Johnston et al., 2001; van Halem et al., 2009). It is estimated that over 150 million people worldwide are exposed to concentrations of geogenic arsenic in drinking water that exceed the World Health Organization (WHO) limit of 10 µg L<sup>-1</sup> (Nordstrom, 2002; Smedley and Kinniburgh, 2002; Mitchell, 2014). Although Bangladesh is one of the most recognized regions of As contaminated groundwater (*e.g.* Nickson et al., 2000; Anawar et al., 2003; Harvey et al., 2006; Van Green et al., 2008; Jung et al., 2012), concentrations of As in groundwater exceeding

WHO guidelines have been measured in over 70 countries on nearly every continent or major land mass (Barringer and Reilly, 2013).

Estimates of the population in Canada exposed to groundwater As concentrations exceeding the Canadian drinking water guidelines of  $10 \mu\text{g L}^{-1}$  (Health Canada, 2012) are less well documented. However, naturally occurring As has been documented at concentrations that exceed these guidelines in all provinces and one territory (Table 8.1). In western Canada, elevated As concentrations are typically associated with igneous and metamorphic bedrock aquifers, and associated glaciofluvial and fluvial sediments (Boyle et al., 1998; Bolton and Beckie, 2011). In eastern Canada, elevated As concentrations have been associated with metasedimentary bedrock aquifers in New Brunswick and Nova Scotia (Bottomley, 1984), igneous bedrock aquifers in Newfoundland, and sandstone aquifers in Prince Edward Island (Somers et al., 1999). Across the Prairie provinces, elevated As concentrations in groundwater are typically observed in glaciofluvial sediments (Lemay et al., 2005; Thompson et al., 1999; Moore, 2005), although groundwater obtained from some wells completed in sandstone and shale aquifers (Cheung et al., 2009) and produced-water from deep oil-field wells (White et al., 1963; Moncur, 2010) have elevated As. Anthropogenic sources of As in groundwater have been reported in many parts of Canada near facilities for wood treatment, gold mining operations (Wang and Mulligan, 2006), waste pond seepage from hydrofluoric acid production and enhanced oil recovery using thermal steam injection methods (Fennell, 2008). For example, As concentrations up to  $2050 \mu\text{g L}^{-1}$  were reported for groundwater down-gradient from a Au-mine tailings impoundment in NW Ontario (Ross et al., 1999).

Table 8-1: Examples of natural and anthropogenic occurrences of As in groundwater across Canada.

Location	Rock Type/Aquifer	Conc. $\mu\text{g L}^{-1}$	Reference
<i>Geogenic As source to groundwater</i>			
Bowen Island, British Columbia (BC)	Metavolcanic and metasediments with sulfides	1-580	Boyle et al., 1998
Langley, BC	Glaciofluvial/marine clay	<1-276	Cavalanti de Albuquerque et al., 2012
Southern West Coast, BC	Igneous bedrock with sulfides and fluvial sediments	<1-2440	Carmichael & Clarkson, 1995; Mattu & Schreier, 2000; Bolton & Beckie, 2011
Meager Creek, BC	Geothermal hot spring water	237-303	Koch et al., 1999
Lussier, Fairmont & Radium Hot Springs, BC	Geothermal hot spring water	92, 74-88, 234 (respectively)	Moncur, 2013 unpublished data
Alberta (AB)	Glaciofluvial/ sedimentary bedrock	<1-119	Fitzgerald et al., 2001
Cold Lake-Beaver River Basin, AB	Glaciofluvial	<10-361	Stein et al., 2000; Lemay et al., 2005
Southern Athabasca Oils Sands Region, AB	Glaciofluvial	<10-30	Lemay, 2003
Central AB	Glaciofluvial/sandstone	<1-780	AHW, 2000
South-Central AB	Cretaceous sandstone/shale	<1-165	Cheung et al., 2009
Ellis Pool, AB	Deep oilfield brine	230	White et al., 1963
Saskatchewan (SK)	Glaciofluvial	<1-117	Thompson et al., 1999
Birsay, SK	Glacial till porewater	3-99	Yan et al, 2000
Virден, Manitoba (MB)	Glaciofluvial	38-44	Moore, 2005
Ontario (ON)	Various	<2.5-68	Health Canada, 2006
Quebec (QC)	Not specified	<10-330	McGuigan et al., 2010
New Brunswick	Igneous and metasediment bedrock	up to 1050	Bottomly, 1984
Prince Edward Island	Permian sandstone	<1-26	Somers et al., 1999
Nova Scotia	Metasediment bedrock with sulfides	3-5000	Meranger et al., 1984
Newfoundland	Igneous and sedimentary bedrock	up to 769	Rageh et al., 2007; Serpa et al., 2009
Carcross, Yukon	Glaciofluvial	12-27	Dayton & Knight, 2010
<i>Anthropogenic As source to groundwater</i>			
Montreal, QC	Glaciofluvial-wood preservative	1-79	Zagury et al., 2003
Cold Lake Oil Sands Region, AB	Glaciofluvial-enhanced thermal recovery of bitumen operations	5-324	CNRL, 2005; Fennell, 2008
Amherstburg, ON	Carbonate bedrock-hydrofluoric acid production	up to 206	Windsor Star, 2006
Gold mine, Balmertown, ON	Sulfide mine tailings porewater-neutral rock drainage (NRD)	300-100,000	McCreadie et al., 2000
Zn-Cu mine, Sherridon, MB	Sulfide mine tailings porewater-acid rock drainage	<10-50,000	Moncur et al., 2005
Gold mine, Yellowknife, NT	Lake sediment porewater impacted by mining operation	16-947	Andrade et al., 2010
Gold mine, Bralorne, BC	Flooded underground mine workings - NRD	up to 5898	Desbarats et al., 2014



Elevated As concentrations have been reported in many smallscale groundwater investigations in the Cold Lake-Beaver River Basin (CLBR) in east-central Alberta, but previous studies did not clearly identify the spatial extent of this groundwater problem or identify whether the elevated concentrations were due to natural geogenic sources, or anthropogenic activities. An early study by Nriagu (1998) sampled 51 residential wells and found that 40% of the wells had As concentrations exceeding Canadian drinking water guidelines of  $10 \mu\text{g L}^{-1}$ . Follow up studies of residential wells in the CLBR basin by Alberta Health and Wellness (AHW, 2000) and Stein et al. (2000), found that 50% of the 59 wells and 54% of the 35 wells sampled respectively, contained As concentrations in groundwater exceeding  $10 \mu\text{g L}^{-1}$ . Lemay et al. (2005) was the first to map the distribution of As concentrations in groundwater across the CLBR basin spatially and within individual formations, but did not provide information regarding the number of wells exceeding drinking water guidelines for As. A study by AHW (2014) that surveyed 152 wells in the CLBR basin found that 48% of groundwater from residential wells contained As concentrations that exceeded guidelines, with As(III) as the dominant species. Javed et al. (2014) characterized sediments from the CLBR basin and observed both arsenian pyrite and arsenopyrite. Arsenic was also found to be adsorbed to sediments and bound to crystalline oxide minerals. The objective of this investigation is the integration of existing and newly collected As groundwater data, including As speciation measurements, with major ion and trace element data to understand processes controlling the spatial distribution of As concentrations in groundwater across the CLBR basin and identify areas of concern. A second objective was to determine sources and potential controls of As mobility in groundwater using geochemical modeling and detailed solid-phase and mineralogical analyses from available aquifer sediments.

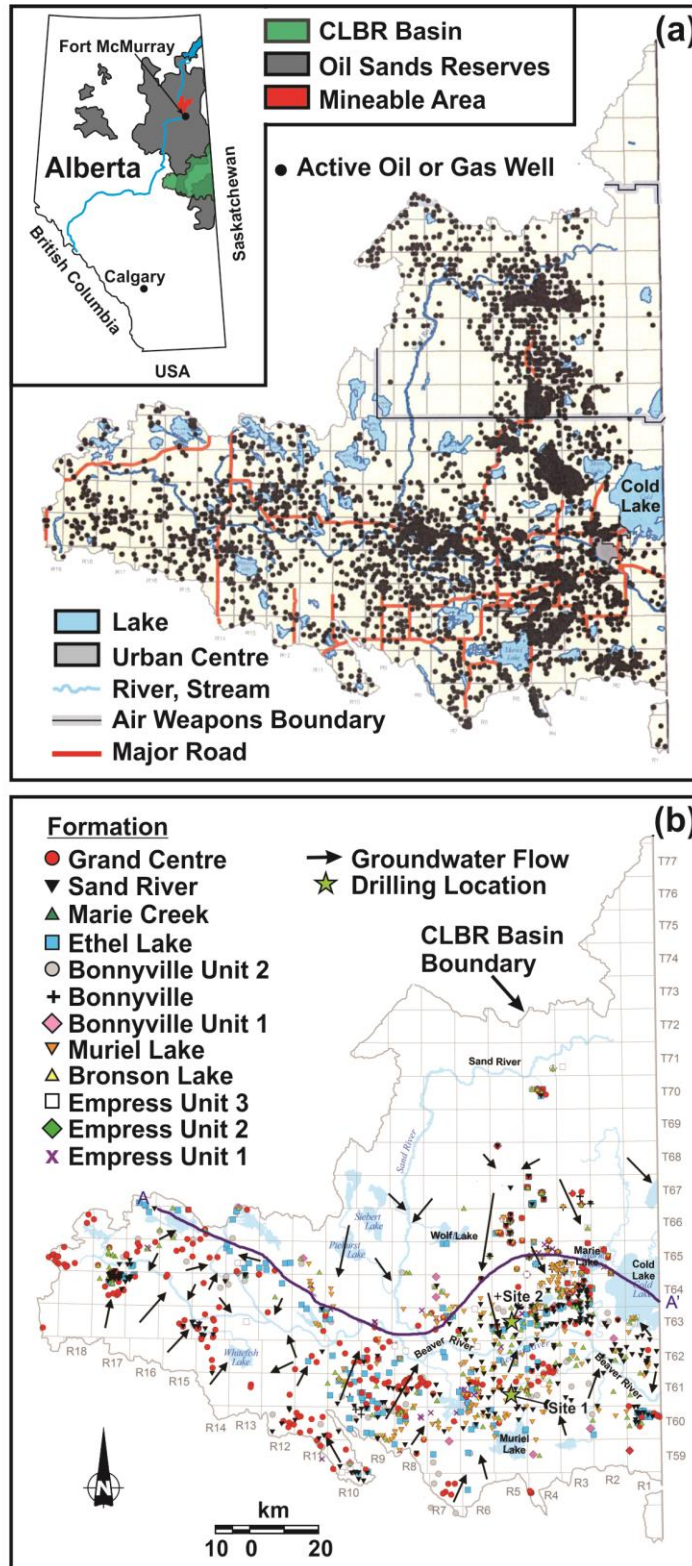


Figure 8-1. Maps show (a) distribution of active energy wells, revised after Lemay (2003) and (b) regional groundwater flow and the location of water wells (symbols are differentiated by geological formation) used in this study. Inset shows the extent of the oil sands and location of the Cold Lake-Beaver River Basin in Alberta, Canada.

### **8.3 Study Area**

The Alberta portion of CLBR basin is approximately 22,000 km<sup>2</sup>, located 400 km northeast of Calgary (Fig. 8.1). The basin encompasses a portion of the Southern Oil Sands Region and the Cold Lake Oil Sands Region (Fig. 8.1). Agricultural lands cover one-third of the watershed. The area also includes considerable heavy oil and gas extraction, with numerous active energy wells (Fig. 8.1). Commercial scale thermal in situ oil sands projects are present west and northwest of Cold Lake. Groundwater is extensively used as a source of water in the CLBR region for industrial, agricultural, municipal, and domestic purposes (AESRD, 2013).

### **8.4 Geological and Hydrogeological Setting**

The general stratigraphy beneath the CLBR basin is comprised of 25–225 m of unconsolidated sediments with the basal deposits composed of Neogene sand and gravel overlain by alternating till and sand and gravel sequences of glacial Quaternary deposits (Fig. 8.2). A clay-till unit blankets most of the upper surface of the CLBR basin. These sediments unconformably rest on thick (>200 m) Cretaceous organic-rich marine shale of the Lea Park and Colorado Group (Prior et al., 2013). Neogene and Quaternary stratigraphy of the area was mapped by Andriashek and Fenton (1989), Andriashek (2003), and Parks et al. (2005). Based on their observations and lithological description of each formation or unit, twelve distinct hydrostatic units were identified as regional aquifers and aquitards (Table 8.2).

Table 8-2: Physical properties of the eight formations in the CLBR glacial drift deposits (revised after Parks et al. (2005)).

Formation	Lithology	Hydrogeology	Area (km <sup>2</sup> )	Volume (km <sup>3</sup> )	Thickness (m)
<i>Quaternary Period</i>					
Grand Center (GC)	till	aquitard	16,000	810	1 - 150
Sand River (SR)	sand/silt	aquifer	5,000	13	1 - 85
Marie Creek (MC)	till	aquitard	12,000	300	1 - 100
Ethel Lake (EL)	silt/sand/gravel	aquifer	4,600	31	1 - 65
Bonnyville Unit 2 (BNV2)	till	aquitard	12,700	310	1 - 150
Bonnyville (BNV)	sand/gravel	aquifer	1,100	8	1 - 65
Bonnyville Unit 1 (BNV1)	till	aquitard	5,200	78	1 - 95
Muriel Lake (ML)	sand/silt/gravel	aquifer	4,800	65	1 - 50
Bronson Lake (BL)	diamicton/clay	aquitard	3,200	34	1 - 100
Empress Unit 3 (E3)	sand/gravel	aquifer	1,600	19	1 - 110
Empress Unit 2 (E2)	clay/silt	aquitard	1,100	13	1 - 55
<i>Neogene Period</i>					
Empress Unit 1 (E1)	sand/gravel	aquifer	2,200	22	1 - 55

Bedrock incisions from preglacial and glacial drainage have produced a network of buried paleovalley and buried glaciofluvial channel aquifers throughout the CLBR basin. As a result, regional groundwater flow in aquifers is constrained by surficial topography, deep surface water bodies, and bedrock topography (Parks et al., 2005). Recharge occurs in the uplands, particularly in the north, with discharge and flowing artesian conditions occurring in the low lands near the confluence of the Sand and Beaver Rivers, eastern reaches of the Beaver River, and near some lakes (Fig. 8.1). Cold Lake is approximately 100 m deep and represents both a groundwater discharge site as well as a source of recharge for hydraulically connected aquifers (Fig. 8.2). In the deeper Empress aquifers, flow is laterally confined by bedrock barrier boundaries, whereas shallower aquifers tend to exhibit stronger influences from topography. Cross-formational flow between shallow and deeper aquifers occurs across till sheets mostly at hydraulic windows associated with cross-cutting sands and gravels deposited during glacial and more recent erosional events (Parks et al., 2005). In general, groundwater flow in all aquifers is downward along the flanks of the CLBR watershed and laterally directed toward the Beaver

River downstream of the Sand River confluence, signifying a strong influence from surficial topography (Fig. 8.1).

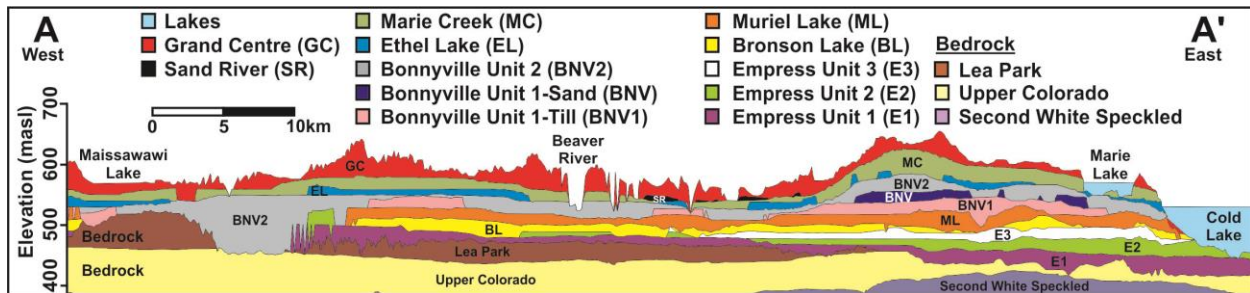


Figure 8-2. Cross-section, A–A' from Figure 8.1b, showing the distribution of stratigraphic units across the Cold Lake-Beaver River Basin (revised after Parks et al. (2005)).

## 8.5 Methods

### 8.5.1 Groundwater Chemistry

The majority of the groundwater geochemistry data used in this study was provided by Alberta Environment and Sustainable Resource Development that included data from the Alberta Water Well Information Database (<http://environment.alberta.ca/01314.html>), AHW (2000), Beaver River Watershed Alliance database, and a number of industry studies. The groundwater database for the CLBR basin included 527,349 entries containing groundwater geochemistry and/or water levels. This database was filtered to remove entries where depth, or latitude and longitude were missing, and geochemistry data with charge balance errors exceeding 10%, and industrial monitoring wells that could potentially be impacted by enhanced thermal in situ oil recovery operations. Statistical analyses such as the median, mean, maximum, minimum, and standard deviation were determined for wells that were sampled multiple times. The final data set was reduced to 1537 wells with geochemistry including pH, alkalinity and major anion and cations, 779 of which also had As concentration data. Additional groundwater chemistry was added to the data set from AHW (2014) and this study to ensure the most complete data set was

interpreted. Alberta Environment provided geochemistry data from their Groundwater Observation Well Network (GOWN), including stable isotopes of  $\delta^{34}\text{S}_{\text{SO}_4}$  and  $\delta^{13}\text{C}_{\text{DIC}}$  and the radiogenic isotope  $^{14}\text{C}_{\text{DIC}}$ . In total 816 wells with As concentrations were used for mapping.

A total of 13 groundwater wells were sampled during this study using a peristaltic pump and 6.4 mm diameter (1/4-in.) polyethylene tubing. Sample tubing was lowered into the well screen and pumped at a low-flow rate following the method of Puls and Barcelona (1996). Water levels were periodically measured during pumping to ensure that no or minimal drawdown was occurring. Measurements of pH, Eh, temperature, electrical conductivity and dissolved oxygen (DO) were made in the field using a Hydrolab with probes sealed in a flow-through cell. All probes in the Hydrolab were calibrated prior to sampling. Water samples were collected when pH and Eh values stabilized. Water samples were collected for major anions and cations, trace metals, and dissolved organic carbon (DOC) from each well. All water samples were filtered with 0.45  $\mu\text{m}$  polyethersulfone filters and stored in prewashed Nalgene bottles. One aliquot of water was acidified with 12 N trace-metal grade  $\text{HNO}_3$  to a pH of <1 for cation and dissolved metals analysis, and other aliquots were left unacidified. All water samples were immediately refrigerated at 4 °C until analyses. Water samples were analyzed using inductively coupled plasma-optical emission spectrometry (ICP-OES) analysis for major cations, inductively coupled plasma-mass spectrometry (ICP-MS) for trace metals, and ion chromatography (IC) for anions. Combustion and infrared detection was used for DOC analysis. Measurements of alkalinity were made in the field on filtered samples using a Hach digital titrator and bromcresol green/methyl red indicator and 0.16 N  $\text{H}_2\text{SO}_4$ .

Maps showing the spatial distribution of As concentrations in groundwater were created using ArcGIS. Shape files for all geological formations in the CLBR basin were provided by the Alberta Geological Survey. Arsenic data was mapped by individual formations/aquifers. All

formation units were mapped except the Bonnyville Unit 1 and 2, Bronson Lake, Empress 2 Formations and bedrock due to limited data points.

### **8.5.2 Arsenic Speciation**

There was a much smaller subset of data with speciated As analysis available from groundwater, including the AHW (2014), the GOWN wells and this study. During the AHW (2014) survey, 132 groundwater samples were speciated into As(III) and As(V) at the University of Alberta by using a HPLC-ICP-MS following the methods of Le and Ma (1998) and Gong et al. (2006). An additional 34 samples from the GOWN wells and nine from this study were speciated into As(III) and As(V) in the field using a modified anion-exchange method of Ficklin (1983) followed by ICP-MS analyses.

### **8.5.3 Geochemical Modeling**

The geochemical model PHREEQC 2.18 (Parkhurst and Appelo, 1999) using the WATEQ4F (Ball and Nordstrom, 1991) database was used to elucidate mineral phases that may be controlling As concentrations in the groundwater. PHREEQC is an equilibrium/mass-transfer model that provides calculations of saturation indices (SI) for discrete mineral phases. To calculate SI for this study, the minimum parameters required from a groundwater sample included pH, Eh, alkalinity ( $\text{mg L}^{-1} \text{CaCO}_3$ ), Ca, K, Mg, Na,  $\text{SO}_4$ , Cl, Al, Fe, As and temperature. For wells with multiple sampling events, the most recent or most complete data set was used for modeling. In total, groundwater speciation calculations were made for groundwater samples collected from 605 wells. The computer program NETPATH (Plummer et al., 1994; Parkhurst and Charlton, 2008) was used to adjust  $^{14}\text{C}_{\text{DIC}}$  groundwater ages.

#### 8.5.4 Solid Phase Analyses and Mineralogy

Solid phase concentrations of As in sediments from the CLBR basin were obtained from Andriashek (2000; n = 175) and Fennell (2008; n = 21). In addition, we analyzed 26 sediment samples for total metal concentrations using HF/HNO<sub>3</sub> extraction followed by ICP-MS. Sediments were collected at two locations in the CLBR basin (Fig. 8.1b) using an auger drill rig equipped with a split-spoon sampler described by Moncur (2010). Sediment samples were collected every 0.25 m over the first 3 m of drilling followed by sampling at 0.5 m intervals for the remaining depths. Samples were collected from Site 1 and Site 2 to depths of 15 m and 13.5 m, respectively (Fig. 8.1b). After collection, samples were immediately frozen.

Samples for mineralogical analysis were shipped frozen to the laboratory where they were air-dried, de-agglomerated, homogenized and split into representative fractions. Eleven sediment samples were analyzed from Site 1, and four sediment samples were analyzed from Site 2. Primary crystalline phases were determined for all samples by X-ray diffraction (XRD) using a RIGAKU D/MAX 2500 rotating-anode powder diffractometer. More detailed identification of individual phases in the secondary precipitates was made using a Rigaku Rapid II rotating anode micro-XRD. For some samples, mineral species identified by XRD were confirmed by energy-dispersive spectrometry (EDS) using a JEOL JXA 8900 electron probe micro-analyzer (EPMA) to provide qualitative information about the composition of the main mineral phases observed in the polished section. Backscattered electron imaging (BSE) and quantitative wavelength-dispersive X-ray spectrometry (WDS) were used to locate and determine the compositions of the main carriers of As. X-ray absorption fine structure spectroscopy (XANES) experiments were carried out at the bending magnet beamline 20-BM at sector 20 of the Advanced Photon Source (APS), Argonne, IL, USA. XANES was used to



determine the oxidation states of As mineral phases in two sediment samples collected at 5.5 and 6 m depths at Site 1 and two sediment samples collected at 1 and 11.5 m depths at Site 2 (Fig. 8.1b). Finely ground and homogenized samples were loaded into Teflon sample holders with Mylar windows. Experiments were carried out at room temperature in the fluorescence mode using a Canberra 13-element detector. A Au foil was used for energy calibration for As K-edge XAFS measurements. Between five to eight scans were made on each sample. Data reduction and analysis were performed with ATHENA (Ravel and Newville, 2005). The least-squares fitting assessment of the XANES spectra were performed with LSFITXAFS (Paktunc, 2004).

## **8.6 Results and Discussion**

### **8.6.1 Sources and Controls of Arsenic**

Results of the solid-phase As analysis of sediments from the CLBR basin are summarized in Table 8.3. Whole rock analyses of 216 unconsolidated sediment samples indicate that the mean As concentration was 6 ppm (min = 0.3; max = 17). These As concentrations are in the range typical for glacial deposits (average = 9; min = 2; max = 170) (Smedley and Kinniburgh, 2002). The mean As concentration measured from the eight Lea Park Formation marine shale samples was 17 ppm (min = 8.4; max = 20). Arsenic concentrations in the glacial drift sediments are relatively constant with depth for most locations (Fig. 8.3), with a few exceptions, including a sharp increase in concentration within the Lea Park marine shale and elevated concentrations at a few other locations. Marine shales typically contain the highest As content in the earth's crust, following gold ores (Nordstrom, 2012). Leckie et al. (1994) found that shales from the Lea Park Formation and Upper Colorado Group that underlie the CLBR basin contained abundant pyrite.

Table 8-3: Total As concentrations measured in sediments from the CLBR basin, including data from Andriashek (2000), Fennell (2008) and this study. All values are in ppm. BR refers to bedrock and n refers to number of samples.

Formation	n	Median	Mean	Minimum	Maximum
Grand Center	64	6.4	6.7	1.2	17
Sand River	4	3.5	3.4	2.4	4.1
Marie Creek	71	5.6	5.9	3.2	14
Bonnyville	67	7.9	6.9	1.2	14
Muriel Lake	10	1.1	1.0	0.3	1.6
Lea Park (BR)	6	18	17	8.4	20
Total – Drift	216	6.3	6.2	0.3	17
Total – Drift + BR	222	6.4	6.5	0.3	20

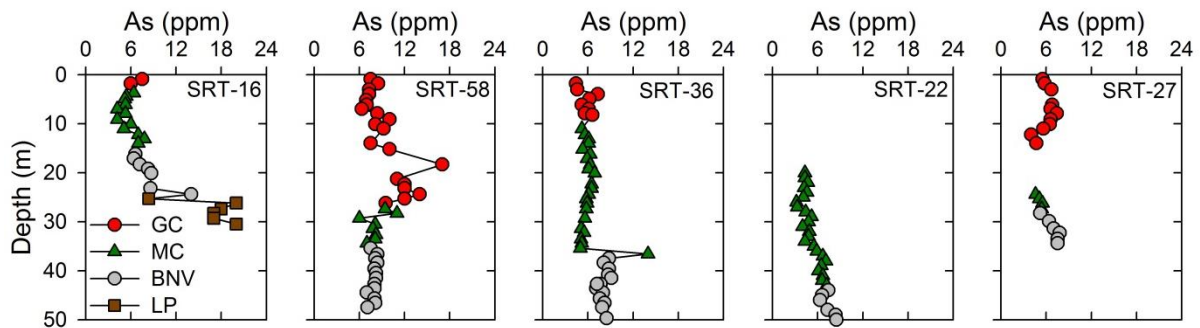
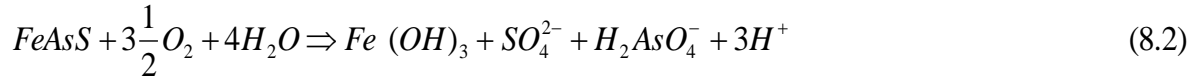
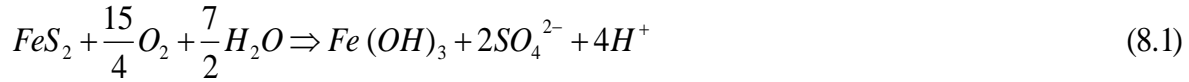


Figure 8-3: Depth profile of total As concentrations from five bore-holes in the Cold Lake - Beaver River basin. GC - Grand Centre; MC - Marie Creek; BNV - Bonnyville; and LP -Lea Park Formations. Data from Andriashek (2000).

The As-bearing sediments in the CLBR basin were glacially deposited, except for the Empress 1 and 2 Formations that were deposited prior to glaciation. During four glaciation events, rock was eroded from the Canadian Shield, Cretaceous age marine shales and Devonian aged carbonates and transported and deposited in the CLBR basin (Andriashek and Fenton, 1989). Most of the sediments observed in CLBR basin sediments are composed of igneous and metamorphic fragments, shale and carbonates. The primary source of As within these source-rocks is likely sulfide minerals. Marine shale from the Colorado Group that underlies much of the CLBR basin, contained 5-8 wt.% pyrite (Rokosh et al., 2009). During glaciation, these sulfide minerals would have been exposed to the atmosphere. Sulfide minerals are unstable when

in contact with oxygen and will oxidize (Nordstrom, 1982). For example, the oxidation of pyrite and arsenopyrite can be expressed as:



The oxidation of pyrite (Eq. (8.1)) and arsenopyrite (Eq. (8.2)) results in formation of secondary Fe oxyhydroxide and the release of  $SO_4$ , arsenate and  $H^+$ . The release of  $H^+$  may reduce the porewater pH, however sediments from the CLBR basin have a high carbonate content (Andriashek and Fenton, 1989) maintaining a circumneutral groundwater pH through buffering. Although not shown in (8.1), pyrite is a common carrier of As (Nordstrom, 2002; Majzlan et al., 2014) and will release arsenic during oxidation. Under circumneutral pH and oxidizing conditions, arsenate will adsorb to Fe oxyhydroxide mineral phases (Dixit and Hering, 2003).

As glaciation in the CLBR basin progressed, previously deposited sediments were buried by advancing glaciation and eventually water tables within the sediments were established, limiting  $O_2$  diffusion into the sediments. In addition, the consumption of  $O_2$  by microbial oxidation of organic carbon [ $CH_2O$ ] will lead to anoxic conditions in the groundwater (Lovley, 1987). Under reducing conditions, As can be released to groundwater through reductive dissolution of arseniferous Fe oxyhydroxides. During the reductive dissolution, Fe reducing bacteria consume  $CH_2O$  and utilize Fe(III)-oxyhydroxide as an electron acceptor for anaerobic respiration (Hansel et al., 2003). The reduction of Fe(III)-oxyhydroxide results in the release of  $Fe^{2+}$ ,  $HCO_3^-$  and sorbed ions such as arsenate to the groundwater as demonstrated by Paktunc (2013) for the mobilization of arsenic as As(III) species following reductive dissolution of goethite in a tailings impoundment. Under reducing conditions, As(V) can be reduced to As(III)

(Smedley and Kinniburgh, 2002; Mukherjee et al., 2012) resulting in increased concentrations and dominance of As(III) in groundwater. Arsenic reducing bacteria such as dissimilatory arsenate respiring prokaryotes catalyze organic carbon using As(V) as an electron acceptor (Zobrist et al., 2000). The source of organic carbon in the sediments that can stimulate Fe/As reduction can be from plant material co-deposited with sediments and from DOC produced by plant or animal degradation and transported by groundwater flow. Another source of organic carbon is from glacially redeposited organic-rich shale fragments within the till matrix and thin interbedded fine grained layers within the sand and gravel. For example, in place Colorado Group shale has a high total organic carbon (TOC) content ranging from 0.27% to 11.04%, with the highest values in the Upper Colorado and Second White Specks (Tu et al., 2007). Other reactants that can promote arsenate reduction include hydrogen, hydrogen sulfide, elemental sulfur and methane (Amend et al., 2014).

In the presence of dissolved  $\text{SO}_4$ , Fe(II) and As(III), reduction may be followed by microbially-mediated (dissimilatory) sulfate reduction (DSR) where sulfate-reducing bacteria catalyze the oxidation of  $\text{CH}_2\text{O}$  reducing  $\text{SO}_4$  to  $\text{H}_2\text{S}$  (Berner, 1985). When  $\text{H}_2\text{S}$  is produced through DSR in the presence of available Fe(II) or other metals and metalloids, a secondary sulfide mineral will precipitate (Berner, 1985). DSR decreases the concentrations of dissolved  $\text{SO}_4$ , Fe(II), and other elements such as As(III), and increases alkalinity and pH in the groundwater (Tuttle et al., 1969; Buschmann and Berg, 2009). Significant isotope fractionation of sulfur enrichment is another important indicator of DSR (Mayer, 2005).

To determine if As-bearing minerals were present in the CLBR basin, a detailed quantitative mineralogical characterization of the sediments was performed in two areas of the watershed (Fig. 8.1b). Both sites were located where the Grand Centre Formation outcrops and were approximately 22 km apart. At Site 1 a borehole was drilled to a depth of 15 m, and at Site

2, a borehole was drilled to a depth of 13.5 m. Sediments were visibly oxidized to depths of 5.8 m and 4.9 m at Sites 1 and 2, respectively. The results of the XRD analyses revealed similar mineralogical compositions in the sediments from Sites 1 and 2, with the crystalline phases consisting mainly of quartz, microcline, albite, calcic plagioclase, calcite, and amphibole, with various amounts of clay minerals such as kaolinite, montmorillonite and mica. No obvious mineralogical differences in the XRD analyses were observed between the brown oxidized and gray unoxidized sediments.

Small pyrite grains, typically framboidal in habit were found throughout the unoxidized sediment samples at Sites 1 and 2 (Fig. 8.4a and b). Although the pyrite does not represent a major mineral phase, it is common throughout the samples. The textural features of the framboidal pyrite grains suggest that pyrite is a neomineral formed within the sediments post deposition. Considering that pyrite is a common As carrier (Nordstrom, 2002), 19 BSE images of individual grains were taken and their compositions were analyzed by WDS to determine whether As was a significant compositional component. The As content of pyrite in samples was variable, reaching 1550 ppm in a sample at Site 1, 6 m depth, and 1840 ppm in a sample from Site 2 at an 11.5 m depth, with averages of 460 and 590 ppm, respectively (Table 8.4). The presence of As in the pyrite grains analyzed suggests that pyrite is an important As carrier in these sediment samples. None of the pyrite grains examined from the unoxidized sediments showed any evidence of oxidation features. Framboidal pyrite was not observed in the sediment samples from the oxidized zone (Site 1-1 m, and Site 2-1 m), but instead spheroidal Fe oxyhydroxide grains with minor S and variable concentrations of As were observed (Fig. 8.4c and d). The habit and composition strongly suggest that these Fe oxyhydroxide grains represent pseudomorphs after framboidal pyrite grains. The As concentrations of the characterized Fe

oxyhydroxide reached values up to 670 ppm in Site 1-1 m and 2270 ppm in Site 2-1 m with averages of 200 and 770 ppm, respectively (Table 8.4).

Table 8-4: Arsenic concentration (ppm) of Fe(III)-oxyhydroxide [FeOOH] and pyrite grains in sediments from Sites 1 and 2, determined by WDS-EPMA.

Location	Site 1	Site 1	Site 2	Site 2
Depth	1 m	6 m	1 m	11.5 m
Mineral	FeOOH	Pyrite	FeOOH	Pyrite
Sediment	oxidized	unoxidized	oxidized	unoxidized
Sample 1	<100	<100	2270	<100
Sample 2	<100	180	440	780
Sample 3	<100	190	710	570
sample 4	280	470	400	410
Sample 5	320	<100	<100	184
Sample 6	370	790		<100
Sample 7	670	<100		320
Sample 8	380	1550		
Sample 9	<100	570		1760
Sample 10	<100	810		180

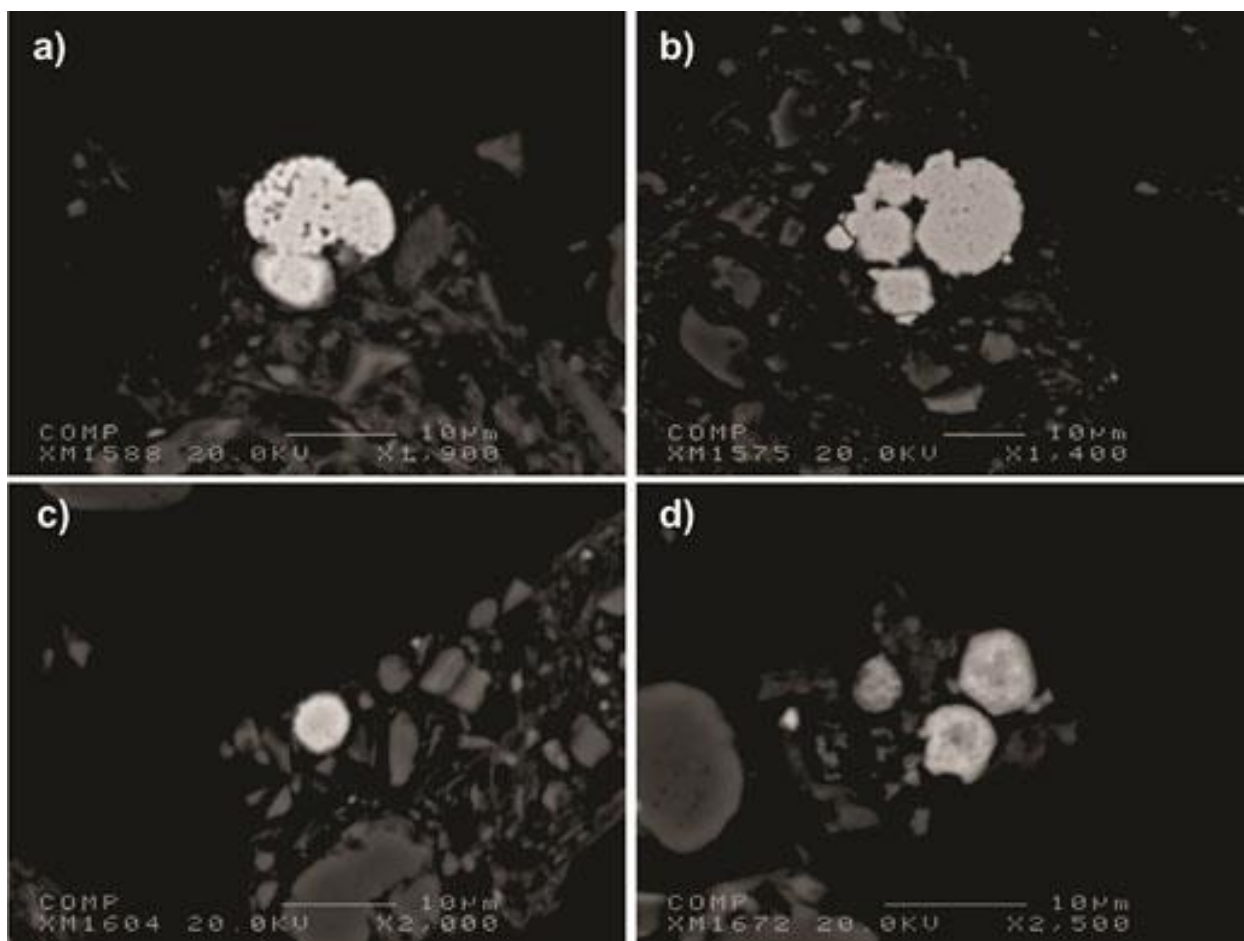


Figure 8-4: BSE images of representative As-bearing mineral phases observed in sediment samples showing frambooidal pyrite at: (a) Site 1, 6 m depth; (b) Site 2, 11.5 m depth. Secondary Fe oxyhydroxide pseudomorphs after frambooidal pyrite at: (c) Site 1, 1 m depth; (d) Site 2, 1 m depth.

K-edge XANES spectra were collected to determine the valence state (-I, III, V) in which As occurs based on the location of the absorption edges. Arsenic can occur within the structure of arsenopyrite and pyrite as As(-I), which is susceptible to oxidation particularly in the frambooidal types of pyrite (Paktunc, 2008). All of the sediments with elevated concentrations of As ( $4.3\text{-}7.4\text{ mg kg}^{-1}$ ) had spectra with the main absorption peak centered at  $11874.7\text{ eV}$  (dashed line) indicating that the dominant species was As(V) (Fig. 8.5). The spectral features above the edge in Figure 8.5 were similar to those of goethite or ferrihydrite with adsorbed As (Paktunc et al., 2004, 2008), suggesting that these Fe(III)-oxyhydroxides are the dominant As carriers in the

sediments with elevated As concentrations. The sediment samples at 5.5 and 6 m depths along bore-hole Site 1-1 m representing oxidized and unoxidized sediments displayed similar XANES spectra dominated by As(V). The spectra collected for oxidized and unoxidized sediment samples from 1 and 11.5 m depths along the Site 2 borehole displayed differences in their As K-edge. The spectrum of an unweathered sample from 11.5 m depth had a shoulder on the lower energy side of the main absorption peak suggesting the presence of reduced As(-I) species in addition to As(V) (Fig. 8.5). The derivative value of this shoulder is 11868.5 eV which is close to those of arsenopyrite and arsenian pyrite suggesting the presence of As(-I) species in addition to As(V). The presence of As(-I) species in the unoxidized portions of the sediments were consistent with the presence of sulfide minerals such as arsenian pyrite and arsenopyrite.

Previous mineralogical analyses of sediments from the Muriel Lake Formation (Fennell, 2008) also indicated the presence of framboidal pyrite in the sediments. In this study, SEM-microprobe analysis of the pyrite detected the presence of As, but only qualitatively at low concentrations. XANES analysis of the sediments identified As(V) as the dominant species, with minor amounts of As(III) present.

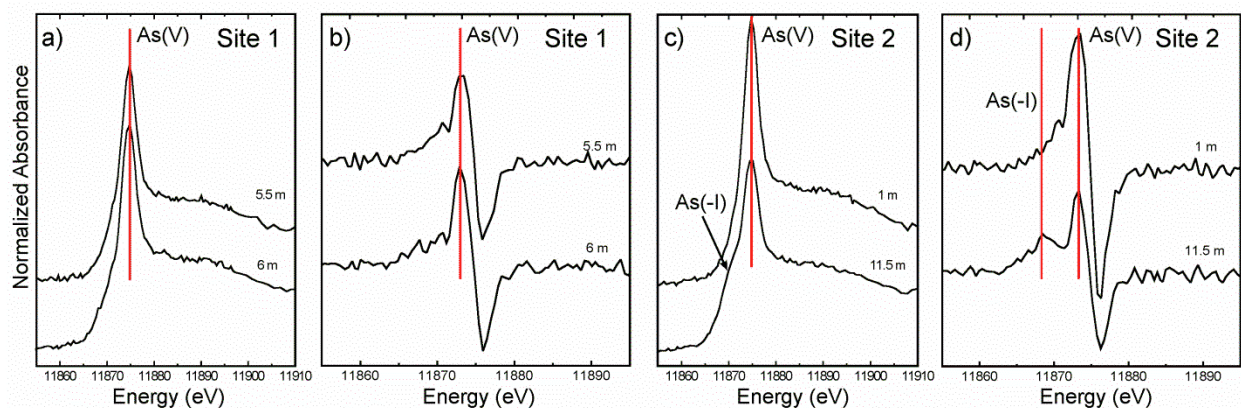


Figure 8-5: Normalized As K-edge XANES spectra for sediment samples collected at: (a) Site 1, 5.5 and 6 m depths (c) Site 2, 1 and 11.5 m depths; and derivatives for samples from (b) Site 1 and (c) Site 2. Vertical line is at 11874.7 eV representing the main absorption peak for As(V) and 11868.5 eV in (d) representing As(-I).



## **8.6.2 Arsenic Distribution in Groundwater**

Understanding the distribution of As concentrations in aquifers is crucial for determining the placement of wells for extraction of potable water and health-risk studies. Arsenic concentrations in groundwater varied spatially across the CLBR basin and within individual formations, with no obvious trends observed along groundwater flow paths (Fig. 8.6). Overall, there were no obvious distribution patterns of As in groundwater except for an area west of Cold Lake where As concentration in some wells are elevated in all formations except the Grand Centre Formation. The heterogeneous nature of glacially deposited sediments likely influences the random distribution of As in both solid and aqueous phases within the CLBR basin.

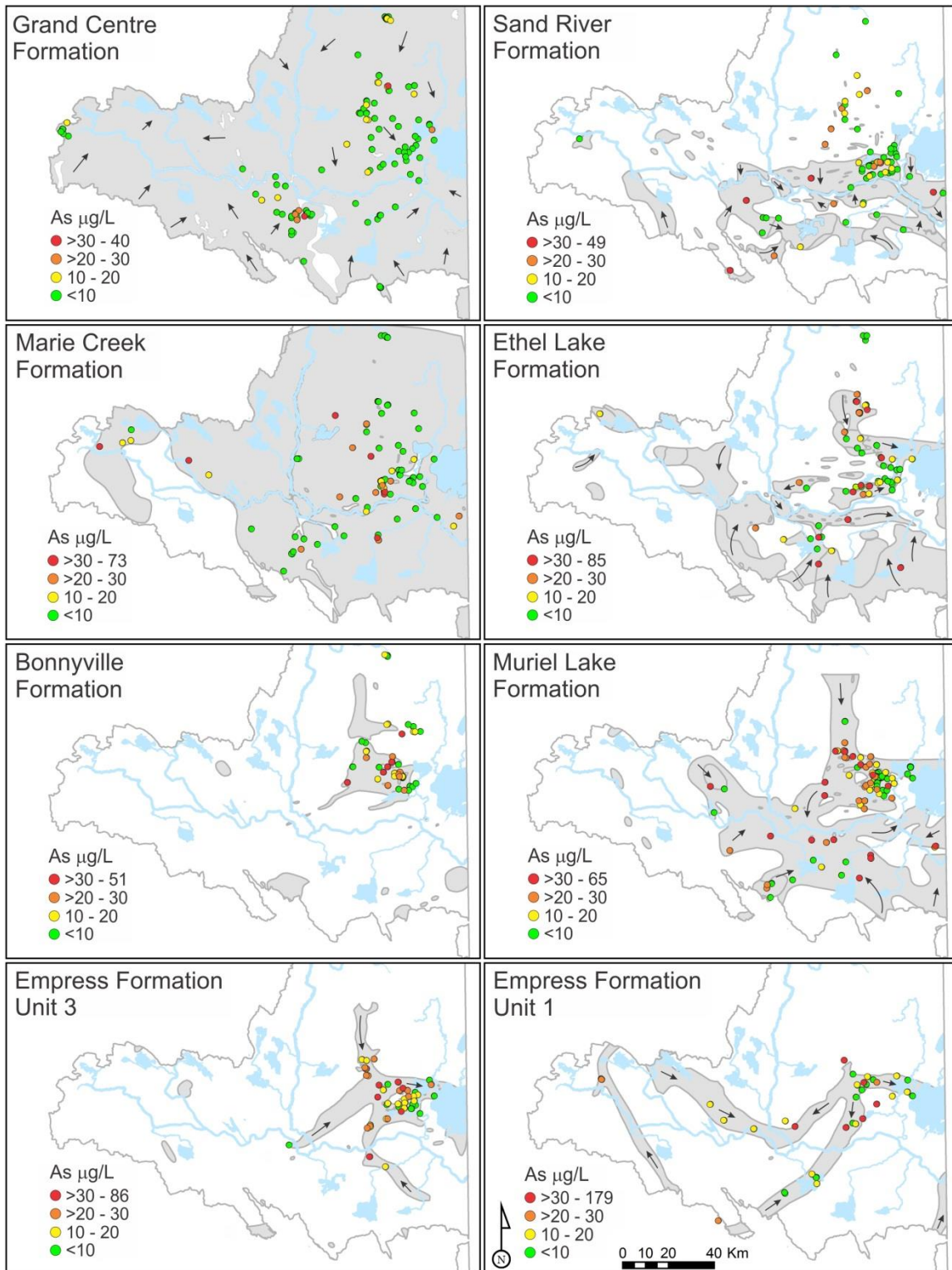


Figure 8-6: Spatial distribution of As in groundwater across the CLBR Basin. Arrows show groundwater flow direction in each formation (modified after Parks et al. (2005)). Gray shading indicates the extent of each formation. There was insufficient data to map groundwater flow in the Marie Creek and Bonnyville Formations. Scale bar and north arrow applicable to all submaps.

The mean concentration of As in all glaciofluvial formation groundwaters was  $15 \mu\text{g L}^{-1}$ , ranging from  $<1$  and  $179 \mu\text{g L}^{-1}$ , with 50% of the wells exceeding  $10 \mu\text{g L}^{-1}$  (Table 8.5). Arsenic concentrations in groundwater were lowest in the uppermost Grand Centre Formation with only 17% of the wells exceeding  $10 \mu\text{g L}^{-1}$ , whereas concentrations were highest in the deeper Empress 3 Formation where 70% of the wells were  $>10 \mu\text{g L}^{-1}$ . There were minimal differences in As groundwater concentrations between aquitard and aquifer units. For example, average concentrations of As in groundwater between the aquitard and aquifer units in the Bonnyville and Empress Formations only differed by a few micrograms per liter. In general, As concentrations in groundwater increased with depth through the unconsolidated sediments. Within the underlying shale units, all seven of the wells sampled had As concentrations that were below  $10 \mu\text{g L}^{-1}$ . It was previously suggested that elevated As concentration in shallow Quaternary aquifers in Alberta could originate from the underlying pyritic shales (AHW, 2000; Fitzgerald et al., 2001). However, the low As concentrations in groundwater from these deep shales suggest that they are not directly contributing to elevated concentrations (Table 8.5). Nevertheless, if these shales were exposed to oxygen by over pumping of a well or if fragments of these shales are present in near-surface sediments, arsenian sulfide minerals could oxidize releasing As to the groundwater.

Groundwater from the CLBR basin had As(III) as the principal species, accounting for 80% of the As (Table 8.5). Groundwater from the Grand Centre Formation had the lowest As(III) ratio making up only 46% of the As. Overall the As(III) ratio increased with depth. At depth, over 80% of the groundwater from aquifer units contained As(III), whereas groundwater from till units had lower percentages of As(III)/As<sub>T</sub>, except for the Bonnyville Unit 1 Till. The dominance of As(III) over As(V) in groundwaters from the CLBR basin indicates a strongly reducing environment.

Table 8-5: Arsenic concentrations in groundwater from formations in the CLBR Basin.

Formation	n	Median $\mu\text{g L}^{-1}$	Average $\mu\text{g L}^{-1}$	Max. $\mu\text{g L}^{-1}$	Min. $\mu\text{g L}^{-1}$	Wells	% Wells	As(III)/As <sub>T</sub>	
						Exceeding 10 $\mu\text{g L}^{-1}$	Exceeding 10 $\mu\text{g L}^{-1}$	(n)	%
Grand Center	149	3	6	70	<1	23	17	23	46
Sand River	79	8	12	61	<1	32	41	27	66
Marie Creek	101	8	11	160	<1	30	33	29	65
Ethel Lake	80	11	15	100	<1	41	51	21	82
Bonnyville Unit 2	33	10	17	110	<1	16	48	14	61
Bonnyville	75	11	14	70	<1	37	51	6	85
Bonnyville Unit 1	21	11	16	50	2.0	11	52	3	88
Muriel Lake	133	17	19	140	<1	89	67	25	82
Bronson Lake	14	22	21	70	<1	8	57	4	72
Empress Unit 3	71	18	19	86	<1	50	70	8	80
Empress Unit 2	10	10	16	100	5.9	5	50	-	-
Empress Unit 1	43	11	17	179	<1	25	58	15	84
Lea Park	2	3	3	3.1	2.9	0	0	-	-
Upper Colorado	3	4	3.3	4.4	2.0	0	0	-	-
2 <sup>nd</sup> White Specks	2	-	5	9	<1	1	0	-	-
Average Glacial	816	11	15	124		27	50	175	74

Arsenic concentrations within groundwater from the CLBR basin appear to be strongly influenced by redox conditions. Arsenic concentrations increased as the Eh decreased, with the highest As concentrations associated with the lowest Eh values (Fig. 8.7). The groundwater samples from reducing environments with elevated As concentrations tended to have lower concentrations of SO<sub>4</sub> and Fe(II). The highest As concentrations were found in groundwater with circumneutral pH conditions and with alkalinities at approximately 600 mg L<sup>-1</sup> CaCO<sub>3</sub>. The average DOC concentrations in the groundwaters across the CLBR basin was 3.1 mg L<sup>-1</sup>, but the

highest As concentrations were found in groundwaters with about 5 mg L<sup>-1</sup> of DOC. These average groundwater DOC concentrations are not particularly high, but even at low concentrations, OC (<1%) in the sediments can promote microbially mediated reduction reactions (Hery et al., 2010). Geochemical modeling calculations indicated that 72% of groundwater from the wells were at equilibrium or undersaturated with respect to ferrihydrite (Fig. 8.7). These calculations suggest that the primary mechanism for As release from the sediments is the reductive dissolution of Fe oxyhydroxides. In addition to the release of As, elevated concentrations of Fe would be expected during reductive dissolution of Fe oxyhydroxides provided that the dissolution is congruent and the Fe species remains in solution. The correlation between As and Fe concentrations in the groundwater were not strong, except for the Bronson Lake Formation ( $R^2 = 0.71$ ). All other As to Fe relations had a  $R^2 < 0.26$ . This poor correlation between As and Fe may be due to scavenging of Fe during siderite [FeCO<sub>3</sub>] precipitation. Speciation model calculations found that 80% of groundwater for the wells was at equilibrium or supersaturated with respect to siderite. The detection limit for siderite by XRD is several percent. If present, it likely would be in trace quantities in the sediment. Siderite precipitation will remove Fe(II) from solution and is known to be an effective sink for As in groundwater (Mumford et al., 2012), sorbing both As(III) and As(V) (Islam et al., 2005), with the sorption of As(III) being the weaker of the two oxidation states (Jonsson and Sherman, 2008). Ferric-oxyhydroxide phases were not identified in the unoxidized sediments during the mineralogical study, yet XANES experiments revealed that over 75% of the solid-phase As concentrations in the sediments was As(V), similar to observations by Javed et al. (2014) who observed 25-75% of As in other areas of the CLBR basin sediments was bound in oxides. In other aquifers with elevated groundwater As concentrations, reductive dissolution of Fe oxyhydroxides has been proposed as the principal process for As release from alluvial and

glaciofluvial sediments, for example in Southeast Asia (Nickson et al., 2000; Fendorf et al., 2010), USA Midwest (Kelly et al., 2005; Erickson and Barnes, 2005), China (Guo et al., 2013) and Alaska (Munk et al., 2011). Although the groundwater chemistry, speciation modeling and mineralogy all are consistent with the prevalence of reductive dissolution of Fe oxyhydroxides in deeper sediments from the CLBR basin, competitive desorption by phosphate or silica (Manning and Goldberg, 1996; Holm, 2002) or desorption from clay minerals cannot be ruled out as additional processes that may be contributing to As release to groundwater.

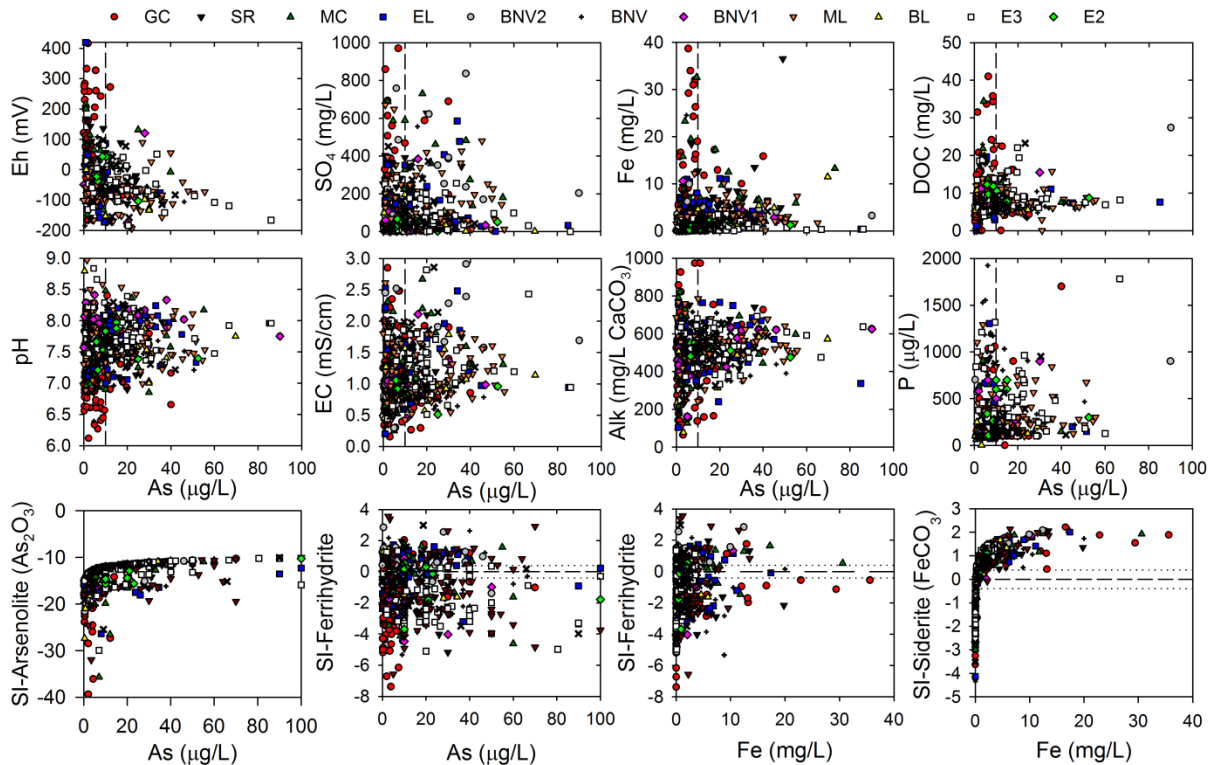


Figure 8-7: The relationship between As concentrations in groundwater and various other aqueous parameters (top two rows). Plots in the bottom row show calculated SI values for arsenolite, ferrihydrite and siderite (near equilibrium conditions  $SI = -0.4$  to  $0.4$ , are represented by the horizontal dashed lines). Symbols are representative of the different formations included in the data set.

There are general trends in pH and Eh conditions related to depth and geological formation (Fig. 8.8). The most oxidizing conditions (Eh and DO) were observed at shallow depths, in the near surface zone of the Grand Centre and Sand River Formations. Groundwater

from the Grand Centre Formation had the lowest pH values which corresponded to the highest concentrations of F, Cl, Si and Ca, Mg, U, and Fe. Chemical weathering occurring in the surficial sediments is likely releasing elevated concentrations of ions to the porewater which is displaced downward into shallow groundwater; this observation is consistent with the mineralogical analyses of the near-surface Grand Centre Formation sediments that showed visibly oxidized sediments and the complete consumption of sulfide minerals in the weathered zones.

Groundwater sampled from 1 m below the oxidized zone in the Grand Centre Formation had a depressed pH and elevated concentrations of major ions in the groundwater. In addition to elevated major anions and cations, elevated concentrations of  $\text{NO}_3$  and DOC were present in the shallow groundwater (Fig. 8.8). The elevated concentrations of  $\text{NO}_3$  and DOC are likely from anthropogenic sources such as the application of fertilizers, feed lots, and sewage seepage from septic tanks and lagoons. Elevated DOC was also observed in deeper groundwater >100 m depth (Fig. 8.8). The source of DOC at depth is likely organic-rich shale that is dispersed throughout the unconsolidated sediments.

In addition to biogeochemical redox reactions that release As from sediments, hydrogeologic properties of the aquifer material will influence groundwater flow and residence time, affecting As concentrations (Smedley and Kinniburgh, 2002). The  $^{14}\text{C}$  and  $^3\text{H}$  data indicate the Grand Center and Marie Creek Formations have the youngest groundwater ages (Table 8.6). Tritium was not detected in any of the samples from the Ethel Lake Formation or deeper, indicating no evidence of post 1950s water in these samples. There was a wide range in  $^{14}\text{C}$  ages for some of the formations, but in general groundwater ages increase with depth. The large range in ages in some formations (*e.g.* Empress Unit 1) are not surprising since the well locations are located along a flow path, and the oldest ages are associated with the more distal reaches of the formation. These long residence times of groundwater flow in the aquifers can influence As

mobilization. For example, the average As concentration in groundwater from the Grand Centre Formation was  $6 \mu\text{g L}^{-1}$  with modern aged water signifying a short groundwater flow path and residence time. Conversely, the average As concentration in the Empress Unit 1 was  $17 \mu\text{g L}^{-1}$  with groundwater ages ranging from 25,000 and 3,000 years before present, indicating a long groundwater flow path and residence time. The long groundwater flow path and residence time can allow As to accumulate in the groundwater to where concentrations become hazardous (Barringer and Reilly, 2013).



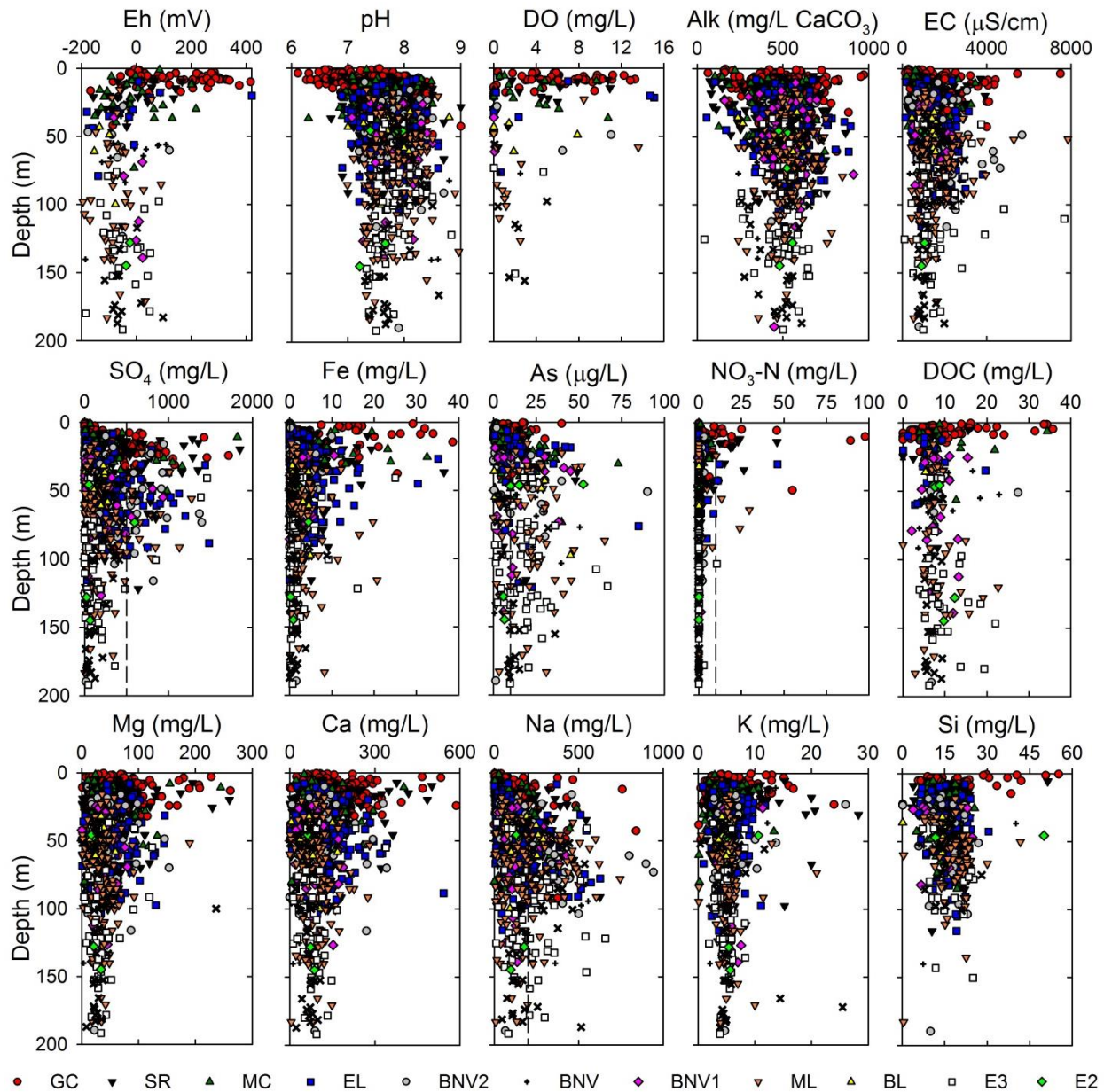


Figure 8-8: Depth profiles of groundwater chemistry from the CLBR basin. The vertical dashed lines represent maximum allowable drinking water limits.

Sulfur isotope ratio determinations on the  $\text{SO}_4$  ion is a valuable tool for determining sources of dissolved  $\text{SO}_4$  in groundwater. Typical values of  $\delta^{34}\text{S}_{\text{SO}_4}$  derived from sulfide oxidation range between -30‰ and +10‰ (Mayer, 2005). With the exception of the data from the Empress Unit 3 Formation, the  $\delta^{34}\text{S}_{\text{SO}_4}$  results for the other formations are consistent with  $\text{SO}_4$  originating from the oxidation of pyrite (Table 8.6). The depleted isotopic composition of

groundwater from the formations suggests the oxidation of sulfides during recharge and glaciation contributed to SO<sub>4</sub> concentrations and that earlier redox conditions in the formations were potentially oxic. Within the Empress Unit 3 Formation, the δ<sup>34</sup>S<sub>SO4</sub> value in groundwater near the recharge zone was +13.8‰, with SO<sub>4</sub> and As concentrations of 42 mg L<sup>-1</sup> and 24 µg L<sup>-1</sup>, respectively. Further down-gradient along the flow-path, δ<sup>34</sup>S<sub>SO4</sub> showed significant enrichment to +36.2‰ corresponding to decreased concentrations of SO<sub>4</sub> and As of 1.3mg L<sup>-1</sup> and 9.6 µg L<sup>-1</sup>, respectively, suggesting that DSR is occurring in the Empress Unit 3 formation and potentially limiting As concentrations in groundwater.

Table 8-6: Stable isotope and radiocarbon data from groundwater in the CLBR basin. NETPATH was used to correct groundwater ages. Number of wells sampled is represented by n. VCDT refers to Vienna Canyon Diablo Troilite.

Formation	Carbon				Tritium (T.U.)	Sulfur	
	n	δ <sup>13</sup> C <sub>DIC</sub> (‰ VPDB)	<sup>14</sup> C <sub>DIC</sub> pMC	Corr. Age (years B.P.)		n	δ <sup>34</sup> S <sub>SO4</sub> (‰ VCDT)
Grand Center	1	-15.2	78.6	Recent	10.2	2	-5.8
Sand River		-	-	-	-	1	-0.2
Marie Creek	2	-15.2 to -14.0	50.9 - 99	1,700 - recent	<0.8 - 14.4	2	-1.1
Ethel Lake	4	-14.9 to -16.1	31.5 - 61.2	6,200 – 1,200	<0.8	2	-4.4
Bonnyville	1	-13.2	54.6	3700	<0.8	1	-6.2
Muriel Lake	3	-20.1 to -6.8	18.1 - 59.6	14,000 - 800	<0.8	3	+0.2
Bronson Lake		-	-	-	-	1	-7.9
Empress Unit 3	2	-18.7 to -15.2	9.9 - 28.5	18,000 – 6,700	<0.8	4	+19.5
Empress Unit 1	7	-22.7 to -13.3	5.5 - 42.4	25,000 – 3,000	<0.8	8	-0.7

### 8.6.3 Long-Term Arsenic Variations

Long-term variability of As concentrations in groundwater were evaluated using data from repeat sampling of groundwater wells from 2001 and 2009 (Fig. 8.9). The database included time-series

data for seven of the eight formations, with only data from the Bronson Lake Formation not available. The temporal variations in As concentrations in the formations were minimal, similar to what has been reported in other temporal studies (Ayotte et al., 2014). These small variations were observed in all formations. The largest variations of As were observed in the Ethel Lake and Empress Formations, although there did not appear to be any correlation in trends between the aquifers. There also did not appear to be strong seasonal variations in any of the formations as other studies have observed in groundwater from Vietnam (Berg et al., 2001), Bangladesh (Cheng et al., 2005), Mongolia (Guo et al., 2013) and the United States (Ayotte et al., 2014). The shallower wells (Sand River and Ethel Lake) showed slight increases in As concentrations, whereas the deeper wells (Bonnyville, Muriel Lake, Empress) exhibited slight decreases. Long-term trends in As concentrations could not be determined for the Grand Centre or Marie Creek wells due to their limited <3 year data set (Ravenscroft et al., 2006). It is reasonable to conclude that natural As concentrations in the groundwater from formations in the CLBR basin are not significantly variable over the long-term. However, for wells where As concentration are near maximum drinking water guidelines, the variability of As concentrations in the groundwater could be large enough to be a potential long-term risk to human health.

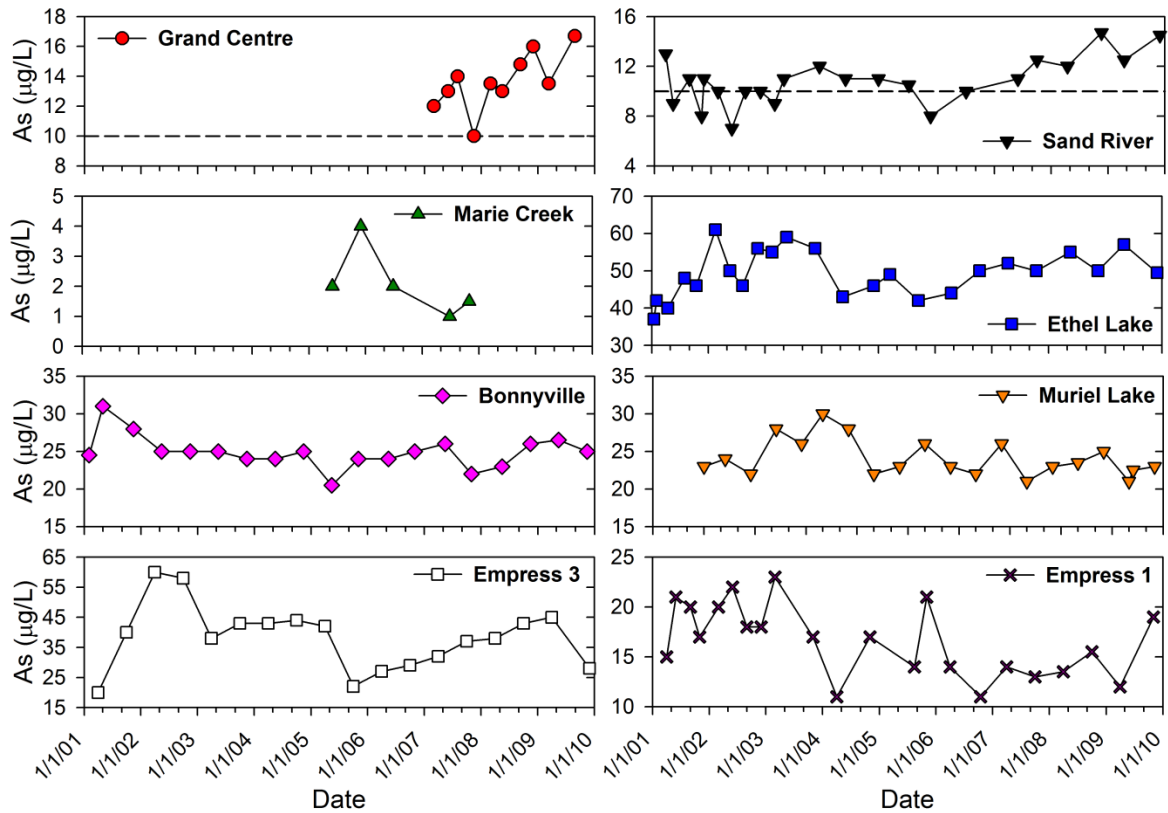


Figure 8-9: Temporal variation of As concentrations in groundwater from wells in eight aquifers within the CLBR basin from 2000 and 2010. Horizontal dashed line represents the As drinking water standard of  $10 \mu\text{g L}^{-1}$ .

## 8.7 Conclusions

Glaciofluvial aquifers of the CLBR basin contained widespread elevated arsenic concentration in groundwater with 50% of the wells exceeding  $10 \mu\text{g L}^{-1}$ . The distribution of As did not show any obvious spatial patterns or trends along groundwater flow paths. Arsenic concentrations measured from groundwater in the underlying marine shale was  $<10 \mu\text{g L}^{-1}$ . Speciation of the arsenic indicated that arsenite, the more mobile and toxic form was dominant in most of the groundwater. The highest concentrations of As was associated with reducing conditions, circumneutral pH and lower concentrations of Fe and  $\text{SO}_4$ . Speciation modeling showed that the majority of groundwater samples were undersaturated with respect to ferrihydrite. These

relations suggested that reductive dissolution of Fe oxyhydroxides may be the source of some of the As in the groundwater.

Arsenic concentrations in glaciofluvial sediment from the CLBR basin ranged from 1 to 17 ppm, with an average of 6 ppm. Mineralogical characterization of unoxidized sediment samples revealed the presence of framboidal pyrite in the deeper sediments with an average As concentration of 530 ppm, reaching up to 1840 ppm. In contrast, the near surface oxidized sediments did not contain framboidal pyrite, but exhibited spheroidal Fe oxyhydroxide with elevated As concentrations, interpreted to be an alteration product of former framboidal pyrite grains. XANES indicated that the oxidized sediments are dominated by As(V) species having spectral features similar to those of goethite or ferrihydrite with adsorbed As, suggesting that Fe oxyhydroxides are the dominant As carriers. In contrast XANES spectra collected on unoxidized sediment samples indicated the presence of a reduced As species (As(-I)) characteristic of arsenopyrite and arsenian pyrite. Ferric-oxyhydroxide phases were not identified in the unoxidized sediments during the mineralogical study, however XANES experiments revealed that over 75% of the solid-phase As concentrations in the sediments was As(V) suggesting that Fe reduction of Fe oxyhydroxides could be the main source of As to the groundwater, consistent with modeling results. Within the near-surface sediments, mineralogical analyses indicate that the oxidation of framboidal pyrite during weathering may be the source of As released to shallow aquifers in this region. Understanding the distribution and form of As present naturally in aquifer material and groundwater in the CLBR is important for managing water resources in the region, including the location of domestic water wells to minimize the potential health risks of As exposure.

# **Chapter 9:**

## *Conclusions*

## 9.1 Summary of Results

Most of the current understanding of the geochemical, mineralogical and microbial processes controlling the release and transport of low pH waters and dissolved metal(oid)s from sulfide-rich tailings has come from field and laboratory investigations on recently decommissioned or active tailings sites (*e.g.* Boorman and Watson, 1976; Blowes et al., 1991; McGregor et al., 1998; Jurjovec et al., 2002; Lindsay et al., 2009; Parviainen et al., 2009). There have been relatively few studies conducted on old tailings impoundments (*e.g.* Blowes et al., 1992; Jacob and Otte, 2004; Hayes et al., 2014), and most of these have focused on providing detailed descriptions of the distributions of geochemical and mineralogical parameters for snap-shots in time, or at best for a couple of seasons of monitoring. Tailings management and remediation requires the ability to predict long-term release and transport of low-pH waters and metals and this has largely been based on extrapolation of short-term results into the future. Studying the geochemical, mineralogical and microbial processes controlling the long-term release and transport of low-pH water and dissolved metals from the Sherridon Mine site has helped address this knowledge gap by providing a field site where the impacts of 60-80 years of oxidation of sulfide-rich tailings can be evaluated. The Sherridon tailings provided a fairly unique opportunity to study the evolution of a deposit that had minimal disturbance between the time the mine ceased operations in 1951 and the time of sample collection. Many similarly aged tailings deposits described in the literature are located at active mine sites where deposition of new tailings or process water, or remediation efforts have occurred making it difficult to clearly isolate the geochemical processes related to aging of the original tailings from the more recent activity (*e.g.*, McGregor et al., 1998; Johnson et al., 2000). In addition, the Sherridon site is located on the Precambrian Shield with well-constrained surface inflows and outflows making it

an ideal geological and structural setting for monitoring net fluxes and loadings of oxidation products from the tailings to receiving water bodies.

Pyrite [ $\text{FeS}_2$ ] and pyrrhotite [ $\text{Fe}_{(1-x)}\text{S}$ ] were the primary minerals oxidizing in the Sherridon tailings resulting in the generation of very low-pH water and elevated concentrations of dissolved  $\text{SO}_4$  and metals. There have been numerous studies on the oxidation of Fe sulfide minerals in mine tailings and subsequent release of dissolved  $\text{SO}_4$  and metals to the environment (*e.g.* Blowes and Jambor, 1990; Nordstrom and Alpers, 1999; Johnson et al., 2000; Levings et al., 2005; Moncur et al., 2006), including many review articles (*eg.* Jambor, 1994; Lottermoser, 2010; Blowes et al., 2014; Jamieson et al., 2015, Lindsay et al., 2015). Most of these studies focused on the release of metals associated with the oxidation of Fe sulfides, but the research described in Chapter 2 also examines the behavior of pyrite and pyrrhotite, and includes other, frequently overlooked Fe bearing minerals in tailings, such as sphalerite [ $(\text{Zn,Fe})\text{S}$ ], magnetite [ $\text{Fe}^{2+}\text{Fe}^{3+}_2\text{O}_4$ ], and to a lesser degree biotite [ $\text{K}(\text{Mg,Fe})_3\text{AlSi}_3\text{O}_{10}(\text{OH})_2$ ]. Weathering of these minerals will also contribute to the generation of  $\text{H}^+$  through Fe oxidation (reactions 1.3 to 1.8).

As part of this thesis (Chapter 2) the data from the Sherridon tailings were used with geochemical and mineralogical data from over 30 other tailings impoundments to develop a sequential list of the relative resistance of various sulfide minerals to oxidation. The list serves as a guide to the susceptibility of different sulfide minerals to oxidation (assuming similar textures and grain sizes). For example, the stability of sphalerite in tailings impoundments is generally greater than that of pyrrhotite, but less than pyrite, which in turn is less than magnetite (Table 2.1). Using the relative resistance of sulfide minerals as a guide, a conceptual model was developed for the sequence of events that typically occurs in an oxidized tailings impoundment over time (Table 2.3). In the earliest stage of oxidation, secondary products are formed predominantly from the alteration of pyrrhotite, with native sulfur, marcasite, Fe sulfate and Fe



oxyhydroxides derived from pyrrhotite during which pyrite shows little or no evidence of alteration. Iron oxyhydroxides typically consist of very fine-grained goethite with a high sorptive capacity. During the next stage of weathering, sphalerite oxidation releases dissolved Zn and Cd to the pore water. Dissolved Ni and Co derived from pyrrhotite, and dissolved Zn and Cd from sphalerite, commonly co-precipitate or absorb into early formed Fe oxyhydroxides. As the tailings system matures, a recycling occurs due to continued leaching from low-pH pore water and because the gradually increased crystallinity of the Fe oxyhydroxides decreases their sorptive capacity. During the late stages of oxidation, after the sulfide minerals have been consumed within the tailings impoundment, the pore water pH will eventually rise and jarosite will become unstable leaving goethite as the dominant secondary mineral.

The lack of remedial efforts at the Sherridon tailings during the past 80 years after deposition has resulted in extensive oxidation of sulfide minerals in the tailings that has produced low pH conditions and extremely high concentrations of dissolved  $\text{SO}_4$  and metals in the tailings pore water. The only Sherridon tailings that were not subjected to such a long period of oxidation were the Fox tailings. These tailings were discharged into Fox Lake and stored for six decades under a shallow 1 m water cover. A number of laboratory and field studies have investigated the short-term storage of tailings under shallow water covers (Davé et al., 1997; Li et al., 1997; Holmström and Öhlander, 1999; Vigneault et al., 2001; Elberling and Damgaard, 2001; Samad and Yanful, 2005), but only a few studies have considered the reactivity of tailings that have been submerged over long time periods (e.g., Jacob and Otte, 2004; Vigneault et al., 2007). Chapter 4 describes a study involving detailed mineralogy, water chemistry, microbiology, and stable isotopic analyses to understand sulfide oxidation and reduction processes in long-term storage of tailings under a shallow water cover. The range in hydrogeochemical settings within the Fox tailings allowed for comparison of geochemical,

mineralogical, microbial and isotopic parameters in an area with exposed tailings (sub-aerial) and an area that was fully-submerged (sub-aqueous). In the sub-aerial zone within the Fox tailings, where the water table was 50 cm below the surface, and where tailings were exposed to atmospheric oxygen, a well-defined, ochreous oxidation zone with extensive sulfide mineral depletion developed from surface to about 40 cm depth. A transitional zone of much weaker oxidation extended from 40 to 60 cm below the tailings surface, and the sulfide mineral assemblage remained unaltered at depths >60 cm. In contrast, in the fully submerged (sub-aqueous) tailings, the oxidation zone was thin, extending <6 cm below the water-tailings interface. Pore water collected from the sub-aerial tailings had low pH, depleted alkalinity, and elevated concentrations of dissolved SO<sub>4</sub> and metal(oid)s, with populations of acidophilic sulfur oxidizing bacteria. However, the sub-aqueous tailings exhibited strong reducing conditions with pore-water characterized by circumneutral pH and low concentrations of dissolved SO<sub>4</sub> and metals. This pore water also exhibited elevated H<sub>2</sub>S concentrations and strong δ<sup>34</sup>S<sub>SO4</sub> fractionation indicative of dissimilatory sulfate reduction. The subaerial tailings porewater had depleted δ<sup>34</sup>S<sub>SO4</sub> values similar to the signature of sulfide minerals in the tailings. Marcasite [FeS<sub>2</sub>] and grains of secondary covellite [CuS] occurred as secondary coatings on primary minerals within 2 cm of sub-aqueous tailings surface. These findings further emphasize the influence of reducing conditions and microbial activity on metal mobility within sub-aqueous mine tailings. Results from this study provide insight into the effectiveness of submerging sulfide tailings under a shallow water cover as a viable method for limiting sulfide-mineral oxidation over extended time periods.

Using organic carbon as a stimulant to induce microbial sulfate reduction to remove metal(oid)s and SO<sub>4</sub> from mining impacted groundwater is a common approach to prevent or treat mine drainage from sulfide tailings oxidation. Successful treatment technologies that aim to

induce sulfate reduction as a method to treat groundwater have included organic-rich permeable reactive barriers (Benner et al., 1999), constructed wetlands (Walton-Day, 2003), and mixing organic carbon with fresh tailings during deposition to prevent the release of metal(oid)s and  $\text{SO}_4$  (Hulshof et al., 2006; Lindsay et al., 2011a). In the Woods tailings, extensive sulfide oxidation over the past 60 years has resulted in elevated concentrations of sulfide oxidation products and low pH values in the unsaturated zone of the tailings ( $\text{SO}_4$  up to  $244 \text{ g L}^{-1}$  and Fe up to  $107,000 \text{ mg L}^{-1}$ ). Concentrations of dissolved metals and  $\text{SO}_4$  decreased beneath the vadose zone in the saturated zone, but remained elevated ( $\text{SO}_4$  up to  $55,000 \text{ mg L}^{-1}$ ; Fe up to  $33,000 \text{ mg L}^{-1}$ ) relative to areas without sulfide oxidation such as the submerged Fox tailings. During precipitation events and the spring freshet, surface seeps developed along the flanks of the tailings impoundment discharging groundwater with low pH values (*e.g.*, as low as 0.39) and elevated concentrations of dissolved metals ( $\text{SO}_4$  up to  $203 \text{ g L}^{-1}$ ; Fe up to  $68 \text{ g L}^{-1}$ ) similar to the composition of pore water in the unsaturated zone. In these seepage zones, efflorescent minerals were observed precipitating, including copiapite, melanterite, rozenite, halotrichite, chalcantite, alpersite, hexahydrate, jurbanite, pickeringite, jarosite and gypsum. There have been numerous field studies describing the occurrence of secondary sulfate minerals from mine drainage and their role in the cycling of  $\text{SO}_4$  and metals in warm climates (*e.g.* Nordstrom and Alpers, 1999; Frau, 2000; Buckby et al., 2003; Hammarstrom et al., 2005; Peterson et al., 2006), however no study has been done on the formation of efflorescent sulfate salts from sulfide mine waste in sub-arctic regions where the annual temperature is near or below  $0^\circ\text{C}$ . Secondary efflorescent minerals play an important role in controlling the impacts from tailings oxidation in that they have the potential to remove  $\text{SO}_4$  and metals from solution. However, laboratory dissolution experiments (described in Chapter 6) have shown that these minerals rapidly dissolved in water, indicating that removal was temporary, and that they would eventually contribute to increased

loadings of dissolved metals and  $\text{SO}_4$  during precipitation events. The concentrations of metals and  $\text{SO}_4$  abruptly decreased ( $\text{SO}_4$   $0.3 \text{ g L}^{-1}$ ;  $\text{Fe}$   $0.0001 \text{ g L}^{-1}$ ) along the groundwater flowpath in the Woods tailings, near the border between the tailings and the discharge area into Woods Lake. This decrease in dissolved metals and  $\text{SO}_4$  coincided with a strong shift towards more positive isotopic  $\delta^{34}\text{S}\text{-SO}_4$  values, consistent with sulfate reduction being responsible for this trend rather than dilution. Core samples of tailings collected from within the Woods Tailings impoundment showed that the tailings were deposited over organic-bearing lake sediments. Piezometric measurements showed that there was an upward vertical hydraulic gradient between the native sediments and overlying tailings. The input of organic carbon into the tailings from the former lake sediments appeared to promote sulfate reduction that substantially decreased the loading of dissolved metals and  $\text{SO}_4$  to the adjacent surface water body. However, metal loadings may increase when the underlying organic-rich lake sediment, which is utilized as a carbon source for bacterial sulfate reduction, is exhausted.

Groundwater and surface water discharging from the Sherridon tailings impoundments directly enter Camp Lake. A 5-year hydrological and geochemical sampling program was initiated at Camp Lake to better understand long-term seasonal variations, mass-loading and impacts of effluent discharging from the mine site. Inflow and outflow from Camp Lake were sampled weekly and biweekly. Although seasonal variations in water quality measured in streams impacted by acid rock drainage (ARD) have been reported in a number of studies (McKnight and Bencala, 1990; Alpers et al., 1992; Brooks et al., 2001; August et al., 2002; Stillings et al., 2008; Butler et al., 2008; Sarmiento et al., 2009, 2012; Gozzard et al., 2011), the majority of these studies were limited to short-term monitoring (1–2 years). This current study is unique in that detailed monitoring of mass loadings over five years addresses watershed-scale impacts to the receiving Kississing Lake.

Outflow from Camp Lake showed a strong seasonal cycle in mass-loadings. During winter months when the lake was ice-covered, discharge water from Camp Lake had a neutral pH with low concentrations of dissolved metals and SO<sub>4</sub> similar to background concentrations. Discharge from Camp Lake had an abrupt increase in dissolved metal and SO<sub>4</sub> concentrations and decreases in pH during the spring freshet that remained relatively constant until fall freeze-up, when dissolved metal concentrations and pH returned to winter values. The annual and interannual variations in loadings measured in Camp Lake are different from those measured at the two streams feeding Camp Lake, revealing the contribution of high-salinity groundwater discharge from the tailings to the lake during dry years and the potential for significant loadings due to the dissolution of efflorescent minerals or flushing of the thick unsaturated zone in the tailings during relatively wet years. The abrupt changes in pH, metal and SO<sub>4</sub> concentrations, and the timing of these changes with the appearance and disappearance of ice-cover on the lakes, suggests a combination of physical and geochemical controls related to shifts in sources of water, mixing and changes in solubility. Despite fairly low average annual metal concentrations measured in Camp Lake discharge, concentrations of Zn and Cu were elevated above background in bottom sediments of Kississing Lake in a zone extending 9.5 km<sup>2</sup> from the location of Camp Lake inflow. These results show that in northern regions during the ice-free period, it is critical to control metal discharge from mine-impacted areas and demonstrate that even when average annual concentrations are only slightly elevated, long-term metal loadings can have a significant impact on receiving aquatic systems.

The insight gained from studying metal(oid) release from sulfide-rich tailings was used to identify processes and controls on the release of metal(loid)s from Quaternary sediments in Alberta's Southern Oil Sands Regions. The concentrations of As in shallow groundwater wells completed in sand and gravel aquifers often exceed drinking water guidelines (10 µg L<sup>-1</sup>) in this

area, but the distribution of As did not show any obvious spatial patterns or trends along groundwater flow paths. Similarities between the vertical profiles of metal(oid) concentrations in porewater through weathered glaciofluvial sediments in the area (Figure 9.1) and those observed in sulfide tailings, suggest that a combination of precipitation/dissolution reactions might control the release and transport of As in groundwater. The same combination of geochemical, mineralogical and isotopic methods used to study the release of metals from tailings was used to better understand the sources and controls on As in shallow groundwater in the area. Speciation of As in groundwater indicated that arsenite, the more mobile and toxic form was the dominant species. The highest concentrations of As were associated with reducing conditions, circumneutral pH and lower concentrations of Fe and SO<sub>4</sub>. It was previously hypothesized that elevated As concentrations in the regional groundwater originated from the underlying As-rich marine shale (AHW, 2000; Fitzgerald et al., 2001). However, groundwater collected from the shale aquifers during this study had As concentrations that were typically <10 µg L<sup>-1</sup>.

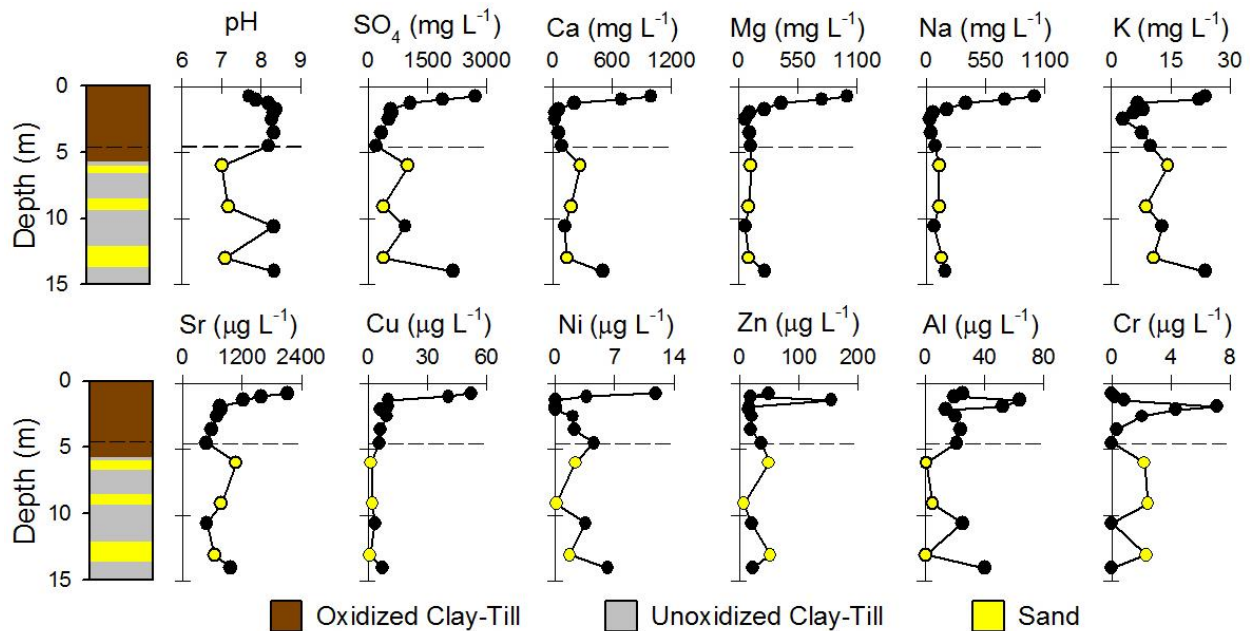


Figure 9-1: Depth profile of water chemistry through glacial till and sand aquifers in NE Alberta, showing a similar weathering trend to oxidized mine tailings. Dashed line represents the water table location.

Sulfide minerals were not observed during mineralogical analyses of the near surface oxidized sediments, but spheroidal Fe oxyhydroxides were present. The Fe oxyhydroxides contained elevated As concentrations and were interpreted to be an alteration product of former framboidal pyrite grains. XANES spectra indicated that these oxidized sediments were dominated by As(V) species with features similar to those of goethite or ferrihydrite with adsorbed As, suggesting that Fe oxyhydroxides are the dominant As carriers. Mineralogical characterization of unoxidized sediment samples revealed the presence of framboidal pyrite in the deeper sediments with an average As concentration of 530 ppm, reaching up to 1840 ppm. In contrast, XANES spectra collected on unoxidized sediment samples indicated the presence of a reduced As species (As(-I)) characteristic of arsenopyrite and arsenian pyrite. Ferric-oxyhydroxide phases were not identified in the unoxidized sediments during the mineralogical study, however XANES experiments revealed that over 75% of the solid-phase As

concentrations in the sediments was As(V) suggesting that Fe reduction of Fe oxyhydroxides could be the main source of As to the groundwater. Speciation modeling showed that the majority of groundwater samples were undersaturated with respect to ferrihydrite, supporting mineralogical results. Understanding the distribution and form of As present naturally in aquifer material and groundwater is important for managing water resources in the region, including selection of locations to install domestic water supply wells to minimize the potential health risks of As exposure.

## **9.2 Scientific Contributions**

Research presented in this thesis resulted in a number of contributions to the understanding of geochemistry and management of acid rock drainage (ARD). New scientific contributions include:

- Delineation and relative importance of a broader range of Fe-bearing minerals which can directly and indirectly contribute to ARD.
- A comprehensive guide outlining the susceptibility of discrete sulfide mineral phases to oxidation including the development of a conceptual model for the sequence of events that typically occurs in an oxidizing tailings impoundment over time.
- Evidence that submergence of sulfide tailings under a shallow water cover is a viable method for long-term management.
- Data showing that concentrations of dissolved metals and  $\text{SO}_4$  were elevated after >50 years of microbial mediated sulfide oxidation reactions, much beyond those observed in younger tailings impoundments.
- Evidence that organic-rich lake sediments underlying the tailings induced bacterial (dissimilatory) sulfate reduction which substantially reduced dissolved metal(oid)s and  $\text{SO}_4$  concentrations in the tailings groundwater.
- Data showing that Sherridon's subarctic climate, abundant efflorescent minerals formed seasonally from hyperacidic seepage waters. The formations of these efflorescent minerals resulted in a temporary removal of  $\text{SO}_4$  and metal(oid)s from solution, however they rapidly dissolved during laboratory dissolution tests which would result in increased loading to receiving surface waters during precipitation events and spring freshet.



- Demonstration that groundwater contributed significant loadings of metals and SO<sub>4</sub> to surface waters, and highlights the potential for very high loadings when dissolution of efflorescent minerals accumulated on the tailings surface and in the unsaturated zone is enhanced during relatively wet years. It is important that a wet year follows a dry year during which salt accumulates on the tailings surface and within the unsaturated zone.
- Data showing that the timing and variations in pH values and metal concentrations suggest a combination of physical and geochemical controls related to shifts in sources of water and mixing and changes in solubility controlling the seasonal and interannual variations in loadings.
- Demonstrating that although the average annual concentrations of dissolved metals and SO<sub>4</sub> discharging over the Camp Weir to Kississing Lake were within or very near regulatory guidelines, this research demonstrates that long-term metal loadings of low metal concentrations can have a significant impact on the receiving aquatic systems.
- Evidence supporting the conclusion that in northern regions, the ice-free period is critical in controlling metal discharge from mine-impacted areas.
- Demonstrating that elevated arsenic concentrations in groundwater from the Cold Lake-Beaver River basin in northeastern Alberta are due to a combination of arsenian pyrite oxidation in shallow sediments and arsenic-rich Fe oxyhydroxide reduction in deeper sediments.

### **9.3 Recommendations**

Hydrogeological, geochemical, and mineralogical investigations of the Sherridon Mine site have shown widespread contamination of groundwater and surface water from poorly managed tailings disposal. It is apparent that a remediation program is required to prevent further degradation of adjacent surface water bodies. The results of this research show that the remedial program should concentrate on managing the fate of dissolved oxidation products released from the tailings rather than focusing on the prevention of sulfide oxidation within the tailings. The most beneficial remediation option should include isolation of the Sherridon Tailings from Camp Lake coupled with a collection and treatment system. The installation of an infiltration cover over the Sherridon tailings would not control AMD completely, but it would be beneficial for controlling the tailings dust and can reduce water flow through piles.

The results of this research indicate that remediation options that focus on sulfide oxidation controls such as water covers and organic material covers may not be that beneficial, given that the oxidation processes are in an advanced stage. Although the submergence of the Fox tailings significantly reduced metal(oid) and acid loading since it was constructed 60 years ago, it is too late to realize these benefits for the Camp and Woods tailings. Attempts to implement a water cover remediation strategy on these late-stage oxidized tailings would result in dissolution of soluble  $\text{SO}_4$  minerals within the unsaturated tailings, which would result in the release of metal(oid)s,  $\text{SO}_4$  and acid, as demonstrated in Chapter 6. Similarly, attempts to use an organic cover over the tailings may also have negative effects, in that it may promote reductive dissolution of Fe oxyhydroxide minerals, which would also result in the release of metals adsorbed, or coprecipitated within the mineral structure. The collaboration between a multidisciplinary team of researchers, government, industry and engineers with substantial expertise in geochemistry and mine closure would be required to select a successful tailings management program. Disconnects between scientific research, government and engineering competence have often delayed effective remedial efforts (Nordstrom et al., 2015).

A key requirement for successful tailings management and remediation planning is the ability to predict long-term release and transport of low-pH waters and metal(oid)s. These types of long-term predictions rely on numerical models and our understanding of the geochemical processes that need to be incorporated into these reactive transport models that have evolved over the last 25 years, primarily based on extrapolation of short-term results into the future. The research conducted at the Sherridon Mine, after 60-80 years of sulfide oxidation, has contributed to closing the previous knowledge gap about long-term effects of sulfide oxidation by identifying the geochemical and microbial processes that have occurred in a variety of different settings across the site. The comprehensive data set of porewater geochemistry and mineralogy collected

from the Sherridon tailings provides an opportunity to calibrate reactive transport models to predict the long-term evolution of water quality from high-sulfide tailings. There is now the opportunity to use data from aged sites like Sherridon to improve our understanding of the mechanisms controlling sulfide oxidation and reactive transport models.

Future research at this site should build on the geochemical, microbial and isotopic analyses conducted by making use of new, advanced mineralogical and geochemical methods (*e.g.* XANES, laser ablation) to improve our understanding of the mechanisms of sulfide oxidation, inorganic and microbial processes. In addition, recent advances in metal isotope analyses should be used in future work to help interpret geochemical and mineralogical data to distinguish reactions controlling the transport of metals, microbial interactions, and secondary mineral formation. Detailed assessments of geochemical processes in older tailings deposits (like those found in the Sherridon tailings), and research using new analytical techniques to improve our understanding of the mechanisms of sulfide oxidation, can be combined to calibrate and improve reactive transport modelling. These models can then be applied to evaluate different tailings management and remediation strategies.

The general approach of combining geochemical, microbial and mineralogical analyses that have been developed to identify geochemical processes controlling the release and transport of metals in sulfide-rich tailings can also be applied to better understand water quality controls in low-sulfide tailings. The same processes that result in the very low-pH, metal-rich waters from sulfide-rich tailings also occur, to a lesser degree, in low-sulfide tailings. For some metal(oid)s, even releases of low concentrations can have a significant impact on water quality, ecosystems and human health, therefore processes controlling even low-concentration releases need to be understood. There are many areas for applying the knowledge gained from tailings studies to understand the geochemical processes and mechanisms of metal release, including oil sands

tailings, in situ oil recovery, geothermal systems, waste rock, shale gas, and the geogenic release of metals to groundwater such as presented in Chapter 8. While these will undoubtedly benefit from the general approach developed for tailings studies, additional research will be required to develop the same level of understanding for different source minerals and processes that occur under different redox conditions.

## References

- Abolfazlzadehdoshanbehbazari, M., Birks, S.J., Moncur, M.C., Ulrich, A.C., 2013. Fate and transport of oil sands process-affected water into the underlying clay till: a field study. *J. contamin. Hydrol.* 151, 83-92.
- AESRD (Alberta Environment and Sustainable Resource Development), 2013. Lower Athabasca region groundwater management framework: supporting document for the Cold Lake – Beaver River (CLBR) area. ISBN: 978-1-4601-1117-8.
- AHW (Alberta Health and Wellness), 2000. Arsenic in groundwater from domestic wells in three areas of northern Alberta. Health Surveillance Report, ISBN (0-7785-0708-4).
- AHW (Alberta Health and Wellness), 2014. Domestic well water quality in the Beaver River Basin 2009, drinking water quality and human health assessment. Alberta Domestic Well Water Quality and Assessment Program. ISBN (978-0-7785-8281-6).
- Al, T.A., Martin, C.J., Blowes, D.W., 2000., Carbonate-mineral/water interactions in sulfide-rich mine tailings. *Geochim. Cosmochim. Acta* 64, 3933-3948.
- Allison, J.D., Brown, D.S., Nova-Gardac, K.L., 1990. MINTEQA2/PRODEFA2, A Geochemical Assessment Model for Environmental Systems, Version 3.0 User's Manual. Environmental Research Laboratory, Office of Research and Development, U.S. EPA, Athens, GA.
- Alpers, C.N., Nordstrom, D.K., Thompson, M.J. 1992. Seasonal variations of Zn/Cu ratios in acid mine waters from Iron Mountain, California. In *Environmental Geochemistry of Sulfide Oxidation*. (C.N. Alpers and D.W. Blowes, eds.) ACS Symposium Series 550. pp. 324-344.
- Alpers, C.N., Blowes, D.W., Nordstrom, D.K., Jambor, J.L., 1994. Secondary minerals and acid mine-water chemistry. In: Jambor, J.L, Blowes, D.W. (Eds.), *Environmental Geochemistry of Sulfide Mine-Wastes*. Mineral. Assoc. Can. Short Course Vol. 22, 247-270.
- Alpers, C .N., Nordstrom, D. K., 1999. Geochemical modeling of water-rock interactions in mining environments. In: Plumlee, G.S., Logsdon, M.J. (Eds.). *Reviews in Economic Geology*, vol. 6A . *The Environmental Geochemistry of Mineral Deposits, Part A, Processes, Methods and Health Issues*, 289-324.
- Alpers, C.N., Jambor, J.L., Nordstrom, D.K., (Eds.), 2000. Sulfate Minerals – Crystallography, Geochemistry, and Environmental Significance. *Reviews in Mineralogy and Geochemistry* Vol. 40.
- Amend, J.P., Saltikov, C., Lu, G.S., Hernandez, J., 2014. Microbial arsenic metabolism and reaction energetics. In: Bowell, R.J., Alpers, C.N., Jamieson, H.E., Nordstrom, D.K.,

- Majzlan, J., (Eds.), *Arsenic: Environmental Geochemistry, Mineralogy, and Microbiology*. Rev. Mineral. Geochem. 79, 391-433.
- Anawar, H.M., Akai, J., Komaki, K., Terao, H., Yoshioka, T., Ishizuka, T., 2003. Geochemical occurrence of arsenic in groundwater of Bangladesh: sources and mobilization. *J. Geochem. Explor.* 77, 109-131.
- Andrade, C.F., Jamieson, H.E., Kyser, T.K., Prahraj, T., Fortin, D., 2010. Biogeochemical redox cycling of arsenic in mine-impacted lake sediments and co-existing pore waters near Giant Mine, Yellowknife Bay, Canada. *Appl. Geochem.* 25, 199-211.
- Andriashek, L.D., Fenton, M.M., 1989. Quaternary Stratigraphy and Surficial Geology of the Sand River Area. Alberta Research Council, NTS 73L, Bulletin 57.
- Andriashek, L.D., 2000. Geochemistry of Selected Glacial and Bedrock Geologic Units, Cold Lake Area, Alberta. Alberta Geological Survey Earth Sciences Report 2000-10.
- Andriashek, L.D., 2003. Quaternary Geological Setting of the Athabasca Oil Sands (In Situ) Area, Northeast Alberta. Alberta Geological Survey Earth Sciences Report 2002-03.
- Assayag, N., Rivé, K., Ader, M., Jézéquel, D., Agrinier, P., 2006. Improved method for isotopic quantitative analysis of dissolved inorganic carbon in natural water samples. *Rapid Commun. Mass Spectrom.* 20, 2243-2251.
- August, E.E., McKnight, D.M., Hrnica, D.C., Garhart, K.S., 2002. Seasonal variability of metals transported through a wetland impacted by mine drainage in the Rocky Mountains. *Environ. Sci. Technol.* 36, 3779-3786.
- Awoh, A.S., Mbonimpa, M., Bussière, B., 2013. Determination of the reaction rate coefficient of sulphide mine tailings deposited under water. *J. Environ. Manage.* 128, 1023-1032.
- Ayotte, J.D., Belaval, M., Olson, S.A., Burow, K.R., Flanagan, S.M., Hinkle, S.R., Lindsey, B.D., 2014. Factors affecting temporal variability of arsenic in groundwater used for drinking water supply in the United States. *Sci. Tot. Environ.* DOI: 10.1016/j.scitotenv.2014.02.057.
- Azcue, J.M., Rosa, F., 1996. Effects of sampling technique on the determination of major ions in sediment pore water. *Wat. Qual. Res. J. of Can.* 31, 709-724.
- Bain, J.G., Mayer, K.U., Blowes, D.W., Frind, E.O., Molson, J.W.H., Kahnt, R., Jenk, U., 2001. Modelling the closure-related geochemical evolution of groundwater at a former uranium mine. *J. Contam. Hydrol.* 52, 109-135.
- Balci, N., Shank III, W.C., Mayer, B., Mandernack, K.W. 2007. Oxygen and sulfur isotope systematics of sulfate produced by bacterial and abiotic oxidation of pyrite. *Geochim. Cosmochim. Acta*, 71, 3796-3811.

- Ball, J.W., Nordstrom, D.K. 1991. User's manual for WATEQ4F with revised thermodynamic data base and test cases for calculating speciation of major, trace and redox elements in natural waters. U.S. Geol. Surv. Open-File Rep. pp. 91-183.
- Barker, J.F., Chatten, S., 1982. A technique for determining low concentrations of total carbonate in geological materials. *Chem. Geol.* 36, 317-323.
- Barringer, J.L., Reilly, P.A., 2013. Arsenic in groundwater: a summary of sources and the biogeochemical and hydrogeologic factors affecting arsenic occurrence and mobility, Chapter 4. In: Bradley, P.M. (Ed.) *Current Perspectives in Contaminant Hydrology and Water Resources Sustainability*. DOI: 10.5772/55354.
- Barry, K.L., Grout, J.A., Levings, C.D., Nidle, B.H., Piercey, G.E., 2000. Impacts of acid mine drainage on juvenile salmonids in an estuary near Britannia Beach in Howe Sound, British Columbia. *Can. J. Fish. Aquat. Sci.* 57, 2032-2043.
- Bayless, E.R., Olyphant, G.A., 1993. Acid-generating salts and their relationship to the chemistry of groundwater and storm runoff at an abandoned mine site in southwestern Indiana, U.S.A. *Journal of Contaminant Hydrology* 12, 313-328.
- Beck, A.E., 1983. Aquatic Impact Assessment of the Sherridon Mine. *Water Standards and Studies Report #83-25*.
- Beck, A.E., 1988. Memorandum report: Data report and summary for data collected during 1988. Manitoba Environmental Management Division.
- Benner, S.G., Blowes, D.W., Gould, W.D., Herbert, R.B., Ptacek, C.J. Geochemistry of a permeable reactive barrier for metals and acid mine drainage. 1999, *Environ. Sci. Technol.*, 33, 2793-27997.
- Benner, S.G., Gould, W.D., Blowes, D.W., 2000. Microbial populations associated with the generation and treatment of acid mine drainage. *Chem. Geol.* 169, 435- 448.
- Berg, M., Tran, H.C., Nguyen, T.C., Pham, H.V., Schertenleib, R., Giger, W., 2001. Arsenic contamination of groundwater and drinking water in Vietnam: a human health threat. *Environ. Sci. Technol.* 35, 2621-2626.
- Berg, P., McGlathery, K.J., 2001. A high-resolution pore water sampler for sandy sediments. *Limnol. Oceanogr.* 46, 203-210.
- Berner, R.A., 1980. *Early Diagenesis: A Theoretical Approach*. Princeton University Press, Princeton, NJ.
- Berner, R.A., 1985. Sedimentary pyrite formation: an update. *Geochim. Cosmochim. Acta* 48, 605-615.
- Bertorino, G., Caredda, A.M., Ibba A., Zuddas, P., 1995. Weathering of Pb-Zn mine tailings in

- pH buffered environment. In: Kharaka, Y.K., Chudaev, O.V. (Eds.), 8<sup>th</sup> International Symposium on Water–Rock Interaction, 859-862.
- Bigham, J.M., Schwertmann, U., Traina, S.J., Winland, R.L., Wolf, M., 1996. Schwertmannite and the chemical modeling of iron in acid sulfate waters. *Geochimica et Cosmochimica Acta* 60, 2111–2121.
- Birks, S.J., Edwards, T.W.D., Remenda, V.H., 2007. Isotopic evolution of Glacial Lake Agassiz: New insights from cellulose and porewater isotopic archives. *Palaeogeogr. Palaeoclimatol. Palaeoecol.* 246, 8-22.
- Blodau, C. 2004. Evidence for a hydrologically controlled iron cycle in acidic and iron rich sediments. *Aquat. Sci.* 66, 47-59.
- Blowes, D.W., Jambor, J.L., 1990. The pore-water chemistry and the mineralogy of the vadose zone of sulfide tailings, Waite Amulet, Quebec. *Appl. Geochem.* 5, 327-346.
- Blowes, D.W., Reardon, E.J., Jambor, J.L., Cherry, J.A., 1991. The formation and potential importance of cemented layers in inactive sulfide mine tailings. *Geochim. Cosmochim. Acta* 55, 965-978.
- Blowes, D.W., Jambor, J.L., Appleyard, E.C., Reardon, E.J., Cherry, J.A. 1992. Temporal observations of the geochemistry and mineralogy of a sulfide-rich mine-tailings impoundment, Heath Steele mines, New Brunswick. *Explor. Min. Geol.* 1, 251-264.
- Blowes, D.W., Al, T.A., Lortie, L., Gould, W.D., Jambor, J.L., 1996. Microbiological, chemical, and mineralogical characterization of the Kidd Creek mine tailings impoundment, Timmins area, Ontario. *Geomicrobiol. J.* 13, 13–31.
- Blowes, D.W., Jambor, J.L., Hanton-Fong, C.J., Lortie, L., Gould, W.D., 1998. Geochemical, mineralogical and microbiological characterization of a sulphide-bearing carbonate-rich gold-mine tailings impoundment, Joutel, Québec. *Appl. Geochem.* 13, 687–705.
- Blowes, D.W., Ptacek, C.J., Jambor, J.L., Weisener, C.G., 2003. The geochemistry of acid mine drainage, pp. 149-204. In: *Environmental Geochemistry* (ed. B.S. Lollar) Vol. 9 *Treatise on Geochemistry* (eds. H.D. Holland, K.K. Turekian). Elsevier–Pergamon, Oxford.
- Blowes, D.W., Al, T., Lortie, L., Gould, W.D., Jambor, J.L., 1996. Microbiological, chemical, and mineralogical characterization of the Kidd Creek Mine Tailings Impoundment, Timmins Area, Ontario. *Geomicrobiol. J.* 13, 13-31.
- Blowes, D.W., Ptacek, C.J., Jambor, J.L., Weisener, C.G., Paktunc, D., Gould, W.D., Johnson, D.B., 2014. The geochemistry of acid mine drainage. Pp. 131-190. In: *Environmental Geochemistry* (ed. B.S. Lollar) Vol. 11, *Treatise on Geochemistry*, 2<sup>nd</sup> Edition (eds. H.D. Holland, K.K. Turekian). Elsevier.



- Bolton, M., Beckie, R., 2011. Aqueous and mineralogical analysis of arsenic in the reduced, circumneutral groundwater and sediments of the lower Fraser River delta, British Columbia, Canada. *Appl. Geochem.* 26, 458-469.
- Boorman, R.S., Watson, D.M., 1976. Chemical processes in abandoned sulphide tailings dumps and environmental implications for Northeastern New Brunswick. *CIM Bull.* 69, 89-96.
- Bottomley, D.J., 1984. Origins of some arseniferous groundwaters in Nova Scotia and New Brunswick, Canada. *J. Hydrol.* 69, 223-257.
- Boulet, M.P., Larocque, A.C.L. 1998. A comparative mineralogical and geochemical study of sulfide mine tailings at two sites in New Mexico, USA. *Environ. Geol.* 33, 130-142.
- Bowell, R.J., Bruce, I., 1995. Geochemistry of iron ochres and mine waters from Levant Mine, Cornwall. *Appl. Geochem.* 10, 237-250.
- Boyle, D.R., Turner, R.J.W., Hall, G.E.M., 1998. Anomalous arsenic concentrations in groundwaters of an island community, Bowen Island, British Columbia. *Environ. Geochem. Health*, 20, 199–212.
- Broman, P.G., Haglund P. Mattsson, E., 1991. Use of sludge for sealing purposes in dry covers- Development and field experiences. In :Second Internat. Conf. Abatement Acidic Drainage Vol. 1, MEND Secretariat, Ottawa, Ontario. pp. 515-528.
- Brookins, D.G., 1988. Eh-pH Diagrams for Geochemistry. Springer-Verlag, New York, p. 176.
- Brooks, P.D., McKnight, D.M., Bencala, K.E., 2001. Annual maxima in Zn concentrations during spring snowmelt in streams impacted by mine drainage. *Environ. Geol.* 40, 1447-1454.
- Buckley, A.N., Wouterlood, H.J., Woods, R., 1989. The surface composition of natural sphalerites under oxidative leaching conditions. *Hydrometall.* 22, 39-56.
- Buckby, T., Black, S., Coleman, M.L., Hodson, M.E., 2003. Fe-sulphate-rich evaporative mineral precipitates from the Rio Tinto, southwest Spain. *Mineralogical Magazine* Vol. 67, 263-278.
- Bufflap, S.E., Allen, H.E., 1995. Sediment pore water collection methods for trace metal analysis: a review. *Wat. Res.* 29, 165-177.
- Buschmann, J., Berg, M., 2009. Impact of sulfate reduction on the scale of arsenic contamination in groundwater of the Mekong, Bengal and Red River deltas. *Appl. Geochem.* 24, 1278-1286.
- Butler, B.A., Ranville, J.F., Ross, P.E., 2008. Observed and modeled seasonal trends in dissolved and particulate Cu, Fe, Mn, and Zn in a mining-impacted stream. *Water Res.* 42, 3135-3145.

- Campbell, K.M., Nordstrom, D.K., 2014. Arsenic speciation and sorption in natural environments. In: *Bowell, R.J., Alpers, C.N., Jamieson, H.E., Nordstrom, D.K., Majzlan, J., (Eds.), Arsenic: Environmental Geochemistry, Mineralogy, and Microbiology. Rev. Mineral. Geochem. 79, 185-216.*
- Cánovas, C.R., Hubbard, C.G., Olías, M., Nieto, J.M., Black, S., Coleman, M.L., 2008. Hydrochemical variations and contaminant load in the Río Tinto (Spain) during flood events. *Journal of Hydrology 350, 25-40.*
- Cánovas, C.R., Olías, M., Nieto, J.M., Galván, L., 2010. Wash-out processes of evaporitic sulfate salts in the Tinto river: hydrogeochemical evolution and environmental impact. *Applied Geochemistry 25, 288-301.*
- Carbone, C., Dinelli, E., Marescotti, P., Gasparotto, G., Lucchetti, G., 2013. The role of AMD secondary minerals in controlling environmental pollution: Indications from bulk leaching tests. *Journal of Geochemical Exploration 132, 188-200.*
- Carmichael, V., Clarkson, L., 1995. Well water survey for arsenic in the Powell River and Sunshine Coast communities of British Columbia – March to June 1994. Report prepared for Coast Garibaldi Health Unit.
- Carr, R.S., Chapman, D.C., 1995. Comparison of methods for conducting marine and estuarine sediment porewater toxicity test-extraction, storage, and handling techniques. *Arch. Environ. Contam. Toxicol. 28, 69-77.*
- Carrara, C., Ptacek, C.J., Robertson, W.D., Blowes, D.W., Moncur, M.C., Sverko, E., Backus, S., 2008. Fate of pharmaceutical and trace organic compounds in three septic system plumes, Ontario, Canada. *Environ. Sci. Technol. 42, 2805–2811.*
- Cavalcanti de Albuquerque, R., Kirste, D., 2012. Arsenic mobilization in a freshening groundwater system formed within glaciomarine deposits. *Appl. Geochem. 27, 2173-2186.*
- CCME (Canadian Council of Minister of the Environment), 2007. Canadian water quality guidelines for the protection of aquatic life: summary table. In *Canadian Environmental Quality Guidelines, 1999, Canadian Council of Ministers of the Environment, Winnipeg.*
- CCME (Canadian Council of Ministers of the Environment), 2002. Canadian sediment quality guidelines for the protection of aquatic life: summary tables. In *Canadian Environmental Quality Guidelines, 1999, Canadian Council of Ministers of the Environment, Winnipeg.*
- Cheng, Z., Van Geen, A., Seddique, A.A., Ahmed, K.M., 2005. Limited temporal variability of arsenic concentrations in 20 wells monitored for 3 years in Araihaazar, Bangladesh. *Environ. Sci. Technol. 39, 4759-4766.*

- Cheung, K., Sanei, H., Klassen, P., Mayer, B., Goodarzi, F., 2009. Produced fluids and shallow groundwater in coalbed methane (CBM) producing regions of Alberta, Canada: Trace element and rare earth element geochemistry. *Int. J. Coal Geol.* 77, 338-349.
- Chou, I-M., Seal, R.R. II, Hemingway, B.S., 2002. Determination of melanterite–rozenite and chalcantite–bonattite equilibria by humidity measurements at 0.1 MPa. *American Mineralogist* 87, 108-114.
- Chou, I-M., Seal, R.R., Wang, A., 2013. The stability of sulfate and hydrated sulfate minerals near ambient conditions and their significance in environmental and planetary sciences. *J. Asian Earth Sci.* 62, 734-758.
- Close, M.E., Magesan, G.N., Lee, R., Stewart, M.K., Hadfield, J.C. 2003. Field study of pesticide leaching in an allophonic soil in New Zealand. 1: experimental results. *Aust. J. Soil Res.* 41, 809–824.
- CNLR (Canadian Natural Resources Ltd.), 2005. Z8 Pad Arsenic Mobility Investigation, Progress Report.
- Cochran, W.G., 1950. Estimation of bacterial densities by means of the ‘‘most probable number’’. *Biometrics* 6, 105–116.
- Combes, J.M., Manceau, A., Calas, G., Bottero, J.Y., 1989. Formation of ferric oxides from aqueous solutions: A polyhedral approach by X-ray absorption spectroscopy. I. Hydrolysis and formation of ferric gels. *Geochim. Cosmochim. Acta* 53, 583–594.
- Cook, N.J., Chryssoulis, S.L., 1990. Concentrations of ‘invisible gold’ in the common sulfides. *Can. Mineral.* 28, 1-16.
- Cook, R.B., Kelly, C.A., Schindler, D.W., Turner, M.A., 1986. Mechanisms of hydrogen ion neutralization in an experimentally acidified lake. *Limnol. Oceanogr.* 31, 134–148.
- Córdoba, E.M., Muñoz, J.A., Blázquez, M.L., González, F., Ballester, A., 2008. Leaching of chalcopyrite with ferric ion. Part II: Effect of redox potential. *Hydrometallurgy* 93, 88–96.
- Courtin-Nomade, A., Bril, H., Neel, C., Lenain, J.F., 2003. Arsenic in iron cements developed within tailings of a former metalliferous mine—Enguialès, Aveyron, France. *Appl. Geochem.* 18, 395-408.
- Curley, E.M., O’Flynn, M.G., McDonnell, K.P., 2011. The use of porous ceramic cups for sampling soil pore water from the unsaturated zone. *Int. J. Soil Sci.* 6, 1-11.
- Curtis, K.R., Cowee, M., Lewis, S., Harris, T., 2008. Livestock Producer Interest in Local Processing. University of Nevada Cooperative Extension Fact Sheet, FS-08-10.
- Davé, N.K., Lim, T.P., Horne, D., Boucher, Y., Stuparyk, R., 1997. Water cover on reactive

- tailings and wasterock: Laboratory studies of oxidation and metal release characteristics. In: 4<sup>th</sup> International Conference on Acid Mine Drainage, May 31-June 6, Vancouver, pp. 779-794.
- Davis, A., Ashenberg, D., 1987. The aqueous geochemistry of the Berkeley Pit, Butte, Montana, U.S.A. *Appl. Geochem.* 4, 23-36.
- Dayton & Knight. 2010. Carcross Water System Upgrades. Feasibility Assessment and Conceptual Options Report. Prepared for Yukon Government Community Services.
- Deditius, A.P., Utsunomiya, S., Reich, M., Kesler, S.E., Ewing, R.C., Hough, R., Walsh, J., 2011. Trace metal nanoparticles in pyrite. *Ore Geol. Rev.* 42, 32-46.
- de Giudici, G., Voltolini, M., Moret, M., 2002. Microscopic surface processes observed during the oxidative dissolution of sphalerite. *Eur. J. Miner.* 14, 757-762.
- de Lange, G.J., Cranston, R.E., Hydes, D.H., Boust, D. 1992. Extraction of pore water from marine sediments: a review of possible artifacts with pertinent examples from the North Atlantic. *Mar. Geol.* 109, 53-76.
- Desbarats, A.J., Parsons, M.B., Percival, J.B., 2014. Arsenic mobility in mildly alkaline drainage from an orogenic lode gold deposit, Bralorne mine, British Columbia. *Appl. Geochem.* <http://dx.doi.org/10.1016/j.apgeochem.2014.11.015>.
- Dingman, S.L., 2002. *Physical Hydrology*, Second Edition. Prentice Hall, 646 pp.
- Dixit, S., Hering, J.G., 2003. Comparison of arsenic(V) and arsenic(III) sorption onto iron oxide minerals: implications for arsenic mobility. *Environ. Sci. Technol.* 37, 4182-4189.
- Dobchuk, B., Nichol, C., Wilson, G.W., Aubertin, M., 2013. Evaluation of a single-layer desulfurized tailings cover. *Can. Geotech. J.* 50, 777-792.
- Dold, B., Blowes, D.W., Dickhout, R., Spangenberg, J.E., Pfeifer, H.R., 2005. Low molecular weight carboxylic acids in oxidizing porphyry copper tailings. *Environ. Sci. Technol.* 39, 2515-2521.
- Dold, B., Spangenberg, J.E., 2005. Sulfur speciation and stable isotope trends of water-soluble sulfates in mine tailings profiles. *Environ. Sci. Technol.* 39, 5650-5656.
- Domènech, C., de Pablo, J., Ayora, C., 2002. Oxidative dissolution of pyritic sludge from the Aznalcóllar mine (SW Spain). *Chem. Geol.* 190, 339-353.
- Druschel, G.K., Baker, B.J., Gihring, T.M., Banfield, J.F., 2004. Acid mine drainage biogeochemistry at Iron Mountain, California. *Geochem. Trans.* 5, 13-32.
- Dubrovsky, N.M., Morin, K.A., Cherry, J.A., Smyth, D.J.A. 1984. Uranium tailings acidification and subsurface contamination migration in a sand aquifer. *Water Poll. Res. J. Can.* 19,

55-89.

- Elberling, B., Damgaard, L.R., 2001. Microscale measurements of oxygen diffusion and consumption in subaqueous sulphide tailings. *Geochim. Cosmochim. Acta* 65, 1897-1905.
- Edmunds, W.M., Bath, A.H., 1976. Centrifuge extraction and chemical analysis of interstitial waters. *Environ. Sci. Technol.* 10, 467-472.
- Edraki, M., Golding, S.D., Baublys, K.A., Lawrence, M.G. 2005. Hydrochemistry, mineralogy and sulfur isotope geochemistry of acid mine drainage at the Mt. Morgan mine environment, Queensland, Australia. *Appl. Geochem.* 20, 789-805.
- Eggleton, J., Thomas, K.V., 2004. A review of factors affecting the release and bioavailability of contaminants during sediment disturbance events. *Environ. Int.* 30, 973-980.
- Elsetinow, A.R., Strongin, D.R., Borda, M.J., Schoonen, M.A., Rosso, K.M., 2003. Characterization of the structural and the surface reactivity of a marcasite thin film. *Geochim. Cosmochim. Acta.* 67, 807-812.
- Equeenuddin, S.M., 2014. Occurrence of alpersite at Malanjkhand copper mine, India. *Environmental Earth Sciences*, DOI: 10.1007/s12665-014-3668-9.
- Environment Canada, 2012. Canadian Climate Normals, 1927-2012, Flin Flon, Manitoba. Accessible at: [http://climate.weatheroffice.gc.ca/Welcome\\_e.html](http://climate.weatheroffice.gc.ca/Welcome_e.html).
- Erickson, M.L., Barnes, R.J., 2005. Glacial sediments causing regional-scale elevated arsenic in drinking water. *Groundwater* 43, 796-805.
- Fanfani, L. Zuddas, P., Chessa, A., 1997. Heavy metals speciation analysis as a tool for studying mine tailings weathering. *J. Geochem. Explor.* 58, 241-248.
- Fares, A., Sanjit, D.K., Fares, S., 2009. Review of vadose zone soil solution sampling techniques. *Environ. Rev.* 17, 215-234.
- Farley, W.J., 1949., Geology of the Sherritt Gordon ore body. *CIM Bull.* 42, 25-30.
- Fendorf, S., Michael, H.A., van Geen, A., 2010. Spatial and temporal variations of groundwater arsenic in South and Southeast Asia. *Sci.* 328, 1123-1127.
- Fennell, J. W., 2008. Effects of aquifer heating on groundwater chemistry with a review of arsenic and its mobility. Ph.D. Thesis, University of Calgary, Calgary, AB, pp. 330.
- Ferris, F.G., Fyfe, W.S., Beveridge, T.J., 1987. Bacteria as nucleation sites for authigenic minerals in a metal-contaminated lake sediment. *Chem. Geol.* 63, 225-232.

- Ficklin, W.H. 1983. Separation of arsenic (III) and arsenic(V) in ground waters by ion exchange. *Talanta*, 30, 371-373.
- Fleet, M.E., Chryssoulis, S.L., MacLean, P.J., Davidson, R., Weisener, C.G., 1993. Arsenian pyrite from gold deposits: Au and As distribution investigated by SIMS and EMP, and color staining and surface oxidation by XPS and LIMS. *Can. Mineral.* 31, 1-17.
- Frau, F., Cidu, R., Ardaù, C., 2012. Short-term changes in water chemistry in the Baccu Locci stream (Sardinia, Italy) affected by past mining. *Appl. Geochem.* 27, 1844-1853.
- Freeze, R.A., Cherry, J.C., 1979. *Groundwater*. Prentice Hall, Englewood Cliffs, New Jersey.
- Fritz, P., Drimmie, R.J., Frappe, S.K., O'Shea, K.J., 1987. The isotopic composition of precipitation and groundwater in Canada. *Isotope Techniques in Water Resources Development*, International Atomic Energy Agency, Vienna, IAEA-SM-299/17, pp. 539-550.
- Fritz, P., Basharmal, G.M., Drimmie, R.J., Ibsen, J., Qureshi, R.M., 1989. Oxygen isotope exchange between sulphate and water during bacterial sulfate reduction. *Chem. Geol., Isot. Geosci. Sect.* 79, 99– 105.
- Fitzgerald, D., Chanasyk, D.S., Neilson, R.D., Kiely, D., Audette, R., 2001. Farm Well Water Quality in Alberta. *Water Qual. Res. J. Can.* 36, 565-588.
- Frau, F., 2000. The formation–dissolution–precipitation cycle of melanterite at the abandoned pyrite mine of Genna Luas in Sardinia, Italy: environmental implications. *Mineralogical Magazine* 64, 995-1006.
- Froese, E., Goetz, P.A., 1981. *Geology of the Sherridon Group in the Vicinity of Sherridon, Manitoba*. *Geol. Surv. Can. Paper* 80-21.
- Furrer, G., Phillips, B.L., Ulrich, K., Pöthig, R., Casey, W.H., 2002. The origin of aluminum flocs in polluted streams. *Sci.* 297, 2245-2247.
- Garrels, R.M., Thompson, M.E., 1960. Oxidation of pyrite by iron sulfate solutions. *Am. J. Sci.* 256, 57-67.
- Gibson, J.J., Birks, S.J., Jeffries, D.S., Kumar, S., Scott, K.A., Aherne, J., Patrick D. Shaw, P.D., 2010. Site specific estimates of water yield applied in regional acid sensitivity surveys across western Canada. *J. Limnol.* 69, 67-76.
- Giesemann, A., Jäger, H.J., Norman, A.-L., Krouse, H.R., Brand, W.A., 1994. On-line sulfur-isotope determination using an elemental analyzer coupled to a mass spectrometer. *Anal. Chem.* 66, 2816–2819.
- Gigowski, B., Vogg, A., Wierer, K., Dobias, B., 1991. Effect of Fe-lattice ions on adsorption, electrokinetic, colorimetric and flotation properties of sphalerite. *Int. J. Miner. Process.*

33, 103-120.

- Gilbert, S.E., Cooke, D.R., Hollings, P., 2003. The effects of hardpan layers on the water chemistry from the leaching of pyrrhotite-rich tailings material. *Environ. Geol.* 44, 687-697.
- Giudici, G. De, Voltolini, M., Moret, M., 2002. Microscopic surface processes observed during the oxidative dissolution of sphalerite. *Eur. J. Mineral.* 14, 757-762.
- Goetz, P.A., Froese, E., 1982. The Sherritt Gordon massive sulfide deposit. *Precambrian Sulfide Deposits, H.S. Robinson Memorial Volume*. Hutchinson, R.W., Spence, C.D., and Franklin, J.M (Eds.). *Geol. Assoc. Can. Special Pap.* 25, pp. 557-569.
- Gong, Z., Lu, X., Watt, C., Wen, B., He, B., Mumford, J., Ning, Z., Xia, Y., Le, X.C., 2006. Speciation analysis of arsenic in groundwater from Inner Mongolia with an emphasis on acid-leachable particulate arsenic. *Anal. Chim. Acta* 555, 181-187.
- Goody, D.C., Clay, J.W., Bottrell, S.H., 2002. Redox-driven changes in porewater chemistry in the unsaturated zone of the chalk aquifer beneath unlined cattle slurry lagoons. *Appl. Geochem.* 17, 903-921.
- Gould, W.D., Kapoor, A., 2003. The microbiology of acid mine drainage In: Jambor, J.L., Blowes, D.W., Ritchie, A.I.M. (Eds.) *Environmental Aspects of Mine Wastes*. Mineral. Assoc. Can. Short Course Vol. 31, 203-226.
- Gould, W.D., Stichbury, M., Francis, M., Lortie, L., Blowes, D.W., 2003. An MPN method for the enumeration of iron-reducing bacteria. In: Spiers, G., Beckett, P., Conroy, H. (Eds.), *Proceedings of Sudbury '03, Mining and the Environment III*. Laurentian University, Sudbury, ON, pp. 153-157.
- Gozzard, E., Mayes, W.M., Potter, H.A.B., Jarvis, A.P., 2011. Seasonal and spatial variation of diffuse (non-point) source zinc pollution in a historically metal mined river catchment, UK. *Environ. Pollut.* 159, 3113-3122.
- Guo, H., Zhang, Y., Jia, Y., Zhao, K., Kim, K., 2013. Spatial and temporal evolutions of groundwater arsenic approximately along the flow path in the Hetao basin, Inner Mongolia. *Chin. Sci. Bull.* 58, 3070-3079.
- Gunsinger, M.J., Ptacek, C.J., Blowes, D.W., Jambor, J.L., 2006a. Evaluation of long-term sulfide oxidation processes within pyrrhotite-rich tailings, Lynn Lake, Manitoba. *J. Contam. Hydrol.* 83, 149-170.
- Gunsinger, M.J., Ptacek, C.J., Blowes, D.W., Jambor, J.L., Moncur, M.C., 2006b. Mechanisms controlling acid neutralization and metal mobility within a Ni-rich tailings impoundment. *Appl. Geochem.* 21, 1301-1321.

- Habicht, K.S., Canfield, D.E., 1997. Sulfur isotope fractionation during bacterial sulfate reduction in organic-rich sediments. *Geochim. Cosmochim. Acta* 61, 5351– 5361.
- Habicht, K.S., Canfield, D.E., Rethmeier, J. Sulfur isotope fractionation during bacterial sulfate reduction and disproportionation of thiosulfate and sulfite. *Geochim. Cosmochim. Acta*, 1998, 62, 2585–2595.
- Hamilton, R., Fraser, W.W., 1978. A case history of natural underwater revegetation: Mandy Mine high sulfide tailings. *Reclam. Rev.* 1, 61-65.
- Hammarstrom, J.M., Seal II, R.R., Meier, A.L., Kornfeld, J.M., 2005. Secondary sulfate minerals associated with acid drainage in the eastern US: recycling of metals and acidity in surficial environments. *Chem. Geol.* 215, 407-431.
- Hansel, C.M., Benner, S.G., Neiss, J., Dohnalkova, A., Kukkadapu, R.K., Fendorf, S., 2003. Secondary mineralization pathways induced by dissimilatory iron reduction of ferrihydrite under advective flow. *Geochim. Cosmochim. Acta* 67, 2977–2992.
- Harris, D.L., Lottermoser, B.G., Duchesne, J., 2003. Ephemeral acid mine drainage at the Montalbion silver mine, north Queensland. *Australian Journal of Earth Sciences* 50, 797-809.
- Harrison, A.G., Thode, H.G., 1958. Mechanism of the bacterial reduction of sulphate from isotope fractionation studies. *Trans. Faraday Soc.* 54, 84–92.
- Harvey, C.F., Ashfaq, K.N., Yu, W., Badruzzaman, A.B.M., Ali, M.A., Oates, P.H., Michael, H.A., Neumann, R.B., Beckie, R., Islam, S., Ahmed, M.F., 2006. Groundwater dynamics and arsenic contamination in Bangladesh. *Chem Geol.* 228, 112-136.
- Hayes, S.M., Root, R.A., Perdrial, N., Maier, R.M., Chorover, J., 2014. Surficial weathering of iron sulfide mine tailings under semi-arid climate. *Geochim. Cosmochim. Acta* 141, 240-257.
- Health Canada, 2003. Federal-Provincial Advisory Committee on Environmental and Occupational Health, Guidelines for Canadian Drinking Water Quality.
- Health Canada, 2006. Guidelines for Canadian drinking water quality: guideline technical document — arsenic. Water Quality and Health Bureau, Healthy Environments and Consumer Safety Branch, Health Canada, Ottawa, ON.
- Health Canada, 2012. Guidelines for Canadian Drinking Water Quality—Summary Table. Water, Air and Climate Change Bureau, Healthy Environments and Consumer Safety Branch, Health Canada, Ottawa, ON.
- Heinrichs, H, Böttcher, G., Brumsack, H.J., Pohlmann, M., 1996. Squeezed soil-pore solutions – a comparison to lysimeter samples and percolation experiments. *Water Air Soil Pollut.* 89, 189-204.



- Héry, M., Van Dongen, B.E., Gill, F., Mondal, D., Vaughan, D.J., Pancost, R.D., Polya, D.A., Lloyd, J.R., 2010. Arsenic release and attenuation in low organic carbon aquifer sediments from West Bengal. *Geobiol.* 8, 155–168.
- Hesslein, R.H., 1976. An in situ sampler for close interval pore water studies. *Limnol. Oceanogr.* 21, 912-914.
- Holm, T. R., 2002. Effects of carbonate/bicarbonate, silica, and phosphate on arsenic sorption to hydrous ferric oxide. *J. Am. Water Works Assoc.* 94, 174-181.
- Holmström, H., Öhlander, B., 1999. Oxygen penetration and subsequent reactions in flooded sulphidic mine tailings: A study at Stekenjokk, northern Sweden. *Appl. Geochem.* 14, 747-759.
- Holmström, H., Ljungberg, J., Ekström, M., Öhlander, B., 1999. Secondary copper enrichment in tailings at the Laver mine, northern Sweden. *Environ. Geol.* 38, 327-342.
- Holmström, H., Öhlander, B., 2001. Layers rich in Fe- and Mn-oxyhydroxides formed at a tailings-pond water interface, a possible trap for trace metals in flooded mine tailings. *J. Geochem. Explor.* 74, 189-203.
- Hvorslev, M.J., 1951. Time lag and soil permeability in groundwater observations. US Army Corps of Engineers, Bull. 36, Waterways Exper. Sta. Corps of Engrs., US Army. Vicksburg, MS, pp. 1–50.
- Huerta-Diaz, M.A., Rivera-Duarte, I., Sanudo-Wilhelmy, S.A., Flegal, A.R., 2007. Comparative distribution of size fractionated metals in pore water sampled by in situ dialysis and whole-core sediment squeezing: implications for diffusive flux calculations. *Appl. Geochem.* 22, 2509-2525.
- Hulshof, A.H.M., Blowes, D.W., Ptacek, C.J., Gould, W.D., 2003. Microbial and nutrient investigations into the use of in situ layers for treatment of tailings effluent. *Environ. Sci. Technol.* 37, 5027-5033.
- Hulshof, A.H.M., Blowes, D.W., Gould, W.D., 2006. Evaluation of in situ layers for treatment of acid mine drainage: A field comparison. *Water Res.* 40, 1816–1826.
- Hydrological Atlas of Canada, 1978. Fisheries and Environment Canada. Surveys and Mapping Branch, Natural Resour. Can., Ottawa.
- Hynek, B.M., McCollom, T.M., Marcucci, E.C., Brugman, K.K., Rogers, K.L., 2013. Assessing environmental controls on acid-sulfate alteration at active volcanoes in Nicaragua: applications to relic hydrothermal systems on mars. 44th Lunar and Planetary Science Conference, March 18-22, The Woodlands, TX, p. 1633.

- Hynek, B.M., McCollom, T.M., McHenry, L.J., Alvarado, G.E., 2014. Assessing hydrothermal alteration on early mars through analog environments in Nicaragua, Costa Rica, Iceland, and Hawaii. 45th Lunar and Planetary Science Conference, March 17-21, The Woodlands, TX, p. 2172.
- Islam, F.S., Pederick, R.L., Gault, A.G., Adams, L.K., Polya, D.A., Charnock, J.M., Lloyd, J.R., 2005. Interactions between the Fe(III)-reducing bacterium *Geobacter sulfurreducens* and arsenate, and capture of the metalloid by biogenic Fe(II). *Appl. Environ. Microbiol.* 71, 8642-8648.
- Istomina, V.S., 1957. *Seepage Stability of Soils*. Moscow.
- Jacob, D.J., Otte, M.L., 2004. Long-term effects of submergence and wetland vegetation on metals in a 90-year old abandoned Pb-Zn mine tailings pond. *Environ. Poll.* 130, 337-345.
- Jambor, J.L., Traill, R.J., 1963. On rozenite and siderotil. *Canadian Mineralogist* 7, 751-763.
- Jambor, J.L., 1994. Mineralogy of sulfide-rich tailings and their oxidation products. In: Jambor, J.L., Blowes, D.W. (Eds.), *Environmental Geochemistry of Sulfide Mine-Wastes*. Mineral. Assoc. Can. Short Course Vol. 22, 59-102.
- Jambor, J.L., Blowes, D.W., 1998. Theory and applications of mineralogy in environmental studies of sulfide-bearing mine wastes. In: Cabri, L.J., Vaughan, D.J. (Eds.), *Modern Approaches to Ore and Environmental Mineralogy*. Mineral. Assoc. Can. Short Course Vol. 27, 367-401.
- Jambor, J.L., Dutrizac, J.E. 1998. Occurrence and constitution of natural and synthetic ferrihydrite, a widespread iron oxyhydroxite. *Chem. Rev.* 98, 2549-2585.
- Jambor, J.L., 1999. Nomenclature of the alunite supergroup. *Can. Mineral.* 37, 1323-1341.
- Jambor, J.L., Blowes, D.W., Ptacek, C.J., 2000a. Mineralogy of mine wastes and strategies for remediation. *Environmental Mineralogy*. In: Vaughan, D.J., Wogelius, R.A. (Eds.), *EMU Notes in Mineral.* Vol. 2, 255-290.
- Jambor, J.L., Nordstrom, D.K., Alpers, C.N., 2000b. Metal-sulfate salts from sulfide mineral oxidation. In: Alpers, C.N., Jambor, J.L., Nordstrom, D.K. (Eds.), *Sulfate Minerals – Crystallography, Geochemistry, and Environmental Significance*. *Rev. Mineral. Geochem.* Vol. 40, 303-350.
- Jambor, J.L., Dutrizac, J.E., Chen, T.T., 2000c. Contribution of specific minerals to the neutralization potential in static tests. In: *Fifth International Conference on Acid Rock Drainage*. *Soc. Min. Metall. Explor.* 1, 551-565.
- Jambor, J.L., Dutrizac, J.E., Groat, L.A., Raudsepp, M., 2002. Static tests of neutralization potentials of silicate and aluminosilicate minerals. *Environ. Geol.* 43, 1-17.

- Jambor, J.L.. 2003. Mine-waste mineralogy and mineralogical perspectives of acid–base accounting. In: Jambor, J.L., Blowes, D.W., Ritchie, A.I.M. (Eds.), *Environmental Aspects of Mine Wastes*. Mineral. Assoc. Can. Short Course Vol. 31, 117-145.
- Jamieson, H.E., Robinson, C., Alpers, C.N., Blaine, R.B., McCleskey, D.K., Nordstrom, R.C. Peterson. 2005. Major and trace element composition of copiapite-group minerals and coexisting water from the Richmond mine, Iron Mountain, California. *Chemical Geology* 215, 387– 405.
- Jamieson, H.E., Walker, S.R., Parsons, M.B., 2015. Mineralogical characterization of mine waste. *Appl. Geochem.* 57, 85-105.
- Janzen, M.P., Nicholson, R.V., Scharer, J.M., 2000. Pyrrhotite reaction kinetics: reactions rates for oxidation by oxygen, ferric iron, and for nonoxidative dissolution. *Geochim. Cosmochim. Acta* 64, 1511 – 1524.
- Jasechko, S., Birks, S.J., Gleeson, T., Wada, Y., Fawcett, P.J., Sharp, Z.D., McDonnell, J.J. Welker, J.M., 2014. The pronounced seasonality of global groundwater recharge. *Water Resour. Res.*, 50, doi:10.1002/2014WR015809.
- Javed, M.B., Kachanoski, G., Siddique, T., 2014. Arsenic fractionation and mineralogical characterization of sediments in the Cold Lake area of Alberta, Canada. *Sci. Tot. Environ.* 500-501, 181-190.
- Jeong, G.Y., Lee, B.Y., 2003. Secondary mineralogy and microtextures of weathered sulfides and manganous carbonates in mine waste-rock dumps, with implications for heavy-metal fixation. *Amer. Mineral.* 88, 1933-1942.
- Jerz, J.K., Rimstidt, J.D., 2003. Efflorescent iron sulfate minerals: Paragenesis, relative stability, and environmental impact. *American Mineralogist* 88, 1919-1932.
- Johnson, R.H., Blowes, D.W., Robertson, W.D., Jambor, J.L., 2000. The hydrogeochemistry of the Nickel Rim mine tailings impoundment, Sudbury, Ontario. *J. Contam. Hydrol.* 41, 49-80.
- Johnston, R., Heijnen, H., Wurzel, P., 2001. Safe Water Technology, Chapter 6. In: *United Nations Synthesis Report on Arsenic in Drinking Water*, World Health Organisation.
- Jönsson, J., Sherman, D.M. 2008. Sorption of As(III) and As(V) to siderite, green rust (fougerite) and magnetite: implications for arsenic release in anoxic groundwaters. *Chem. Geol.* 255, 173-181.
- Jung, H.B., Bostick, B.C., Zheng, Y., 2012. Field, experimental, and modeling study of arsenic partitioning across a redox transition in a Bangladesh aquifer. *Environ. Sci. Technol.* 46, 1388-1395.

- Jurjovec, J., Ptacek, C.J., Blowes, D.W. 2002. Acid neutralization mechanisms and metal release in mine tailings: a laboratory column experiment. *Geochim. Cosmochim. Acta* 66, 1511-1523.
- Kadzialko-Hofmokl, M., Delura, K., Bylina, P., Jeleńska, M., Kruczyk, J., 2008. Mineralogy and magnetism of Fe-Cr spinel series minerals from podiform chromitites and dunites from Tapadła (Sudetic ophiolite, SW Poland) and their relationship to palaeomagnetic results of the dunites. *Geophys. J. Int.* 175, 885-900.
- Kaplan, I.R., Rittenberg, S.C., 1964. Microbiological fractionation of sulphur isotopes. *J. Gen. Microbiol.* 34, 195– 212.
- Kalinowski, B.E., Schweda, P., 1996. Kinetics of muscovite, phlogopite, and biotite dissolution and alterations at pH 1-4, room temperature. *Geochim. Cosmochim. Acta* 60, 367-385.
- Kawano, M., Tomita, K., 2001. Geochemical modeling of bacterially induced mineralization of schwertmannite and jarosite in sulfuric acid spring water. *American Mineralogist* 86, 1156-1165.
- Keith, D.C., Runnells, D.D., Esposito, K.J., Chermak, J.A., Levy, D.B., Hannula, S.R., Watts, M., Hall, L., 2001. Geochemical models of the impact of acidic groundwater and evaporative sulfate salts on Boulder Creek at Iron Mountain, California. *Applied Geochemistry* 16, 947-961.
- Kelln, C.J., Wassenaar, L.I., Hendry, M.J., 2001. Stable isotopes ( $\delta^{18}\text{O}$ ,  $\delta^2\text{H}$ ) of pore water in clay-rich aquitards: a comparison and evaluation of measurement techniques. *Ground Water Monit. Rem.*, Spring, 108-116.
- Kelly, W.R., Holms, T.R., Wilson, S.D., Roadcap, G.S. 2005. Arsenic in glacial aquifers: sources and geochemical controls. *Ground Water* 43, 500-510.
- Kimball, B.A., Wetherbee, G.A., 1989. Instream chemical reactions of acid mine water entering a neutral stream near Leadville, Colorado. In U.S. Geological Survey Toxic Substances Hydrology Program Proceedings of the Technical Meeting. (G.E. Mallard and S.E. Ragone, eds.) Phoenix, AZ. pp. 71-79.
- Kimball, B.A., D.M., McKnight, D.M., Wetherbee, G.A., Harnish, R.A., 1992. Mechanisms of iron photoreduction in a metal-rich, acidic stream (St. Kevin Gulch, Colorado, U.S.A.). *Chem. Geol.* 96, 227-239.
- Kimball, B.A., Runkel, R.L., Walton-Day, K., Bencala, K.E., 2002. Assessment of metal loads in watersheds affected by acid mine drainage by using tracer injection and synoptic sampling: Cement Creek, Colorado, USA. *Appl. Geochem.* 17, 1183-1207.
- Kinniburgh, D.G., Trafford, J.M., 1996. Unsaturated zone pore water chemistry and the edge effect in a beech forest in southern England. *Water Air Soil Pollut.* 92, 421-450.

- Klapper, H., Schultze, M., 1997. Sulfur acid mining lakes in Germany, ways of controlling geogenic acidification. In Proc. 4th Internat. Conf. Acid Rock Drainage, Vancouver, BC. pp. 1727-1744.
- Knezovich, P.J., Harrison, F.L., Wilhelm, R.G. 1987. The bioavailability of sediment-sorbed organic chemicals: a review. *Water Air Soil Pollut.* 32, 233–245.
- Knöller, K., Fauville, A., Mayer, B., Strauch, G., Friese, K., Veizer, J., 2004. Sulfur cycling in an acid mining lake and its vicinity Lusatia, Germany. *Chem. Geol.* 204, 303-323.
- Koch, I., Feldmann, J., Wang, L., Andrewes, P., Reimer, K.J., Cullen, W.R., 1999. Arsenic in the Meager Creek hot springs environment, British Columbia, Canada. *Sci. Tot. Environ.*, 236, 101-117.
- Koehler, G., Wassenaar, L.I., Hendry, M.J., 2000. An automated technique for measuring  $\delta D$  and  $\delta^{18}O$  values of porewater by direct  $CO_2$  and  $H_2$  equilibration. *Anal. Chem.* 72, 5659-5664.
- Korte, M.E., Fernando, Q., 1991. A review of arsenic (III) in groundwater. *Critical Rev. Environ. Control* 21, 1-39.
- Koski, R.A., Munk, L, Foster, A.L., Shanks III, W.C., Stillings, L.L., 2008. Sulfide oxidation and distribution of metals near abandoned copper mines in coastal environments, Prince William Sound, Alaska, USA. *Appl. Geochem.* 23, 227-254.
- Kossoff, D., Dubbin, W.E., Alfredsson, M., Edwards, S.J., Macklin, M.G., Hudson-Edwards, K.A., 2014. Mine tailings dams: characteristics, failure, environmental impacts, and remediation. *Appl. Geochem.* 51, 229-245.
- Krouse, H.R., Gould W.D., McCready R.G.L., Rajan, S, 1991.  $^{18}O$  incorporation into sulfate during the bacterial oxidation of sulfide minerals and the potential for oxygen isotope exchange between  $O_2$ ,  $H_2O$  and oxidized sulfur intermediates. *Earth Planet. Sci. Lett.* 107, 90–94.
- Lapakko, K.A., Antonson, D.A., 2012. Duluth complex rock dissolution and mitigation techniques: A summary of 35 years of DNR research. Minnesota Department of Natural Resources, St. Paul, MN, USA. 50 p.
- Le, X.C., Ma, M., 1998. Short-column liquid chromatography with hydride generation atomic fluorescence detection for the speciation of arsenic. *Anal. Chem.* 70, 1926-1933.
- Leckie, D.A., Bhattacharya, J.P., Bloch, J., Gilboy, C.F., Norris, B., 1994. Cretaceous Colorado/Alberta Group of the Western Canada Sedimentary Basin. Chapter 20, Geological Atlas of the Western Canada Sedimentary Basin, pp. 335-352.

- Lemay, T.G., 2003. Arsenic concentrations in Quaternary drift and Quaternary-Tertiary buried channel aquifers in the Athabasca Oil Sands (in situ) Area, Alberta. Alberta Energy and Utilities Board, Alberta Geological Survey, Geo-Note 2002-04.
- Lemay, T., Parks, K., Andriashek, L.D., Michael, K., Jean, G., Kempin, E. Stewart, S., 2005. Regional Groundwater Quality Appraisal, Cold Lake-Beaver River Drainage Basin, Alberta. Alberta Geological Survey Special Report 73.
- Leverett, P., Williams, P.A., 2007. Unusual post-mining sulfates from the Peelwood and Lloyd mines, New South Wales, and a comment on wattevilleite. *Austral Mineral* 13, 41–46
- Levings, C.D, Varela, D.E., Mehlenbacher, N.M., Barry, K.L, Piercey, G.E., Guo, M., Harrison, P.J., 2005. Effects of an acid mine drainage effluent on photoplankton biomass and primary production at Britannia Beach, Howe Sound, British Columbia. *Mar. Pollut. Bull.* 50, 1585-1594.
- Lewis, B.A. and Gallinger, R.D., 1999. Poirier site reclamation program. In: *Proceedings Sudbury'99 Mining and the Environment II*, Sudbury, ON, Canada, Vol. 2., pp. 439-448.
- Leybourne, M.I, Johannesson, K.H., Asfaw, A., Measuring arsenic speciation in environmental media: sampling, preservation, and analysis. In: *Bowell, R.J., Alpers, C.N., Jamieson, H.E., Nordstrom, D.K., Majzlan, J., (Eds.), Arsenic: Environmental Geochemistry, Mineralogy, and Microbiology. Rev. Mineral. Geochem.* 79, 371-390.
- Li, M., Aubé, B., St-Arnaud, L., 1997. Consideration in the use of shallow water covers for decommissioning reactive tailings. In: *4th International Conference on Acid Mine Drainage*, May 31-June 6, Vancouver, BC, pp. 115-130.
- Light, T.S., 1972. Standard solution for redox potential measurements. *Anal. Chem.* 44, 1038-1039.
- Lindsay, M.B.J., Blowes, D.W., Condon, P.D., Ptacek, C.J., 2009a. Managing pore-water quality in mine tailings by inducing sulfate reduction. *Environ. Sci. Technol.* 43, 7086–7091.
- Lindsay, M.B.J., Condon, P.D., Jambor, J.L., Lear, K.G., Blowes, D.W., Ptacek, C.J., 2009b. Mineralogical, geochemical, and microbial investigation of a sulfide-rich tailings deposit characterized by neutral drainage. *Appl. Geochem.* 24, 2009, 2212-2221.
- Lindsay, M.B.J., Blowes, D.W., Condon, P.D., Ptacek, C.J., 2011a. Organic carbon amendments for passive in situ treatment of mine drainage: Field experiments. *Appl. Geochem.* 26, 1169–1183.
- Lindsay, M.B.J., Wakeman, K.D., Rowe, O.F., Grail, B.M., Ptacek, C.J., Blowes, D.W., Johnson, D.B., 2011b. Microbiology and geochemistry of mine tailings amended with organic carbon for passive treatment of pore-water. *Geomicrobiol. J.* 28, 229-241.

- Lindsay, M.B.J., Moncur, M.C., Bain, J.G., Jambor, J.L., Ptacek, C.J., Blowes, D.W., 2015. Geochemical and mineralogical aspects of sulfide mine tailings. *Appl. Geochem.* 57, 157-177.
- Lock, K., De Schampelaere, K.A.C., Janssen, C.R., 2002. The effect of Lindane on terrestrial invertebrates. *Arch. Environ. Contam. Toxicol.* 42, 217-221.
- Lottermoser, B.G., 2010. Mine Waste, characterization, treatment and environmental impacts, 3<sup>rd</sup> Edition. Springer-Verlag, Berlin Heidelberg, p. 400.
- Lovley, D.R., 1987. Organic matter mineralization with the reduction of ferric iron: a review. *Geomicrobiol. J.* 5, 375-399.
- Lu, J., Alakangas, L., Jia, Y., Gotthardsson, J., Evaluation of the application of dry covers over carbonate-rich sulphide tailings. *J. Hazard. Mater.* 244-245, 180-194.
- Maia, F., Pinto, C., Waerenborgh, J.C., Gonçalves, M.A., Prazeres, C., Carreira, O., Sérgio, S., 2012. Metal partitioning in sediments and mineralogical controls on the acid mine drainage in Ribeira da Água Forte (Aljustrel, Iberian Pyrite Belt, Southern Portugal). *Appl. Geochem.* 27, 1063-1080.
- Majzlan, J., Drahota, P., Filippi, M., 2014. Parageneses and crystal chemistry of arsenic minerals. In: *Bowell, R.J., Alpers, C.N., Jamieson, H.E., Nordstrom, D.K., Majzlan, J., (Eds.), Arsenic: Environmental Geochemistry, Mineralogy, and Microbiology. Rev. Mineral. Geochem.* 79, 17-184.
- Malmström, M., Banwart, S., Lewenhagen, L.D., Bruno, J., 1996. The dissolution of biotite and chlorite at 25°C in the near-neutral pH region. *J. Contam. Hydrol.* 21, 201-213.
- Malmström, M.E., Berglund, S., Jarsjö, J., 2008. Combined effects of spatially variable flow and mineralogy on the attenuation of acid mine drainage in groundwater. *Appl. Geochem.* 23, 1419-1436.
- Manheim, F.T., 1966. A hydraulic squeezer for obtaining interstitial water from consolidated and unconsolidated sediments. *U.S. Geol. Sur. Prof. Paper* 550-C: 256-261.
- Manning, B. A., and Goldberg, S., 1996. Modeling competitive adsorption of arsenate with phosphate and molybdate on oxide minerals. *Soil Sci. Soc. Am. J.* 60, 121-131.
- Manson, R., Bloom, N., Cappellino, S., Gill, G., Benoit, J., and Dobbs, C. 1998. Investigation of porewater sampling methods for mercury and methylmercury. *Environ. Sci. Technol.* 32, 4031-4040.
- Mattu, G., Schreier, H., 2000. An investigation of high arsenic levels in wells in the Sunshine Coast and Powell River regions of B.C. Report prepared for the Coast Garibaldi Community Health Services Society.

- Maurel, C., 1978. Stabilité de la blende dans le système Zn-Cd-S. *Bull. Minéral.* 101, 406-411.
- Mayer, B., 2005. Assessing sources and transformations of sulfate and nitrate in the hydrosphere using isotope techniques. In: Aggarwal, P.K., Gat, J.R., Froehlich, K.F.O., (Eds.), *Isotopes in the Water Cycle: Past, Present and Future of a Developing Science*. International Atomic Energy Agency, Springer, Dordrecht, Netherlands, p. 67-89.
- McCreadie, H., Blowes, D.W., Ptacek, C.J., Jambor, J.L., 2000. Influence of reductive reactions and solid-phase composition on porewater concentrations of arsenic. *Environ. Sci. Technol.* 34, 3159-3166.
- McDonald, C.M., Gould, W.D., Lindsay, M.B.J., Blowes, D.W., Ptacek, C.J., Condon, P.D., 2013. Assessing cellulolysis in passive treatment systems for mine drainage: A modified enzyme assay. *J. Environ. Qual.* 42, 48-55.
- McGuigan, C.F., Hamula, C.L.A., Huang, S., Gabos, S., Le, C., 2010. A review on arsenic concentrations in Canadian drinking water. *Environ. Rev.* 18, 291-307.
- McGuire, M.M., Edwards, K.J., Banfield, J.F. Hamers, R.J., 2001. Kinetics, surface chemistry, and structural chemistry of microbially mediated sulfide mineral dissolution. *Geochim. Cosmochim. Acta* 65, 1243-1258.
- McKnight, D.M., Bencala, K.E., 1990. The chemistry of iron, aluminum, and dissolved organic material in three acidic, metal-enriched, mountain streams, as controlled by watershed and in-stream processes. *Water Resour. Res.* 26, 3087-3100.
- Meranger, J.C., Subramanian, K.S., 1984. Arsenic in Nova Scotia groundwater. *Sci. Tot. Environ.* 39, 49-55.
- Mineral Resources Branch, 1978. Sherridon Mine. Reference-Manitoba Card #839. A Compendium. *Natural Resour. Can.*, Ottawa.
- Mitchell, V.L., 2014. Health risks associated with chronic exposures to arsenic in the environment. In: *Bowell, R.J., Alpers, C.N., Jamieson, H.E., Nordstrom, D.K., Majzlan, J., (Eds.), Arsenic: Environmental Geochemistry, Mineralogy, and Microbiology*. *Rev. Mineral. Geochem.* 79, 435-450.
- Moncur, M.C., Ptacek, C.J., Blowes, D.W., Jambor, J.L., 2005. Release, transport and attenuation of metals from an old tailings impoundment. *Appl. Geochem.* 20, 639-659.
- Moncur, M.C., Ptacek, C.J., Blowes, D.W., Jambor, J.L., 2006. Spatial variations in water composition at a northern Canadian lake impacted by mine drainage. *Appl. Geochem.* 21, 1799-1817.
- Moncur, M.C., Ptacek, C.J., Hayashi, M., Birks, S.J., Blowes, D.W., Bright, D.A. 2007. Seasonal cycle of metals discharging from an abandoned mine site in northern Canada. In: *Sudbury 2007, Mining and the Environment IV*, Sudbury ON, October 19-27. pp. 1-10.



- Moncur, M.C., Jambor, J.L., Ptacek, C.J., Blowes, D.W., 2009a. Mine drainage from the weathering of sulfide minerals and magnetite. *Appl. Geochem.* 24, 2362-2373.
- Moncur, M.C., Ptacek, C.J., Mayer, B., Blowes, D.W., Birks, S.J., 2009b. Tracing the sulfur cycle at an abandoned high-sulfide tailings impoundment using chemical and isotopic techniques. In: *Proceedings of the 11<sup>th</sup> International Symposium on Environmental Issues and Waste Management in Energy and Mineral Production*, Banff, AB, November 16-19. pp. 316-324.
- Moncur, M.C., 2010. Uranium anomalies in shallow groundwater near Bonnyville, Alberta. *Water for Life: Knowledge and Research Series*. ISBN No. 978-0-7785-9952-4.
- Moncur, M.C., Ptacek, C.J., Blowes, D.W., Lindsay, M.B.J., 2012. Long-term storage of sulfide-rich tailings under a shallow water cover. In: Price, W.A. (Ed.), *9<sup>th</sup> International Conference on Acid Rock Drainage*. Ottawa, ON. May 20-26.
- Moncur, M.C., Smith, L.J.D., 2012. Processed kimberlite porewater geochemistry from Diavik Diamond Mines, Inc. In: Price, W.A. (Ed.), *9<sup>th</sup> International Conference on Acid Rock Drainage*. Ottawa, ON. May 20-26.
- Moncur, M.C., Blowes, D.W., Ptacek, C.J., 2013. Pore-water extraction from the unsaturated zone. *Can. J. Earth Sci.* 50, 1051-1058.
- Moncur, M.C., Ptacek, C.J., Hayashi, M., Blowes, D.W., Birks, S.J., 2014. Seasonal cycling and mass-loading of dissolved metals and sulfate discharging from an abandoned mine site in northern Canada. *Appl. Geochem.* 41, 176-188.
- Moncur, M.C., Ptacek, C.J., Lindsay, M.B.J., Blowes, D.W., Jambor, J.L., 2015. Long-term mineralogical and geochemical evolution of sulfide-rich mine tailings under a shallow water cover. *Appl. Geochem.* 57, 178-193.
- Moore, K., 2005. Treatment of Arsenic Contaminated Groundwater using Oxidation and Membrane Filtration. MSc. Thesis, University of Waterloo, Waterloo, ON.
- Mukherjee, A., Scanlon, B.R., Fryar, A.E., Saha, D., Ghosh, A., Chowdhuri, S., Mishra, R., 2012. Solute chemistry and arsenic fate in aquifers between the Himalayan foothills and Indian craton (including central Gangetic plains): influence of geology and geomorphology. *Geochim. Cosmochim. Acta* 90, 283-302.
- Mumford, A.C., Barringer, J.L., Benzel, W.M., Reilly, P.A., Young, L.Y., 2012. Microbial transformations of arsenic: mobilization from glauconitic sediments to water. *Wat. Res.* 46, 2859-2868.
- Munk, L., Fraure, G., Pride, D.E., Bigham, J.M., 2002. Sorption of trace metals to an aluminum precipitate in a stream receiving acid rock-drainage; Snake River, Summit County, Colorado. *Appl. Geochem.* 17, 421-430.

- Munk, L., Hagedorn, B., Sjoström, D., 2011. Seasonal fluctuations and mobility of arsenic in groundwater resources, Anchorage, Alaska. *Appl. Geochem.* 26, 1811-1817.
- Murakami, T., Utsunomiya, S., Yokoyama, T., Kasama, T., 2003. Biotite dissolution processes and mechanisms in the laboratory and in nature: Early stage weathering environments and vermiculitization. *Am. Mineral.* 88, 377-386.
- Murphy, R., Strongin, D.R., 2009. Surface reactivity of pyrite and related sulfides. *Surf. Sci. Rep.* 64, 1-45.
- Mycroft, J.R., Nesbitt, H.W., Pratt, A.R., 1995. X-ray photoelectron and Auger electron spectroscopy of air-oxidized pyrrhotite: Distribution of oxidized species with depth. *Geochim. Cosmochim. Acta* 59, 721-733.
- Nelson, S.T., 2000. A simple, practical methodology for routine VSMOW/SLAP normalization of water samples analyzed by continuous flow methods. *Rapid Commun. Mass Spectrom.* 14, 1044-1046.
- Nicholson, R.V., Gillham, R.W., Cherry, J.A., Reardon, E.J., 1989. Reduction of acid generation in mine tailings through the use of moisture-retaining cover layers as oxygen barriers. *Canadian Geotech. J.* 26, 1 -8.
- Nicholson, R.V., Scharer, J.M., 1994. Laboratory studies of pyrrhotite oxidation kinetics. In: Alpers, C.N., Blowes, D.W. (Eds.), *Environmental Geochemistry of Sulfide Oxidation*, Am. Chem. Soc. Symp. Ser., vol. 550, pp. 14– 30.
- Nickson, R.T., McArthur, J.M., Ravenscroft, P., Burgess, W.G., Ahmed, K.M., 2000. Mechanisms of arsenic release to groundwater, Bangladesh and West Bengal. *Appl. Geochem.* 15, 403-13. Nordstrom D. K., 1982. Aqueous pyrite oxidation and the consequent formation of secondary iron minerals. In: Kittrick, J.A., Fanning, D.F., Hossner, L.R. (Eds.), *Acid Sulfate Weathering*, Soil Sci. Soc. Am. Spec. Publ. 10, p. 37– 56.
- Nielsen, D.R., van Genuchten, M. TH., Biggar, J.W., 1986. Water flow and solute transport processes in the unsaturated zone. *Water Resour. Res.* 22, 89S-108S.
- Nordstrom, D.K., 1977. Thermochemical redox equilibria in Zobell's solution. *Geochim. Cosmochim. Acta* 41, 1835-1841.
- Nordstrom, D.K., 1982. Aqueous pyrite oxidation and the consequent formation of secondary minerals. In: Kittrick, A., Fanning, D.S., Hossner, L.R. (Eds.), *Acid Sulphate Weathering*. Soil Sci. Soc. Am. Special Pub. 10, 37-56.
- Nordstrom, D.K., Southam, G., 1997. Geomicrobiology of sulfide mineral oxidation. In: Banfield, J.F., Nealson, K.H. (Eds.), *Geomicrobiology: Interactions between Microbes and Minerals*. *Rev. Mineral.* 35, 361-390.

- Nordstrom, D.K., Alpers, C.N., 1999. Geochemistry of acid mine waters. In: Plumlee, G.S., Logsdon, M.J. (Eds.), *The Environmental Geochemistry of Mineral Deposits. Part A: Processes, Techniques, and Health Issues*. *Rev. Econ. Geol.* 6A, pp. 133-160, 1999.
- Nordstrom, D.K., Alpers, C.N., 1999. Negative pH, efflorescence mineralogy, and consequences for environmental restoration at the Iron Mountain Superfund site. In: *National Academy of Sciences USA*, Vol. 96, 3455-3462.
- Nordstrom, D.K., Alpers, C.N., Ptacek, C.J., Blowes, D.W., 2000. Negative pH and extremely acidic mine waters from Iron Mountain, California. *Environmental Science and Technology* 34, 254–258.
- Nordstrom, D.K., 2002. Worldwide occurrence of arsenic in ground water. *Sci.* 21, 2143-2145.
- Nordstrom, D.K., 2009. Acid rock drainage and climate change. *J. Geochem. Explor.* 100, 97-104.
- Nordstrom, D.K., 2011. Hydrogeochemical processes governing the origin, transport and fate of major and trace elements from mine wastes and mineralized rock to surface waters. *Appl. Geochem.*, 26, 1777-1791.
- Nordstrom, D.K., 2012. Arsenic in the geosphere meets the anthroposphere. In: Ng, J.C., Noller, B.N., Naidu, R., Bundschuh, J., Bhattacharya, P., (Eds.), *Proceedings of the 4<sup>th</sup> International Congress on Arsenic in the Environment*, CRC Press, 15-19.
- Nordstrom, D.K., Campbell, K.M., 2014. Modeling low-temperature geochemical processes, pp. 27-68. In: *Surface and Groundwater, Weathering and Soils* (ed. J.I. Drever) Vol. 7, *Treatise on Geochemistry*, second Edition (eds. H.D. Holland, K.K. Turekian). Elsevier.
- Nordstrom, D.K., Blowes, D.W., Ptacek, C.J., 2015. Hydrogeochemistry and microbiology of mine drainage: an update. *Appl. Geochem.* 57, 3-16.
- Nriagu, J.O., 1998. Arsenic in groundwater in the Cold Lake area. *Sessional Paper* 560199.
- Olías, M., Cánovas, C.R., Nieto, J.M., Sarmiento, A.M., 2006. Evaluation of the dissolved contaminant load transported by the Tinto and Odiel rivers Basin (South West Spain). *Appl. Geochem.* 21, 1733-1749.
- Ouangrawa, M., Molson, J., Aubertin, M., Bussiere, B., Zagury, G.J., 2009. Reactive transport modeling of mine tailings columns with capillary-induced high water saturation for preventing sulfide oxidation. *Appl. Geochem.* 24, 1312-1323.
- Paktunc, A.D., Davé, N.K., 2002. Formation of secondary pyrite and carbonate minerals in the Lower Williams Lake tailings basin, Elliot Lake, Ontario, Canada. *Amer. Mineral.* 87, 593–602.

- Paktunc, D., Dutrizac, J.E., 2003. Characterization of arsenate-for-sulfate substitution in synthetic jarosite using X-ray diffraction and X-ray absorption spectroscopy. *Can. Mineral.* 41, 905-919.
- Paktunc, D., Foster, A., Heald, S., Laflamme, G., 2004. Speciation and characterization of arsenic in gold ores and cyanidation tailings using X-ray absorption spectroscopy. *Geochim. Cosmochim. Acta* 68, 969-983.
- Paktunc, D., 2004. A computer program for analysing complex bulk XAFS spectra and for performing significance tests. *J. Synchrotron Rad.* 11, 295–298.
- Paktunc, D., Kingston, D., Pratt, A., McMullen, J., 2006. Distribution of gold in pyrite and in products of its transformation resulting from roasting of refractory gold ore. *Can. Mineral.* 44, 213–227.
- Paktunc, D., 2008. Speciation of arsenic in pyrite by micro-X-ray absorption fine-structure spectroscopy (XAFS). *Proc. 9th Int. Cong. App. Mineral. (ICAM2008)* 8-10 September 2008, Brisbane, Queensland, Australasian Inst. Mining Metall., 155-158.
- Paktunc, D., Dutrizac, J., Gertsman, V., 2008. Synthesis and phase transformations involving scorodite, ferric arsenate and arsenical ferrihydrite: Implications for arsenic mobility. *Geochim. Cosmochim. Acta* 72, 2649-2672.
- Paktunc, D., 2013. Mobilization of arsenic from mine tailings through reductive dissolution of goethite influenced by organic cover. *Appl. Geochem.* 36, 49-56.
- Palenik, C.S., Utsunomiya, S., Reich, M., Kesler, S.E., Wang, L., Ewing, R.C., 2004. Invisible gold revealed: Direct imaging of gold nanoparticles in a Carlin-type deposit. *Amer. Mineral.* 89, 1359-1366.
- Papelis, C., Hayes, K.F., Leckie, J.O., 1988. HYDRAQL: A program for the computation of chemical equilibrium composition of aqueous batch systems including surface complexation modeling of ion adsorption at the oxide/solution interface. Technical Report 306. Stanford University, Palo Alto, California.
- Parkhurst, D.L., Appelo, C.A.J., 1999. User's guide to PHREEQC (version 2) - a computer program for speciation, batch-reaction, one-dimensional transport, and inverse geochemical calculations. *US Geol. Survey, Water-Resour. Inv. Rep.* 99-4259, pp. 312.
- Parkhurst, D.L., Charlton, S.R., 2008. NetpathXL – an Excel interface to the program NETPATH: *U.S. Geological Survey Techniques and Methods* 6-A26, p. 11.
- Parkhurst, D.L., Appelo, C.A.J., 2013. Description of input and examples for PHREEQC version 3—A computer program for speciation, batch-reaction, one-dimensional transport, and inverse geochemical calculations. *U.S. Geological Survey Techniques and Methods, Book 6, Chapter A43*, 497.

- Parks, K., Andriashek, L.D., Michael, K., Lemay, T., Stewart, S., Jean, G., Kempin, E., 2005. Regional Groundwater Resource Appraisal, Cold Lake-Beaver River Drainage Basin, Alberta. Alberta Geological Survey Special Report 74.
- Patterson, R.J., Frape, S.K., Dykes, L.S., McLeod, R.A., 1978. A coring and squeezing technique for the detailed study of subsurface water chemistry. *Can. J. Earth Sci.* 15, 162-169.
- Patrick, R.A.D., Mosselmans, J.F.W., Charnock, J.M., 1998. An X-ray absorption study of doped sphalerites. *Eur. J. Mineral.* 10, 239-249.
- Parvianinen, A., Cruz-Hernández, P., Pérez-López, R., Miguel Nieto, J., Delgado-López, J.M., 2015. Raman identification of Fe precipitates and evaluation of As fate during phase transformation in Tinto and Odiel River Basins. *Chemical Geology* 398, 22-31.
- Peine, A., Peiffer, S. 1998. In-lake neutralization of acid mine lakes. In: Geller, W., Klapper, H., Salomons, W., (Eds.), *Acid Mining Lakes: Acid Mine Drainage, Limnology, and Reclamation*. pp. 47-63.
- Pedersen, T.F., 1985. Early diagenesis of copper and molybdenum in mine tailings and natural sediments in Rupert and Holberg inlets, British Columbia. *Can. J. Earth Sci.* 22, 1474-1484.
- Pedersen, T.F., Mueller, B., McNee, J.J. 1993. The early diagenesis of submerged sulphide-rich mine tailings in Anderson Lake, Manitoba. *Can. J. Earth Sci.* 30, 1099-1109.
- Perez, I.P., Dutrizac, J.E., 1991. The effect of the iron content of sphalerite on its rate of dissolution in ferric sulphate and ferric chloride media. *Hydrometall.* 26, 211-232.
- Peters, C.A., Healy, R.W., 1988. The representativeness of pore water samples collected from the unsaturated zone using pressure-vacuum lysimeters. *Ground Water Monit. Rem.* 8, 96-101.
- Peterson, R.C., Hammarstrom, J.M., Seal II, R.R., 2006. Alpersite (Mg,Cu)SO<sub>4</sub>•7H<sub>2</sub>O, a new mineral of the melanterite group, and cuprian pentahydrate: Their occurrence within mine waste 91, 261-269.
- Pitzer K. S., 1973. Thermodynamics of electrolytes: I. Theoretical basis and general equations. *J. Phys. Chem.* 77, 268-277.
- Plumlee, G.S., 1999. The environmental geology of mineral deposits. *The Environmental Geochemistry of Mineral Deposits*. In: Plumlee, G.S., Logsdon, M.J. (Eds.), Part A: Processes, Techniques, and Health Issues, *Rev. Econ. Geol.* Vol. 6A, 71-116.
- Plummer, L.N., Prestemon, E.C., Parkhurst, D.L., 1994. An interactive code (NETPATH) for modeling NET geochemical reactions along a flow PATH, version 2.0: U.S. Geological Survey Water-Resources Investigations Report 94-4169. p. 130.

- Poling, G.W., Ellis, D.V., Murray, J.W., Parsons, T.R., Pelletier, C.A., 2002. Underwater tailings placement at Island Copper Mine: A success story. Soc. Mining, Metallurgy and Exploration, Inc. Littleton, CO, pp. 204.
- Praharaj, T., Fortin, D., 2008. Seasonal variations of microbial sulfate and iron reduction in alkaline Pb–Zn mine tailings (Ontario, Canada). *Appl. Geochem.* 23, 3728–3740.
- Pratt, A.R., Muir, I.J., Nesbitt, H.W., 1994a. X-ray photoelectron and Auger electron spectroscopic studies of pyrrhotite and mechanisms of air oxidation. *Geochim. Cosmochim. Acta* 58, 827-841.
- Pratt, A.R., Nesbitt, H.W., Muir, I.J., 1994b. Generation of acids from mine waste: Oxidative leaching of pyrrhotite in dilute H<sub>2</sub>SO<sub>4</sub> solutions at pH 3.0. *Geochim. Cosmochim. Acta* 58, 5147-5159.
- Prietzl, J., Mayer, B. 2005. Isotopic fractionation of sulfur during formation of basaluminite, alunite, and natroalunite. *Chem Geol.* 215, 525-535.
- Pring A., Tarantino, S.C., Tenailleau, C., Etschmann, B., Carpenter, M.A., Zhang, M., Liu, Y., Withers, R.L., 2008. The crystal chemistry of Fe-bearing sphalerites: an infrared spectroscopic study. *Amer. Mineral.* 93, 591-597.
- Prior, G.J., Hathway, B., Glombick, P.M., Pană, D.I., Banks, C.J., Hay, D.C., Schneider, C.L., Grobe, M., Elgr, R., Weiss, J.A., 2013. Bedrock geology of Alberta. Alberta Energy Regulator, AER/AGS Map 600, scale 1:1 000 000.
- Ptacek C.J., Blowes, D.W., 1994. Influence of siderite on the pore-water chemistry of inactive mine-tailings impoundments. *Environmental Geochemistry of Sulfide Oxidation.* (C.N. Alpers and D.W. Blowes, eds.), American Chemical Society, Symposium Series Vol. 550, pp. 172-189.
- Ptacek, C.J., Blowes, D.W., 2000. Predicting SO<sub>4</sub>-mineral solubility in concentrated waters. In: Alpers, C.N., Jambor, J.L., Nordstrom, D.K. (Eds.), *Sulfate Minerals – Crystallography, Geochemistry, and Environmental Significance*, *Rev. Mineral. Geochem.*, 40, pp. 513–540.
- Puls, R.W., Barcelona, M.J., 1996. Low-flow (minimal drawdown) ground-water sampling procedures. *USEPA Ground Water Issue*, EPA/540/S-95/504, pp. 11.
- Rageh, O.M, Coles, C.A., Lye, L.M., 2007. Statistical analysis of Newfoundland drinking water sources containing arsenic. In *Ottawa Geo2007 – 60<sup>th</sup> Canadian Geotechnical Conference, 8<sup>th</sup> CGS/IAH-CHC Groundwater Conference*, Ottawa, ON, pp. 2287-2291
- Rasmuson, A., Collin, M., 1988. Mathematical modelling of water and oxygen transport in layered soil covers for deposits of pyritic mine tailings. In: *Proceedings Internat. Conf. Control Environ. Problems from Metal Mines*, Roros, Norway, pp. 32.

- Ravel, B., Newville, M., 2005. ATHENA, ARTEMIS, HEPHAESTUS: data analysis for X-ray adsorption spectroscopy using IFEFFIT. *J. Synchrotron Radiat.* 12, 537–541.
- Ravenscroft, P., Howarth, R.J., McArthur, J.M., 2006. Comment on “Limited temporal variability of arsenic concentrations in 20 wells monitored for 3 years in Araihasar, Bangladesh”. *Environ Sci. Technol.* 40, 1716-1717.
- Reardon, E.J. and Moddle, P.M., 1985. Gas diffusion measurements on uranium mill tailings: implications to cover layer design. *Uranium* 2, 111-131.
- Rimstidt, J.D., Chermak, J.A., Gagen, P.M., 1994. Rates of reaction of galena, sphalerite, chalcopyrite and arsenopyrite. In: Alpers, C.N., Blowes, D.W. (Eds.), *Environmental Geochemistry of Sulfide Oxidation*, vol. 550, Am. Chem. Soc. Symp. Ser., pp. 2–13.
- Robertson, J.D., 1992. Subaqueous disposal: a promising method for the effective control of reactive waste materials. In: 24<sup>th</sup> Annual Meeting of the Canadian Mineral Processors Conference, January 21-23, Ottawa, ON, Paper 33. p. 10.
- Robertson, J.D., Tremblay, G.A., Fraser, W.W., 1997. Subaqueous tailings disposal: A sound solution for reactive tailings. In: 4<sup>th</sup> International Conference on Acid Rock Drainage, May 31-June 6, Vancouver, BC, Canada, Vol. 3, pp. 1027-1044.
- Robertson, W.D., 1994. The physical hydrogeology of mill-tailings impoundments. In: Jambor, J.L., Blowes, D.W. (Eds.), *Environmental Geochemistry of Sulfide Mine-Wastes*. Mineral. Assoc. Can. Short Course Vol. 22, 271-292.
- Robertson, W.D., Russell, B.M., Cherry, J.A., 1996. Attenuation of nitrate in aquitard sediments of southern Ontario. *J. Hydrol.* 180, 267-281.
- Rokosh, C.D., Pawlowicz, J.G., Berhane, H., Anderson, S.D.A., Beaton, A.P., 2009. Geochemical and sedimentological investigation of the Colorado Group for shale gas potential: initial results. ERCB/AGS Open File Report 2008-09.
- Rollo, H.A., Jamieson, H.E., 2006. Interaction of diamond mine waste and surface water in the Canadian Arctic. *Appl. Geochem.* 21, 1522-1538.
- Romero, A., González, I., Galán, E., 2006. The role of efflorescent sulfates in the storage of trace elements in stream waters polluted by acid mine-drainage: the case of Peña del Hierro, southwestern Spain. *Can Mineral* 44, 1431–1446.
- Ross, C.S., Bain, J.G., Blowes, D.W., 1999. Transport and attenuation from a gold mine tailings impoundment. In: Goldsack, D.E., Belzile, N., Yearwood, P., Hall, G.J., (Eds.), *Sudbury '99, Mining and the Environment II*, Vol. 2., pp. 745-754.
- Rowe, R.K., Hosney, M.S., 2013. Laboratory investigation of GCL performance for covering arsenic contaminated mine wastes. *Geotext. Geomembr.* 39, 63-77.

- Rimstidt, D.J., Vaughan, D.J., 2003. Pyrite oxidation: a state-of-the-art assessment of the reaction mechanism. *Geochim. Cosmochim. Acta* 67, 873-880.
- Rinker, M.J., Nesbitt, H.W. Pratt, A.R., 1997. Marcasite oxidation in low-temperature acidic (pH 3.0) solutions: Mechanism and rate laws. *Amer. Mineral.* 82, 900-912.
- Rye, R.O., Bethke, P.M., Wasserman, M.D., 1992. The stable isotope geochemistry of acid sulfate alteration. *Econ. Geol.* 87, 225–262.
- Sabelli, C., 1985. Refinement of the crystal structure of jurbanite,  $\text{Al}(\text{SO}_4)(\text{OH})\cdot 5\text{H}_2\text{O}$ . *Zeitschrift für Kristallographie* 173, 33-39.
- Samad, M.A., Yanful, E.K., 2005. A design approach for selecting the optimum water cover depth for subaqueous disposal of sulfide mine tailings. *Can. Geotech. J.* 42, 207-228.
- Savage, K.S., Tingle, T.N., O'Day, P.A., Waychunas, G.A., Bird, D.K., 2000. Arsenic speciation in pyrite and secondary weathering phases, Mother Lode gold district, Tuolumne County, California. *Appl. Geochem.* 15, 1219-1244.
- Saquet, M., Halden, N.M., Babaluk, J., Campbell, J.L., Nejedly Z., 2002. Micro-PIXE analysis of trace element variation in otoliths from fish collected near acid mine tailings: potential for monitoring contaminant dispersal. *Nucl. Instrum. Methods Phys. Res.* 189, 196-201.
- Sarmiento, A.M., Caraballo, M.A., Sanchez-Rodas, D., Nieto, J.M., Parviainen, A., 2012. Dissolved and particulate metals and arsenic species mobility along a stream affected by acid mine drainage in the Iberian Pyrite Belt (SW Spain). *Appl. Geochem.* 27, 1944-1952.
- Sarmiento, A.M., Nieto, J.M., Olías, M., Cánovas, C.R., 2009. Hydrochemical characteristics and seasonal influence on the pollution by acid mine drainage in the Odiel river Basin (SW Spain). *Appl. Geochem.* 24, 697-714.
- Sayles, F.L., Wilson, T.R.S., Hume, D.N., Mangelsdorf, P.C., 1973. In situ sampler for marine sedimentary pore waters: evidence for potassium depletion and calcium enrichment. *Sci.* 181, 154-156.
- Seal, R.R., 2003. Stable-isotope geochemistry of mine waters and related solids. In: Jambor, J.L., Blowes, D.W, Ritchie, A.I.M. (Eds.), *Environmental Aspects of Mine Wastes*. Mineral. Assoc. Can. Short Course Vol. 31, pp. 303-334.
- Serpa, C., Batterson, M., Guzzwell, K., 2009. The influence of bedrock and mineral occurrences on arsenic concentrations in groundwater wells in the Gander Bay Area, Newfoundland. Newfoundland and Labrador Department of Natural Resources Geological Survey, Report 09-1, pp. 315-337.
- Singer, P.C., Stumm W., 1970. Acid mine drainage-rate determining step. *Sci.* 167, 1121–1123.



- Smedley, P.L., Kinniburgh, D.G., 2002. A Review of the source, behaviour and distribution of arsenic in natural waters. *Appl. Geochem.* 17, 517-568.
- SMEWW (Standard Methods for the Examination of Water and Wastewater), 2005. American Health Association, Washington, D.C.
- Smith, L.J.D., Moncur, M.C., Neuner, M., Gupton, M., Blowes, D.W., Smith, L., Sego, D.C., 2012. The Diavik waste rock project: design, construction and instrumentation of field-scale experimental waste rock piles. *Appl. Geochem.* 36, 187-199.
- Smyth, D.J.A., 1981. Hydrology and geochemical studies above the water table in an inactive uranium impoundment near Elliot Lake, Ontario. M.Sc. Project, University of Waterloo, Waterloo, Ontario.
- Sodermark, B., Lundgren, T., 1988. The Bersbo project - The first full scale attempt to control acid mine drainage in Sweden. In: *Proceedings Internat. Conf. Control Environ. Problems from Metal Mines, Roros, Norway*, p. 17.
- Sobron, P., Alpers, C.N., 2013. Raman Spectroscopy of Efflorescent Sulfate Salts from Iron Mountain Mine Superfund Site, California. *Astrobiology* 13, 270-278.
- Somers, G., Raymond, B., Uhlman, W., 1999. P.E.I. Water Quality Interpretive Report. Report prepared for the Canada - Prince Edward Island Water Annex.
- Stanton, M.R., Gemery-Hill, P.A., Shanks III, W.C., Taylor, C.D., 2008. Rates of zinc and trace metal release from dissolving sphalerite at pH 2.0-4.0. *Appl. Geochem.* 23, 136-147.
- Starr, R.C., Ingleton, R.A., 1992. A new method for collecting core samples without a drill rig. *Ground Water Monit. Rem.* 12, 91-95.
- Stein, R., Dudas, M., Klebek, M., 2000. Occurrence of arsenic in groundwater near Cold Lake, Alberta. *Alberta Environment*.
- Stillings, L.L., Foster, A., Koski, R.A., Munk, L.A., Shanks, III, W.C., 2008. Temporal variation and metals flux from the historic Beatson Mine, Prince William Sound, AK, *Appl. Geochem.* 23, 255-278.
- Suzuki, I., 1999. Oxidation of inorganic sulfur compounds: chemical and enzymatic reactions. *Can. J. Microbiol.* 45, 97-105.
- Tassé, N., Germain, M.D., Bergeron, M., 1994. Composition of interstitial gases in wood chips deposited on reactive mine tailings. In: Alpers, C.N., Blowes, D.W. (Eds.), *Environmental geochemistry of sulfide oxidation*. Am. Chem. Soc. Symp. Series, 550, 631-634.
- Taylor, B.E., Wheeler, M.C., Nordstrom, D.K. 1984a. Isotope composition of sulfate in acid mine drainage as measure of bacterial oxidation. *Nat.* 308, 538-541.

- Taylor, B.E., Wheeler, M.C., Nordstrom, D.K. 1984b. Stable isotope geochemistry of acid mine drainage: Experimental oxidation of pyrite. *Geochim. Cosmochim. Acta*, 48, 2269-2678.
- Theobald, P.K., Lakin, H.W., and Hawkins, D.B., 1963. The precipitation of aluminum, iron, and manganese at the junction of Deer Creek with the Snake River in Summit County, Colorado. *Geochim. Cosmochim. Acta*. 27, 121-132.
- Thode, H.G., Monster, J. 1965. Sulfur isotope geochemistry of petroleum, evaporates and ancient seas. *Am. Assoc. Petrol. Geol. Mem.* 4, 367-377.
- Thompson, T.S., Le, M.D., Kasick, A.R., Macaulay, T.J., 1999. Arsenic in well water supplies in Saskatchewan. *Bull. Environ. Contam. Toxicol.* 63, 478-483.
- Thornber M.R., Wildman, J.E., 1984. Supergene alteration of sulfides, VI. The binding of Cu, Ni, Zn, Co, and Pb with gossan (iron bearing) minerals. *Chem. Geol.* 44, 399-434.
- Tischendorf, G., Förestter, J.H., Gottesmann, B., 2001. Minor-and trace-element composition of trioctahedral micas: a review. *Mineral. Mag.* 65, 249-276.
- Toole, J., Thompson, J., Wilson, T.R.S., Baxter, M.S., 1984. A sampling artifact affecting the uranium content of deep-sea pore waters obtained from cores. *Nat.* 308, 263-266.
- Turnipseed, D.P., Sauer, V.B., 2010. Discharge measurements at gauging stations. U.S. Geological Survey Techniques and Methods, 3-A8 87.
- Tu, Q., Schröder-Adams, C.J., Craig, J., 2007. A New Lithostratigraphic Framework for the Cretaceous Colorado Group in the Cold Lake Heavy Oil Area, East-Central Alberta, Canada. *Nat. Resour. Res.* 16, 17-30.
- Tuttle, J.H., Dugan, P.R., Randles, C.I. 1969. Microbial sulfate reduction and its potential utility as an acid mine water pollution abatement procedure. *Appl. Microbiol.* 17, 297-302.
- Uhlig, I., Szargan, R., Nesbitt, H.W., Laajalehto, K., 2001. Surface states and reactivity of pyrite and marcasite. *Appl. Surf. Sci.* 179, 222-229.
- UMA Engineering Ltd., 2004. Site-Specific Assessment of Human Health and Ecological Risks from the Abandoned Mine Site, Sherridon/Cold Lake Manitoba. Report submitted to Manitoba Conservation.
- Valente, T., Grande, J.A., de la Torre, M.L., Santisteban, M., Cerón, J.C., 2013. Mineralogy and environmental relevance of AMD-precipitates from the Tharsis mines, Iberian Pyrite Belt (SW, Spain). *Applied Geochemistry* 39, 11-25.
- van Green, A., Zheng, Y, Goodbred Jr., S, Horneman, A., Aziz, Z., Cheng, Z., Stute, M., Mailloux, B., Weinman, B., Hoque, M.A., Seddique, A.A., Hossain, M.S., Chowdhury, S.H., Ahmed, K.M., 2008. Flushing history as a hydrogeological control on the regional

- distribution of arsenic in shallow groundwater of the Bengal basin. *Environ. Sci. Technol.* 42, 2283-2288.
- van Halem, D., Bakker, S.A., Amy, G.L., van Dijk, J.C., 2009. Arsenic in drinking water: a worldwide water quality concern for water supply companies. *Drink. Water Eng. Sci.* 2, 29-34.
- Vigneault, B., Campbell, P.G., Tessier, A., De Vitre, R., 2001. Geochemical changes in sulfidic mine tailings stored under a shallow water cover. *Water Res.* 35, 1066-1076.
- Vigneault, B., Kwong, Y.T.J., Warren, L., 2007. Assessing the long term performance of a shallow water cover to limit oxidation of reactive tailings at Louvicourt Mine. MEND Report 2.12.2.
- Walker, G.B., 1930. Report No. 353, Flotation test on ore samples from Sherritt-Gordon Mines, Ltd., Sherridon, Manitoba. Investigations in Ore Dressing and Metallurgy. Dept. Mines Rep. 724. Natural Resources Canada, Ottawa.
- Walton-Day, K., Filipek, L.H., Papp, S.E., 1990. Mechanisms controlling Cu, Fe, Mn, and Co profiles in peat of the Filson Creek Fen, northeastern Minnesota. *Geochim. Cosmochim. Acta* 54, 2933-2946.
- Walton-Day, K., 2003. Passive and active treatment of mine drainage. In: Jambor, J.L., Blowes, D.W., Ritchie, A.I.M. (Eds.), *Environmental Aspects of Mine Wastes*. Mineral. Assoc. Can. Short Course, Vol. 31, 335-359.
- Walton-Day, K., Mills, T.J., 2015. Hydrogeochemical effects of a bulkhead in the Dinero mine tunnel, Sugar Loaf mining district, near Leadville, Colorado. *Appl. Geochem.* <http://dx.doi.org/10.1016/j.apgeochem.2015.03.002>.
- Wang, S., Mulligan, C., 2006. Occurrence of arsenic contamination in Canada: sources, behavior and distribution. *Sci. Total Environ.* 366, pp. 701-721.
- Weisener, C.G., 2002. The reactivity of iron and zinc sulfide mineral surfaces: adsorption and dissolution mechanisms. PhD Thesis, Univ. S. Australia, Adelaide.
- Weisener, C.G., Smart, R.St.C., Gerson, A.R., 2003. Kinetics and mechanisms of the leaching of low Fe sphalerite. *Geochim. Cosmochim. Acta* 67, 823-830.
- White, D.E., Hem, J.D., Waring, G.A., 1963. Data of Geochemistry, 6<sup>th</sup> ed. M. Fleischer, (Ed). Chapter F. Chemical Composition of Sub-Surface Waters. US Geol. Surv. Prof. Pap. 440-F.
- Wiersma, C.L., Rimstidt, J.D., 1984. Rates of reaction of pyrite and marcasite with ferric iron at pH 2. *Geochim. Cosmochim. Acta* 48, 85-92.

- Wilson, S.A., Raudsepp, M., Dipple, G.M., 2009. Quantifying carbon fixation in trace minerals from processed kimberlite: a comparative study of quantitative methods using X-ray powder diffraction data with applications to the Diavik Diamond Mine, Northwest Territories, Canada. *Applied Geochemistry* 24, 2312-2331.
- Winch, S., Mills, H.J., Kostka, J.E., Fortin, D., Lean, D.R.S., 2009. Identification of sulfate-reducing bacteria in methylmercury-contaminated mine tailings by analysis of SSU rRNA genes. *FEMS Microbiol. Ecol.* 68, 94–107.
- Windsor Star, 2006, May 11. Town groundwater tainted by arsenic. Accessed April 14, 2014. [http://www.canada.com/story\\_print.html?id=92734581-cf0b-4a17-afeb-fb205368685f&sponsor](http://www.canada.com/story_print.html?id=92734581-cf0b-4a17-afeb-fb205368685f&sponsor).
- Winger, P.V., Lasier, P.J., Jackson, B.P., 1998. The influence of extraction procedure on ion concentrations in sediment pore water. *Arch. Environ. Contam. Toxicol.* 35, 8-13.
- Yan, X.P., Kerrich, R., Hendry, M.J., 2000. Distribution of arsenic(III), arsenic(V) and total inorganic arsenic in porewaters from a thick till and clay-rich aquitard sequence, Saskatchewan, Canada. *Geochim.Cosmochim. Acta* 64, 2637–48.
- Yanful, E.K., Aube, B.C., Woysner, M., ST-Arnaud, L.C., 1994. Field and laboratory performance of engineered covers on the Waite Amulet tailings. In: *Internat. Land Reclamation Mine Drainage Conf. and Third Internat. Conf. Abatement Acidic Drainage* Vol. pp. 8-147, U.S. Dept. Interior, Bureau of Mines Special Publication SP 06A-94.
- Yanful, E.K., Simms, P.H., 1997. Review of Water Cover Sites and Research Projects, p. 136. MEND report 2.18.1.
- Younger, P.L., Blachere, A., 2004. First-flush, reverse first-flush and partial first-flush: dynamics of short- and long-term changes in the quality of water flowing from deep mine systems. In: Price, W.A., Bellefontaine, K. (Eds.), *Proceedings of the 10<sup>th</sup> Annual British Columbia ML/ARD Workshop, Performance of ARD Generating Wastes, Material Characterization and MEND Projects*.
- Zagury, G.J., Samson, R., Deschênes, L., 2003. Occurrence of metals in soil and ground water near chromated copper arsenate-treated utility poles. *J. Environ. Qual.* 32, 507-514.
- Zanini, L., Robertson, W.D., Ptacek, C.J., Schiff, S.L., Mayer, T., 1998. Phosphorous characterization in sediments impacted by septic effluent at four sites in central Canada. *J. Contam. Hydrol.* 33, 405-429.
- Zieliński, P.A., Larson K.A., Stradling, A.W., 2000. Preferential deportment of low-iron sphalerite to lead concentrates. *Mineral. Eng.* 13, 357-363.
- Zobrist, J., Dowdle, P.R., Davis, J.A., Oremland, R.S., 2000. Mobilization of arsenite by dissimilatory reduction of adsorbed arsenate. *Environ. Sci. Technol.* 34, 4747-4753.